STUDIES IN X-RAY ASTRONOMY

by

Udaya Bhaskaram Jayanthi
Physical Research Laboratory
Ahmedabad-9, India

A thesis

submitted for the Ph.D. degree

of the

Gujarat University

043

B5109

March, 1973

to my uncle
m. chalapathi rau

STATEMENT

Realising the advantage of conducting experiments in X-ray astronomy from equatorial latitudes due to the prevailing low charged particle background, the X-ray astronomy group at the Physical Research Laboratory, planned a comprehensive programme in this field in 1967. The author as a member of the X-ray astronomy group under Prof. U.R. Rao has been involved almost since its inception in the design and fabrication of both balloon and rocket borne payloads for conducting these experiments. For the rocket borne payloads, Xenon-Methane proportional counters with slat collimators have been extensively used. Most of the experiments conducted so far on the rockets from the Thumba Equatorial Rocket Launching Station, Trivandrum (8° 32' N, 76° 51' E), have mainly concentrated in the 2-20 KeV X-ray range and have consequently used 3 mil beryllium entrance windows for counters. Sodium Iodide crystals with plastic scintillator anticoincidence in combination with graded shield, have been used for the balloon borne experiments. Balloon payloads were mounted on oriented platforms, to track the pre-selected stars to an accuracy better than 2°.

The author was involved in the study of time variations of Sco XR-1 and Cen XR-2 in the rocket experiments conducted from Thumba, late in 1968. The author also made some studies on the time variations of X-ray flux from Cen XR-4 and Nor XR-2 in 1969. Both the stars Cen XR-2 and Cen XR-4 have shown spectacular behaviour typical of optical novae. Using the earth as shutter, the cosmic diffuse X-ray background has also

been evaluated by comparing the observed background intensities when the payload looked towards the sky and the earth. The reprints embodying the results of various experiments carried out from Thumba are appended at the end of the thesis.

The main body of the thesis deals with the study of X-ray flux from Sco XR-1 source both in low energy (2-20 KeV) and high energy (20-120 KeV) ranges. Amongst all sources discovered to date, the X-ray source Scorpio XR-1, has been studied in a considerable detail by a number of workers. This X-ray source, besides being the brightest in the sky, is one of the few sources which has been identified both in the optical and the radio regions of the electromagnetic spectrum. The most significant feature of this source is its time variation in X-ray, optical, radio and infrared regions. In the optical region, the X-ray source has been shown to exhibit both long term and short term variations, with the optical blue magnitude varying between 12.2 to 13.2. When the optical luminosity is brighter than 12.5 mag., the source is often seen to exhibit flare like enhancements. Similar flare like enhancements in X-ray region have also been discovered. A number of attempts have been made in the last few years to correlate the variability in the observed X-ray flux with the time variations in other regions of electromagnetic spectrum through simultaneous observations. The establishment of correlation in time variations between different regions of electromagnetic spectrum is essential to understand the X-ray production mechanism in the source.

The author has devoted a considerable effort in conducting simultaneous X-ray and optical observations of Sco XR-1 source. Four rocket flights, two from the Thumba Equatorial Rocket Launching Station (India) and two from the Kagoshima Space Centre (Japan) in collaboration with the X-ray Astronomy group of the Institute of Aeronautical and Space Science, Tokyo, were conducted during the period April-August 1969. These rockets carried instrumented payloads of identical nature to measure X-ray flux from Sco XR-1 in the 2-20 KeV range. Attempts were made to monitor the optical magnitude of this source simultaneously from Tokyo Astrophysical Observatory, Tokyo. The present thesis fully describes the results obtained during these flights and a critical discussion of these in relation to other similar observations. A series of balloon experiments have also been conducted from Hyderabad (17° 25'N, 78° 55' E) for measuring the time variation of X-ray flux from Sco XR-1 in the energy range 20-100 KeV. The observations obtained from the flights have been compared with other balloon and rocket observations to understand the spectral behaviour of the source at high energies and its theoretical implications.

The important results from all the above experiments which are discussed in detail, in the main body of the present thesis are briefly summarised below:

1. The Scorpio XR-1 source has an energy spectrum of an exponential nature indicating thermal bremsstrahlung from a hot thin plasma as the possible source of production. The temperature and the flux show wide variability.

2.   Simultaneous X-ray and optical observations show that simple relations exist between temperature, volume emission measure and optical luminosity during quiet periods.

3.   Based on these relationships, a self consistent plasma cloud model for the star has been formulated. The observed X-ray spectrum has been extrapolated into the optical region and an attempt is made to explain the observed optical fluxes through this semi-opaque plasma model. Using this model an estimate of the physical parameters of the source has been obtained. The source is characterised by a temperature of about $10^7 - 10^8$ K, a density of about $10^{16} - 10^{17}$ cm^{-3} and a radius of about $10^8 - 10^9$ cm.
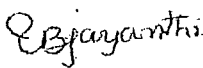
4.   The size of the source is very small comparable to or slightly smaller than the size of a white dwarf. This size is consistent with a distance at which a gas of this temperature is confined by the gravitational force of a central body of approximately solar mass. The study of interrelations between the physical parameters, favoursfor Sco XR-1 a hot plasma cloud deriving energy through accretion of matter from a secondary in a binary system on to a primary star of solar mass and dimension $\sim 10^8 - 10^9$ cm.

5.   The high energy X-ray flux observations also favour thermal bremsstrahlung emission upto about 45 KeV in our experiment, with the temperature being $\sim 9 \times 10^7$ K. This value lies within the range of temperatures observed in the low energy region

($<$ 20 KeV) by rocket experiments. However, an examination of the flux obtained by different workers in the 20-120 KeV range shows that in general power law spectrum with the exponent around $\sim$3.0 fits the data better. In other words the spectrum at higher energies cannot be treated simply as an extension of the low energy spectrum. This means there exists a possibility for different mode of emission, at higher energies, unlike low energy spectrum which follows thermal bremsstrahlung.

(U.R. RAO)
Professor-in-charge.

March 24, 1973

(U.B. JAYANTHI)

PUBLICATIONS

1. Time Variation of the Optical Intensity of Sco X-1 X-ray
   Source.

   U.R. Rao, A.S. Prakasarao and U.B. Jayanthi
   Nature, Vol.222, 846, 1969.

2. X-ray Flux from Centaurus X-2 in the Energy Range 2-20 KeV.

   U.R. Rao, E.V. Chitnis, A.S. Prakasarao and U.B. Jayanthi
   The Astrophysics Journal (Letters), Vol.157, L127, 1969.

3. Energy Spectrum and Time Variation of Sco XR-1

   U.R. Rao, U.B. Jayanthi and A.S. Prakasarao
   The Astrophysics Journal (Letters), Vol.157, L133, 1969.

4. Energy Spectrum and the Absolute Flux of Various Celestial
   X-ray Sources

   U.R. Rao, E.V. Chitnis, A.S.Prakasarao and U.B. Jayanthi
   Proc. of Indian Academy of Science, Vol.70, 257, 1969
   Proc. I.A.U. Symposium No.37 on Non Solar X and Gamma ray
   Astronomy, Rome, May 1969 (Ed.L.Gratton), p.85, 1970.

5. Diffuse X-ray Background Measurements in the Energy Range
   2-18 KeV

   A.S. Prakasarao, D.P. Sharma, U.B. Jayanthi and U.R. Rao
   Astrophysics and Space Science, Vol.10, 150, 1971.

6. X-ray Observations from Cen XR-4 and Nor XR-2

   U.R. Rao, E.V. Chitnis, D.P. Sharma, A.S. Prakasarao and
   U.B. Jayanthi
   Nature, Vol.229, 248, 1971.

7. Time Variation of the X-ray Spectrum and Optical Luminosity
    of Sco X-1

    T. Kitamura, M. Matsuoka, M. Miyamoto, M. Nakagawa, M. Oda,
    Y. Ogawara, K. Takagashi, U.R. Rao, E.V. Chitnis,
    U.B. Jayanthi, A.S. Prakasarao and S.M. Bhandari.

    Astrophysics and Space Science, Vo.1, 2, 378, 1971
    Proc. 12th International Conf.on Cosmic Rays, Hobart,
    August 1971, Vol.1, 2, 1971.

8. Balloon Observations of Sco X-1 in the Energy Interval
    17-106 KeV

    A.K. Jain, U.B. Jayanthi, K. Kasturirangan and U.R. Rao
    Astrophysics & Space Science (In Press).

9. X-ray Emission from Cyg X-1 at Energies Greater than 20 KeV

    A.K. Jain, U.B. Jayanthi, D.P. Sharma, K. Kasturirangan and
    U.R. Rao

    Comm.to 13th Intl.Cosmic Ray Conference, Denver.

10. Hard X-ray Emission from Her X-1

    D.P. Sharma, A.K. Jain, K. Kasturirangan, U.B. Jayanthi and
    U.R. Rao

    Comm.to 13th Intl.Cosmic Ray Conference, Denver.

. . . . .

ACKNOWLEDGMENTS

Finally I would like to record my appreciation of the understanding and cooperation shown by my parents and my wife Kasi Annapurna throughout this work.

(U.B. JAYANTHI)

TABLE OF CONTENTS

. . . . .

CHAPTER I

INTRODUCTION

Astronomical observations till recent past, were mostly
confined to the narrow window in the visible region of the
electromagnetic spectrum augmented only few decades ago by
observations in the radio region. The opaqueness of the atmos-
phere to a large part of the ultraviolet, infrared and high
energy electromagnetic radiation caused by atmospheric absorpt-
ion and the image distortion produced even in the allowed
wavelengths by the changing thermal properties of the earth's
atmosphere have been largely responsible for this limitation.
Restriction of observation to visual astronomy meant that we
could hope to understand the physical nature of only those
objects which emitted purely thermal radiation at a temperature
of about a few thousands of degrees, which meant that most of
their energy was radiated in the form of visible light.

Extension of investigations to other parts of the electro-
magnetic spectrum has immediately allowed us to look into rare
environments of the universe which are characterised by special
features such as abnormally high temperatures, extending to
several hundreds of million degrees, high densities upto
several millions of tons per cc. and presence of very high
magnetic fields of the order of $10^{14} - 10^{15}$ gauss. Thus with
the availability of simultaneous information about our universe
in different wavelength regions extending from gamma rays to
radio wavelengths, it is now possible to devise and carry out

decisive experiments to test almost any hypothesis in astrophy-
sics.

1.1 Cosmic X-Rays

Until the accidental discovery of X-ray emission from the
general direction of Scorpio constellation by Rossi and his
collaborators in 1962, X-ray studies were limited to the Solar
X-ray measurements. Since then, a large number of experiments
have been conducted on balloons, rockets and satellites, with
much better energy and directional resolution, by a number of
workers. In the last 10 years, more than 130 discrete X-ray
sources, some of them emitting energy in X-rays nearly three to
four orders of magnitude or more than the entire energy emitted
by Sun, have been discovered. The recent X-ray satellite UHURU,
with its large area detector has significantly added to our
knowledge of the sources. Out of the total number of sources
observed nearly 40 are of extragalactic origin whereas the
remaining are of galactic origin.

X-ray astronomy studies have been primarily conducted in
the photon energy range of 200 eV to 200 KeV. The absorption
of photons in the atmosphere demands that these studies be
conducted, either at balloon or preferably at rocket (or sate-
llite) altitudes. Figure 1 shows absorption curves for ele-
ctromagnetic radiation of different wavelengths in the atmos-
phere, from which the attenuation of photons of different
energies at different altitudes can be evaluated. Soft X-rays
of energy less than 12 KeV can only be observed at altitudes
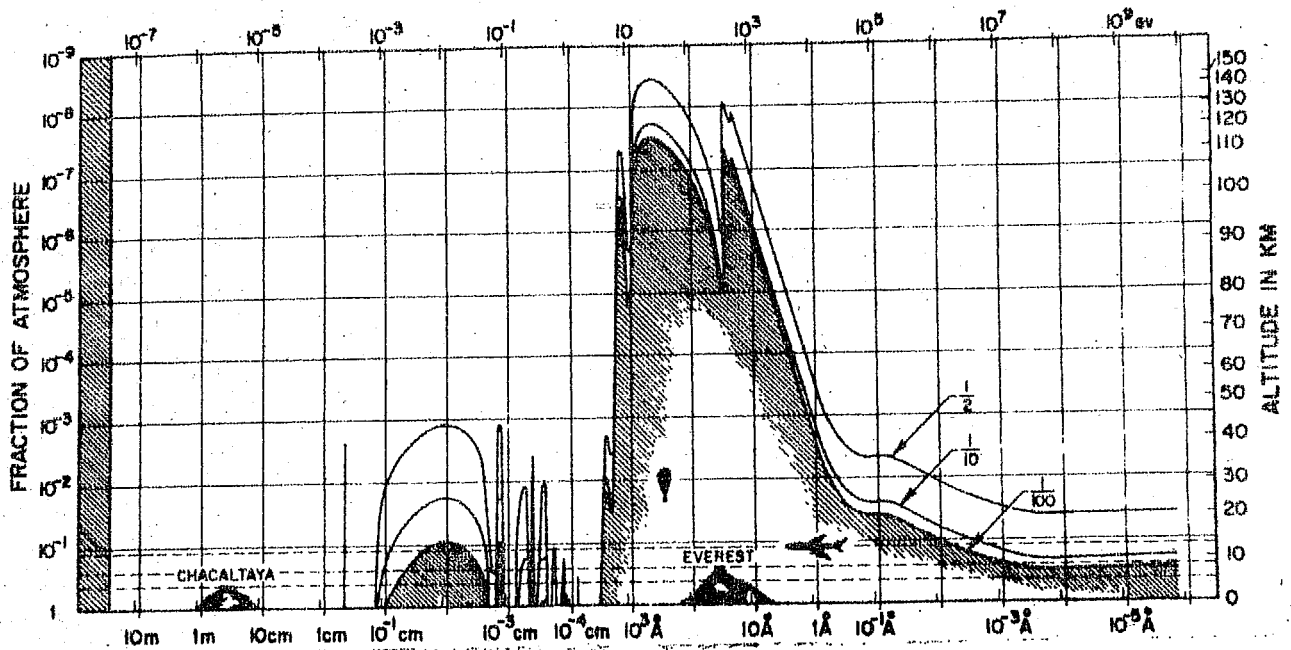
Fig. 1 – Attenuation of electromagnetic radiation in the atmosphere. Solid curves indicate altitude at which given attenuation occurs for a radiation of given energy.
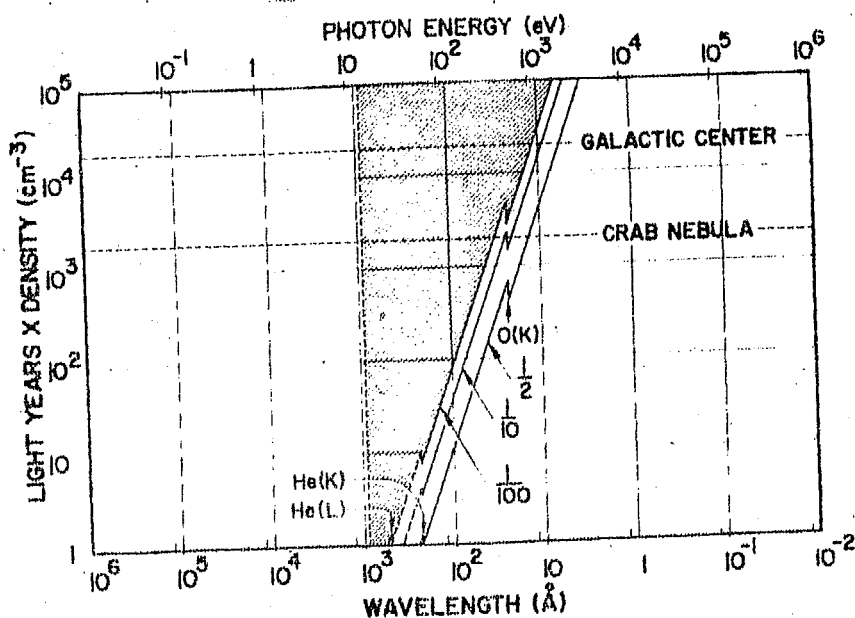
Fig. 2 – Attenuation of X-rays in interstellar space.

greater than 80 Km., which is attained by rockets or space vehicles. Hard X-rays with energies greater than 20 KeV can penetrate to altitudes about 35 Km. which is within the range of balloons.

Besides the atmospheric absorption which can be overcome by experimentation at very high altitudes, severe limitations on the measurements at very low energies ($<$ 1 KeV) is imposed by the interstellar absorption. A precise knowledge of inter-stellar absorption is necessary to compute the absolute fluxes from different X-ray sources particularly at energies below 2 KeV. Figure 2 shows the interstellar absorption in which the product of density of interstellar matter (in atoms per cm^3) and the distance (in light years) corresponding to various degrees of attenuation is plotted against photon energy. The nomenclatures O (K), He (K) and He (L) indicate the K and L characteristic absorption edges of Oxygen and Helium. The parameters pertaining to the Crab nebula and the galactic center are also plotted in the same figure. These parameters have been calculated using the known distance to these objects and assumed particle densities of 0.3 atoms per cm^3 and one atom per cm^3 for the Crab and the galactic center respectively. Considering the average value of density of interstellar matter to be of the order of 0.5 hydrogen atoms per cm^3, it is seen that the galaxy is transparent to wavelengths below about 6 Å ($>$ 2 KeV), while radiation longer than 100 Å ($<$ 120 eV) can reach the earth only from sources closer than 100 light years.

From the point of observational requirements it is customary to divide the X-ray region of spectrum into two regions.

a) Soft X-rays extending from the low energy cut off due to interstellar absorption to about 20 KeV. The observations of soft X-rays can only be carried out at altitudes above 100 Kms and thus require the use of rocket or artificial satellites. Many rocket experiments and UHURU satellite equipped with proportional counters have provided valuable data in this region.

b) Hard X-rays extending from 20 KeV to 0.5 MeV. Since the spectrum of high energy photons is very steep, longer time of observation is essential. Most of the presently existing information on hard X-rays have been provided by balloon borne detectors consisting of inorganic scintillators. A few satellite measurements are also available in this energy region.

Besides the discovery of X-ray sources, the early rocket flights also revealed the existence of surprisingly large steady flux of X-radiation. This diffuse radiation, extragalactic in nature, exhibits near isotropy in space and is of great cosmological significance. Many production mechanisms have been proposed to explain the X-ray emission from celestial objects. Comprehensive reviews summarising the various mechanisms are available in literature (Hayakawa et al. 1966; Gould 1967; Friedman 1967; and Oda 1968). We shall, in the next section describe, in brief, the important production mechanisms in the light of the experimental observations on diffuse background and discrete sources enumerated in the following

sections. From such a discussion we will attempt to arrive at self consistent models for these sources as well as for background radiation.

1.2 X-Ray Production Mechanisms

The three basic processes of importance for the production of photons in the energy range 1 - 100 KeV are (1) Thermal bremsstrahlung radiation, (2) Electron-synchrotron radiation and (3) Inverse compton radiation, the latter two being non-thermal processes. In this section we briefly discuss these production mechanisms.

1.21 Thermal Radiation from a Hot Thin Plasma

Bremsstrahlung or free-free radiation, occurs during the coulomb scattering of the electrons by ions and is the dominant energy loss process in a hot thin plasma at temperatures above 10^{7} k. Since the energy of the observed photons is a substantial part of the energy of the primary electron, the observed X-radiation can be produced by electrons in KeV range. The differential cross-section for the production of a photon with energy E in dE, by an electron of velocity β and energy E_e is expressed as

$$\frac{d\sigma}{dE} = \alpha \frac{Z^2 n_e^2}{\beta^2} G(E, E_e, Z) \frac{1}{E} \qquad \dots 1.1$$

where α is the fine structure constant, n_e is the classical radius of the electron, and Z is the atomic number of the nuclei. The factor G (Gaunt factor) is a slowly varying function of E and E_e and may be regarded as constant as a first order

approximation.

For a maxwellian distribution of electrons at temperature T (in degrees) in a Volume V, encountering ions of charge Z the emission spectrum is given by

$$\frac{dN}{dt\ dV\ dE} = 1.03 \times 10^{-11}\ a(\mathcal{T})\ n_e\ T^{-\frac{1}{2}}E^{-1}\left[\sum_Z Z^2\ n_Z\ G(E,E_e,Z\ )\right]$$
$$\exp\left(-\frac{E}{kT}\right)\quad \text{photons.cm}^{-3}.\text{sec}^{-1}.\text{KeV}^{-1} \quad \dots\ 1.2$$

where k is Boltzmann's constant and E is in KeV. The opacity of the plasma for the radiation, modifies the otherwise exponential function through a $(\mathcal{T})$ which is a function of optical depth $(\mathcal{T})$. This function essentially becomes unity for $E > kT$ and the energy spectrum becomes purely exponential.

In addition to the bremsstrahlung radiation, a hot plasma would emit photons by radiative recombination, characteristic line emission and dielectronic recombination. In radiative recombination, photons are emitted when electrons combine with ions which result in a continuum. This process yields a maximum intensity at temperatures around $5 \times 10^{6}\ ^{O}$K. Radiation from characteristic line emission occurs during transitions of excited electrons to lower levels. The line emission intensity begins at temperatures $\sim 10^{5}$K, has inverse dependence with temperatures and becomes relatively less significant above temperatures $\sim 5 \times 10^{6}$K. Dielectronic recombination radiation is emitted by electron transition, which has been excited not in the initial ionisation, but by the transition of an originally highly excited electron. The radiation from this process is

of importance at temperatures of the order of $10^6 - 10^7$K.

The relative intensities of radiation from these processes depend on the chemical abundances and the temperature of the plasma. In a plasma with chemical abundances as are usually encountered in astrophysics, bremsstrahlung radiation predominates at temperatures higher than 10^7K. Extensive treatments of low density plasma have been given by Tucker & Gould (1966) and Tucker (1967).

1.22 Black-Body Radiation

Significant flux of X-rays can be produced by blackbody radiation if the temperature is high enough. The flux emitted by a blackbody at surface temperature T , where photons of energy E will be in equilibrium with material particles, is given by

$$-\frac{dN}{dt\,dE\,dS} = 9.9 \times 10^{31}\ E^2 \left[\exp\ (E/\ kT)\ -\ 1 \right]^{-1}$$

$$\text{photons.cm}^{-2}. \text{sec}^{-1}. \text{KeV}^{-1} \qquad \dots 1.3$$

where k is Boltzmann's constant, S is the surface area of the star and E is in KeV. To explain galactic X-ray sources it is necessary to postulate an object which is a strong emitter of X-rays, but with negligible emission at optical and radio wavelengths.

1.23 Synchrotron Radiation

When relativistic electrons spiral in a magnetic field they emit synchrotron radiation also known as magnetic bremsstrahlung. Two difficulties associated with this mechanism

are (1) the extremely high energy electrons required to produce X-rays in magnetic fields at 10^{-3} to 10^{-4} gauss and (2) the short radiative life times of these electrons which is of the order of year.

A relativistic electron with energy E_e KeV in a field of H gauss produces a wide spectrum of photon energies but with a peak at

$$E_p = 1.9 \times 10^{-17} \; H_{\perp} \; E_e^2 \quad \text{KeV} \qquad \ldots 1.4$$

where $H_{\perp}$ is the component of the field perpendicular to the electron velocity. For photon energies much greater than the E_p, the spectral function behaves as

$$\backsim \frac{E}{E_c} \quad \exp\left(-\frac{E}{E_c}\right) \qquad \ldots 1.5$$

where $E_c = 3.45 \; E_p$. The spectrum of photons from a source, will further depend on the spectrum of the electrons and the range of magnetic fields present within the object.

For the case where the directions of magnetic field are random and the electron density distribution is isotropic in volume V and is consistent with a power law spectrum in energy

$$\frac{dN_e}{dVdE_e} = -K E_e^{-\gamma} \text{electrons.cm}^{-3}. \text{KeV}^{-1} \qquad \ldots 1.6$$

the spectrum of photons emitted by the synchrotron process is

$$\frac{dN}{dVdtdE} = 3.85 \times 10^{21} \; a(\gamma) \; K \left[\frac{6.6 \times 10^{-17} H_{\perp}}{E} \right]^{\frac{(\gamma + 1)}{2}}$$

$$\text{photons.cm}^{-3}. \text{sec}^{-1}. \text{KeV}^{-1} \qquad \ldots 1.7$$

where E is the photon energy in KeV and the function $a(\gamma)$ is approximately 0.1 for γ between 1 and 5 (Ginzburg & Syrovatski

1965). Thus we see the observed spectrum is also a power law as considered in equation (1.7).

In any X-ray source the electron spectrum would get modified with time, due to its finite half life which is usually given by

$$T = \frac{5 \times 10^8}{H_\perp^2} \left(\frac{mc^2}{E_e} \right) \text{ seconds} \qquad \ldots 1.8$$

Electrons of energy = 3×10^{10} KeV, in magnetic field of intensity 3×10^{-4} gauss, lose their energy via soft X-ray emission in a couple of years. Thus we need continuous injection or acceleration of higher energy electrons in the X-ray sources which are nearly time invariant e.g. Tau XR-1.

Synchrotron radiation from any single electron is highly polarised unlike the photon emission from thermal bremsstrahlung. It is polarised along the electron velocity vector with a cone of half angle (Jackson 1962)

$$\Theta_{max} = \frac{mc^2}{E_e} \qquad \ldots 1.9$$

The overall polarisation of radiation depends on the extent of areas over which the magnetic field remains constant in direction.

1.24 Inverse Compton Effect

In this process compton interactions between high energy electrons and low energy photons produce X-rays. The effect is called 'Inverse compton effect' as the energy of the photon is increased in the interaction. An electron of energy E_e

colliding with thermal photons of average energy E_p (= 2.7 kT)
produces scattered photons with an average energy $\overline{E}$ where
(Ginzburg & Syrovatski 1964)

$$\overline{E} = 1.33 \ E_p \ (\frac{E_e}{mc^2})^2 \qquad \text{... 1.10}$$

for $E_p < m \ c^2$. For production of X-rays of KeV, electrons having
energy > 20 MeV are needed in the presence of few eV photons.
The X-ray spectrum depends on the electron spectrum and for a
power law distribution of electrons of the form $Ke^{-\gamma}$ it is

$$\frac{dN}{dVdtdE} \ = \ 1.3 \times 10^{-17}. \ (57)^{3-\gamma} \ n_p \ E_p \ K \ T^{-(\frac{\gamma+3}{2})} \ E^{-(\frac{1+\gamma}{2})}$$
$$\text{photons.cm}^{-3}. \text{ sec}^{-1}. \text{ KeV}^{-1} \qquad \text{... 1.11}$$

where n_p is the low energy photon density in Cm^{-3} and E_p and E
are in eV. Thus the power law electron spectrum is reflected
in the photon spectrum with the exponent differing by 0.5.

Even though the simple mechanisms described above predict
unique spectral shape for a given X-ray source depending on the
nature of the process that is responsible for their emission,
in practice, deduction of origin from the observed spectral
characteristics is quite difficult. This essentially arises
due to the fact that extremely simplifying assumptions have been
made in the theoretical derivation of the spectral characterist-
ics from various processes which in practice are far from being
realistic. For example a synchrotron source emits a power law
spectrum only if the energy distribution of electrons themselves
follow a power law in addition to magnetic field being uniform.
A sharp high energy cut off in the electron energy distribution,

can make the synchrotron spectrum appear exponential over considerable energy range as shown by Manley (1966). Likewise even the thermal free-free emission is simple exponential, only when the emitting plasma is thin and at a single temperature. Sartori & Morrison (1967) have shown that the spectrum can take the form of power law if temperature gradients exist in the plasma. Thus a unique identification of the source production mechanism from their observed energy spectrum is unfortunately not possible. Nevertheless the observed spectral features can give an important clue to their origin.

1.3 Diffuse X-Radiation

Extensive data is now available on the X-ray background in the energy range 280 eV to 1 MeV obtained using a variety of different techniques aboard balloons, rockets and satellites. Investigations of detailed characteristics of the cosmic X-ray background which has a low flux value of about six photons $\cdot$ cm^{-2} sec^{-1} above 1 KeV, requires rather careful experimentation and use of sophisticated analytical procedures. In the balloon experiments, the extraterrestrial cosmic component can be clearly demarcated by the upward trend in the counting rate as the detector rises above 15 gm. cm^{-2} altitude. Substraction techniques, like occultation due to earth's atmosphere or employing two similar detectors with one of them having opaque entrance window have been employed in rocket experiments to differentiate the cosmic X-rays from the locally produced background.

1.31 Spectrum and Isotropy

The detailed spectral characteristics of the diffuse cosmic X-radiation has been a subject of considerable controversy in the last few years. In general it was found to follow a power law spectrum above 1 KeV. In the 2-15 KeV range most of the experimenters including our group have reported an exponent of 1.7 ± 0.25 (Gorenstein et al. 1969; Boldt et al. 1969; and Prakasarao et al. 1971). At higher energies most of the balloon and OSO III satellite observations have reported a much higher spectral index of about 2.5 in the 20 - 100 KeV range. It was, however, been recently pointed out that the balloon observations, in particular suffer from the fact that adequate correction for multiple compton scattering of X-rays ($\lessdot 40$ KeV) in the residual atmosphere (Kasturirangan & Rao 1972; and Manchanda 1971) has not been applied. The satellite observations on the other hand are often contaminated by spurious effects in alkali halides arising due to particle bombardment (Dyer & Morfil 1971). When these corrections are applied, the entire spectrum in the 2 KeV - 1 MeV range (figure 3) can be adequately represented, as pointed out by Kasturirangan & Rao (1972) by a power law spectrum with an exponent of $2.0 + 0.2$. The data of Seward et al. (1967) and Toor et al. (1970) with a single detector over the energy range 2 - 40 KeV, lend support to this conclusion. Similarly the experiments in the 0.2 - 1 MeV range (Metzer et al. 1964; Vette et al. 1970; Golentski et al. 1972; and Clark et al. 1971) also indicate a value around 2.0 for the exponent. At lower energies below 1 KeV the results are
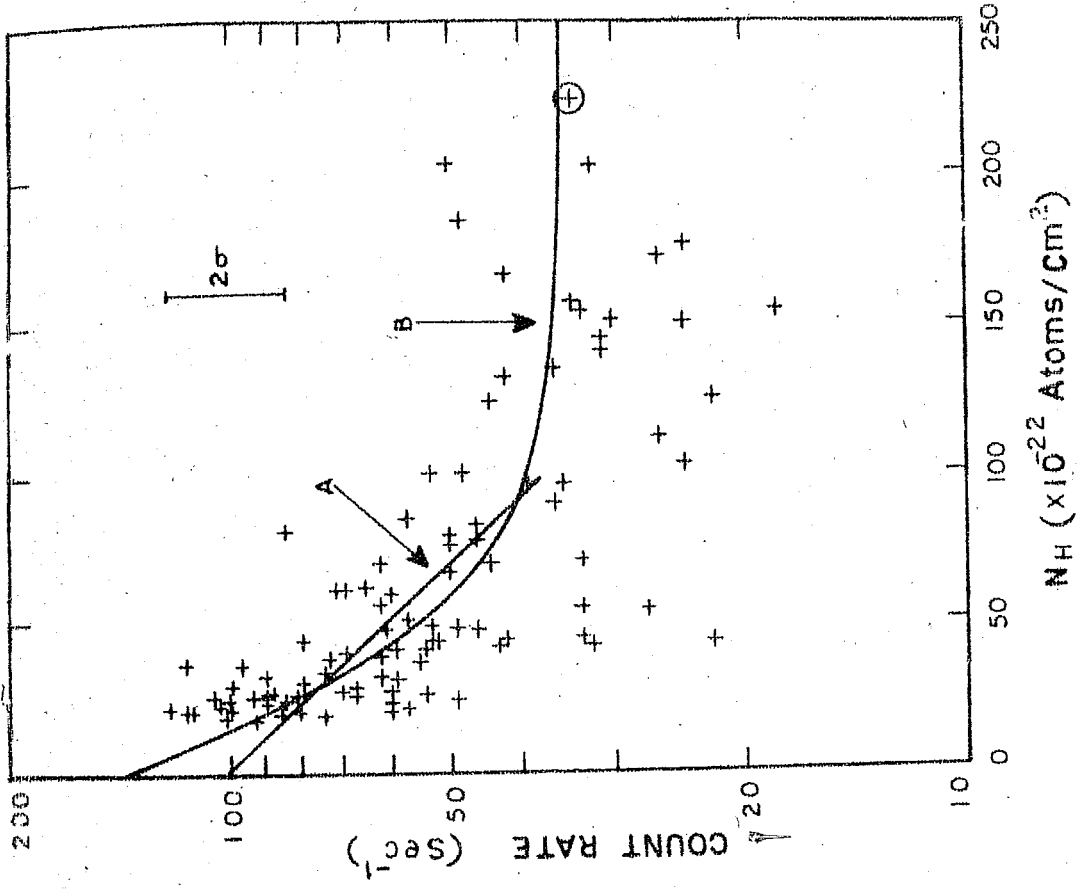
Fig. 4 — Correlation plot of the 250 eV X-ray background flux versus the hydrogen density.
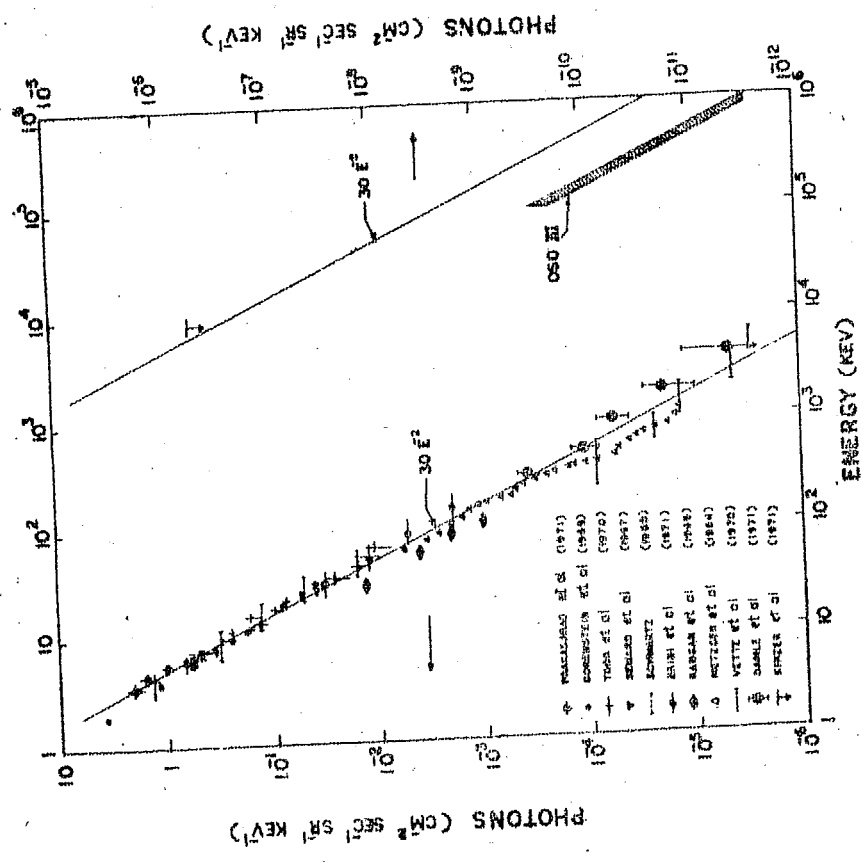
Fig. 3 — Spectrum of the diffuse X-ray and Gamma rays with the baloon observations corrected for multiple compton scattering of X-rays.

ambiguous. Although there are discrepancies by a factor of two
in the reported fluxes, the soft X-ray flux is not simply an
extension of the background observed at higher energies. In
addition it is possible that the spectral nature deviates
below 1.5 KeV as pointed out by Shukla et al. (1971), Palmeri
et al. (1971) and Davidson et al. (1972), who concluded that
an exponential shape fit the soft energy observations better,
with characteristic temperatures around 2-4 x 10^6K.

The isotropy of this background X-radiation above 1 KeV
has been now quite well established by a number of experiment-
ers (Seward et al. 1967; Matsuoka et al. 1968; and·Shwartz et al.
1971) to within 10%. The soft X-ray flux below 1 KeV, on the
other hand, shows a much greater intensity at higher galactic
latitudes compared to that at lower latitudes (Bunner et al.
1969; Hayakawa et al. 1971; Davidson et al. 1972; etc.).
Figure 4 shows the variation of count rate with neutral hydro-
gen density observed by Davidson et al. in the transmission
window around 280 eV. The cosmic flux at galactic latitudes
$>30^{\circ}$ show correlation with neutral hydrogen density indicating
that the observed anisotropy is caused due to the attenuation
of extragalactic isotropic flux by neutral hydrogen. Below
30° latitudes, however, there is no correlation and it indi-
cates an excess flux. This excess in the galactic frame for
energies below 1 KeV has been attributed to the presence of a
galactic component in addition to the omni-directional extra-
galactic background radiation. Curve A in the figure is an
attempt to represent the 280 eV data by a pure extragalactic

source model and B is for a two component model. Extensive survey with narrow opening angle telescopes having a high count rate is essential to determine the degree of anisotropy below the present limit.

1.32 Models for Diffuse X-radiation

The energy density of the isotropic background in the energy range 2-1000 KeV for an exponent of 1.7 for the spectrum, is 6×10^{-5} eV·cm^{-3} which is ten times the metagalactic radiation in the radio region (1-1000 MHz) while the energy density due to 2.7°K blackbody radiation is 0.3 eV cm^{-3}. Thus to understand this X-ray diffuse background radiation, two kinds of models have been suggested, (1) those which interpret the X-ray background as an integrated effect of the discrete sources present in galaxies and (2) those which involve emission mechanisms that operate throughout the intergalactic medium. The details of the two models have been worked out both by neglecting cosmological effects and by taking into account some model of cosmological evolution.

a) Models not Involving Cosmology

The super position model has an inherent draw back in that the X-ray flux from a typical galaxy is ambiguous and besides the X-ray spectral shape cannot be explained uniquely. The superposed X-ray energy from all galaxies, with average density ($\sim 3 \times 10^{-75}$ cm^{-3}) within the Hubble distance ($=10^{28}$cm) and having an average flux similar to our galaxy $\sim 10^{40}$ ergs.

Sec^{-1}, is estimated at 3 x 10^{-6} eV.cm^{-3} (Sciama 1969; and Oda 1965). This estimate falls short by a factor of 20 compared to the observed intensity. To account for the observed flux, galaxies with intense emission ($\sim$10^{43} ergs sec^{-1}) such as M-87 or quasars have been invoked. However, in view of the low spatial densities of these objects ($\sim$10^{-6} MPC^{-3}) estimated by Schmidt (1968), the superposition model has difficulty in accounting for the observed intensity of cosmic background.

Felten & Morrison (1966) have proposed that the X-ray background can be understood as due to compton collisions between the high energy metagalactic electrons (0.5 to 5 BeV) and 2.7 K microwave photons. However, the electrons needed to produce X-ray background can produce radio emission far excess of the observed radio radiation through synchrotron mechanism. If both X-ray and radio background have to be explained simultaneously one has to invoke very low magnetic fields much lower than the present estimates. This theory has the merit of relating the X-ray spectrum directly to the electron spectrum. They have suggested that the electrons with spectral index $\sim$2.6 leaking from radio galaxies can produce compton scattered X-rays of photon index $\sim$1.8. However, the intensity estimates fall short by a factor of 100. Brecher & Morrison (1969) have considered in addition normal galaxies. However, in view of the energy requirements this hypothesis does not seem to be plausible (Setti & Rees 1970).

In addition to the inverse compton effect, thermal and nonthermal bremsstrahlung processes over extended regions can also be considered. Even though the suprathermal electrons with different spectral exponents can explain the observed spectrum through non-thermal bremsstrahlung process, the energy requirements are severe because of the low efficiency ($\sim 1\%$) of this process. Thermal bremsstrahlung process cannot be accepted in view of the observed nonthermal spectrum above 1 KeV, without postulating temperature gradients. However, in general the extragalactic component of the soft X-radiation (< 1 KeV) is attributed to emission from hot dense intergalactic medium. Davidsen et al. (1972) from their observations infer a closure density $\sim 10^{-5}$ cm^{-3} for the hydrogen plasma at $R = \frac{1}{2} R_H$, and temperature $T \sim 4 \times 10^6$K. The temperature in the real universe is a function of the epoch and will be larger at higher $\bar{Z}$ and as the emmissivity of X-radiation depends on T, better spectral determinations are necessary for verifying the details of the theories. However, it can be categorically stated that all the above mentioned processeswhich do not involve cosmological effects are not able to satisfactorily explain the observed cosmic background.

b) Models Involving Cosmology

In evolutionary cosmology, the intergalactic gas would have been denser in the past and the primevial radiation field more intense besides the energetic events being more frequent. All the above mentioned models have been extended to include the evolutionary effects.

Silk (1968 , 1969) has treated the discrete source models by including the evolutionary cosmological effects. It was pointed out, that subject to sufficient increase in the X-ray luminosity of individual galaxies with redshift, one can account for the observed diffuse background by counting normal galaxies. However, the large redshifts ($\bar{Z} = 15$) invoked in this model are not compatible with cosmological time scales. Additionally the same evolution, increases the radio power much beyond the observed extragalactic radio background (Setti & Rees 1970). Treatment for evolution in the case of quasars lead to an intensity inadequate by a factor of 10 compared to the observed value, while in the case of radio galaxies strong evolution cannot be considered because of the limit set by the radio background.

Bergamini et al.(1967) pointed out, that when evolution of temperature and radiation are considered, the observed radiation could be explained by compton interactions of thermal radiation with electrons leaking from radio galaxies. In an evolutionary universe, the temperature of the blackbody radiation is proportional to $(1+\bar{Z})$, $\bar{Z}$ being the redshift, owing to the adiabatic cooling. The photon energy density W_{ph}, will be

$$W_{ph} \propto (1 + \bar{Z})^4. \qquad \qquad \dots 1.12$$

This means that at large redshifts the energy of relativistic electrons can be converted more rapidly into X-rays. Consequently the permitted magnetic field to fit the radio data can be increased in proportion to W_{ph}. The observed X-ray flux can

be explained by applying a cut off at $\bar{Z} = 5$. Beyond $\bar{Z} > 5$ the electrons responsible for radio emission have their half life times reduced considerably. Similar conclusions have been reached by Brecher & Morrison (1967).

Another model by Rees & Setti (1968) proposes an adiabatic expansion in the source and the bulk of X-rays are emitted during that phase of evolution of the radio source when the debris following the initial explosion, in which high energy particles are created, escape and interact with the galactic medium. This adiabatic expansion involves additional energy losses competing with compton losses for the relevant electrons. One needs to assume that the X-ray emission is mainly from a region of small window of red shifts, so that the break is not smeared out.

Silk & McCray (1969) attempted to fit the observed spectrum using a nonthermal bremsstrahlung model in an evolving universe. This process is more efficient at large redshifts because of the higher density of intergalactic gas and the authors postulate that sub-relativistic electrons with suitable spectrum are injected at a redshift ~ 10. The break in the electron spectrum is explained as a result of coulomb losses, which flatten the electron spectrum at low energies. The source of the electrom spectrum is chosen in an ad hoc fashion and besides there is a possibility of the electron spectrum getting modified as they escape into the intergalactic space.

Thus both the models i.e. the radiation from intergalactic space and the superposition of discrete sources are capable of explaining the observed intensity and spectrum under certain circumstances. The restrictions are less severe in the case of compton scattering model. The bounds on the break at 3 GeV in the electron spectrum of the sources, required to replenish the electron content in the compton scattering will vanish in the light of present findings of the absence of a break in the diffuse spectrum beyond 20 KeV.

The recent discovery of NGC 1275, a Seyfert galaxy, as an intense extragalactic X-ray object, leads us to believe that significant contribution to the observed diffuse background comes from extragalactic objects. If all the Seyfert galaxies which form 1% of the population of all spiral galaxies, emit X-rays at the same luminosity of NGC 1275 ($\sim 3 \times 10^{44}$ ergs sec^{-1}), the estimated superposed energy will be much more than the observed background intensity even without the consideration of evolutionary effects. However, the intensity of other Seyfert galaxies NGC 4157 and NGC 1018 falls far short of the required average luminosity. As the uncertainties involved are large, sophisticated experiments are needed to provide information on the relative abundances of various kinds of sources. In addition the flux determinations with good angular resolution may map the patchiness that is expected in either models.

1.4 Discrete Sources

The distribution of various X-ray sources in the sky in our galactic frame of reference is shown in figure 5. These X-ray stars differ very widely in intensity as well as in distribution in space. Broadly speaking, the sources are mostly concentrated at a low galactic latitudes and in particular around the galactic centre. About 40 sources located at high galactic latitudes are interpreted as extra galactic sources. Nevertheless it is clear from the figure that the present instrumentation favours the detection of sources in our galaxy.

1.41 Galactic Sources

Of the ninety and odd galactic sources that have been discovered todate many of the sources seem to also emit in the optical and radio wavelengths. Like the optical objects many of the sources are point sources even though some nebular regions are also found to emit X-rays. Among the galactic sources some ten sources have been identified with the known objects. Of these seven sources have been identified with known supernova remnants (e.g. Crab, Tycho, CasA, Cyg.Loop, etc.). The strongest X-ray source, Sco XR-1 has been identified with a blue star of magnitude ~12.5 and having typical characteristics of an old nova. Likewise Cyg XR-1 has been optically identified with a reasonable degree of certainty. The intensity of X-ray sources is spread over about three decades. The energy flux in the 1 - 10 KeV interval varies from $\sim 5 \times 10^{-7}$ ergs.cm^{-2} sec^{-1} for the brightest source Sco XR-1 to $\sim 10^{-10}$
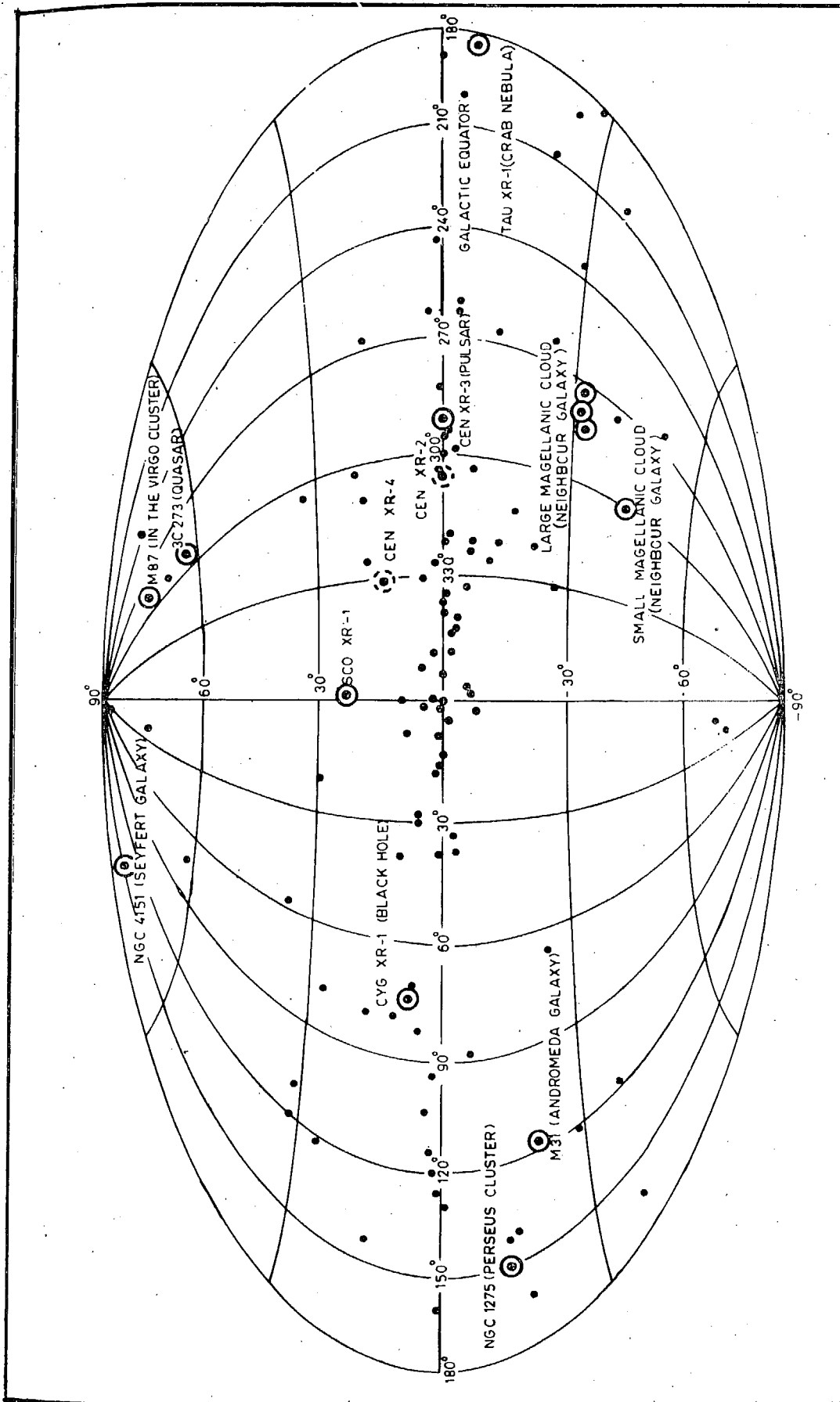
Fig. 5 : Distribution of X-ray sources in galactic coordinates.

ergs.cm^{-2} sec^{-1} for the faint sources like Cyg XR-4, Lyr XR-4, etc., the lower limit of flux being due to the limitation of the presently available detection techniques. Taking distances into account, the average X-ray luminosity of sources is estimated to be about 10^{38} - 10^{39} ergs.sec^{-1}. With the increasing number of X-ray sources detected, the X-ray astronomy studies are fast becoming like optical astronomy studies. It is now possible to draw the luminosity (S) - number (N) distribution for the known galactic sources, which is seen to indicate a slope much less than unity for logS-logN curve — contrary to expectation based on equal probability of distribution in space. At the present time, it is believed that the observed slope of 0.5 is indicative of the existence of a large number of low luminosity sources which are yet to be detected.

Although a considerable amount of spectral information is available about many stars in the 2-15 KeV region, information available on either side of this energy range is totally inadequate. At higher energies, the poor statistics have been the limiting factor. At lower energies the main difficulties have been the instrumentation as well as the reduction in flux values due to interstellar absorption. In spite of these difficulties it is expected that the experiments in the coming years will concentrate on these energy ranges and provide valuable information concerning the spectra and flux characteristics of these sources.

In general most of the X-ray stars seem to follow either a power law energy spectrum (e.g. Tau XR-1) with an energy

exponent value in the range of 0.5 to 2.0 or an exponential spectrum (e.g. Sco XR-1 and Cyg XR-2) characteristic of thermal bremsstrahlung emission, with temperatures of the order of twenty million degrees or more. A few instances where the sources seem to exhibit a flat spectrum (e.g. G X 304 - 1) or a black body radiation spectrum as with GX 340+0 (Bowyer et al. 1971) have also been discovered. Very few experiments have been conducted to date to detect line emissions and polarisation characteristics. The polarisation measurements in the case of Tau XR-1 (Novick et al. 1972) even though indicate the possibility of synchrotron radiation commonly associated with supernova remnants, the evidence is by no means conclusive. On the other hand the very soft X-ray source and old supernova remnant Cygnus-Loop seems to favour thermal emission with a characteristic exponential spectrum (Gorenstein et al. 1970).

It is interesting to note that there is an indication that in many stars the spectral character is not the same throughout the X-ray energy range. This complex behaviour of the sources, if inherent, does probably reflect different physical conditions in the sources like electron energy distribution, magnetic field, temperature, particle density, etc. So far not much work has been done on this aspect as all the spectral and structural details are known rather poorly. With the presently available evidence, we cannot yet definitely exclude the possibility of these differences being due to the different detection methods employed for the different energy regions.

Another most interesting feature of some of the X-ray sources is the time variation of their intensity. Some of the stars have exhibited spectacular and sudden appearance followed by equally spectacular disappearance. Some others seem to exhibit, more gradual, nonetheless extremely interesting time variations. Most spectacular amongst these has been the sudden appearance and disappearance of two stars both in the constellation of Centaurus. The sources Cen XR-2 and Cen XR-4, suddenly flared up and materialised into X-ray stars attaining nearly twice the intensity of Sco XR-1 in a week and decayed gradually in two months, a behaviour which is typical of optical novae. In two of the subsequent rocket flights after the decay of the star, Cen XR-2 was again observed (Rao et al. 1969) much above the threshold of detection.

Another remarkable X-ray star is the Tau XR-1 which seems to have within it the radio pulsar NP 0532. Like the radio counterpart, the X-ray star in the crab nebula also seems to pulsate, the energy in pulsation being about 10% of the total X-ray energy output. This 33 millisecond pulsar is found to have different intensities relative to the steady component in the radio, optical and X-ray regions. Similarly Cen XR-3, an X-ray pulsar with 4.7 sec period has also been discovered by the UHURU satellite. It is believed that this is a binary system with the X-ray star being occulted by a massive component star once in every two days as seen from its X-ray intensity changes. The X-ray star Cyg XR-1, also seems to typically exhibit pulsations, with a fundamental harmonic at 73 m.sec.

in the 2-10 KeV range (Oda et al. 1971), even though at higher
energies no such periodicity has been observed (Manchanda et al.
1972).

The study of time variations of Sco XR-1, the brightest
X-ray star, forms an important chapter in the history of time
variation of X-ray stars. Being the brightest X-ray source with
known optical and radio counterparts, the time variation of the
photon flux in all the wavelength ranges have been studied in
considerable detail. This will be separately discussed in the
following section since this forms the basis of the main body
of the present thesis. The time variation characteristics of
many other less spectacular X-ray stars like Lup XR-1 have also
been studied but the available data being meagre and the fluxes
involved being small, definitive quantitative estimates have
not been established.

Distribution in longitude of these galactic sources is
highly irregular as shown in figure 5. Strong clustering of
sources is observed towards the galactic centre, with the gala-
ctic nucleus itself emitting X-rays (Kellog et al. 1971). Nearly
forty sources are situated in the Scorpious - Sagattarius
constellations ($L_{II} \approx 280\text{-}40^{\circ}$) and other concentrations are found
in Cygnus and Cepheus-Lacertus regions ($L_{II} \approx 60\text{-}120^{\circ}$). These
groups seem to suggest that the galactic sources are strung
along the spiral arms (Friedman 1969; Gursky et al.
1967). Various known objects such as supernova remnants, old
novae, high temperature objects, pulsars and H I regions have

been suggested at different times as conceivable candidates for X-ray stars. But the spatial distribution of X-ray stars do not comply with any of these objects.

Very recently Ananthakrishnan & Ramanathan (1969) and Edwards et al. (1969), have reported interesting observations concerning the effect of celestial X-ray sources on terrestrial phenomena. Some of the powerful sources such as Sco XR-1 seem to cause significant enhancement in the ionisation of the D-region ionosphere at night. Eventhough considerable uncertainty regarding the theoretical interpretation existed in the past, recently Sharma et al. (1972) have quantitatively worked out the effect of various ionizing agencies on the night time ionosphere and have shown that the observed enhanced absorption coinciding with the passage of intense X-ray stars is consistent with theoretical calculations. Other secondary effects such as increase in air glow emission associated with the transists of Sco XR-1 and Tau XR-1 at night have also been reported in literature (Rao 1971). The terrestrial methods of monitoring, once understood, provide a simple means of continuous observation of some of the bright X-ray stars.

1.42 Extragalactic X-ray Objects

Evidence for X-ray emission from an extragalactic object was first reported about seven years ago by Byram et al. (1966) who observed X-rays from the vicinity of M-87, a radio galaxy in the Virgo cluster. Since then, particularly due to the observations from X-ray detector onboard UHURU satellite,

more than forty extragalactic objects have been detected. Of these sources about 12 have been identified with known objects, six of which are complex clusters ($\sim 0.5^{\circ}$ wide) such as Abel 347, 1367, Coma, Virgo. The Large Megallanic Cloud at 65 KPC contains some three sources. Various radio galaxies such as Cyg A, Cen A, etc. and quasar 3C273 have also been found to emit intense X-ray radiation.

Among the extragalactic objects, NGC 1273, a Seyfert galaxy, is the most intense energetic object with energy emission about $\sim 10^{44}$ ergs.sec^{-1}. cm^{-2} in the 2-10 KeV range (Fritz et al. 1971; and Gursky et al. 1971). The Seyfert galaxies, NGC 1275 and NGC 4151 are essentially infrared objects as their X-ray and optical energy emission is much less. For the distance at which the Virgo object is situated the flux emission is of the order of 10^{42} ergs. per sec. Inspite of the low number of extragalactic objects discovered todate, attempts have been made to draw LogS-LogN curve which seems to indicate unlike for galactic X-ray sources, a clear equispatial distribution.

There is very little information about the spectral character of these extragalactic sources. The rocket and balloon results favoured power law in the case of M-87, suggesting synchrotron emission which is consistent with the M-87, being a strong radio wave emitter. However, the X-ray emission from this Virgo cluster is not due to M-87 alone but comes from an extended region which includes the optical object M-84; the conclusion regarding the spectral shape has to be confirmed

with better observations. In general the sources, for which spectral measurements have been made, seem to satisfy both exponential and power law fits, primarily due to the poor statistics. Further improved statistics coupled with better spatial resolution especially for extended sources are essential to draw definitive conclusions on spectral shape. The sharp cut off observed in few sources at about 2 to 3 KeV may arise out of interstellar or intrastellar absorption of X-rays.

1.43 Models for Discrete Sources

(a) Galactic Sources

Among the peculiar objects suspected as galactic X-ray stars, neutron star figures prominently. This star, suspected as an end product of stellar evolution, will have nearly a core temperatures $\sim 10^{10}$K at its formation. Chiu & Salpeter (1964) suggested that a neutron star with surface temperature 10^7K is capable of emitting X-rays through black body radiation. However, at these high temperatures the neutron star cools down essentially through emission of neutrinos probably bringing down the surface temperature to less than 1% of the core temperature. Thus the cooling time of 1 year at 10^7K is incompatible with any known X-ray star. These estimates can be said to be accurate to within an order of magnitude. Accretion of interstellar matter on to a neutron star in certain conditions may result in blackbody emission at 10^6K and was considered by Morgan et al. (1972) in the case of GX 340+0.

Bremsstrahlung emission from hot thin plasma surrounding some stars was considered. Bless et al. (1968) and Wallerstein (1968) have suggested Wolf-Rayet stars with their hot coronas as strong X-ray emitters. Tucker (1967), de Loore & de Jager (1969), Bierman (1969) and Westphal et al. (1968) have examined the possibility of observing X-rays from coronas during flares. The maintenance of hot corona through ejection of matter or pumping of mechanical energy is limited by thermodynamical consideration. Hot plasma could be produced by the shock heating of the envelope around novae or supernovae or might occur in the ejecta of matter (Tucker 1967). Sartori & Morrison (1967) have considered this possibility of thermal bremsstrahlung at different temperatures in the case of Tau XR-1. In Cygnus loop, the emission can be understood as from a hot thin plasma as the spectrum and line emission observed support this hyphothesis. The synchrotron emission postulated for supernova remnants, has the essential drawback in that, the high energy electron life times associated with X-ray emission is small.

Manley & Olbert (1969) proposed extars, which are clouds of plasma in the process of condensing to form stars. It is supposed that the X-rays are being emitted by the synchrotron process and that the necessary magnetic fields and high energy electrons are present in the clouds, the energy being gravitational in origin. By considering the magnetoactive plasma, they concluded that a modified fermi acceleration is able to pump and maintain relativistic electrons with sharp high

energy cut-off, which will explain the form of X-ray spectrum of Sco XR-1. This calls for a detailed study regarding the condensing phases in stellar evolution.

Hayakawa & Matsuoka (1964) suggested that X-ray sources might be generated by gas streams in early type binaries. The presence of large reservoir of gravitational energy in such a system, can sustain the emission from hot plasma, created by mass transfer from an extended component to another compact star of the binary. Shklovsky (1967) suggested a neutron star for the compact object while Cameron & Mock (1967) put forth a white dwarf instead. Prendergast & Burbidge (1968) investigated this model in detail regarding the mass transfer and the possible configuration of the binary system.

The rotation of the magnetic neutron stars, which explained the pulsar phenomenon (Gold 1968 and Pacini 1968), is invoked by many for the high energy activity in X-ray stars (Pacini 1968; Gold 1969; Gunn & Ostriker 1969 a, b; Finzi & Wolf 1969; Tucker 1969; Coppi & Treves 1971; etc). Particularly the slowing down of NP 0532, as due to a torque on a rotating neutron star implies a rotational energy loss rate comparable to the luminosity of the nebula. The various theories differ on the interaction between the spinning star and the surrounding plasma and furthermore on the nature of the radiation process. Pacini (1967, 1968) and Gunn & Ostriker (1969) suggested low frequency magnetic dipole radiation for acceleration of the particles, while Gold (1969) and Goldreich & Julian (1969)

emphasised the rigid corotation of the magnetosphere resulting
in angular momentum loss to the plasma. The radiation processes
which have been suggested are essentially induced scattering
(Ginzburg et al. 1969; and Bertotti et al. 1969) and Synchrotron
radiation (Gold 1969; Michel & Tucker 1969). Davidson et al.
(1971), Coppi & Ferrari (1971) and Coppi & Trevis (1971) consi-
dered bremsstrahlung emission from the surrounding plasma of a
rotating neutron star for compact sources like Sco XR-1.

b) Extragalactic objects

Broadly speaking the extragalactic sources can be classi-
fied into three classes (Brecher & Burbidge 1972). (1) normal
galaxies similar to our own in which X-ray emission originates
in discrete sources perhaps in binary stars and supernova rem-
nants as discussed earlier, (2) galaxies and quasars which are
known to be powerful nonthermal sources of radio and infrared
flux and have intensely active nuclei and (3) the extended
X-ray sources with sizes ranging from 10^5 to 10^6 PC which seem
to be centred on clusters which contain active galaxies.

The observations made so far give little evidence in
support of the idea that X-ray emission from clusters is a
result of the presence of a hypothetical intergalactic medium
filling the clusters. Synchrotron X-rays which require strong
magnetic field and high energy electrons is possible if only
a number of localised regions are present and as the present
spatial resolution is insufficient it cannot be over emphasized.
The most acceptable hypothesis for X-ray production seems to

be inverse compton effect (Fritz et al. 1971; Adams et al.1969; and Brecher & Burbidge 1972) in small as well as large dimensional extragalactic objects, due to the presence of large flux of relativistic electrons in nucleus of a galaxy. If the X-ray source coincides with the nucleus of a galaxy, compton scattering of the electrons with nonthermal radio, microwave or infrared photons generated in the nucleus, is quite likely to explain the X-rays. X-ray production due to compton effect of electrons generated by the galaxy with the extended microwave photon radiation field can explain the extended sources. The detailed study of spatial configuration, temporal behaviour, and spectral nature of extragalactic sources in the X-ray, optical, radio and microwave regions is essential for any understanding of the source models.

1.5 Experimental Investigations on Sco XR-1

Since this thesis deals mainly with the X-ray source Sco XR-1, in this section we describe in somewhat greater detail, the characteristics of this source as a background to the work presented in the following chapters.

1.51 Characteristics of Sco XR-1

Sco XR-1 is the strongest X-ray source in the sky with an intensity around 6×10^{-7} ergs.sec^{-1}.cm^{-2} in the X-ray energy range. The first detailed spectrum of Sco XR-1 in the 2-20KeV range was obtained by Grader et al. (1966). They conclusively showed that the spectrum, the energy flux per unit frequency followed an exponential function with respect to frequency,

and obtained a value ~5.8 x 10^7K for the characteristic tempe-
rature of the plasma. Peterson & Jacobson (1966) measured the
spectrum over an extended energy range from 20-50 KeV, with
instrumentation on balloon and concluded that the major emiss-
ion was from a thin plasma at temperature ~5 x 10^7K. At
energies above about 40-50 KeV, the spectral characteristics
are not very well known. The observations of Buselli et al.
(1968) favour a power law fit with photon exponent of ~3.4
over the free-free emission fit with temperature ~15 x 10^7K in
the 20-120 KeV range. There is a strong belief that the spect-
rum flattens above 40 KeV.

Friedman et al. (1966) using ¼ mil. and 1 mil. mylar windows
for Argon and Helium filled counters (filter photometry) made
the first determination of flux from Sco XR-1 below 1 KeV.
This experiment along with another NRL flight (Fritz et al.1968),
obtained 30^{+3}_{-10} KeV. cm^{-2}. sec^{-1}. KeV^{-1} for energy flux at 0.25 KeV,
a value which lies on the 1.5 - 15 KeV extrapolated spectrum
measured simultaneously. The soft energy results (Hill et al.
1968; Rappaport et al. 1969) indicate little absorption due to
interstellar matter and can only be understood either by assum-
ing Sco XR-1 as an intense soft X-ray emitter or the interstel-
lar hydrogen density determined by the 21 cm line emission in
the direction of Sco XR-1 as much lower than the previous
estimates. However, Grader et al. (1970), from a series of
experiments, quoted low values of flux in this region and have
suggested the necessity of cool matter $\not> 10^{21}$ atoms to explain
the continuity in the region 0.2 - 10 KeV. In figure 6, the
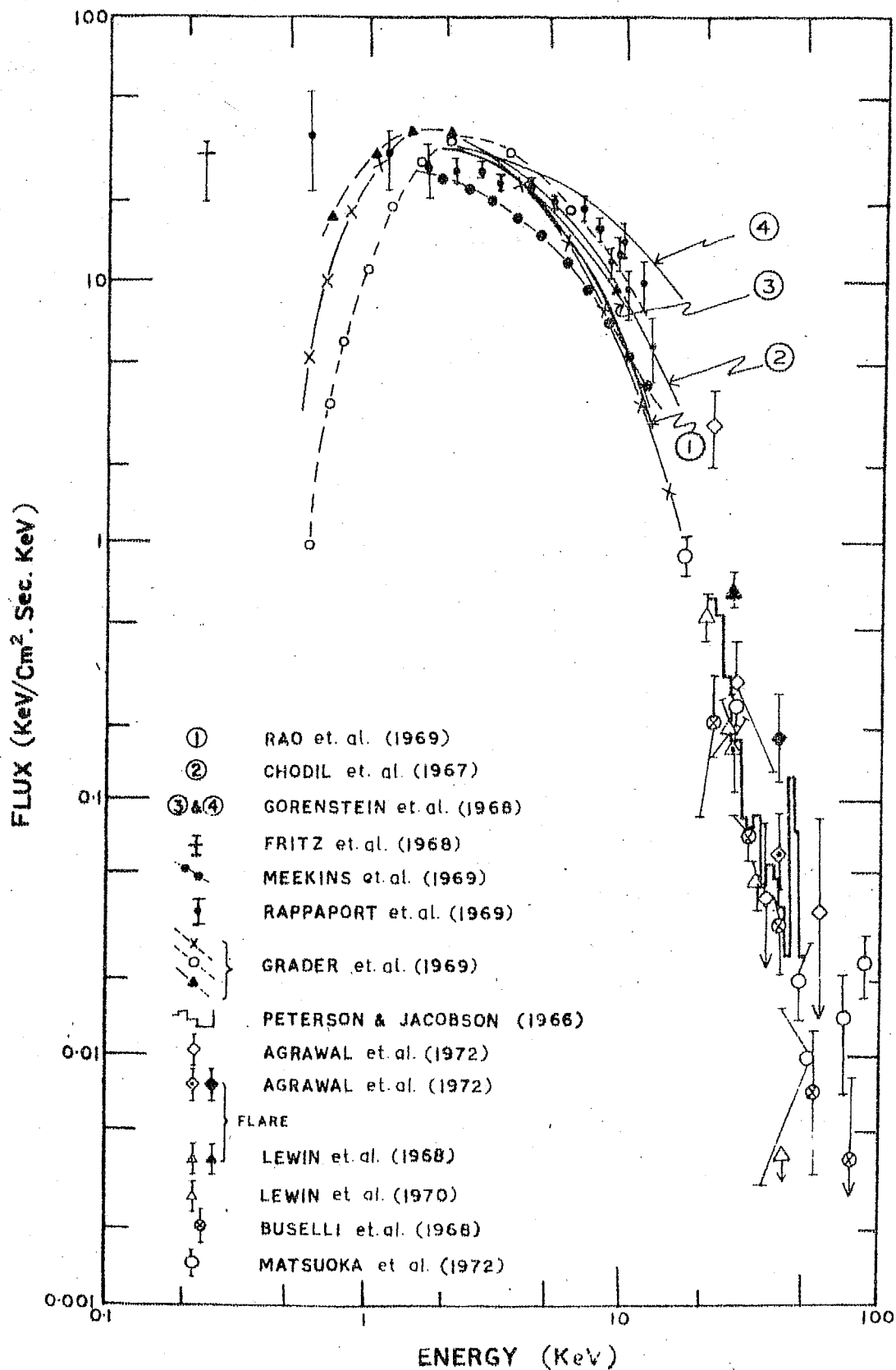
Fig. 6 — Compilation of energy spectrum of Sco XR-1.

various X-ray spectral measurements in the 200 eV to 120 KeV range are presented.

There are very few polarisation and line emission measurements. The X-ray polarimeter experiment of Angel et al. (1969) set an upper limit for the polarisation of Sco XR-1 at about 6% in the 6-18 KeV range. Acton et al. (1970) with large area proportional counter telescope observed Iron line emission at 6 KeV at 6σ confidence level, in contradiction to the negative results reported by Fritz et al. (1969), Holt et al. (1970) and Pounds et al. (1969). This along with the failure of Kestenubaum et al. (1972) to observe Sulphur emission line at 2.6 KeV, are in complete disagreement with the line strengths predicted by Tucker & Gould (1966) and Jordan (1969) on the basis of universal abundances in this star.

The size and the accurate possible locations of Sco XR-1 were determined by ASE/MIT scientists (Gursky et al. 1966) employing modulation collimator in front of the detector on an Aerobee rocket flown in March 1966. The modulation collimator with a broad field of view had high resolution of the order of a few tens of arc seconds, achieved by suitably placed thin wire grids. Equipped with star sensors, the counters scanned the region and located two equally probable positions (Fig. 7a) at

1. Rt. Ascension (1950) = 16^h 17^m 7^s $\pm$ 4^s; Decl. (1950) = $- 15^{\circ}$ $30'$ $54"$ $\pm$ $30"$ and

2. Rt. Ascension (1950) = 16^h 17^m 19^s $\pm$ 4^s; Decl.(1950) = $- 15^{\circ}$ $35'$ $20"$ $\pm$ $30"$

RESPONSE TO A
POINT SOURCE

UHURU

5'
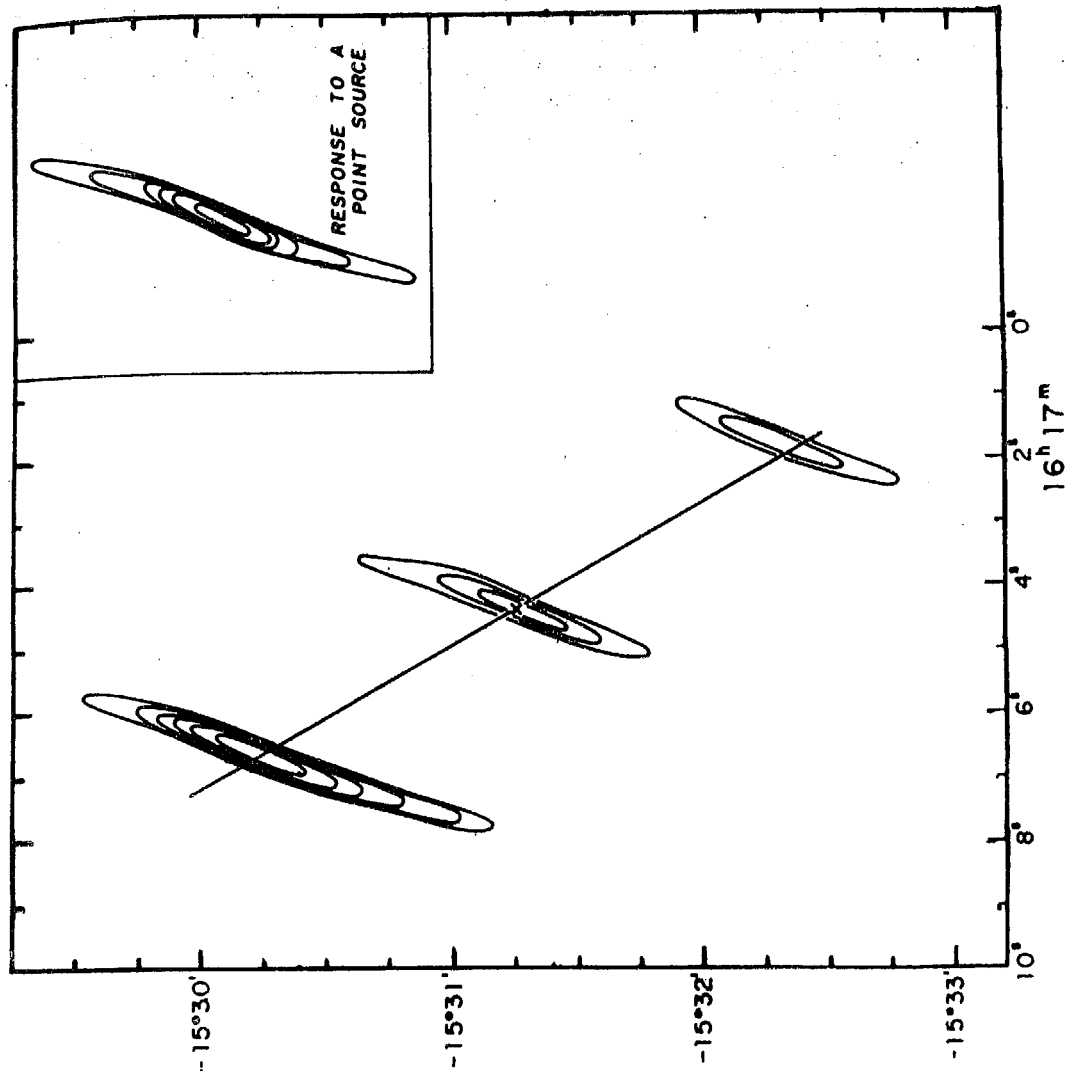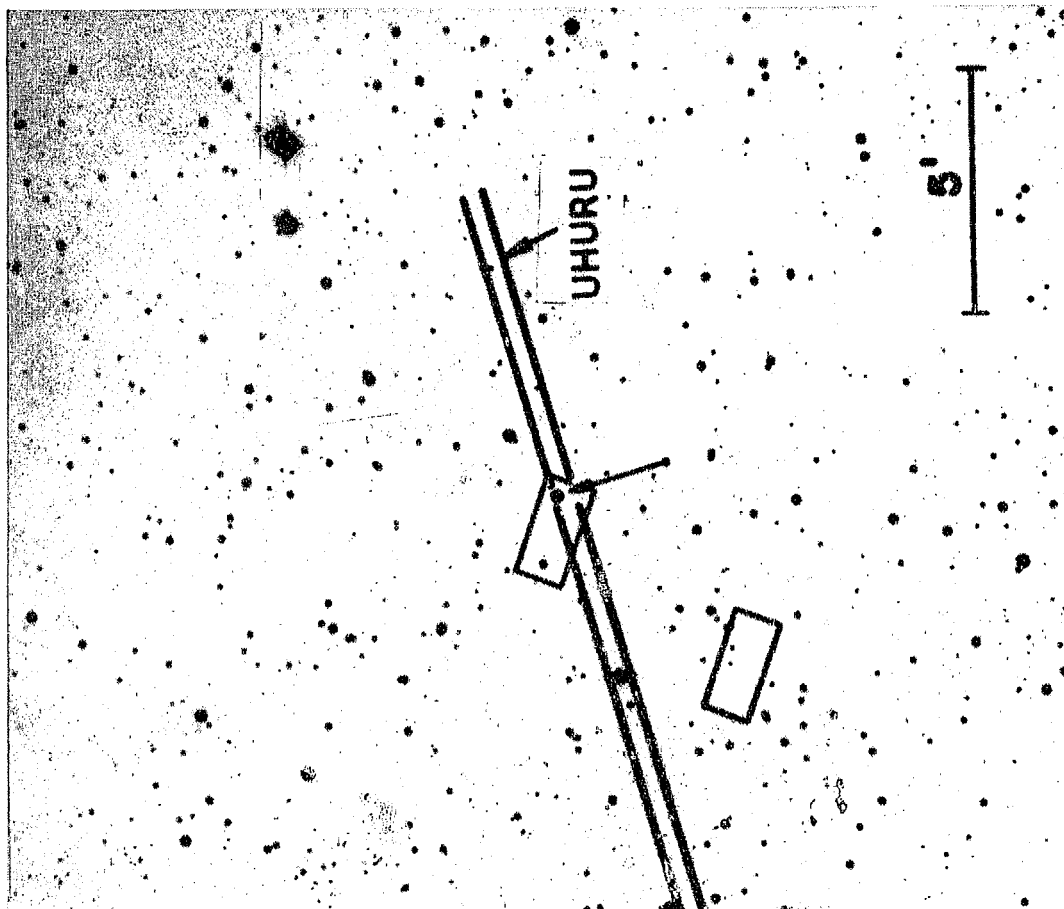
Figure 7 : a) Palomar Sky Survey print of the region surrounding Sco XR–1. The arrow shows the optical object identified with Sco XR–1. X-ray survey with rocket (Squares) and UHURU Satellite are also shown. b) The radio survey shows the central component coincident with Sco XR–1.

The physical dimension of this star is found to be less than 20 arc seconds.

From the extrapolation of X-ray spectrum to the optical region, Sco XR-1 was expected to be a blue star of about 12.5 app. magnitude for its dimension (<20 arc seconds) and to have excess ultraviolet emission compared to normal stars (Oda et al. 1965; and Gursky et al. 1966). Attempts were made in 1965-66 to search the suspected region of the sky for UV excess objects by two colour image methods; at Tokyo Astrophysical Observatory and Palomar Observatory. A 12.5 mag. star at R.A (1950) = 16^h 17^m 7^s and Decl. (1950) = -15° 31' 31" within a precision of 5 arc seconds, was suspected as the candidate star (Ichumura et al. 1966; and Johnson & Stephenson 1966). Figure 7a is a reproduction of Palomar sky survey print where the squares represent the X-ray locations of Sco XR-1 from ASE/MIT experiment, and the UV excess peculiar star was located in one of them. This optical identification of Sco XR-1 (Sandage et al. 1966) was further confirmed by the UHURU satellite (Tananbaum et al. 1971), as can be seen by the long narrow band of width 2 σ enclosing the optical object.

The UBV photometric data of optical Sco XR-1 by Sandage et al. (1966) and Mook (1967) is summarised in Figure 8. The three colour diagram show clearly Sco XR-1 as an UV excess object, with constant B-V. The spectrograms taken at Palomar and other observatories (Sandage et al. 1966; Mook 1967; Wallerstein et al. 1967; and Westphal et al. 1968) showed many

Fig. 8 - Three colour diagram U - B versus B-V. Colour indices corresponding to Sco XR-1 (X Sandage et al. 1967; & Mook 1967). Spectra of some white dwarfs (o), main sequence stars are shown.

Fig. 9 - Microphotometer tracings of spectra of Sco XR-1.

emission features of Sco XR-1. Figure 9, microphotometer tracings of Sco XR-1, indicate the presence of faint Balmer emission lines, intense He II lines (λ4686) and the complex of high excitation lines due to CIII, NIII and OIII, superimposed on a flat strong continuum. Surprisingly no absorption lines except the interstellar CaII (K line) were seen. Hiltner (1967) has not noticed appreciable polarisation in the visible spectrum.

Neugebauer et al. (1969) conducted the photoelectric scanner observations in the 3315 to 10830 $\overset{o}{A}$ range and simultaneously monitored the infrared flux at 1.6 μ and 2.2 μ. The average infrared flux was observed to be 10^{-23} ergs cm^{-2} sec^{-1} Hz^{-1} and seems to drop fast with increasing wavelength. Andrew & Purton (1968) observed radio emission from Sco XR-1 at 4.6 cm. Interferometric observations (Wade & Hjellming 1971) of Sco XR-1 at 11.5 and 2 cms showed three major components on an approximately straight line as shown in figure 7b with the central component coincident with Sco XR-1. These measurements showed quiet time flux at 0.01 flux units and at higher wavelengths only upper limits were provided by Apparao (1971) at 334 MHz. Thus in the infrared and radio regions the flux falls of rapidly.

Sco XR-1 is essentially an X-ray star as its X-ray emission is many magnitudes higher than the quiet sun and its emissions through visible and radio radiation is much smaller.
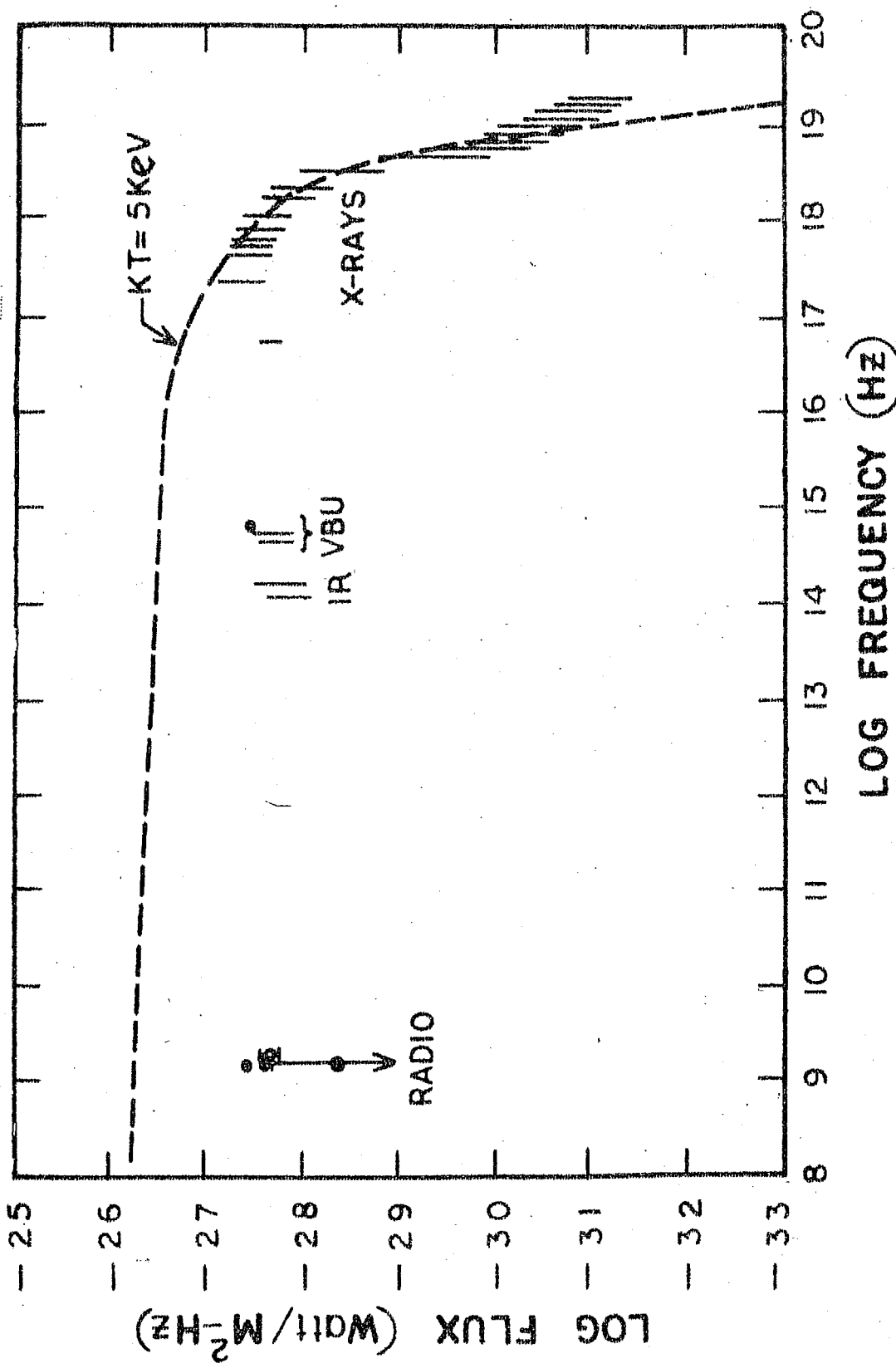
Fig. 10.— Observed energy distribution of Sco XR-1 from the X-ray range to radio range. The energy distribution of thermal radiation by a thin hot plasma at 5 KeV is indicated.

The typical average flux of Sco XR-1 in the various electro-magnetic radiation bands is presented in figure 10.

1.52 Time Variations in Flux and Spectrum

The experimental investigations on Sco XR-1 throughout the electromagnetic spectrum established time variations both in intensity and spectral character. Extensive photometric obser-vations have been conducted on Sco XR-1 for many days and showed variations in V and B in the range of 12.2 to 13.4 app. magnitude (Mook 1967; Hiltner & Mook 1967 a, b; Stiepen 1968; and Westphal et al. 1968). The character of light (figure 11) can be described as (a) continuous flickering that is a rather high frequency variation of a few hundredths of a magnitude and a time scale of minutes, (b) flares of about 0.2 mag. lasting for 10 to 20 minutes with remarkably steep rise and decay and (c) slower variations of characteristic time of some hours and more than half a magnitude amplitude. The spectral features show large intensity variations of hydrogen emission lines from night to night. As all these optical features are associated with old novae optical tests for periods in the range of seconds to many hours have been made. Hiltner & Mook (1967b), reported no clear period upto 1 hour. From power spectral analysis Rao et al. (1968) found periods varying around 3 hrs. Ephmeral effects have been suspected at 0.5276 days (Van Genderen 1969; Oda 1968). Persistent post-flare oscillations with 4 minute period were analysed and attributed to accoustic oscillations in the plasma by
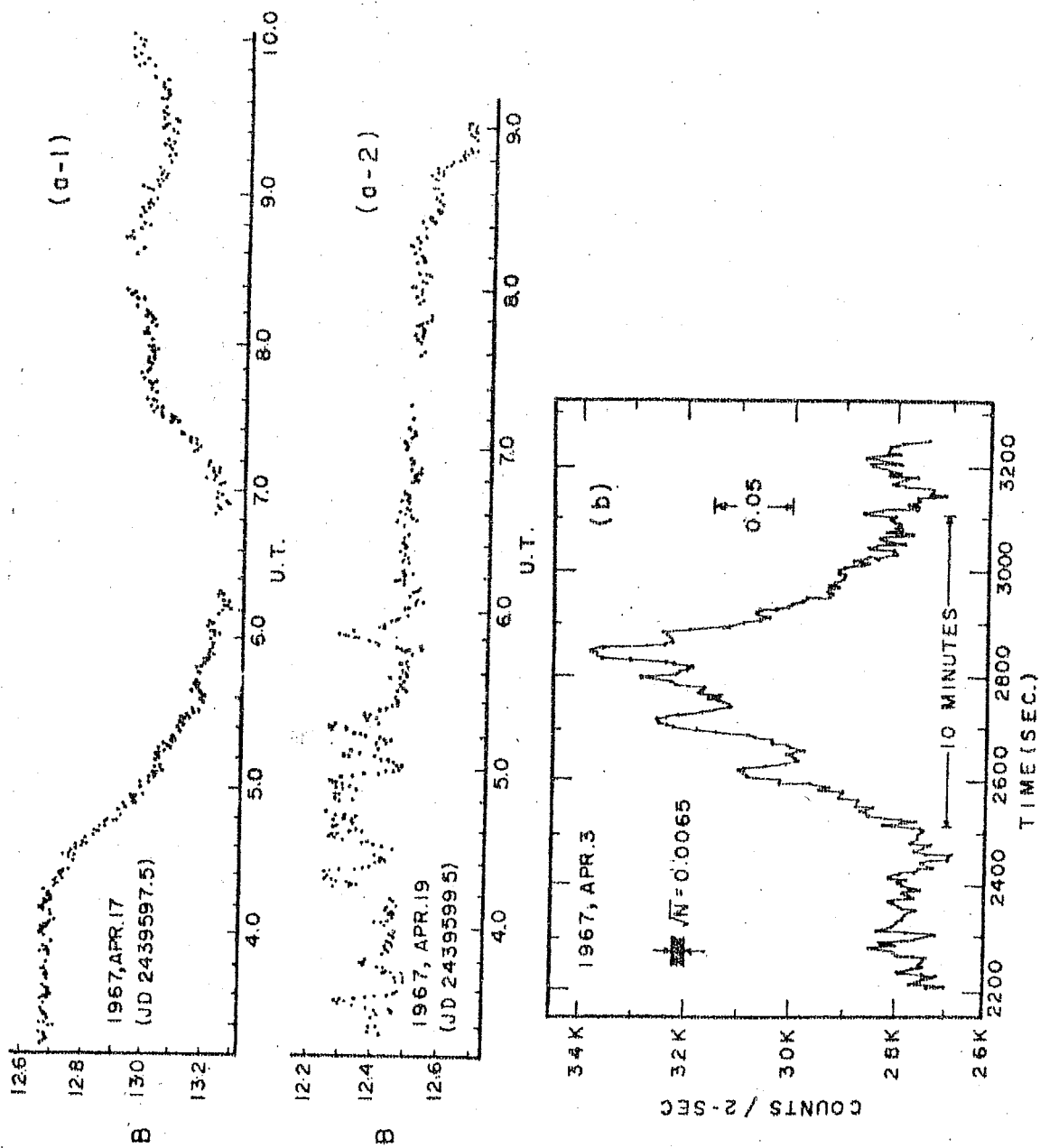
Fig. 11 – Typical examples of the light curve of Sco XR-1.
(a) Hiltner & Mook (1967), (b) Westphal et al. (1968).

Feldman et al. (1970).

Results of the various X-ray experiments to determine
Sco XR-1 flux showed different X-ray luminosities and spectra
on different occasions. The effective temperature corresponding
to thermal bremsstrahlung emission from thin plasma in the
2-20 KeV X-ray range varied between 5×10^7 and 10^8K and seems
to decrease with increase in flux (Kitamura et al. 1971).
Rao et al. (1969) from a compilation felt the flux has a long
term variation. The existence of gradual time variations,
flares and flickers in this region (2-10 KeV) were established
by Vela Satellite detector (Evans et al. 1970) as shown in
figure 12. Flares lasting for tens of minutes were observed in
balloon flights (Lewin et al. 1970; and Agrawal et al. 1970).
The results of Hudson et al. (1970), Lewin et al. (1970) and
Matsuoka et al. (1972) did not find any change in the charact-
eristic temperature at flare time in the 20-40 KeV range, in
contradiction to Lewin et al. (1968) who reported a steepening
of the spectrum and Agrawal et al. (1970) a hardening of the
spectrum. In the higher energy range above 40 KeV the flux and
spectrum obtained by various workers (Agrawal et al. 1972;
Matsuoka et al. 1972; Jain et al. 1972; Webber et al. 1971; etc.)
show anamalous time variations and is discussed in chapter IV
in greater detail.

The intensity and spectrum in the infrared region showed
highly irregular variations with one order of magnitude change
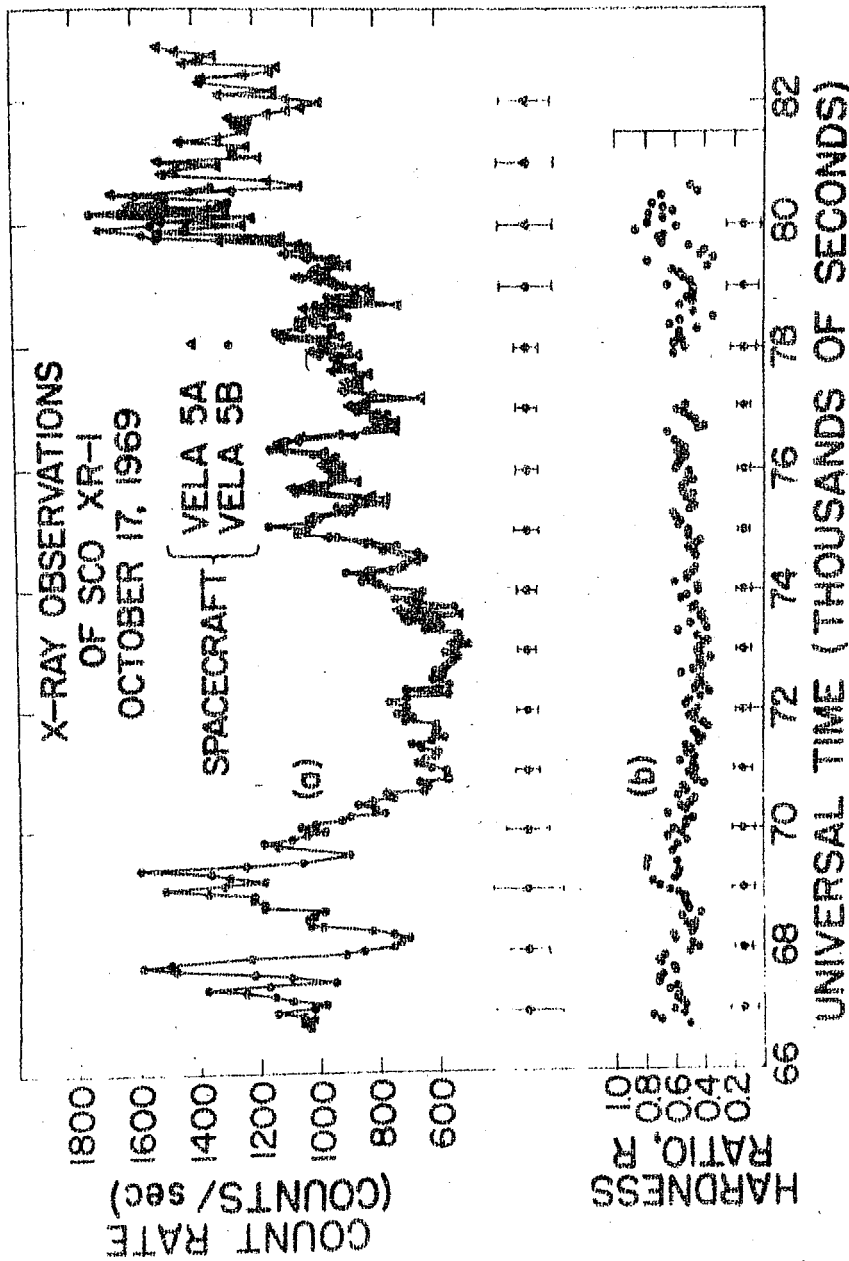
Fig. 12 – X-ray observation of Sco XR-1 by Vela Satellite in the 3-12 KeV range. The hardness ratio defines the count rate in 6-12 KeV range vs. 3-6 KeV.

in flux.   Ables (1969) first reported flux variations in
Radio Sco XR-1 at 4.6 cms with periods of an hour.   The exten-
sive study by Hjellming & Wade (1971) confirmed this hourly
variation and in addition observed flickers and flares .at
2695 MHz and 8085 MHz.   The detailed picture showed that Radio
Sco (1) has a major flare in progress about ·15% of time (2) is
in dormant or steady state for about 20% of the time and (3) is
relatively weak and continuously erratic during the remaining
time.   The detailed radio spectral study has not been done
although the existing information shows irregular variation of
the power index varying between 0.5 to 1.0.

If the emission of optical, X-ray and other electromagnet-
ic radiation can all be attributed to a single mechanism such
as bremsstrahlung, one expects correlated intensity changes.
Because of the highly irregular variations, simultaneous monit-
oring in different wavelength regions may help in understanding
the source mechanisms and physical conditions.   Number of
simultaneous optical and X-ray observations have been made to
date; (a) by LRL group (Chodil et al. 1968; Mark et al. 1969;
and Grader et al. 1970),(b) by a collaborative group of PRL
and ISAS (Kitamura et al. 1971),(c) by the group of UCSD
(Hudson et al. 1970; and Peterson 1970), (d) by Garmire et al.
(1971),(e) by Evans et al. (1970) and (f) by TIFR-ISAS groups
(Matsuoka et al. 1972).

The observations in the 2-20 KeV range by LRL group
(Mark et al. 1969), Garmire et al. (1971) and Kitamura et al.

(1971), as well as the observations of Pelling et al. (1969)
and Matsuoka et al. (1972) in the 20-40 KeV range indicate a
definite trend in the increase of X-ray intensity with the
increase in optical brightness. The existence of definite
correlation in intensities were noted during flare time by
Hudson et al. (1970), Evans et al. (1971) and Matsuoka et al.
(1972) in the 2-100 KeV region. Some correlated short term
oscillations with a 20 sec period for about 2 mts have been
detected by Kestenbaum et al. (1971). In general, in the
2-20 KeV range during quiet time, there seems to be a definite
correlation between the optical intensity and the characterist-
ic temperature of the plasma derived from the X-ray spectrum.
However, during flares and in the 20-100 KeV range no clear
relationship between the source spectral character and inten-
sity has yet emerged.

. . . . .

CHAPTER II

ROCKET BORNE X-RAY EXPERIMENTS

Two identical X-ray astronomy experiments were flown on Nike-Apache rockets from Thumba, South India: N.A.40.04 at 1700 U.T. on April 26 and N.A.40.05 at 1704 U.T. on April 28 in 1969. These along with the experiments from Kagoshima Space Centre (Japan), on K-9M-27 and S-210 rockets on 6 and 7 August, 1969 respectively were conducted under joint collaboration between the group at the Physical Research Laboratory, Ahmedabad (India) and Prof. Minoru Oda's group at the Institute of Space and Aeronautical Science, Tokyo (Japan).

The prime purpose of these four rocket flights, was to measure the X-ray flux and spectrum in the 2-20 KeV range from Scorpious XR-1 source simultaneously along with the optical luminosity of the same source from Tokyo Astrophysical Observatory, Tokyo (Japan). In addition the author has taken very active part in many rocket-borne low energy X-ray experiments (Table I), aimed at the spectral study of some discrete X-ray sources and diffuse X-ray background radiation.

This chapter describes in detail the basic experimental set-up employed for the detection of 2-20 KeV X-rays in these rocket flights and also the analytical methods employed to understand the nature of the source. Table I lists all the rocket flights and the balloon flights carrying X-ray payloads in which the author participated. For the purposes of this thesis, however, we have only considered the results obtained

TABLE I

	Launch		Date	Time (UT)	Altitude (max.)	Telescope Area (cm²)	Collimation (FWHM)	Objects
	Vehicle	Place						
1.	Centaure	TERLS	Nov. 3, 68	0319	135 Km	61	9°x17°	Sco XR-1, Cen XR-2
2.	Nike Apache	"	Nov. 7, 68	0305	140 "	61	9°x17°	Sco XR-1, Cen XR-2 & Tau XR-1
3.	"	"	April 26, 69	1700	145 "	110	10.5x35°	Sco XR-1
4.	"	"	April 28, 69	1704	150 "	110	10.5x35°	Sco XR-1
5.	K-9M-27	KSC	Aug. 7, 69	1215	350 *	76	7°x34°	Sco XR-1, Cen XR-4
6.	S-210-2	"	Aug. 8, 69	1220	140 "	76	7°x34°	Sco XR-1, Cen XR-4
7.	Centaure	TERLS	Dec. 7, 69	0035	125 "	60	7°x15°	Nor XR-2, Cen XR-4 and diffuse back-ground
8.	3m.c.ft. Balloon	HYDERABAD	Nov.18, 70	0112	4.7 mb	95	14°	Sco XR-1
9.	"	"	Nov.15, 71	0138	5.6 "	95	11.6°	Sco XR-1
10.	"	"	March 29, 72	0116	5.6 "	76	19°	Cyg XR-1
11.	"	"	Dec. 28, '72	0155	4.9 "	81	13.5°	Her XR-1
12.	"	"	Jan. 18, '73	0216	4.7 "	81	13.5°	Her XR-1, Cyg XR-1

from a few of these flights. This chapter, therefore, contains only a detailed description of the experimental set up employed only in these flights. However, the details of the experiment- al set up and the results obtained in the rest of the rocket flights are appended at the end of the thesis for the sake of completeness.

2.1 Description of the Experiment

The Nike-Apache rocket used in the experiments described here is a solid fuelled, spin stabilised vehicle which gave on both the occasions, approximately 200 seconds of useful data. The payload was mounted inside the nose-cone of the vehicle. A photograph of the X-ray telescope along with the associated electronics is shown in Figure 13. X-rays were detected by a pair of proportional counters, mounted back to back, so that the two counters looked in the opposite directions in azimuth, thus each counter acting as a veto counter to the other to reduce the charged particle background. Copper etched Colli- mators of rectangular geometry defined the field of view to $65^{\circ} \times 21^{\circ}$, with the long axis parallel to the spin axis of the rocket. Two radioactive sources were attached to the inside surface of the nose-cone in the field of view of the counters for inflight calibration. A timer controlled pyrotechnic device was employed to axially eject the nose cone at about 60 Kms., after which the proportional counters were exposed to the celestial sky. The combined precession and spin motion
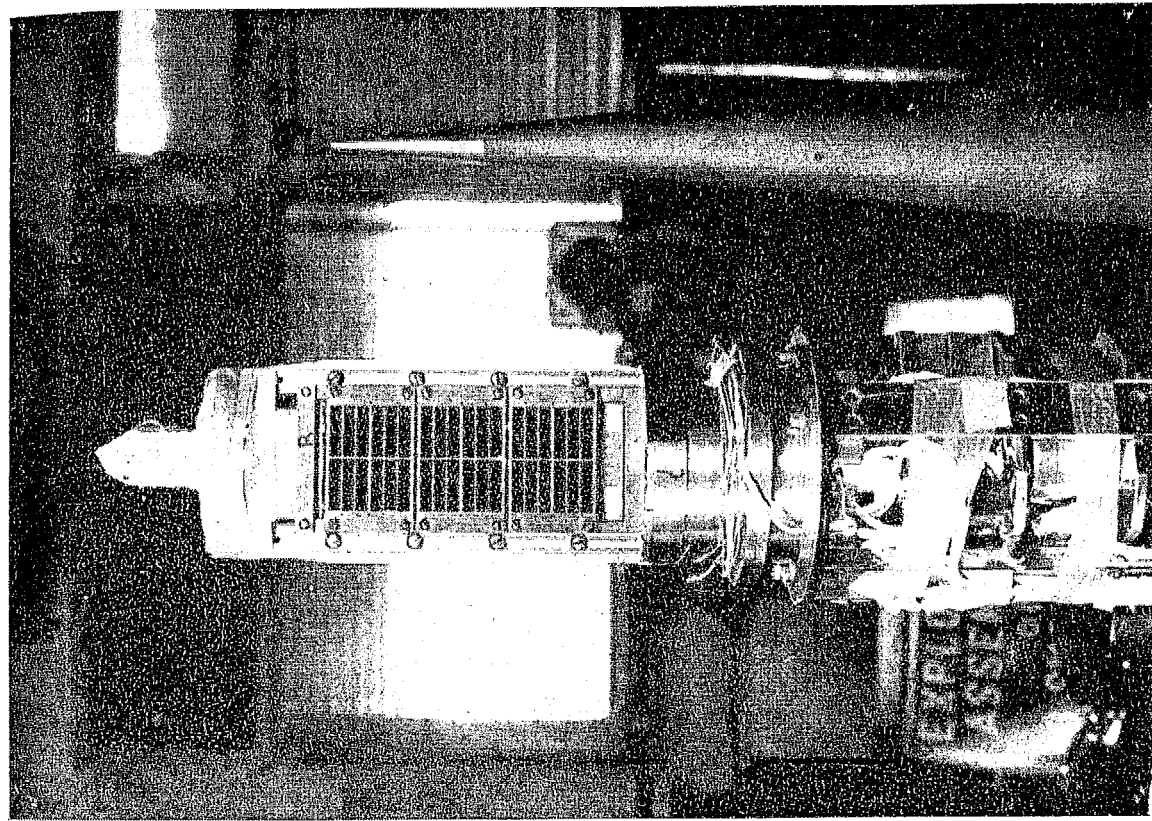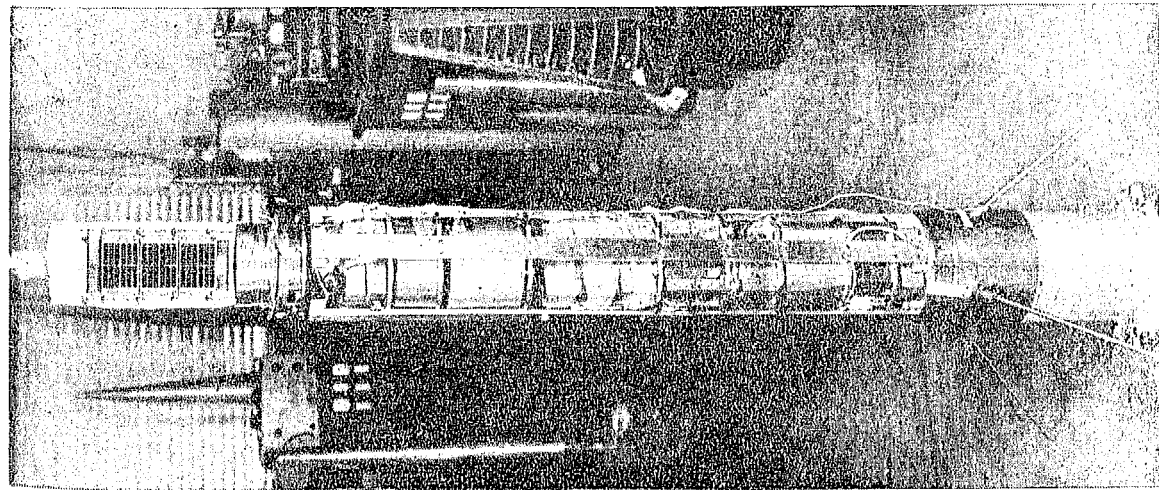
Figure 13 : Photographs of the complete assembly of the payload and X-ray telescope on N.A.40.05

of the rocket allowed a band of the sky along the horizon to be viewed by the counters.

A block diagram of the payload is shown in Figure 14. The output from each X-ray detector was pulse height analysed by a five channel pulse height analyser into five contiguous energy channels corresponding to 2-3.5, 3.5-5.0, 5.0-8.0, 8-14, and 14-20 KeV. The look direction of the counter was determined by two crossed flux gate magnetometers, one mounted perpendicular to the spin axis of the vehicle, perfectly aligned with the counter normal direction and another along a direction parallel to the spin axis of the vehicle. The pulse height analyser information and the aspect information were continuously telemetered to the ground, in real time, using standard IRIG FM/FM telemetry system.

The main bus power systems for the experiment of 16 ± 2 volts and -16 ± 2 volts were supplied by Silver-Zinc batteries in the rocket battery pack, from which +12 and -12 volts regulated power was derived using power regulators. The total input current for the system, excluding the telemetry transmitter and timer was, 500 mA at +15V and 300 mA at -15V.

2.11 Proportional Counters

The output pulse from a proportional counter is proportional to the energy deposited in the counter gas. This together with the internal amplification of about 1000, and a high efficiency, makes the proportional counter an ideal
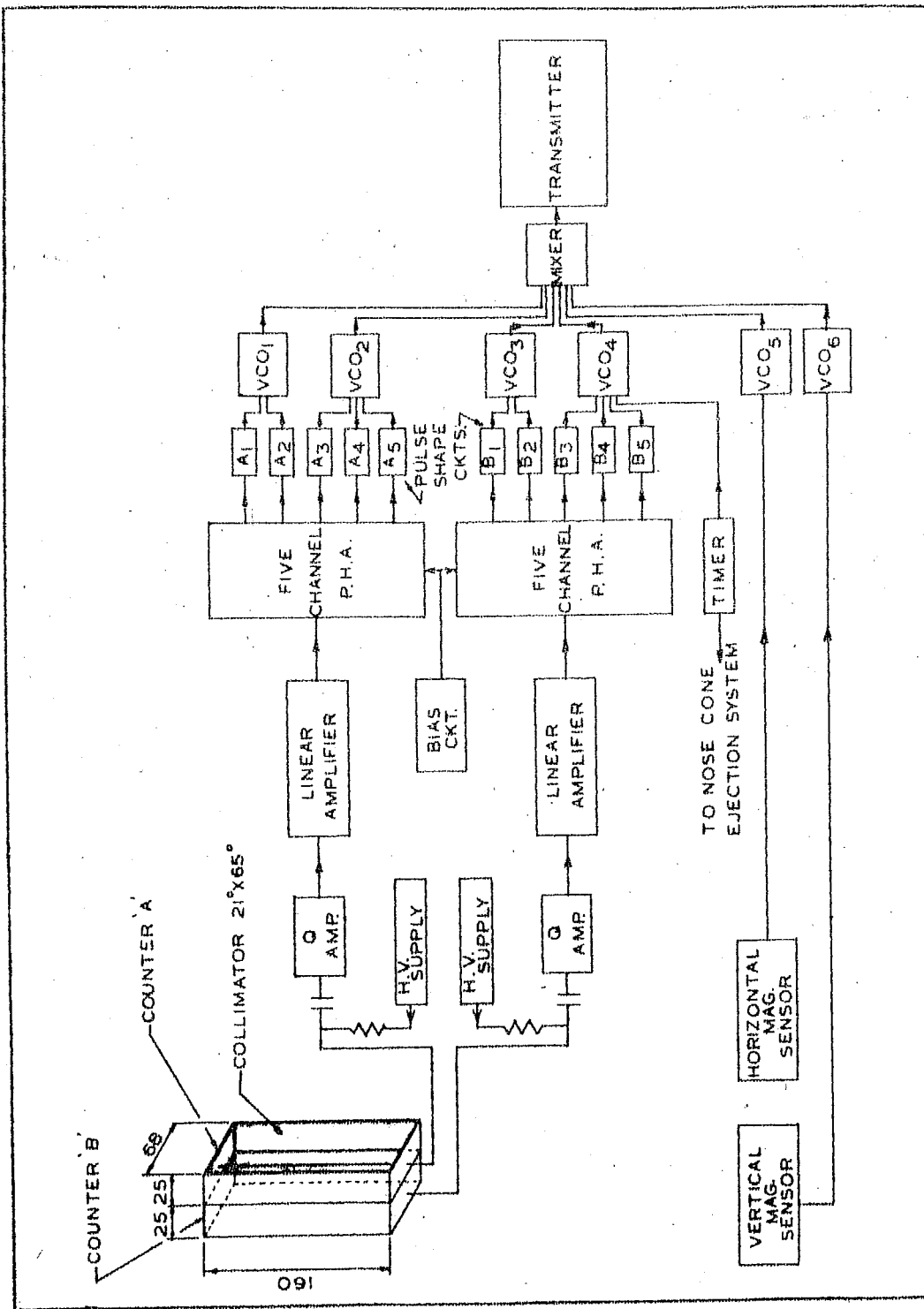
Fig. 14 - Block diagram of the X-ray astronomy rocket payload.

detector of X-rays in the 2-20 KeV energy range.

Basically an X-ray is absorbed in the counter gas and produces a number of ion pairs proportional to the energy deposited in the counter (for Xenon the mean energy per ion pair is 22 eV). The rectangular gas container acts as a cathode and a thin Tungsten wire along the axis of the counter acts as the anode. The electrons produced due to ionisation caused by the passing of an X-ray through the counter are attracted towards the anode; as they get close to the wire they gain sufficient energy in one mean free path to cause secondary ionisation because of high intense electric field close to the wire. In this way an avalanche of electrons is built-up and the amplification factor is independent of the initial number of electrons or where they formed, provided the counter is properly designed. A full discussion of proportional counters, and their mode of operation is given by Rossi & Staub (1949), Curran & Wilson (1965) and Charles & Cooke (1968).

The proportional counters used in these experiments were filled with Xenon-Methane gas mixture (90 - 10% by volume) at one atmospheric pressure. The entrance windows were beryllium foils of average thickness 115 microns (18.5 mg/cm^2). The effective window area of each detector was 96 sq.cm., determined after taking into account the occultation caused by struts and collimator. The aluminium body of the counter produces flourescent X-rays of 1.5 KeV, well below the lower channel at 2 KeV.

However, the copper etched collimator of 1.5 cm.height contaminates the count rate slightly as its K-escape peak lies around 8 KeV.

Xenon has been used as the counter gas because of its higher cross-section for the absorption of X-rays and causes a higher energy loss by charged particles than any other gas. Minimum ionising charged particles will deposit about 18 KeV per inch (Barkas & Berger 1964); more than 75% of the charged particles incident from random directions would be rejected in the 1 inch thick counter. The proportion will increase at lower energies as the energy loss increases. The addition of 10% Methane acts as the quenching gas to prevent continuous avalanche production due to the ultraviolet photon bombardment of the counter walls.

The counters were operated at 2100 volts, which was very well regulated using a corona tube. The current pulse from the proportional counter causes a voltage drop across the load resistor and the resulting voltage pulse was fed to the amplifier through a coupling capacitor and short coaxial cable.

The actual pulse height corresponding to a monoenergetic X-ray shows a wide spread distribution due to the statistical processes involved in the absorption of photon and multiplication process, the spread increasing as the photon energy decreases. The spectral resolution of a counter is traditionally defined in terms of the full width at half maximum (FWHM) of the distribution of pulses, produced by a monoenergetic
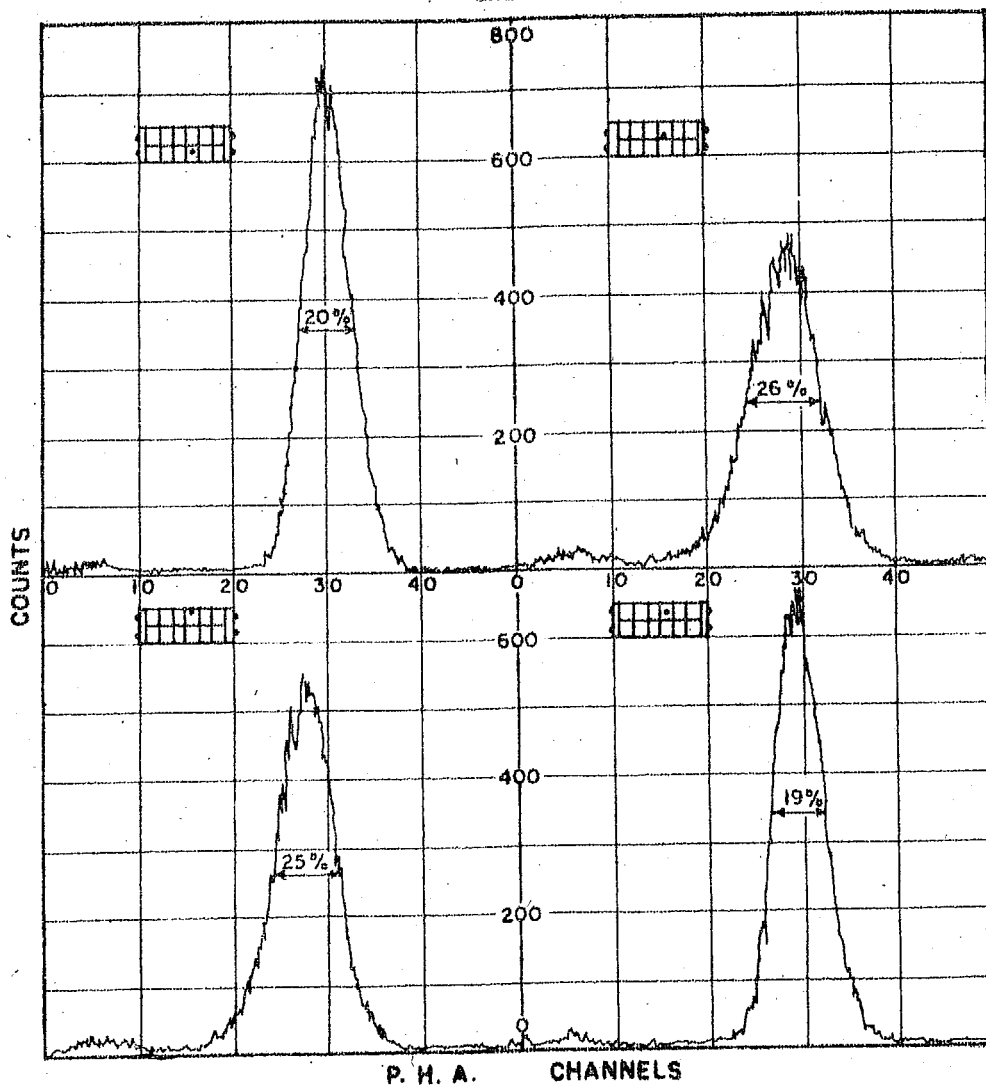
Fig. 15- Pulse height distribution due to Fe^{55} in a two-sectional proportional counter.
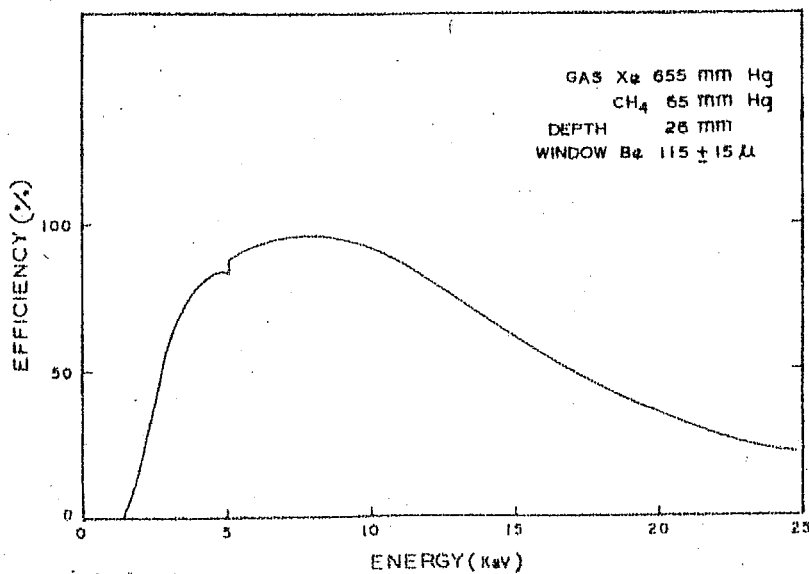
Fig. 16 - Theoretical efficiency of the proportional counter.

height. Figure 15 shows the typical pulse height distribution curves of the two sectional counter used in the present investigation obtained using 5.98 KeV X-ray line from Fe^{55} radio active source. The FWHM for the counters used in the present experiment was typically found to be about 19-25% at 6.0 KeV (Fe^{55}) and 14-18% at 22 KeV (Cd^{109}).

The efficiency of the counter i.e. the probability of detecting a photon of a given energy that is incident on the counter window is given by the product of two factors, the probability of transmission of the photon through the window and the probability of absorption in the gas, i.e.

$$(E) = \exp(-\mu_w \, \rho_w \, X_w) \left[1 - \exp(\mu_g \, \rho_g \, X_g) \right] \quad \ldots \ 2.1$$

where μ is the mass absorption coefficient in gm/cm^2, ρ is the density, X is the thickness, and the subscripts w and g refer to the window material and the counter gas. The calculated efficiency using mass absorption coefficient tables (Victoreen 1949) is shown in figure 16. The decrease of efficiency at low energies is due to the absorption in window while the deterioration at higher energies is caused by lack of opacity of Xenon. The escape peak effects due to K and L edges of Xenon are negligible.

2.12 Pulse Processing Circuitary

The positive pulse output from the preamplifier attached to each counter, with about 1 microsecond rise time and 6 microseconds width was fed to a chain of three negative feed back amplifiers. The gains were properly adjusted to give an output of about 1.1 volts at the output of second stage and final output of about 5 volts for 6 KeV X-rays of Fe^{55}.

The schematic of the five channel pulse height analyser using six discriminators, coincidence gates and univibrators is shown in figure 17. The amplifier signals were fed to the
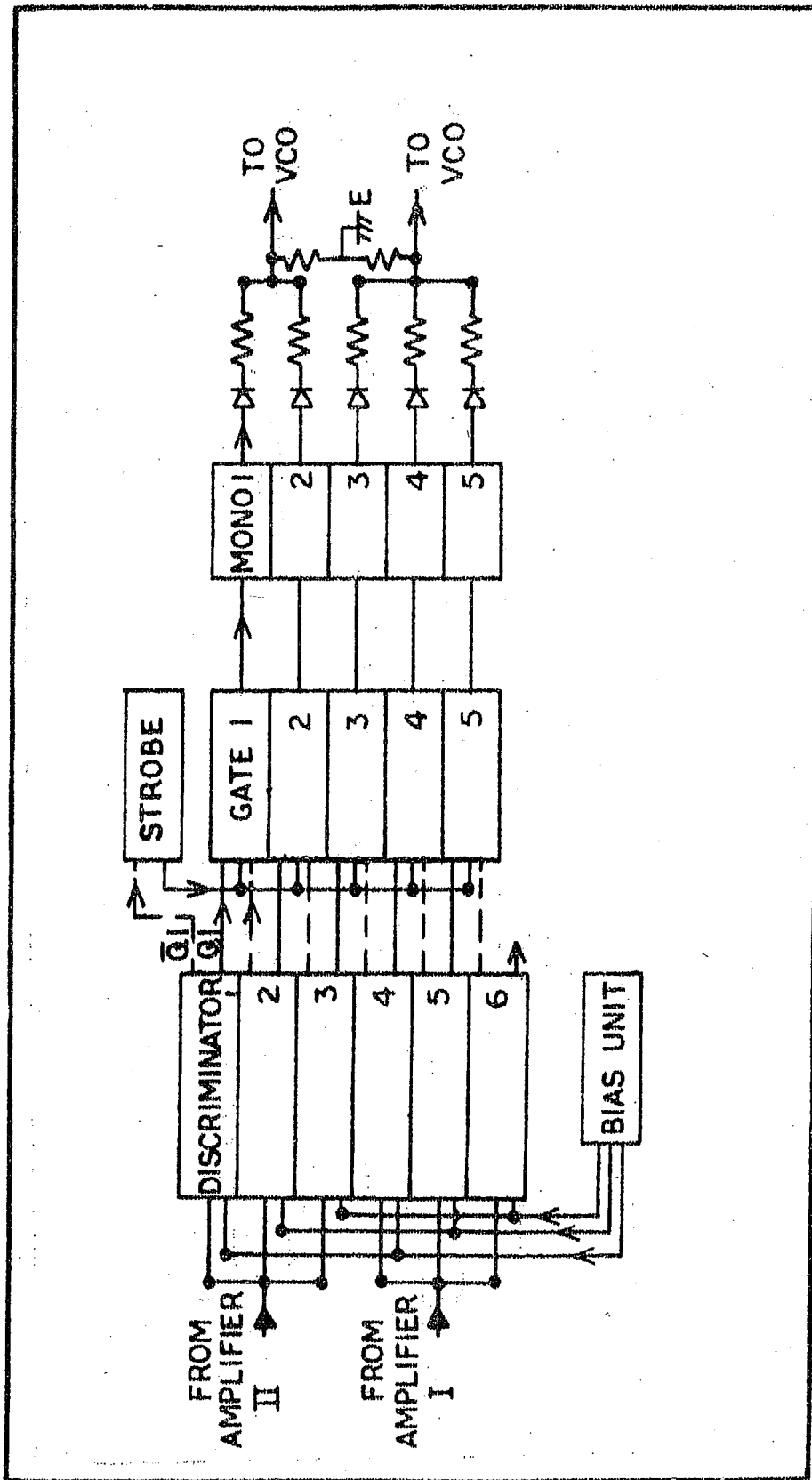
Fig. 17 — Schematic of the five channel pulse height analyser

discriminators whose thresholds were adjusted through appropriate D.C. bias. Each discriminator generated two pulses, Q, a positive pulse (0.5 - 8 volts) and $\overline{Q}$, a negative pulse (8 - 0.5 volts). These signals were fed to the coincidence gates along with a delayed strobe pulse (S) which was generated from the first discriminator so as to avoid false coincidence due to electronic delays. The input for the gates and the description of the output pulses are shown below.

Gate	Inputs	Energy channels
G1	SQ2 $\overline{Q}$1	Ch 1
G2	SQ3 $\overline{Q}$2	Ch 2
G3	SQ4 $\overline{Q}$3	Ch 3
G4	SQ5 $\overline{Q}$4	Ch 4
G5	SQ6 $\overline{Q}$5	Ch 5

The pulses from the two lowest energy channels were shaped to different heights and widths in the corresponding univibrator and fed to a voltage controlled oscillator. Similarly the remaining three energy channels modulated another voltage controlled oscillator.

2.13 Telemetry

The six signals, consisting of two analog aspect informations, four encoded pulse height information - two for each detection system; were fed to six voltage controlled oscillators. Standard IRIG FM/FM telemetry subcarrier frequencies, for which the ground receiving system was compatible, were used.

All these units were operated on an independent power regulator. The outputs of the VCO'S with suitable tapering were mixed in a mixer amplifier. The output of the mixer amplifier was fed to a Bendix type FM transmitter. Checks for the R.F. interference from the transmitter and power supply pickups were made by monitoring counter signals, and necessary shielding precautions, under worst case simulation, were performed.

2.14 Construction and Environmental Testing

The payload was arranged in the Nike-Apache rocket in a number of decks of about six inches in diameter, in the cylindrical portion of the nose cone as shown in figure 13. All the electronic modules were given a conformal coating of epoxy resin (Araldite) and then potted with Eccofoam FPH (Dow Corning Company) to stand the rigors of shock, vibration and temperature. Monitoring leads for signals and D.C. Voltage from all modules were broughtout on terminal strips and were coated with silicone rubber (RTV731) before final closure of cylinder prior to the launch. All the connections to the battery and telemetry sections were given through a 5 pin Cannon Connector. The entire payload was controlled and monitored through a 27 pin umblical connector. Sub-assemblies as well as the entire payload was vibrated to the specified level and were also tested for temperature and vacuum effects.

2.15 Launch and Recording

The purpose of the experiment being to conduct simultaneous observation of Sco XR-1 in optical and X-ray bands, the

flights were to be conducted during night time. The launch time was selected so that the source Sco XR-1 is above the Thumba horizon and have the maximum possible elevation at Tokyo (Japan) from where optical observations were conducted.

The payload was monitored through an umblical cable and by a check out system installed in a block house about 300 ft away from the launch pad. The telemetry signals during the flight were recorded simultaneously on a magnetic tape recorder and/slow run (10 inches per second) paper recorder, along with 0, 2.5 and 5 volt signals corresponding to the VCO'S 7.5% deviations. Time signals of standard NASA 100 p.p.s. time code from a time code generator, synchronised to UT have been recorded. A portion of the paper recording obtained during the Nike Apache 40.04 flight is shown in figure 18. Subsequently, paper records at a speed of 60 inches per second for the flights were made for the analysis.

2.2 Rocket Attitude Analysis

The motion of a rocket in the force-free environment above the atmosphere is well known problem in the dynamics of rigid bodies. The longitudinal axis of the rocket is an axis of symmetry. The moments of inertia about the two lateral axis are equal and much larger than the moment of inertia about the longitudinal axis. It can be shown that the motion of such a body consists of a spin about the longitudinal axis and the precession of this axis about a cone; with both the spin and

- 63 -
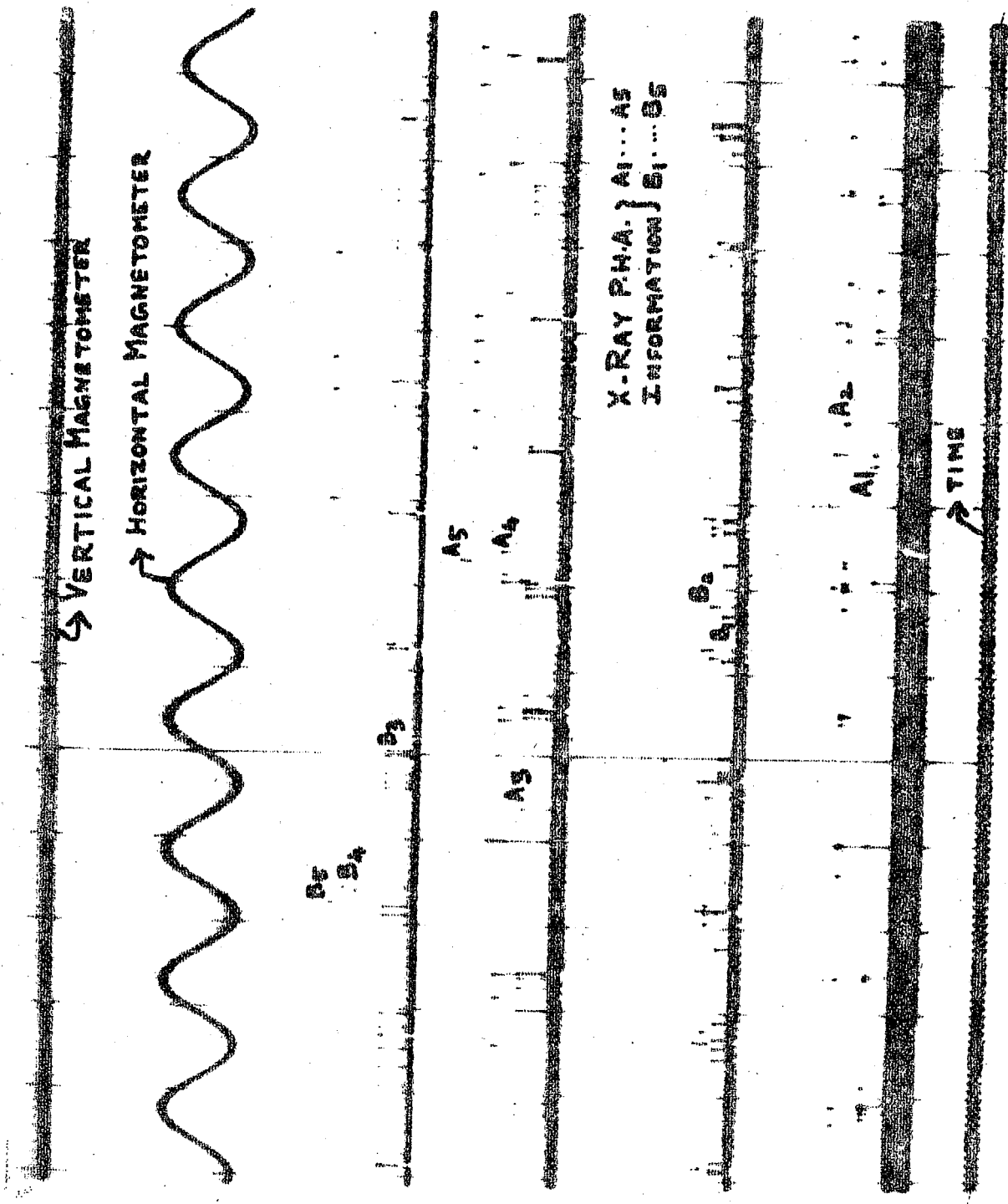
Fig. 18 - Sample data chart record of N.A.40.04 flight.

precession in the same sense (Goldstein 1960).

2.21 Determination of the Attitude Parameters

Information about the vehicle attitude parameters, the spin and precession rates, the half cone apex angle and the precession axis point in the celestial sky can be derived from applying the laws of rocket dynamics, to the data derived from vehicle radar tracking and from magnetic and other aspect sensors.

In the course of initial thrust, the two stage solid fuel rockets are spun to several revolutions per second for stabilisation of the flight. In the two Nike-Apache flights, N.A.40.04 and N.A.40.05 the spin rates were about 8.5 and 9 RPS respectively. If the rockets are not purposely despun, (or no devices exit out of the total system) the rocket will maintain approximately this spin frequency until it reenters the atmosphere where it starts tumbling. The axial ejection of the nose cone, in flight N.A.40.04 caused precession and the spin rate settled to 6.5 RPS after the initial perturbation. However, the N.A.40.05 rocket essentially maintained the initial spin rate with slight noticeable precession.

The half-apex angle of the precession cone, (or half cone angle $\wp$) in a rigid body motion is related to the precession and spin frequencies (ω_p and ω_s) by the formula

$$\text{Cos } \wp = \frac{\omega_s}{\omega_p} \cdot \frac{I_1}{I_2 - I_1} \qquad \qquad .. \; 2.2$$

where I_1 and I_2 are moments of inertia relative to the spin axis and a direction perpendicular to it. At high spin frequencies, the half apex angle of precession cone is small and as the spin frequency decreases, the precession cone increases. Table 2 gives the moments of inertia, calculated theoretically from the known parameters for the two flights. The parameters clearly show no precession at all till the opening of the nose cone.

TABLE II

Moments of Inertia

	N.A.40.04	N.A.40.05
I_1 (Slugs.sq.ft.)	0.4742	0.4729
I_2 "	181.14	180.98

The conservation of total angular momentum requires, $(\omega_s + \omega_p)$ to remain constant. Since, however, the rocket may not exactly behave like a rigid body, slight changes in ω_s, ω_p and β with time during the observation period do occur. The variation of $(\omega_s + \omega_p)$ with time 't' can be fitted to an equation of the type

$$\omega_s + \omega_p = \omega_o + At + Bt^2 \qquad \dots 2.3$$

where ω_o, A and B are constants. Normally it is sufficiently accurate to take the first order term into consideration. These constants are derived from magnetometer data.

Initially, the behaviour of the angle between the instantaneous position of the spin axis and a fixed direction in space is investigated. In the sketh, OM is a fixed direction, OP is the axis of the precession cone about which the spin axis OS moves. The angle $P\widehat{O}S$ is the half cone angle of precession (ς) and is a constant. Since OP and OM remain fixed in space, the angle $P\widehat{O}M$ is also a constant. The angle $S\widehat{P}M$ increases during the flight and can be expressed as

$$\phi = \omega_p t + \text{Constant} \qquad \ldots 2.4$$

Hence by spherical geometry

$$\cos S\widehat{O}M = \cos \varsigma \cdot \cos P\widehat{O}M + \sin \varsigma \cdot \sin P\widehat{O}M \cdot \cos \phi$$

$$= A + B \cos (\omega_p t + C) \qquad \ldots 2.5$$

where A and B are constants. For positions of S on either side of precession axis, P, A and B can be determined; then

$$\varsigma + P\widehat{O}M = \text{arc } \cos (A - B)$$
$$\varsigma - P\widehat{O}M = \text{arc } \cos (A + B) \qquad \ldots 2.6$$

and values can be determined for ς and $P\widehat{O}M$ although it is not possible to say immediately which is which. The above formulae can be applied directly, for the determination of half cone angle ς and precession axis, from the magnetic and X-ray or optical sensors information.
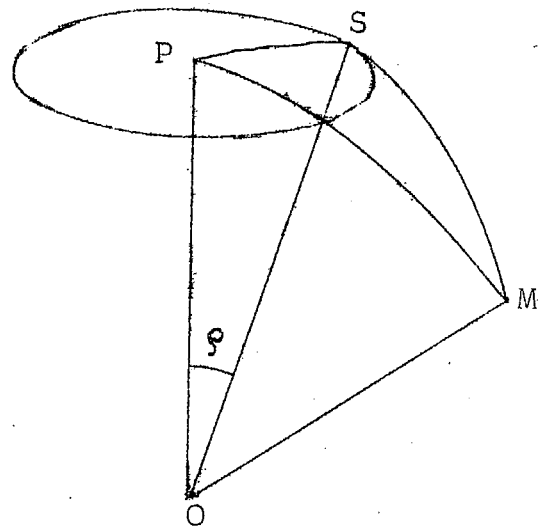
The sample chart record of the data shown in figure 18 is insufficient to show the modulation of the amplitude during one complete precession cycle. The magnetic sensor mounted parallel to the spin axis (vertical magnetometer) produces a sinusoidal output of the form M Cos $\widehat{SOM}$ with respect to the local total magnetic vector M and will give the precession time information. The horizontal magnetic sensor whose output is also a sinusoid, registers a maximum amplitude equal to

$$M_H = M \ Sin \ \widehat{SOM}. \qquad \dots 2.7$$

The peak to peak output amplitude of this sensor recorded during a spin period, will go through a complete cycle of variation in one precession period, the amplitude of this cycle being larger for larger precession cone angles. The acquisition time difference, registered by the horizontal sensor when it crosses the north or south direction, in spins corresponding to the same phase of two successive precessions has been used to obtain ($\omega_s + \omega_p$). Successive precession phases and precessions are used to obtain the time variation of ($\omega_s + \omega_p$) for the duration of the flight. Figure 19 shows the variation of the vertical magnetometer output and the peak to peak amplitude of the horizontal sensor during the two flights. The sensitivity of the vertical sensor is deliberately increased because of the magnetic field vector at Thumba is essentially horizontal.
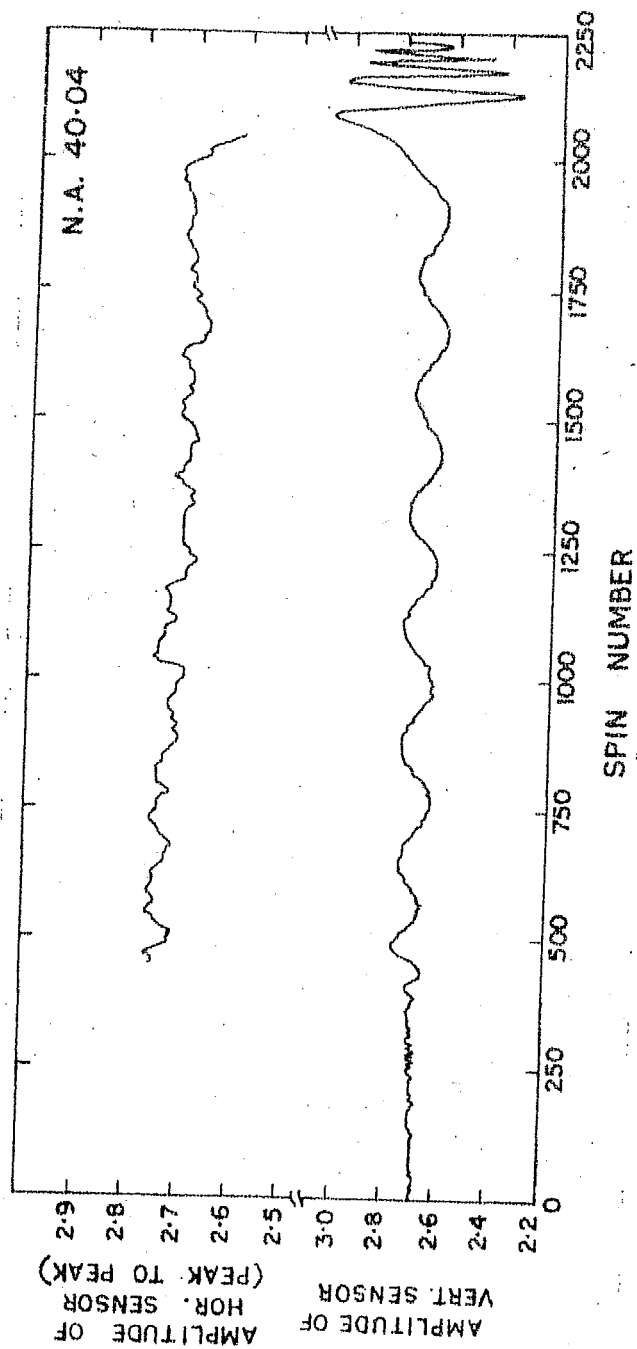
Fig. 19 — Magnetometer data plotted against spin number for N.A. 40.04.
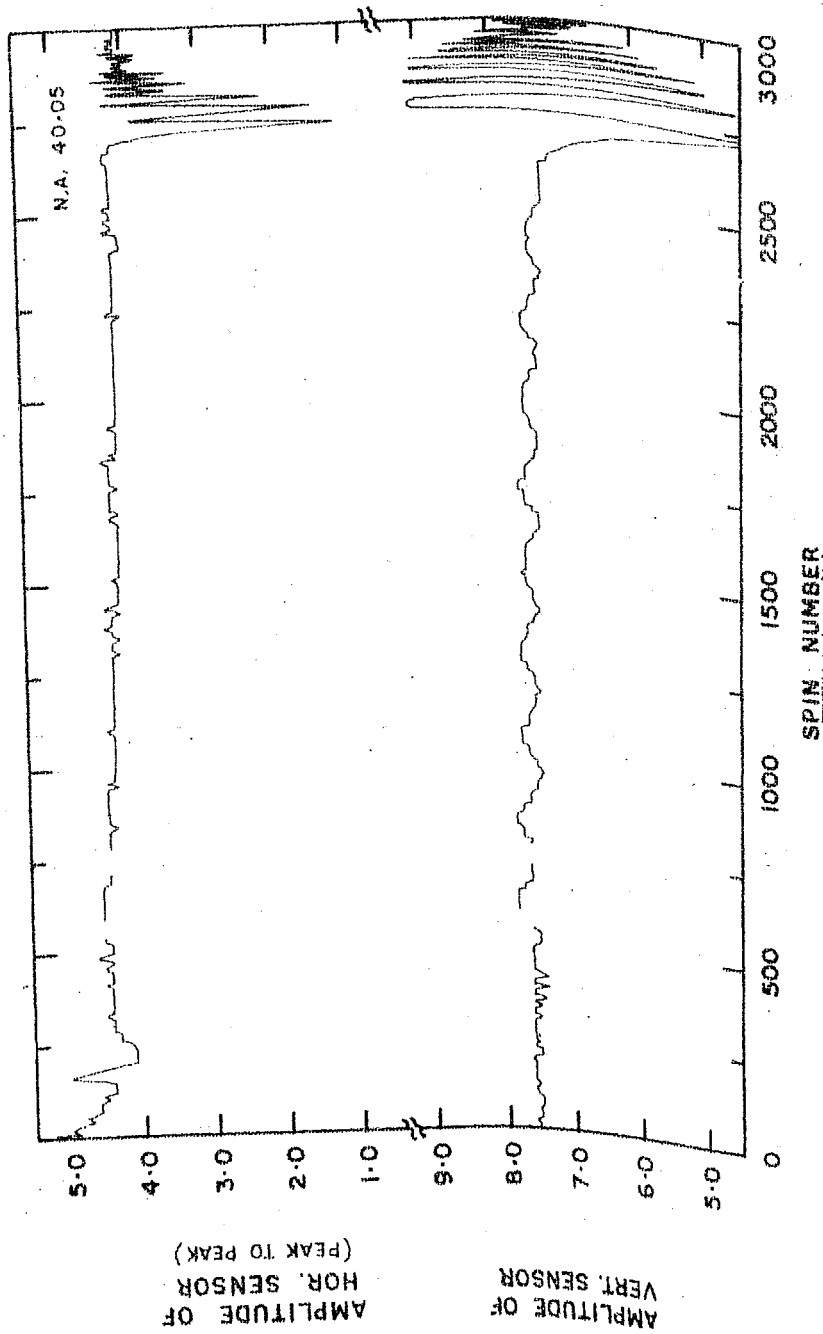
Fig. 19 — Magnetometer data plotted against spin number for N.A. 40.05.

The sensitivity measurements and zero level checks of the magnetometers performed on the ground are of limited value due to changes in the magnetic environment of the rocket which cannot be evaluated readily. These changes are due to (i) change in the permanent magnetism of the rocket which is equivalent to a zero shift and (ii) the induced magnetism of the rocket which is equivalent to a change in sensitivity. These changes commonly occur during the jettisioning of stages or due to the heating of the rocket body.

The correction for the changes in sensitivity was made by effectively calibrating the magnetometer in flight. The determination of the magnetic field M is made possible, from the peak to peak amplitude of the horizontal sensor at precession phase corresponding to SOM equal to 90° from the rocket re-entry time data. In addition, the response or sensitivity of the two magnetometers relative to each other is also checked. The magnetic field sensed in flight is to be corrected for the known ground value. If the simple dipole approximation is used the field strength can be expressed as

$$M = M_o \ (1 - 5,5 \times 10^{-4} \ h) \qquad \qquad \ldots \ 2.8$$

where M_o is the sea level intensity and h is the altitude in kilometers.

Hence from equation 2.7 and 2.8

$$\text{Sin} \ \widehat{\text{SOM}} = \frac{M_H}{M_o \ (1 - 5.5 \times 10^{-4} \ h)} \qquad \ldots \ 2.9$$

The angle $\widehat{XOM}$ during the whole precession can be evaluated from the peak to peak amplitude data of the horizontal sensor data or from the vertical magnetic sensor response. From the precession response of the vertical sensor and horizontal sensor the half cone angle and the angular distance of the magnetic field direction is estimated within the allowed accuracy. In the above estimates and calibration, the data of horizontal and vertical magnetic fields, declination and inclination for the particular day were obtained from the magnetic observatory at Trivandrum.

Although the magnetic information defines the position of the precession axis with respect to the geomagnetic field, this by itself is not adequate to define the position of this axis in space. Triangulation methods for determining the position of precession axis is achieved with known optical or X-ray objects. As no optical sensor was provided for, the well established position of the intense X-ray star Sco XR-1 was used for determining the attitude in absolute terms. The intensity modulation for the known triangular response of the collimator during a precession will be little, if the precession angle is small and the distance of the object from the collimator normal falls in the insensitive part of the response function.

Further refinement of the attitude parameters obtained from the above mentioned amplitude-precession phase method can be derived from the spin – precession phase response of

celestial stars and of magnetic field vector, as described in detail by Wada et al. (1969). Referring to figure 20 let the right ascension and declination of the precession axis, P, be α and δ and let an object A be at an angular distance χ from P and at a precession azimuth $\widehat{APS}$ (measured from AP) with the spin axis S progressing along the precession cone with radius β and a phase ϕ. Let the angular distance SA be denoted by θ and phase angle by ψ^1. Both ψ and θ change with the precession phase. Two new parameters ψ_D and ψ are defined as follows

$$\psi_D = \psi^1 + \phi + \pi/2$$
$$\psi = \psi^1 + \phi + \lambda \qquad \qquad \dots 2.10$$

where ψ_D is called the bearing angle (Giacconi et al. 1966) and ψ is called the spin phase (Wada et al. 1969). The precession phase starts when the spin axis is farthest from the North Pole (N.P) of the celestial sphere and the spin phase when the sensor passes through the North Pole at the starting position of the precession phase.

The precession – spin phase response diagram for an object at a distance χ from the precession axis shows the variation of ψ as a function of ϕ, with a parameter β for precession cone angle and will be described by:

$$\left.\begin{array}{l} \cos\theta = \cos\beta \cdot \cos\chi + \sin\beta \cdot \sin\chi \cdot \cos\phi \\[2mm] \sin\psi^1 = \dfrac{\sin\phi \cdot \sin\chi}{\sin\theta} \\[4mm] \text{and} \quad \cos\psi^1 = \dfrac{\cos\chi - \cos\beta \cdot \cos\theta}{\sin\beta \cdot \sin\theta} \end{array}\right\} \dots 2.11$$
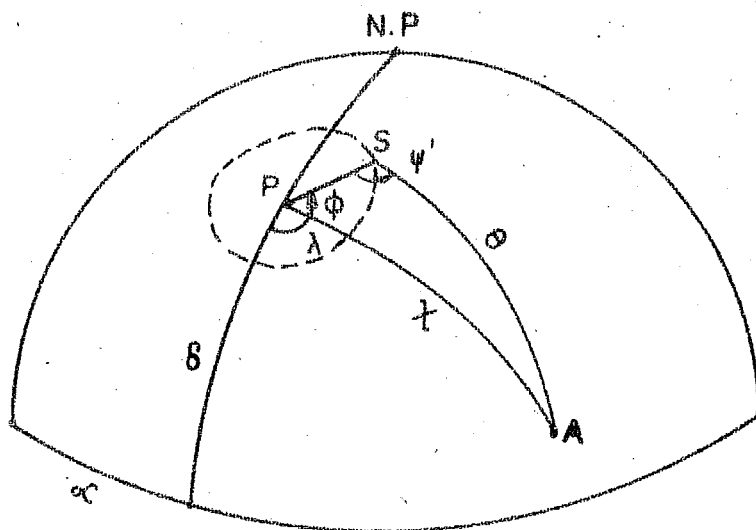
Fig. 20 – Schematic showing the motion of spin axis relative
to an object.
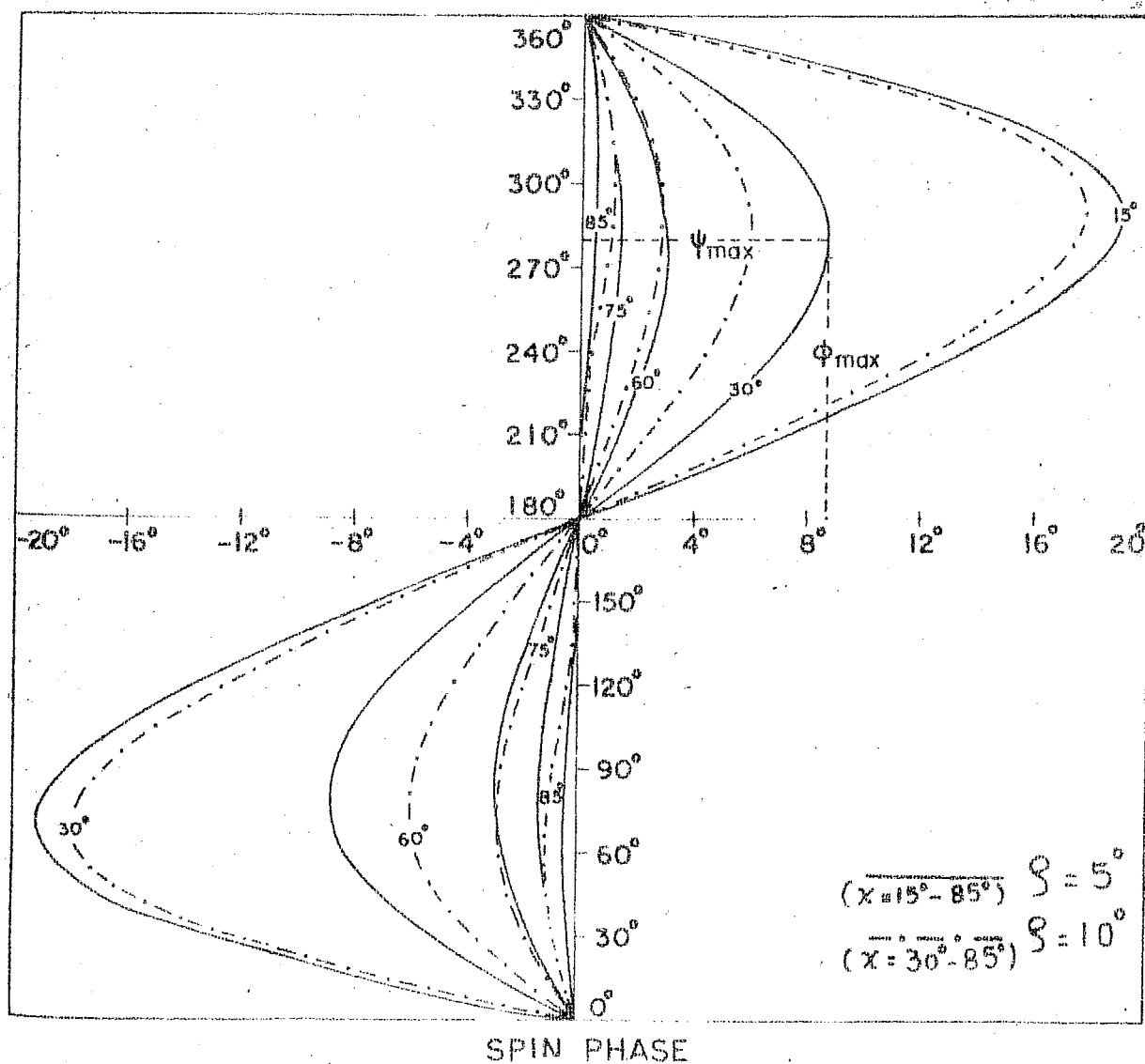
Fig. 21 – Simulated spin-precession diagram for different
values of χ and φ

Knowing $\wp$, λ and χ the phase ψ^1 can be determined and thus ψ.

Now if we consider a magnetic vector or Sco XR-1 object for this analysis, the precession - spin phase diagram constructed from their acquisition time in the data, can be matched against a theoretical response for assumed attitude parameters. In figure 21, a set of curves obtained theoretically for assumed parameters is shown. The two quantities ψ_{max}, the maximum deviation of the spin phase from the average value and ϕ_{max}. the corresponding precession phase will help for accurate determination of $\wp$ and χ within an accuracy of better than one degree, provided there is appreciable precession or the objects are at shorter angular distances from the precession axis. For smaller precession angles $\wp \leqslant 8°$, we observed in our two flights, the accuracy is limited.

As an additional check the information provided by the radar tracking of the vehicle is also used in the analysis. It is known that during the time of rocket motion under thrust, the attitude and the velocity vector coincide. Once out of the atmosphere, where air resistance encountered is negligible, the velocity vector remained constant, until the nose cone opens. The effect of the nose cone ejection in the two flights under consideration was negligible with practically no change in the position of the precession axis. The determination of precession axis, using radar data is accurate to within 2.0° arc angle, in celestial coordinate sky, for the near equatorial
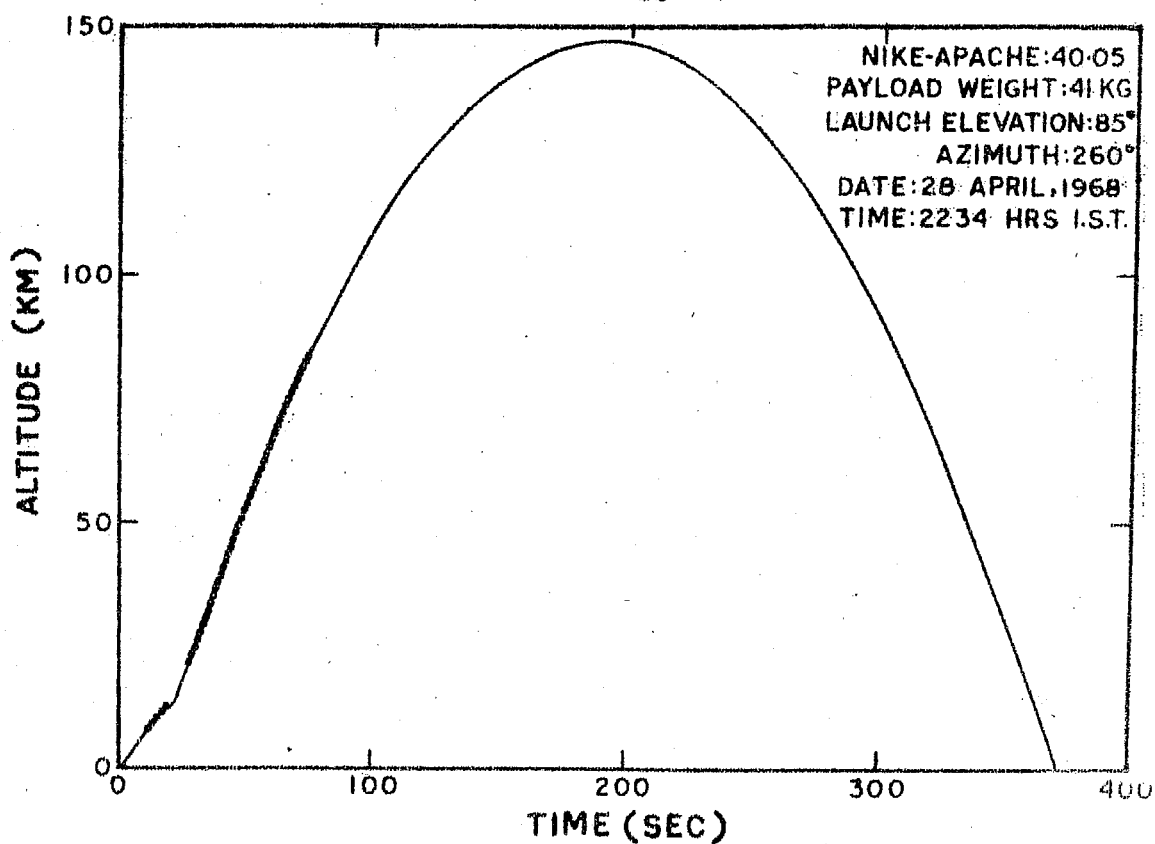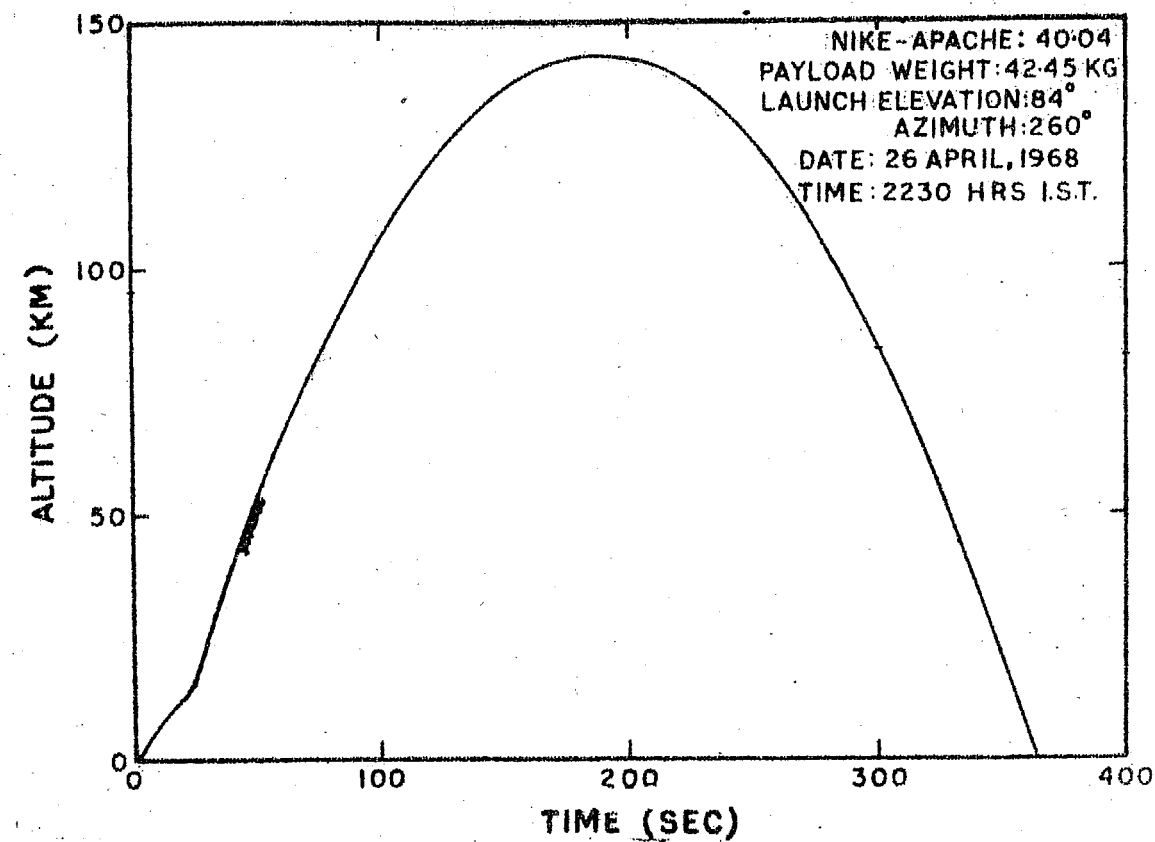
Fig. 22- Theoretical vehicle trajectories for N.A. 40.04 and
N.A. 40.05. Dots indicate radar observations.

position of the Thumba launching station. In figure 22, the
radar track data and the theoretical vehicle trajectory for
N.A.40.04 and N.A.40.05 rockets are shown. The attitude solut-
ions, obtained from methods described above, for the two flights
N.A.40.04 and N.A.40.05, are presented in the table 3.

TABLE III

ASPECT PARAMETERS

	N.A. 40.04	N.A.40.05
Date	April 26, 1969	April 28, 1969
Flight time	1700 UT	1704 UT
Precession Rate (Deg.Sec^{-1})	10.6	12.9
Spin Rate (Deg.Sec^{-1})	2337	3158
Half cone angle (Deg.)	6 ± 2	3 ± 2
Magnetic Elements:		
Dip	$-0^{\circ}\ 59'$	$-0^{\circ}\ 57'$
Declination	$2^{\circ}\ 54'W$	$2^{\circ}\ 54'W$
Zenith Coordinates:		
Right ascension	$12\ \ 26^{m}$	$12\ \ 39^{m}$
Declination	$8^{\circ}\ 33'$	$8^{\circ}\ 33'$
Precession Axis:		
Right ascension	$177^{\circ} \pm 2^{\circ}$	$182^{\circ} \pm 2^{\circ}$
Declination	$6^{\circ}\ 30' \pm 2^{\circ}$	$8^{\circ}\ 47' \pm 2^{\circ}$

2.22 X-ray Telescope Aspect

The determination of the path of the X-ray telescope
normal in the celestial sky during the flight for the given

parameters of the rocket motion will be briefly described here. The basic astronomical formulae for the determination of the siderial time and conversion between several astronomical coordinate systems are available in standard text books and hence will not be dealt here.

It is convenient to consider a number of different frames of reference for the detector aspect analysis, each defined by mutually perpendicular X, Y, Z cartesian coordinates. Let X_k, Y_k and Z_k be a fixed system of coordinates in the celestial sky and X_p, Y_p and Z_p be the precession system of coordinates (Precession frame of reference), with the precession axis coincident with Z_p. If X_p and Y_p make an angle ϕ with respect to X_k and Y_k then the coordinates X_p, Y_p and Z_p at any instance ~~of any point P~~ with respect to X_k, Y_k and Z_k coordinates are given by the matrix equation

$$\begin{bmatrix} X_p \\ Y_p \\ Z_p \end{bmatrix} = \begin{bmatrix} \cos\phi & \sin\phi & 0 \\ -\sin\phi & \cos\phi & 0 \\ 0 & 0 & 1 \end{bmatrix} \begin{bmatrix} X_k \\ Y_k \\ Z_k \end{bmatrix} \qquad \ldots 2.12$$

The spin axis of the rocket is at an angle ζ to the OZ_p axis, ζ being the half apex angle of precession. Let X_s, Y_s and Z_s be a new frame of reference (spin frame) where OZ_s is the spin axis and X_s lies in the X_p, Y_p plane. Then

$$\begin{bmatrix} X_s \\ Y_s \\ Z_s \end{bmatrix} = \begin{bmatrix} 1 & 0 & 0 \\ 0 & \cos\zeta & \sin\zeta \\ 0 & -\sin\zeta & \cos\zeta \end{bmatrix} \begin{bmatrix} X_p \\ Y_p \\ Z_p \end{bmatrix} \qquad \ldots 2.13$$

The rocket spins about its axis $(OZ_s \equiv OZ_r)$ and if X_r, Y_r and Z_r is a new frame of reference (rocket frame of reference) and the angle between X_s and X_r is ψ, then

$$\begin{bmatrix} X_r \\ Y_r \\ Z_r \end{bmatrix} = \begin{bmatrix} \cos\psi & \sin\psi & 0 \\ -\sin\psi & \cos\psi & 0 \\ 0 & 0 & 1 \end{bmatrix} \begin{bmatrix} X_s \\ Y_s \\ Z_s \end{bmatrix} \quad \dots 2.14$$

The angles ϕ and ψ vary smoothly with time as

$$\dot{\phi} = \phi_o + \omega_p (t - t_o) \quad \text{and}$$
$$\psi = \psi_o + \omega_s (t - t_o) \quad \dots 2.15$$

where t is the time, and ϕ_o and ψ_o are initial values at epoch t_o. The relative configuration of these frames of reference are shown in figure 23 (Giacconi et al. 1965). In this figure ϕ is designated as ϕ_p^s and ψ as ϕ_s and $\int$ as $\pi/2 - \lambda_p^s$.

If we assume that the detector axis forms an angle $\lambda_r^d = \lambda_s^d$ with the (X_r, Y_r) plane of the rocket (in the present experiments $\lambda_r^d = 0$) then the elevation of the detector in the precession frame of reference will oscillate between $\lambda_r^d + \int$ to $\lambda_r^d - \int$ during each spin. The detector axis will describe a sinusoidal curve (on a rectangular grid of $\dot{\phi}_p$ and λ_p) with an amplitude equal to $\int$ and a phase that changes from one spin to the next. Thus the region of the sky explored by the detector becomes wider as the apex angle of precession cone increases.
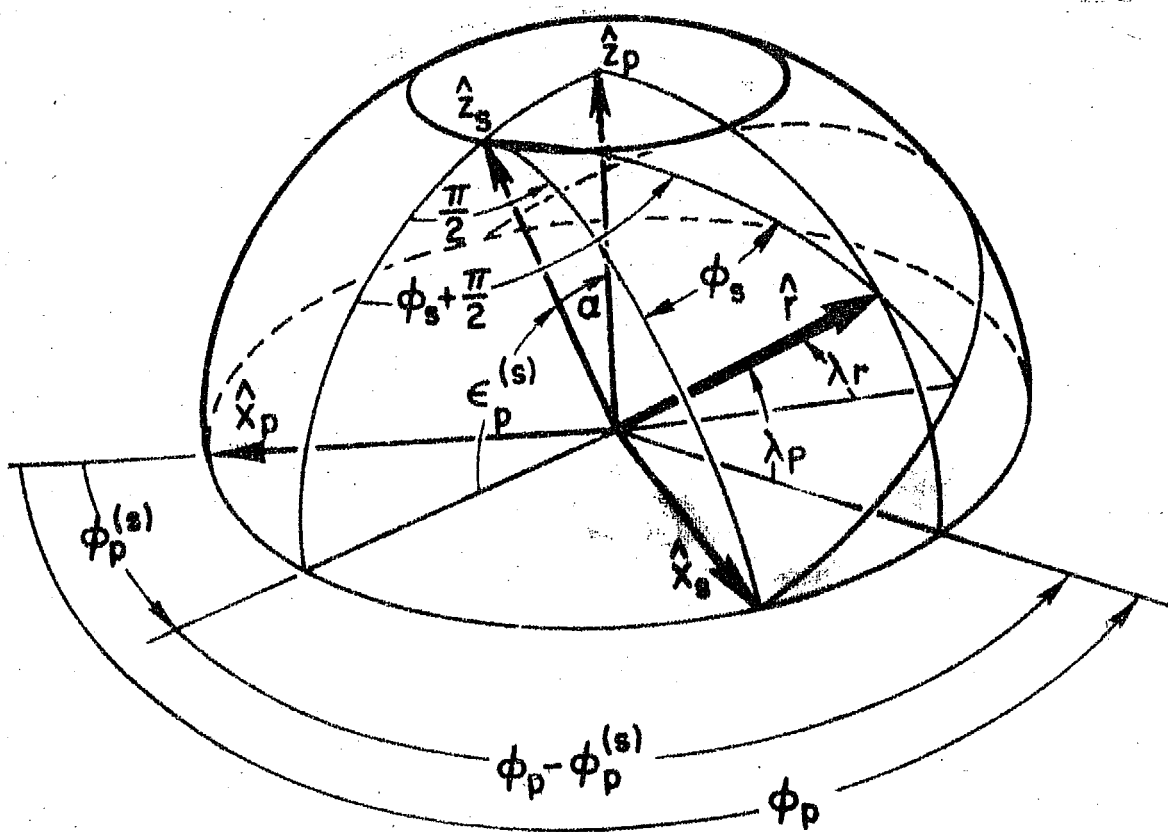
Fig.23 - Relative configuration of different frames of reference.

Using the three coordinate conversions as described earlier the following equation is obtained.

$$\begin{bmatrix} X_r \\ Y_r \\ Z_r \end{bmatrix} = T \begin{bmatrix} X_k \\ Y_k \\ Z_k \end{bmatrix} \qquad \dots 2.16$$

where T is the product of the three matrices of the three conversions in sequence. Since these matrices are orthogonal; it can be written as

$$\begin{bmatrix} X_k \\ Y_k \\ Z_k \end{bmatrix} = \bar{T} \begin{bmatrix} X_r \\ Y_r \\ Z_r \end{bmatrix} \qquad \dots 2.17$$

where $\bar{T}$ is the inverse of the matrix T. For simplification writing C and S as abbreviations for cosine and sine respectively

$$\begin{bmatrix} X_k \\ Y_k \\ Z_k \end{bmatrix} = \begin{bmatrix} C\phi & -S\phi & 0 \\ S\phi & C\phi & 0 \\ 0 & 0 & 1 \end{bmatrix} \begin{bmatrix} 1 & 0 & 0 \\ 0 & C\wp & S\wp \\ 0 & -S\wp & C\wp \end{bmatrix} \begin{bmatrix} C\psi & -S\psi & 0 \\ S\psi & C\psi & 0 \\ 0 & 0 & 1 \end{bmatrix} \begin{bmatrix} X_r \\ Y_r \\ Z_r \end{bmatrix}$$
$$\dots 2.18$$

The rocket axes in the longitudinal and lateral directions are coincident with X-ray telescope collimator surface and as such the detector normal is given by $X_d = X_r$ and Y_r and Z_r are equal to zero.

Then the motion of OX_r or OX_d axis is given by

$$\begin{bmatrix} X_k \\ Y_k \\ Z_k \end{bmatrix} = \begin{bmatrix} C\phi \cdot C\psi & - & S\phi \ C\wp \cdot S\psi \\ S\phi \cdot C\psi & - & C\phi \cdot C\wp \ S\psi \\ S\wp \cdot S\psi & & \end{bmatrix} \qquad \dots 2.19$$

If a celestial frame of reference X_c, Y_c and Z_c with Z_c aligned with the celestial north pole and X_c coincident with vernol equinox is considered, and if OX_k is assigned the southern direction for convenience, then X_k makes an angle R with X_c and Z_k makes an angle $(90-\delta)$ with Z_c where R and δ are the right ascension and declination of the precession axis.

Now
$$\begin{bmatrix} X_c \\ Y_c \\ Z_c \end{bmatrix} = \begin{bmatrix} CR.S\delta & -SR & CR \\ SR.S\delta & CR & SR \\ -C\delta & 0 & S\delta \end{bmatrix} \begin{bmatrix} X_k \\ Y_k \\ Z_k \end{bmatrix} \qquad \ldots 2.20$$

The constants ϕ_o and ψ_o at epoch t_o are evaluated when the spin axis in the precession cycle is southmost, making them equal to 180° and 90° respectively. With the above transformations the trajectory of the detector axis can be described in the celestial coordinates.

2.3 Analysis of X-Ray Data

Because of the small precession associated with both the rocket experiments and also the large admittance angle of the X-ray telescope, Scorpious XR-1 was seen in every spin during the period when the rocket was above 60 Kms. The times of the flight and the collimator design were chosen keeping in mind the main objective of the flight i.e. simultaneous measurement of X-ray flux and optical B magnitude. Figure 24 shows the detectors scan direction in celestial coordinates, along with the local horizons at the time of launch from Thumba for N.A.40.04 and N.A.40.05. In these flights besides Sco XR-1,

- 82 -
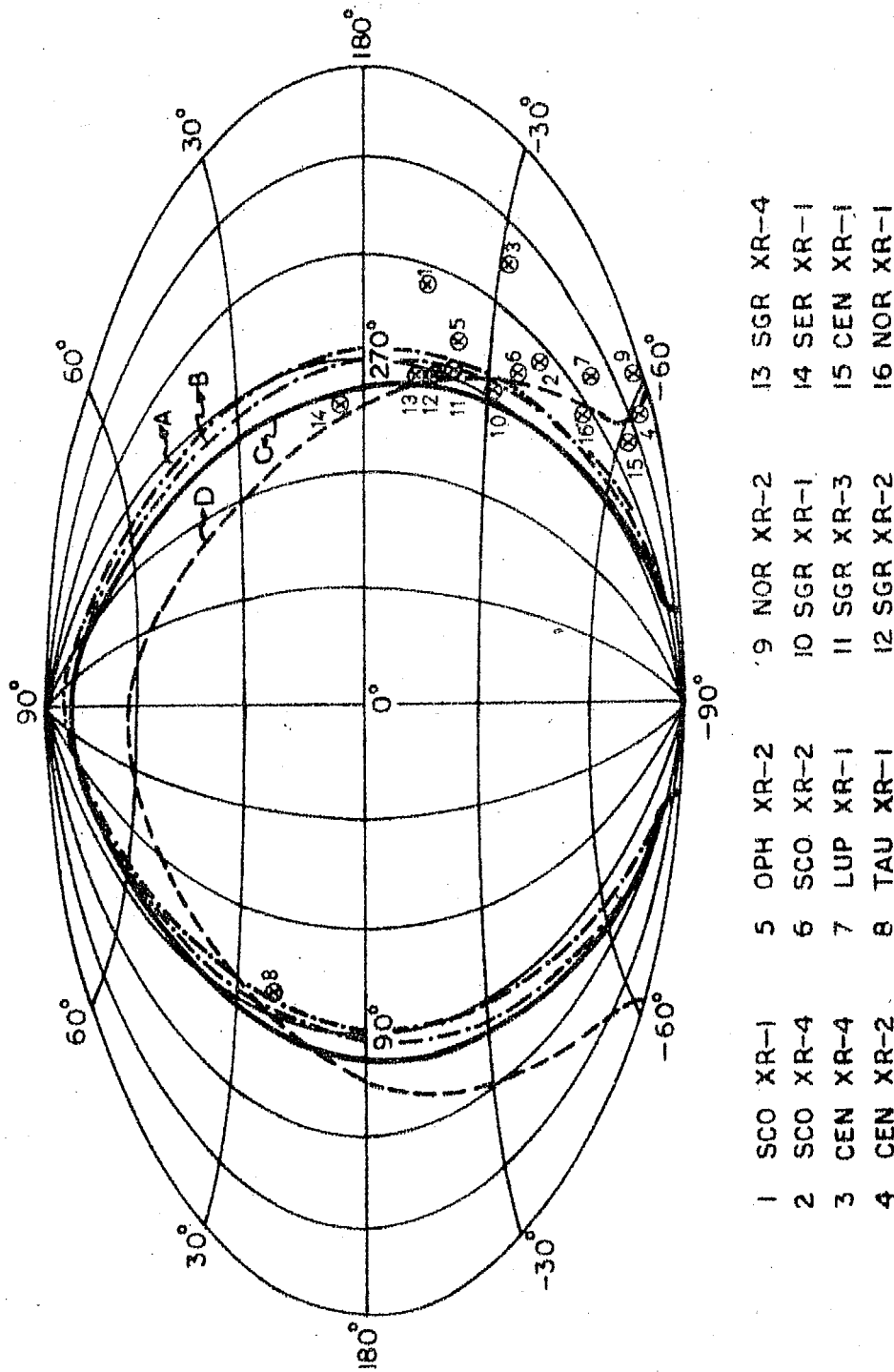
Fig. 24— Plot in celestial coordinates of trajectories of sky scans for the N.A.40.04 (A) and N.A.40.05 (B) flights. Thumba Horizon at the flight time (C) and Galactic equator (D) are shown.

1 SCO XR-1	5 OPH XR-2	9 NOR XR-2	13 SGR XR-4
2 SCO XR-4	6 SCO XR-2	10 SGR XR-1	14 SER XR-1
3 CEN XR-4	7 LUP XR-1	11 SGR XR-3	15 CEN XR-1
4 CEN XR-2	8 TAU XR-1	12 SGR XR-2	16 NOR XR-1

the cluster of sources in the galactic centre also came into the field of view of the detectors even though their contribution, (because of the small fluxes) is comparatively small and can be corrected for.

2.31 Data Processing

The data received from the rocket consisted of two sets of discrete pulses corresponding to the data from the two counters. Each pulse in the telemetry record shown in figure 18 corresponds to one photon detected in the particular energy range of PHA, and the corresponding photon arrival time can be read to an accuracy of one millisecond. Pulses A1 to A5 correspond to the detection system A and B1 to B5 are outputs from counter B. As the two detectors face in opposite directions, the observations by the two counters were out of phase by a time equal to half of the spin period with respect to each other. The sample chart shows clearly the discrete alternate clustering of PHA information of Sco XR-1.

The counters were calibrated with Fe^{55} radio active sources both on the ground prior to the launch and also in flight till 60 seconds after launch. The 6.0 KeV line with 22% FWHM resolution allowed an effective calibration of the discriminator level to within an accuracy of 3 5%. The counters were exposed to the celestial sky after ejection of nose cone along with which the calibration source is also ejected. Between 60 Kms to 80 Kms the count rate was due to high energy

charged particles, gamma rays and secondary particles produced by nuclear interactions in the rocket. Between 80 to 140 Kms the count rate underwent a gradual increase due to detection of celestial X-rays which did not penetrate any further into the atmosphere. The magnitude of increases depend on the look direction of the counter in azimuth and elevation. The rockets collected useful data for nearly 200 seconds above 100 Kms altitude after which they reentered the atmosphere.

Once out of the atmosphere the total angular momentum of the rocket is conserved, and the spin period, above 80 Kms remains essentially constant. The spin period was then divided into 120 bins each 3° wide in azimuth in the rocket frame of reference, and the entire data of PHA information was distributed within the 120 bins. As the two rockets had only $\sim6^{\circ}$ and $\sim3^{\circ}$ as half cone precession angles, the position of a source with respect to collimator normal does not appreciably change in the precession frame of reference for a good number of successive spins. Accordingly each precession was divided into six phases. The data or the count rate for all the precessions was approximately superposed in the precession phase sequence. The data for the two identical counters in each flight was found to be well within the allowed variation and consequently they have been added in the spin phase to improve statistics.

The count rate for the two flights N.A.40.04 and N.A.40.05, in each energy channel above 100 Km, for all spins and precessions summed up is exhibited in figures 25 and 26 respectively.
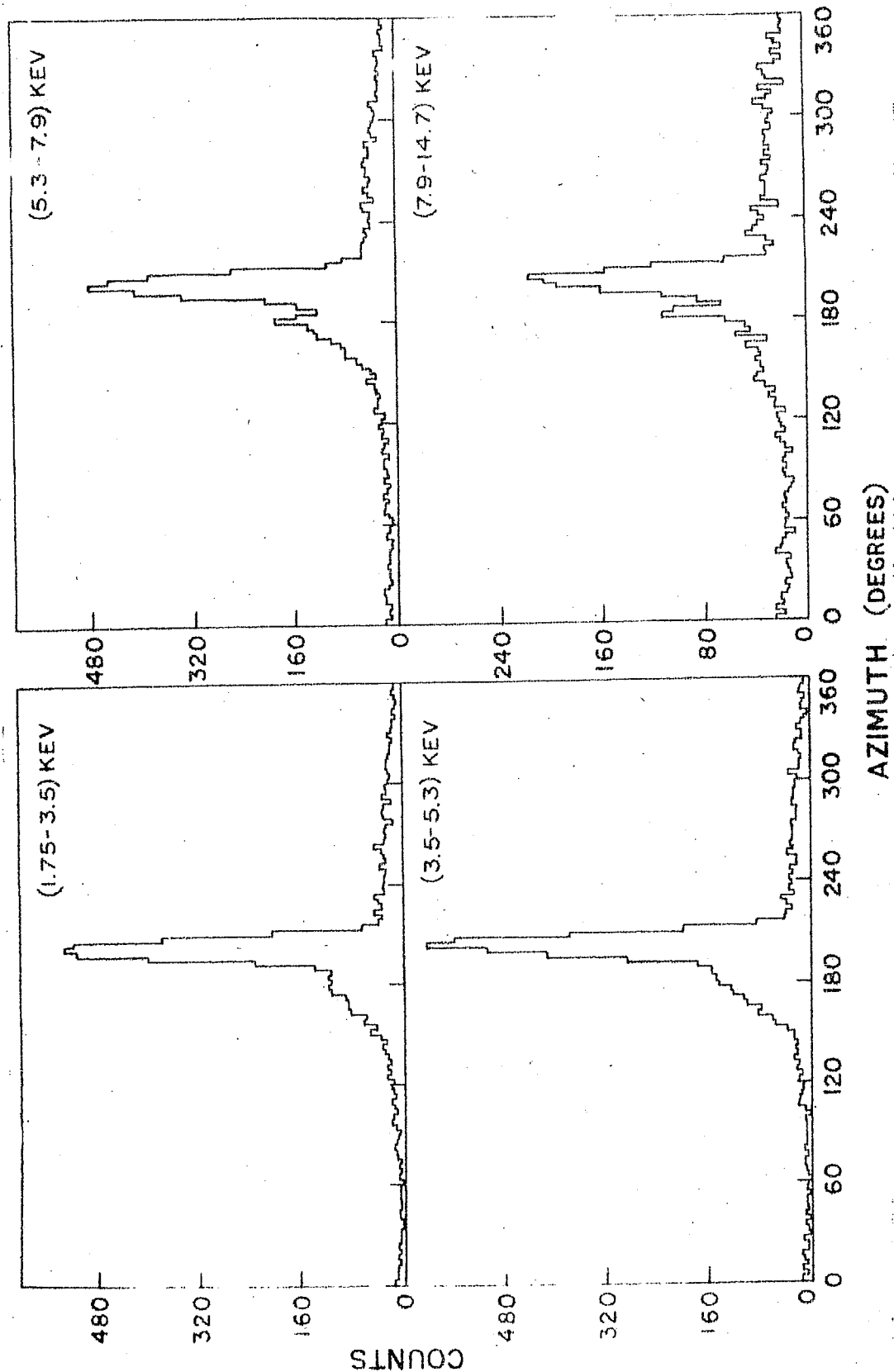
Fig. 25— Observed X-ray counting rates in the various energy channels for flight N.A.40.04.
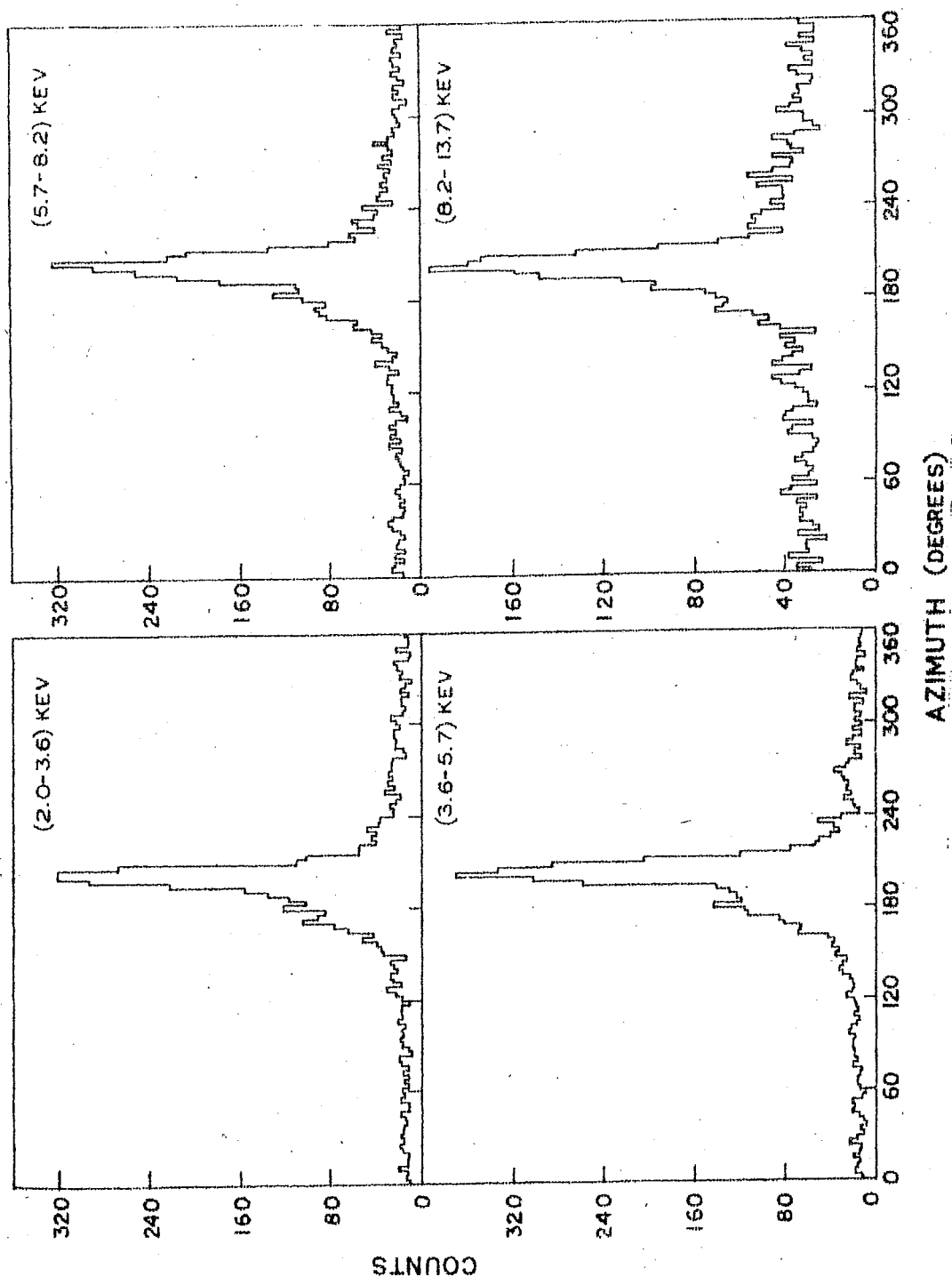
Fig. 26. Observed X-ray counting rates in the various energy channels for flight N.A. 40.05.

Above 100 Kms there was little attenuation of the incoming celestial X-rays of energy above 2 KeV. The figure clearly shows the omnidirectional and secondary background superimposed on which discrete sources show up as distinctive peaks. The spin phase starting from North shows a clear peak in the count rate due to Sco XR-1 and other galactic centre sources. As the precession axis of the rockets is nearly 10° due west, the counters dip more towards the horizon in the west. Thus the diffuse background X-rays are detected more on the eastern azimuth phase than the western.

The counting rate of any discrete X-ray source is seen as an anisotropic signal superimposed on nearly isotropic background. The X-ray background consists of three parts, (1) the isotropic diffuse cosmic X-ray background of cosmic origin, (2) atmospheric X-rays generated by cosmic rays through electron-photon cascades in the atmosphere and (3) induced X-ray background produced by the interactions of charged particles and neutral radiation (γ rays and neutrons) in and around the vicinity of the detector. It is obvious that for improved signal to noise ratio, the background has to be minimised. Whereas the cosmic diffuse X-ray radiation is independent of the location where the experiment is conducted, the cosmic ray induced X-ray flux is strongly dependent on the latitude. The very high geomagnetic cut off prevailing over equatorial regions has a decided advantage over other locations in this regard.
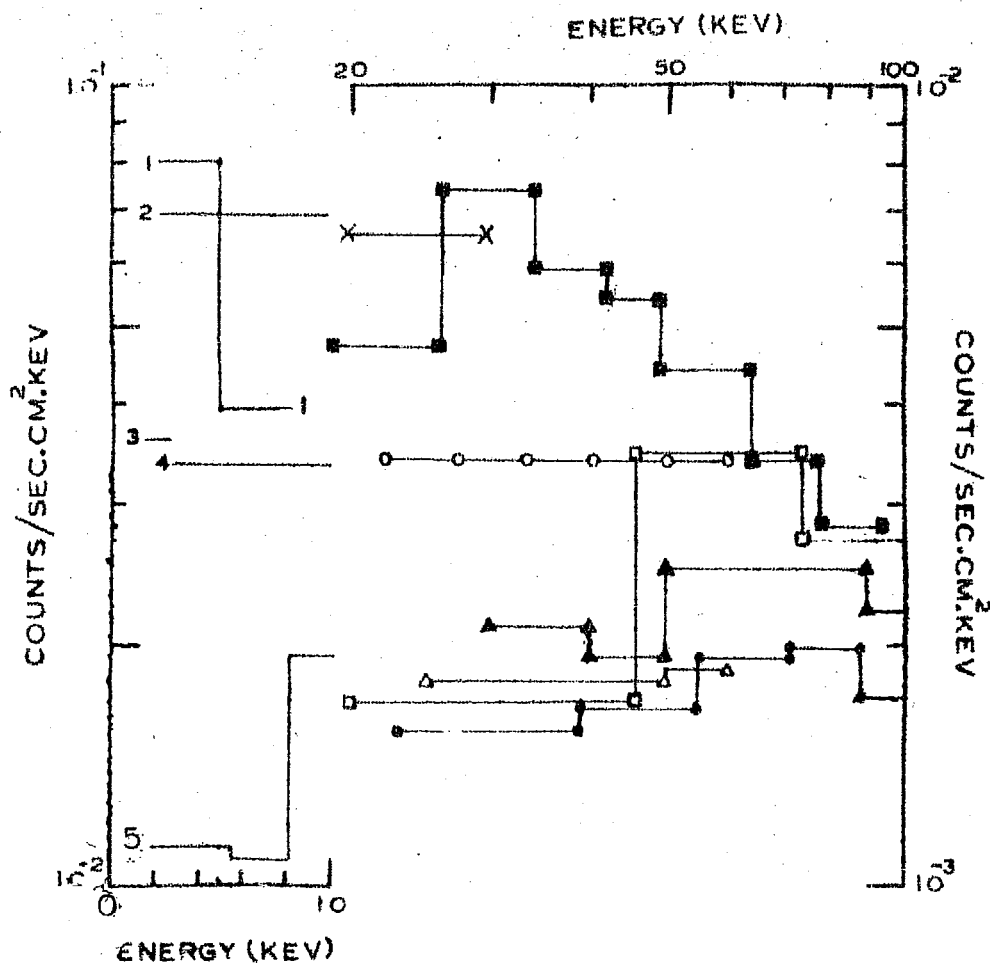
Fig. 27. Background count rates in different rocket and balloon experiments listed below.

Experimenter	Symbol	Place	Cut-Off Rig. (~GV)	Detector			
				FWHM (Deg)	Solid angle ($Sr.cm^{-2}$)	Thickness (mm)	Altitude (~$gms.cm^{-2}$)
Harris (1968)	1	Woomera	5.0	35x10	–	25	
Matsuoka et al. (1968)	2	Kagoshima	14.0	38x 6	0.0175	47	
Palmieri et al. (1971)	3	Kauai (Hawai)	13.0	20x 1	0.008	–	
Chodil et al. (1968)	4	"	13.0	15x 5	–	–	
Present	5	Thumba	17.5	32x10	0.104	26	
Present	▲	Hyderabad	17.5	14	0.05	12.5	5.0
Kasturirangan (1971)	☐	"	17.5	20	0.44	12.7	7.8
Agrawal (1972)	●	"	17.5	12	0.045	4	6.3
Reigler et al. (1968)	O	Palestine (Texas)	4.0	11	0.17	2	3.2
Webber & Reinert (1970)	△	"	4.0	6x20	–	25	3
Lewin et al.(1967)	X	Mildura	4.0	13	–	–	3
Bleeker & Deerenberg(1970)	▨	Aire-Sur L'Adour	5.0	35	0.4	12.5	4

The background count rates registered at various latitudes by different experimenters using rocket and balloon borne payloads are plotted in figure 27 with the necessary details. The analysis is a simple comparison and is not a rigorous, as no attempt is made to normalise the different factors of importance like detector geometry, float altitude, etc. In the case of rocket experiments, the flux of X-rays registered when the detector looks/toward the earth is considered as the cosmic more or less induced background. The figure clearly shows that the rocket background (1-10 KeV) at Thumba (8.5°N) situated on geomagnetic equator is lower by factors 6$\smile$3 compared to those at high latitude stations like Woomera (**32°**S), Australia or Kauai (22.5N), Hawaii.

In the balloon experiments which register high energy X-ray flux (**20**-100 KeV) the cosmic ray induced background becomes a major noise source. The experiments of Bleeker and Deerenberg (1970) have clearly shown the variation in intensity of atmospheric X-rays due to the different latitudes, the count rate decreasing with increase in cut off rigidity. The count rates registered at Hyderabad by the different Indian groups as shown in the figure clearly show that the cosmic ray induced background over Hyderabad is less by a factor of $\smile$3 compared to that observed at middle and higher latitudes. The observed background at Hyderabad even with the simplest detector is comparable to the most sophisticated detector employed by Webber & Reinert (1970). It is therefore obvious that meaningful

experiments can be done at equatorial latitudes even with much simpler detectors due to the enormous reduction in the background.

2.32 Evaluation of Position and Count Rate from Sco XR-1

The response of the counters for the rectangular geometry of the collimators due to a discrete source along any given scan has a triangular step with a base equal to $T \times \frac{21^O}{360^O}$ seconds, where T is the spin period (0.156 sec. for flight N.A.40.04 and 0.119 sec. for flight N.A.40.05). As the two rockets had high spin frequencies the product of the counter effective area and time for each azimuthal bin is small. For improved statistical accuracy we have considered each precession phase as a unit of time. For each given precession phase, there were about seven count rate data points at different energies for the 21° base angle response, which were used for the positional determination of the source.

The presence of galactic sources, near to Sco XR-1, do contaminate by contributing to the observed flux from that direction. It is imperative to estimate the contributions from these sources to the observed count rate to establish the flux level of the Sco XR-1 source. Fortunately many of these sources were sighted in earlier experiments performed by the NRL, Lockheed and ASE/MIT scientists, from which results, the flux, positional information of these sources is known sufficiently accurate to enable us to make adequate correction for the contamination due to these sources. Using the catalogue

prepared by Matsuoka and Oda (1971) the contribution of the galactic sources to the observed count rate of Sco XR-1 is estimated for the various aspect parameters of the telescope.

The count rate due to Sco XR-1, in any azimuthal bin, in a given precession phase for each energy channel, is obtained by substracting the general background count rate and the galactic sources count rate from the total count rate. These count rates have been used for the determination of absolute count rate due to Sco XR-1 for normal incidence. A least square technique has been used to fit the collimator response to the count rate data first on the individual precession phases and then to the data observed in different phases.

The observed data consisted of a series of count rates, $X_p(A_i)$ for a precession phase, in an azimuth bin centered at A_i. Let the triangular collimator response function be $g(A_p - A_i)$ with $g(0) = 1$, then the theoretical response from a point source will be of the form $S_p \cdot g(A_p - A_i)$ where S_p is the source strength incident for the particular precession phase and A_p is the azimuth where the response is maximum. If S_p and A_p are so chosen as to make the sum of the squares of the deviations as small as possible, i.e.

$$E_p = \sum_i \left[X_p(A_i) - S_p \, g(A_p - A_i) \right]^2 \qquad \text{..... 2.22}$$

is minimised. Each count rate point is weighted equally. At the minimum the partial derivates will be zero and S_p is given by

$$S_p = \frac{\sum_i X_p(A_i) \cdot g(A_p - A_i)}{\sum_i \left[g(A_p - A_i) \right]^2} \qquad \ldots 2.23$$

The variance of S_p, for poisson statistics can be written as

$$V(S_p) = \frac{\sum_i X_p(A_i) \left[g(A_p - A_i) \right]^2}{\left(\sum_i \left[g(A_p - A_i) \right]^2 \right)^2} \qquad \ldots 2.24$$

Along a given precession phase the response function $g(A)$ was triangular with $21°$ base width B. In the analysis S_p and $V(S_p)$ were computed for various values of A_p, the correct A_p being that which minimised error function E_p. The variance in A_p is given by

$$V_p(A_p) = \frac{B}{N S_p} \sum V\left[X_p(A_i) \right] \qquad \ldots 2.25$$

where S_p is known from equation 2.23 and N is the number of data bins. Thus the intensity, the response maximum in azimuth and the variance in each is determined for all the precession phases.

For a favourable position of the source and large precession angle, the intensity and the azimuth angle vary in different precession phases as mentioned in the earlier section. Figure 28 is a three dimensional plot of count rate for N.A.40.04 and N.A.40.05 showing the count rate and azimuthal distribution against precession phase. The $12°$ and $6°$ variationsin elevation of Sco XR-1 in a precession, cover only a part of $85°$ base width of the collimator longitudinal response angle. As such there is count rate modulation during a
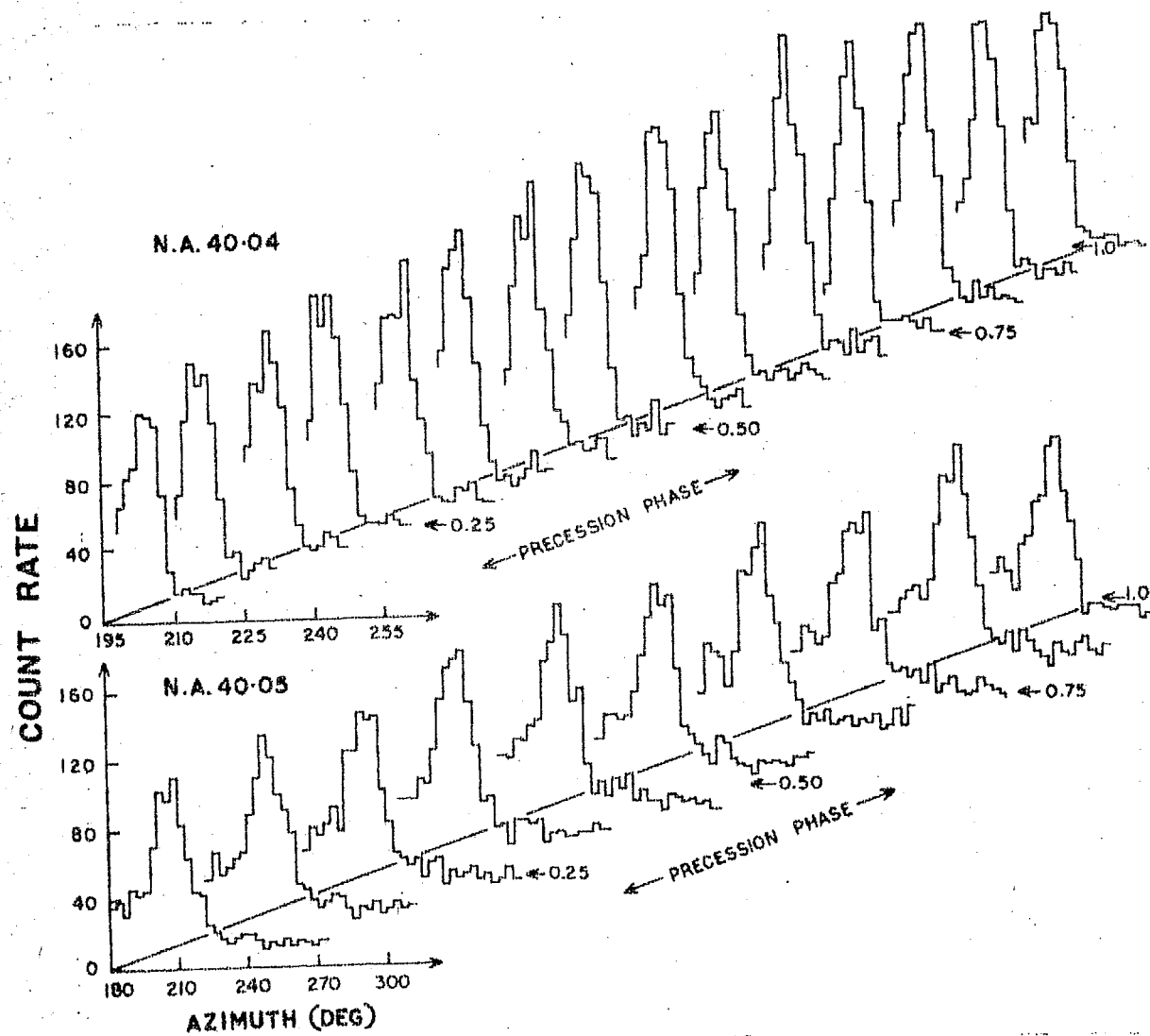
Fig. 28 - Three dimensional plot of total count rate in
different precession phases for N.A.40.04 and
N.A.40.05.

precession, especially so in the case of N.A.40.04 data. In both the flights, the transit in azimuth did not show deviation by more than one 3° azimuthal bin in the different phases. These aspects were consistent with the precession axis position in sky and the half cone angle determined by radar track data and magnetic sensor information. The average elevation of Sco XR-1 with respect to the detector normal is $\sim 19^{\circ}$ and 24° in the precession frame of reference for N.A.40.04 and N.A.40.05 respectively. Using a similar least square fit to the data of the different phases, the elevation response is evaluated with the known attitude parameters and the absolute count rate of Sco XR-1 for normal incidence is determined for each energy channel.

2.33 The Absorption of X-Rays in the Atmosphere

It is necessary to know the effect of the residual atmosphere above the rocket on the incoming celestial X-rays. The absorption of X-rays depend on their energy and on the zenith angle of their arrival direction.

The intensity of X-rays reaching the detector from a source of strength I_0 is given by

$$ I = I_0 \exp \left(-\mu \int \rho \, dx \right) \qquad \ldots \ 2.26 $$

where μ is the mass absorption coefficient of air in $gm^{-1}.cm^2$ and $\int \rho \, dx$ is the amount of matter traversed in $gm.cm^{-2}$. The mass of atmosphere along the line of sight from various rocket altitudes at various zenith angles was calculated from the U.S.

Fig. 30 - Mass absorption coefficient for air.

Fig. 29 - Mass of atmosphere in gms. cm⁻² between the rocket and a celestial object for different altitude and zenith angles.

Standard Atmosphere (1962) and is shown in figure 29. The mass
absorption coefficient of air (Victoreen 1948) is shown in
figure 30. The joint use of these two figures and equation 2.26
allowed the attenuation of any given energy X-rays to be deter-
mined for any attitude and zenith angle. Provided $\int \rho \, dx$ is less
than 10^{-4}, there was negligible absorption over the energy
range 2 to 20 KeV. Sco XR-1 had a maximum of 65° zenith angle
in these experiments and the data used was from heights above
110 Km, the attenuation is negligible.

2.34 Spectral Analysis and Results

The problem was initially turned around, the incident
X-rays were assumed to have various two parameter spectra, and
the expected count rates in each energy channel is estimated.
Sco XR-1 spectrum is quite well known and is found to follow an
exponential function. Electron bremsstrahlung from a thin hot
plasma in the X-ray range produces

$$\frac{dN}{dE} (E) = KE^{-1} \exp\left(-\frac{E}{T_e}\right) \text{ photons cm}^{-2} \text{ sec}^{-1} \text{ KeV}^{-1} \quad .. \ 2.27$$

where T_e is the effective temperature of the plasma in KeV and
K is a constant.

This spectrum of X-rays was traced through the detection
system to determine the resultant count rates in the pulse
height analyser channels. The spectrum of photons in the
counter can be written as

$$\frac{dN}{dE} (E) = KE^{-1} \exp\left(-\frac{E}{T_e}\right) A(E) \in (E) \quad \quad .... \ 2.28$$

where A(E) is the atmospheric attenuation and $\in$ (E) is the efficiency of the counter system.

This spectrum will be distorted by the finite resolution of the counter. The theoretical resolution of a proportional counter can be calculated from the statistical processes which take place and is approximated by

$$FWHM = 44E^{-\frac{1}{2}} . \qquad \qquad \dots 2.29$$

However, in the two flights the proportional counters had approximately 22% and 16% resolutions (FWHM) at 6 KeV (Fe^{55}) and 22 KeV(Cd^{109}) respectively. The FWHM at any energy is obtained by a linear relation between these observed values. The spectrum of output pulses was then given by the convolution integral

$$\frac{dN}{dE} (E_o) = \int_0^\infty \frac{1}{\sqrt{2\pi}\sigma} \exp\left[\frac{(E - E_o)^2}{2\sigma^2}\right]\in(E)\cdot A(E)\cdot KE^{-1} \exp\left(-\frac{E}{T_e}\right) \qquad \dots 2.30$$

where $\sigma = \frac{FWHM}{2.35}$ E. The effect of the counter resolution on the pulse height spectrum from the proportional counter is shown in figure 31.

Assuming for physical parameters K and T_e certain values, the convolution as stated by equation 2.30 is carried over the discrete energy channels. The true values are those which match the convolution integral output with the observed count rate in the PHA channels. The analysis have excluded channel
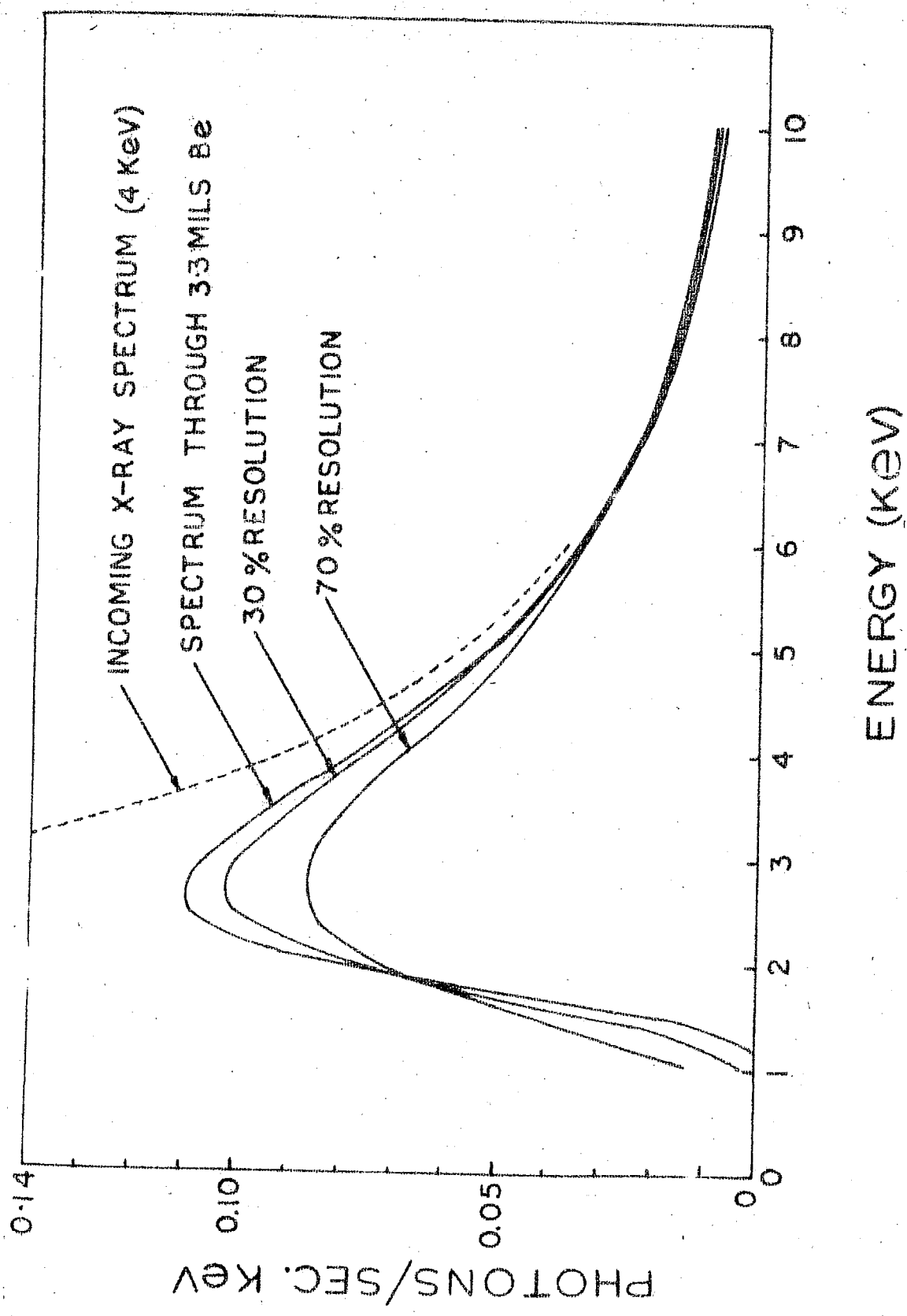
Fig. 31- The effect of the counter resolution on an incoming exponential spectrum.

five, as the count rate in this channel is not satisfactory.
From the two flights the exponential spectrum of Scorpious XR-1
can be described as

$$\frac{dN}{dE}(E) = 65 \exp\left(\frac{-E}{5 \pm 0.8}\right) E^{-1} \text{photons.cm}^{-2}.\text{sec}^{-1} \text{KeV}^{-1}$$

$$\dots 2.31$$

on April 26, 1969 at 1700 U.T. and

$$\frac{dN}{dE}(E) = 47 \exp\left(\frac{-E}{6.8 \pm 0.9}\right) E^{-1} \text{photons.cm}^{2}.\text{sec}^{-1} \text{KeV}^{-1}$$

$$\dots 2.32$$

on April 28, 1969 at 1705 UT. The above spectral results have
been plotted in figure 32. The points represent the average
flux value in the particular energy channel and the errors
represent statistical 1 σ limits.

Thus these experiments have measured Sco XR-1 to emit
50.5 $\pm$ 8.2 and 41 $\pm$ 7.5 photons.cm^{-2}.sec^{-1} in the 2-15 KeV
range. The two different temperatures, 58 and 80 million
degrees and the different flux values, when compared along with
the results of other experimenters, clearly establish real
time variations, inherent with the source as discussed in
Chapter IV.

As the thesis in part deals with the simultaneous obser-
vations attempted by PRL - ISAS groups during April - August
1969 the results along with the observations of other experi-
menters is discussed in detail in Chapter IV.

. . . .
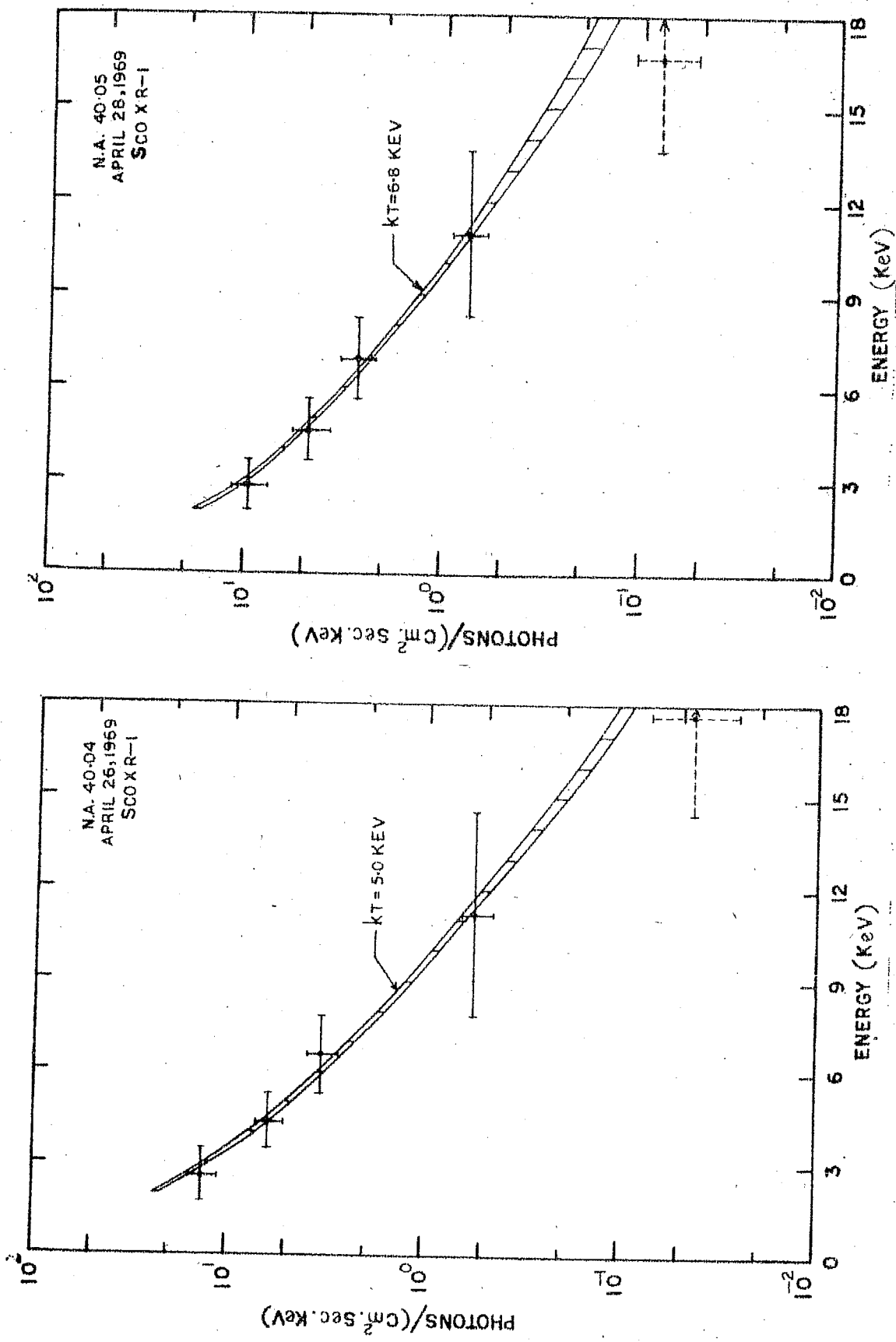
Fig. 32 — Sco XR-1 photon spectrum observed in the two flights.

CHAPTER III

X-RAY BALLOON EXPERIMENT

Investigation of Sco XR-1 in the high energy X-ray region
(E > 20 KeV) was conducted using balloon borne payloads from
Hyderabad, India (17° 25' N and 78° 55' E). Due to the very
high geomagnetic cut off (> 17 GeV) over Hyderabad, the second-
ary cosmic ray produced background is relatively small and con-
sequently Hyderabad offers an excellent site for conducting
balloon borne X-ray astronomy experiments. Two identical X-ray
telescopes were flown on oriented platforms with the help of
3 mcft. balloons on November 17, 1970 and November 15, 1971 to
measure X-ray flux from Sco XR-1 in the 20-120 KeV energy range.
In this chapter we describe these experiments.

3.1 Balloon Borne X-Ray Telescope

The X-ray telescope consists of a Na I (Tl) crystal of six
inches diameter as a primary detector. The crystal has an
entrance window of 0.032 inch aluminium foil. The 0.5 inch
thick crystal was viewed by an optically coupled RCA 8055
photomultiplier. A set of hexagonal tubes, made up of lead
and brass placed above the radiation window of the crystal
defined the field of view of the detector to 11.2° (FWHM) in
the forward direction for X-rays in the 20-120 KeV range. The
entire detector assembly was enclosed within an active shield
which itself was surrounded by a passive shield.
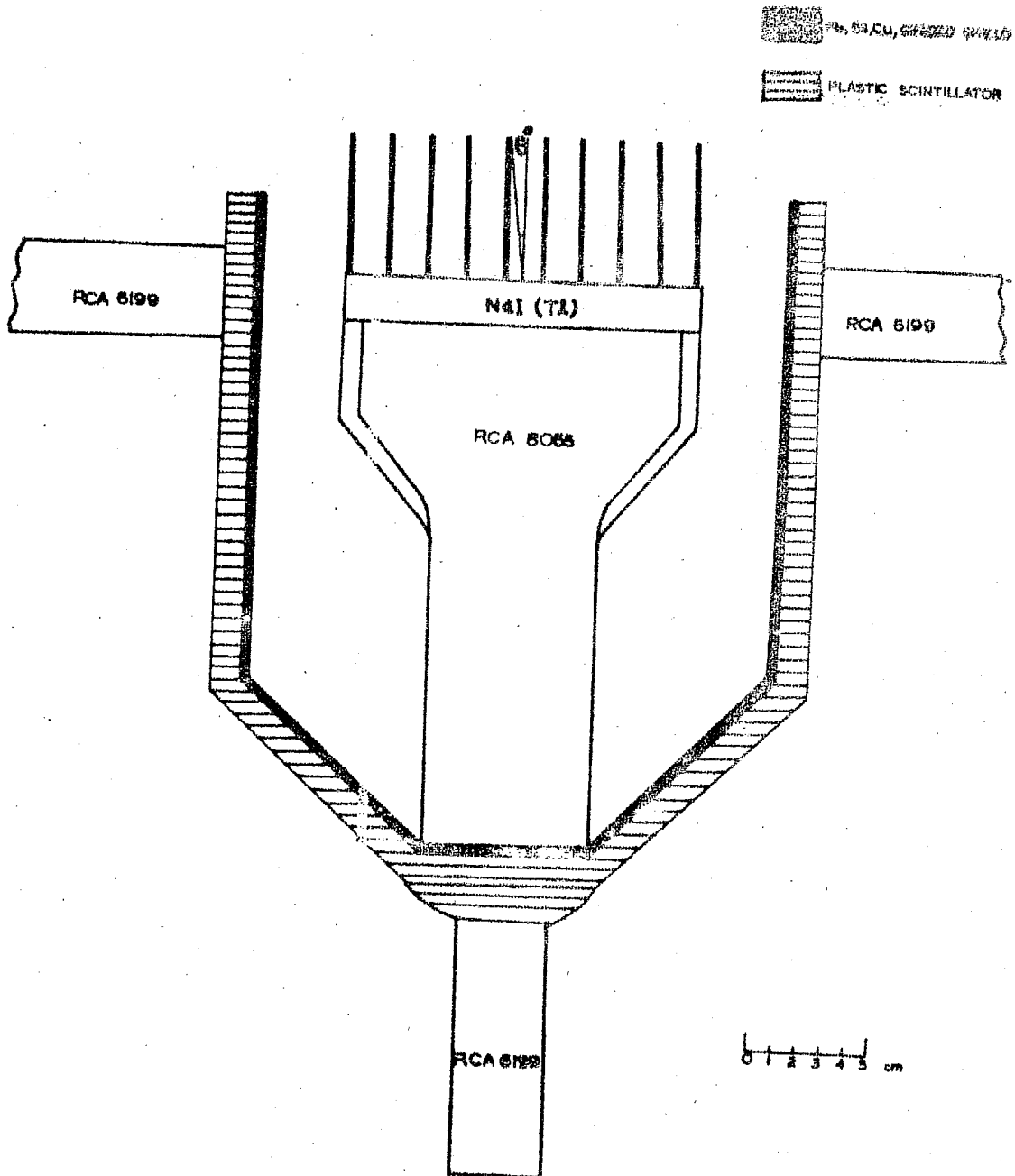
Fig. 33 — Schematic of the X-ray telescope.

The passive shield consisted of graded shielding system comprising lead, tin and brass cylinders arranged concentrically in descending order of their atomic weights. High energy photons are absorbed in the outermost shield of Pb and the subsequent flourescent X-rays, after successive absorption in inner shields are degraded below the threshold of the lowest energy channel of interest. The shield had an opacity of 95% for 150 KeV X-rays coming from sides.

The active shield is a 1 cm thick plastic scintillator of cylindrical shape. This cylinder was viewed by three RCA 6199 photomultipliers optically coupled to the scintillator as shown in figure 33. Relativistic muons or protons deposit nearly 2.5 MeV in the 1 cm thick plastic. Using an Am^{241} source, which emits alpha particles of 5.5 MeV energy, the detection threshold of the plastic anticoincidence scintillator was set at 200 KeV for electrons. The system had about 60 – 70% efficiency for charged particle rejection.

A block diagram of the experimental system is shown in figure 34. The output pulses from RCA 8055 photomultiplier coupled to the NaI (Tl) crystal were suitably amplified and analysed by an eight channel pulse height analyser. The energy channels in the pulse height analyser were adjusted to accept X-rays in the energy ranges 17-25, 25-32, 32-42, 42-53, 53-67 and 67 to 107 KeV. The same events were further independently monitored in two sum channels 17-42 KeV and 42-107 KeV, to
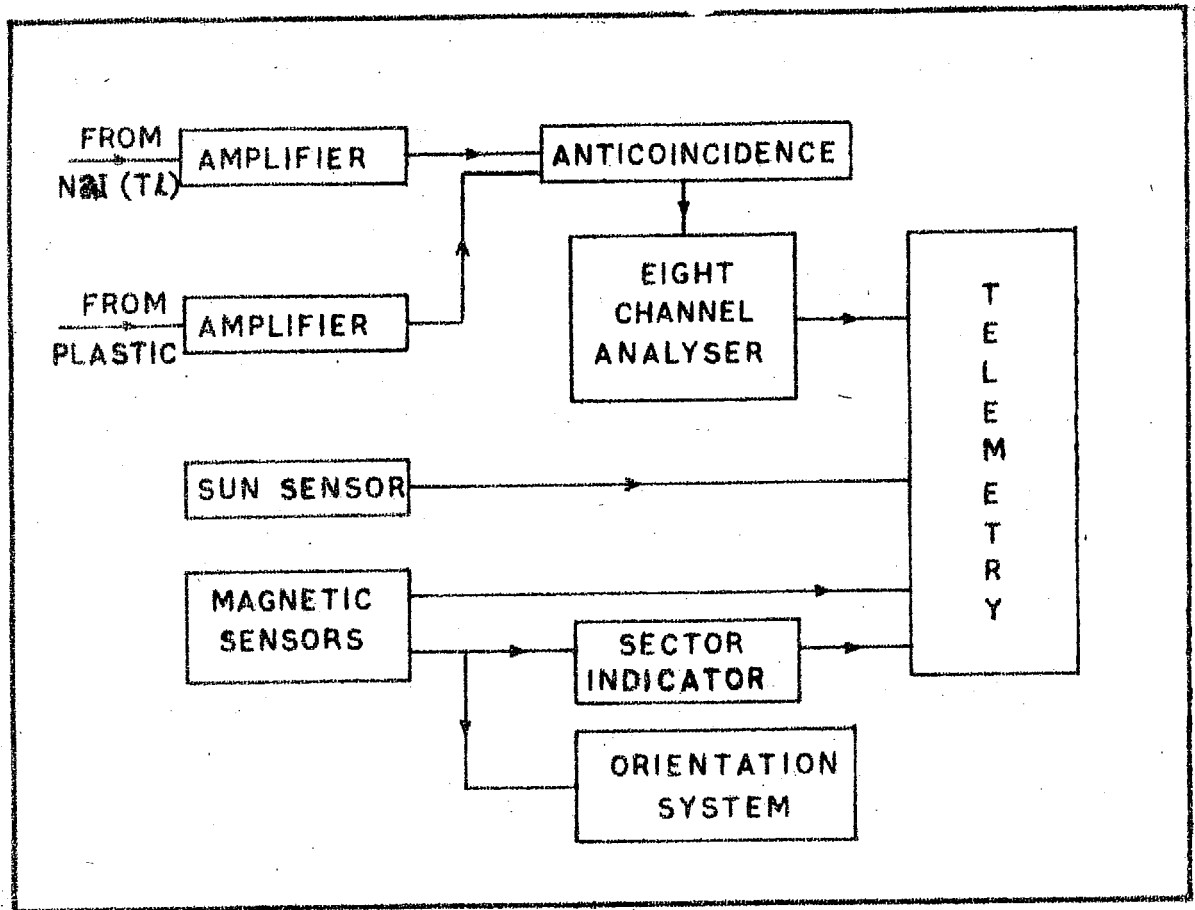
Fig. 34. Schematic of the Balloon X-ray astronomy experiment.

provide independent check of the entire circuitary. An Am^{241} source was placed in the system for calibration once in every five minutes.

The telescope was mounted on an orientation platform and fixed to servocontrolled gimbals to point along preprogrammed azimuthal directions, at a fixed inclination with respect to local zenith. The azimuth aspect was derived from a pair of flux gate magnetic sensors and a sun sensor to an accuracy of better than $\sim 1.5^{\circ}$. The pulse height analyser information as well as the aspect information were continuously telemetered to ground using standard IRIG FM/FM telemetry system.

An onboard aneroid element provided continuous recording of pressure. The balloon was tracked by radar to provide additional altitude information. A thermistor temperature sensor recorded the temperature within the payload throughout the flight.

3.11 Response of the NaI (Tl) Crystal Assembly to X-Ray Photons

The three main processes by which the energy of a photon is deposited in a scintillation counter are photoelectric absorption, compton scattering and pair production. Upto few hundred KeV, photoelectric absorption dominates while at energies above a few MeV pair production becomes important. At the intermediate energies, compton effect is important.
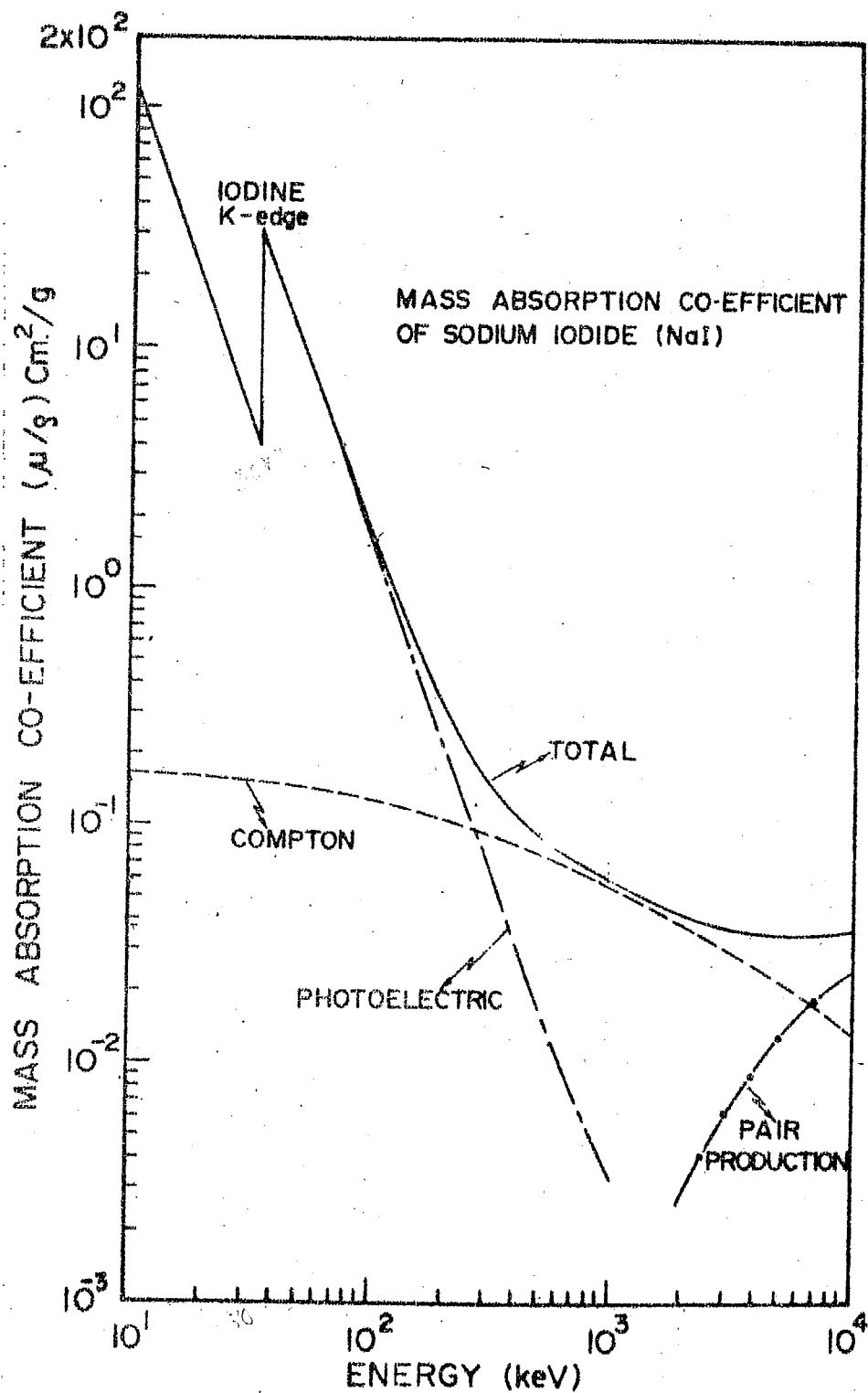
Fig. 35- Mass absorption coefficient of sodium iodide as a function of photon energy.

In the case of photoelectric absorption the entire photon energy is deposited in the crystal and the energy estimation is unambiguous. The attenuation coefficient for the photoelectric effect is strongly dependent on the atomic number Z of the material, therefore in order to achieve a high detection efficiency   a high Z detector is essential. Sodium iodide doped in Thallium gives very large scintillation pulses due to the high photoelectric absorption of the iodine constituents, these crystals are very suitable for X-ray spectrometry. The absorption coefficients for various interaction processes in the Sodium crystal are shown in figure 35. It may be seen from the figure that the photoelectric absorption process is the only dominant process upto about 200 KeV while compton scattering starts dominating above 250 KeV upto an energy of several MeV. The response of the Sodium iodide crystal is quite linear from 20 KeV to 200 KeV for the 0.5 inch crystal. About 10% of the energy dissipated in the NaI (Tl) crystal is converted into visible light. Thus an absorption of 100 KeV photon in the crystal results in the production of 300 optical photons. The emitted photons have a distribution with a maximum around the wavelength 4200 $\overset{\text{o}}{\text{A}}$, and decay with a time constant 250 nanoseconds. The photons are collected at the photocathode of the photomultiplier; RCA 8055 photomultiplier tube has a 5 inch cathode surface with S-11 response i.e. having a peak response for photons around 4400$\overset{\text{o}}{\text{A}}$. The quantum efficiency of the photocathode is about 10%. The typical multiplication factor of
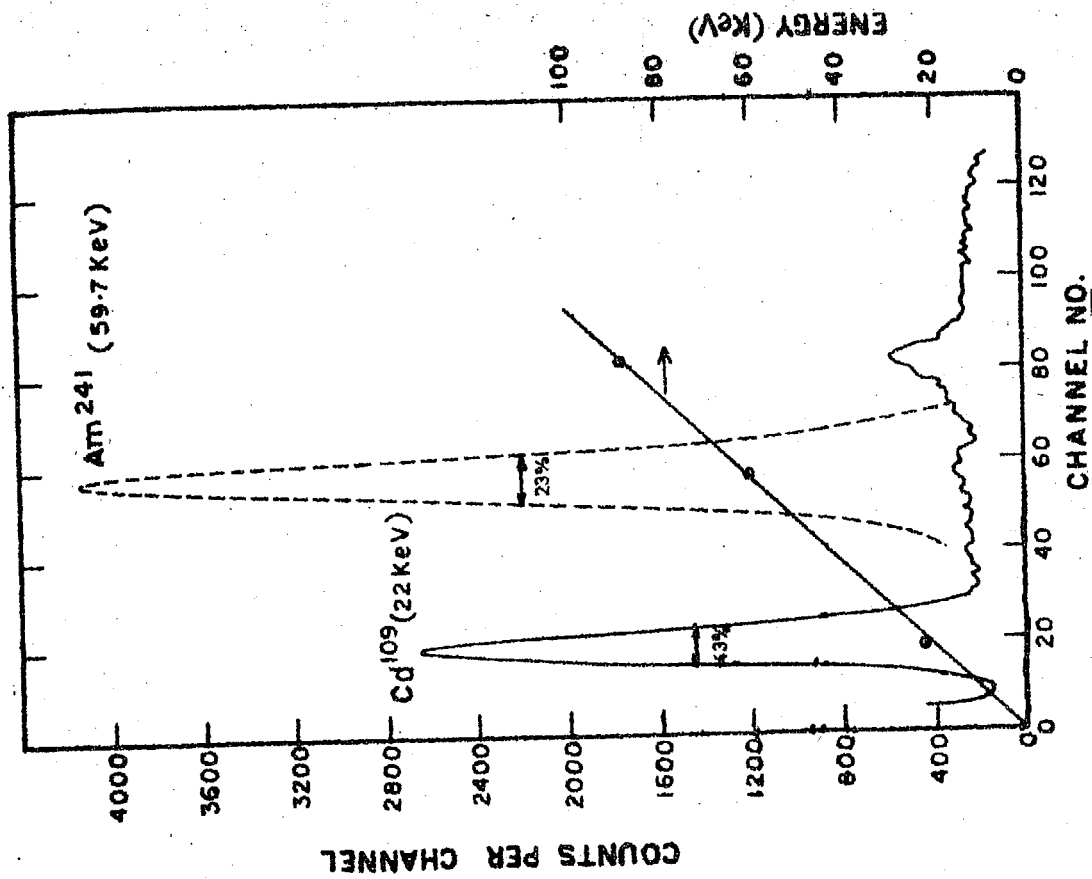
Fig. 37— Variation of detector resolut-
ion with photon energy.
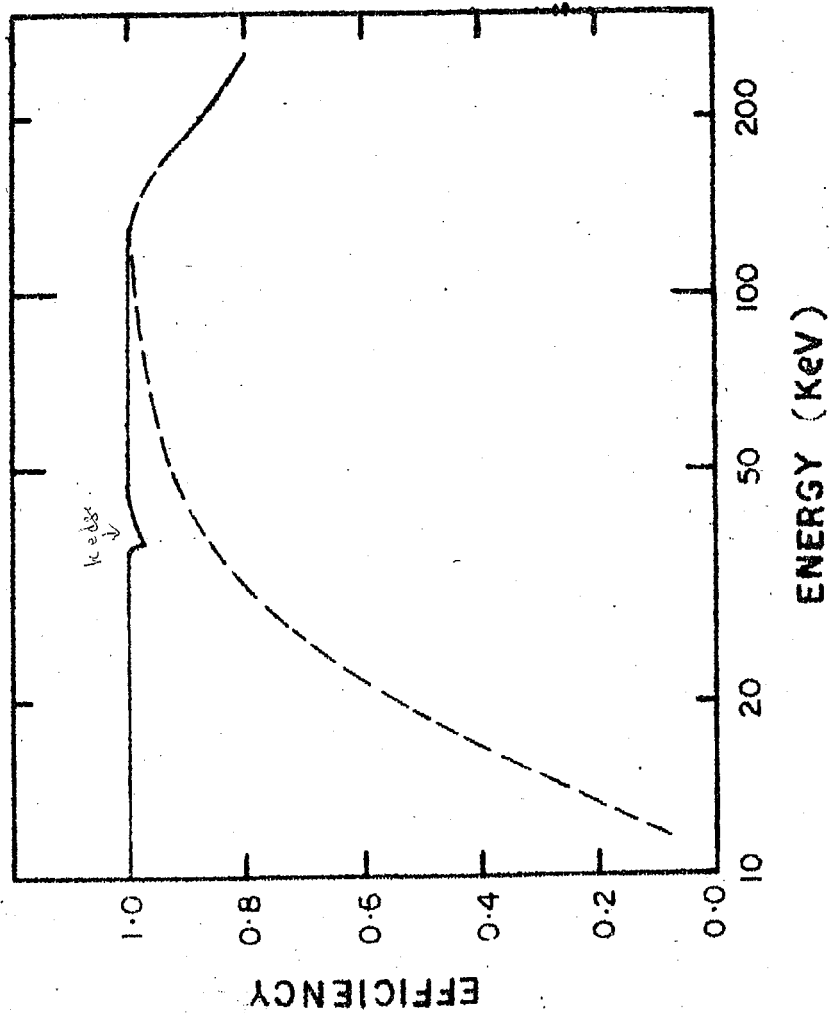
Fig. 36— Detection efficiency for 0.5 inch thick
NaI(Tl) crystal. Dashed line indicates
transmission through 0.032 inch
aluminium window.

this tube according to manufacturers is 1.5×10^6 at an operating voltage of 1000 volts.

The efficiency of the detection system for a collimated beam is defined as

$$\varepsilon (E) = \exp (-\mu_w (E) d_w) \left[1 - \exp (- \mu_c (E) d_c) \right] .. \quad 3.1$$

where d is the thickness in $gm.cm^{-2}$, $\mu(E)$ is mass absorption coefficient in $cm^2.gm^{-1}$, and subscripts w and c represent window material and crystal. The computed values of the efficiency for the detector assembly, 0.5 inch sodium crystal with 0.032 inch aluminium window, at various energies is plotted in figure 36. At lower energies the entrance window limits the transparency of photons for detection in the crystal. On the other hand the efficiency is 100% for higher energies of interest upto 150 KeV. The X-ray edges, at $E_\alpha = 28.6$ KeV and $E_\beta = 32.5$ KeV, for the 0.5 inch thickness of the crystal, have negligible effect on the efficiency.

The various processes that occur starting from the energy loss in the crystal to the final output at the photomultiplier anode are subject to statistical fluctuations. The quantitative theory of the nature of these fluctuations have been treated by Breitenberger (1955). Because of this effect even if the incident photons are monoenergetic, the output pulse height at the anode exhibits considerable distribution. The NaI crystal was calibrated using Cd^{109} (22, 88 KeV) and Am^{241} (16.5, 60 KeV) radio active sources. The pulse height distri-

bution curves are shown in figure 37. The detector system had energy resolution of about 40-50% at 22 KeV and 22 to 33% at 60 KeV.

3.12 Pulse Processing Circuitry

The block diagram of the pulse processing circuit is shown in figure 38. Pulses from the anode of the photomultiplier were amplified and shaped in a charge sensitive preamplifier. The positive pulses from the preamplifier attached to the main crystal, NaI (Tl), were amplified by a set of three amplifiers, which use high gain negative feed back for stable linear ampli- fication. The gains were so adjusted to give for the 22 KeV and 88 KeV X-rays of Cd^{109}, 0.75 volts and 3.0 volts at the second stage, and 2.2 volts at the final stage and saturation. The outputs of the three preamplifiers belonging to the plastic scintillator, were suitably mixed and the combined output is amplified to generate an Inhibit anticoincidence pulse for charged particle rejection.

Two independent high voltage power units supplied the nece- ssary voltages to the NaI (Tl) detector system and to the three photo-tubes coupled to the anticoincidence plastic scintillator. The voltages were generated from a +12V regulated supply using conventional Cockroft - Walton voltage multiplier technique. The regulation of the high voltage was achieved by corona discharge tubes and sufficient filtering was provided for ripple suppression.
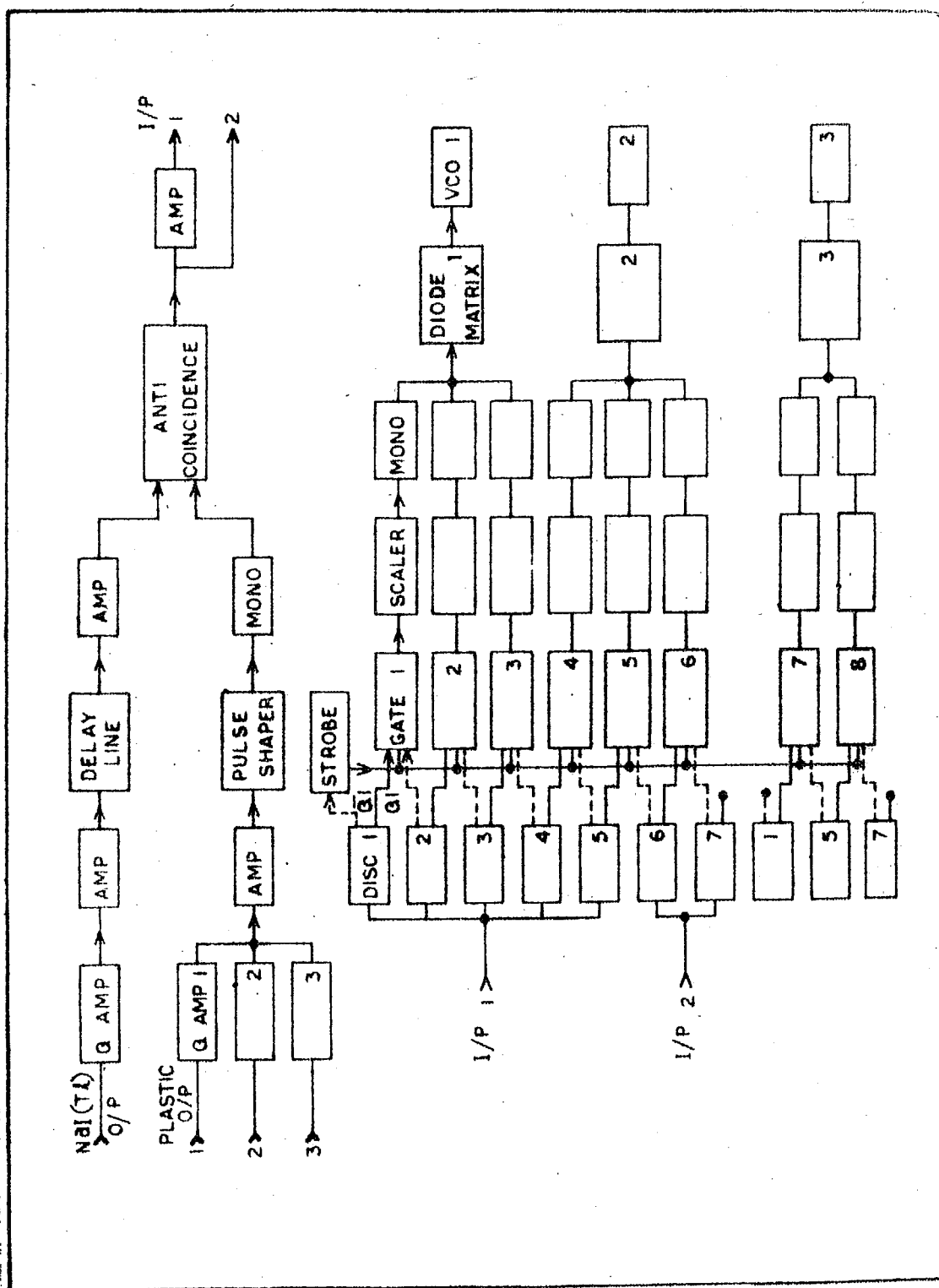
Fig. 38 - Schematic diagram of the pulse height analyser.

The output pulses from the main detector were pulse height analysed by a set of discriminators and coincidence gates. The count rates from each pulse height channel were prescaled with appropriate scaling factors. Two or three channels were mixed and fed to voltage controlled oscillators to modulate the subcarrier frequencies.

3.13 Orientation System

The need for locking the detector look directions in space is achieved by an orientation system, which uses the earth's magnetic field for reference. In order to achieve this, a servo system and magnetic sensors were employed (Seshadri et al. 1970). The telescope and the magnetic sensors were mounted on a circular platform. The inclination of the axis of the telescope with respect to local zenith, needed for the experiment was fixed before the flight. This circular platform was mounted through a thrust bearing on to an outer platform of square shape which was tied to the balloon. The detector platform is rotated with respect to the outer platform with friction drive by a D.C. motor fixed to it. The D.C. motor controlled by a servo system is suitably geared to roll the detector at 10 R.P.M.

The servo system is activated by an error signal generated by the magnetic sensor which senses the earth's magnetic field. Figure 39 shows the block diagram of the orientation system. The sensing element of the magnetic sensor consists of an
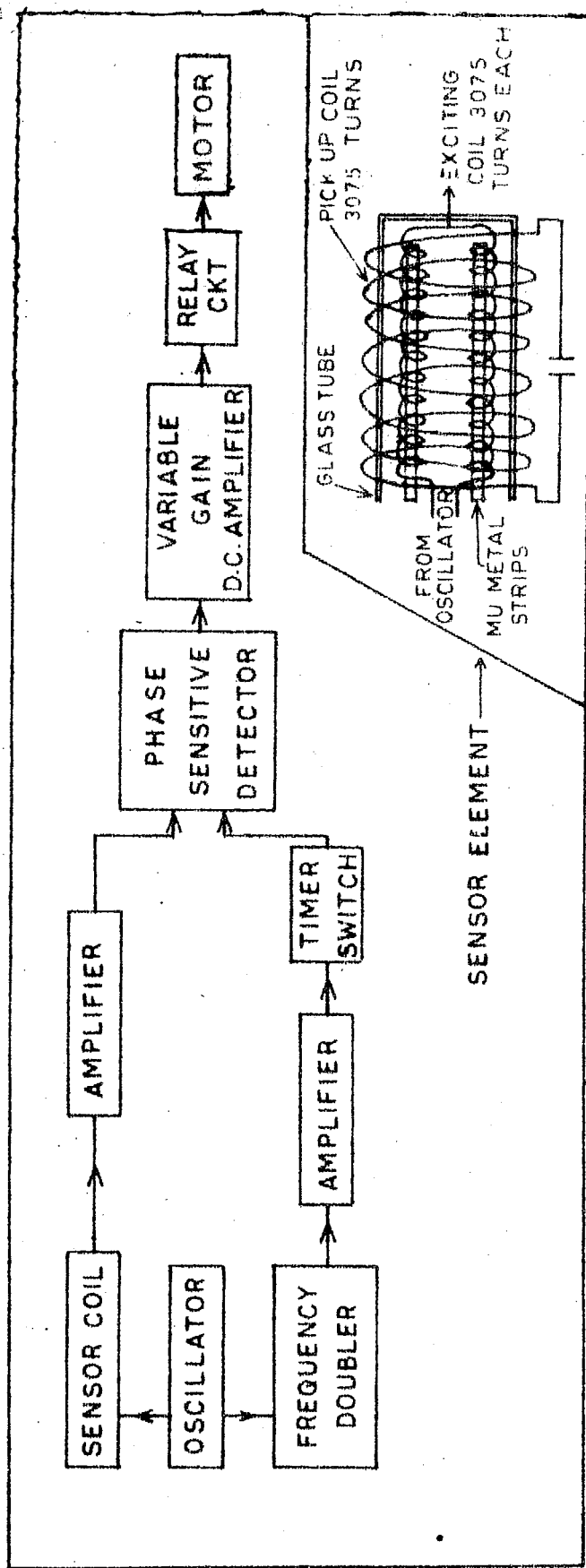
Fig. 39 — Block diagram of the orientation system. Inset shows the magnetic sensor coil.

exciting coil and a pickup coil wound over it. An oscillator at 4 kHz excites the exciting coil which consists of two parallel coils wound in opposite directions on a square loop hysteresis core (Mu metal). Only in the presence of an external magnetic field, a signal at twice the exciting frequency is present at the output of the sensing element. This signal after amplification is compared in a phase sensitive detector, against a reference signal generated from the oscillator, to sense the direction and intensity of magnetic field. This signal is then amplified in a variable gain amplifier to activate the D.C. Motor.

An East-West aligned magnetic sensor coil, for small perturbation of the balloon produces an error signal at the output of the phase sensitive detector. The variable gain amplifier, operating on the principle of pulse width modulation rotates the motor faster for greater deviations and controls the hunting normally associated with the correction.

An on board programmer, a Duncan timer motor, forms part of the circuitary as shown in figure 39, controls the look directions of the detector once in every five minutes during the flight. The programmer locks the detector, in the direction of South for 3.5 minutes, for 1.5 minutes due North and a few rotations in azimuth for 40 seconds in that order. During the rotation period the detector system and the magnetic sensors were calibrated. In addition the sun sensor comes to life during this period to provide attitude information.

This system allowed us to control the look direction of the detector to better than 1.5° in azimuth. Information regarding deviations greater than 1.5° in the South was obtained from two crossed horizontal sensors. This sector information, in the form of step voltage function, modulated the VCO'S provided for X-ray information.

3.14 Telemetry

The X-ray pulse height information as well as the attitude information was telemetered to ground through standard FM/FM telemetry technique. The aspect sector information, sun sensor information and X-ray pulse height information modulated the 5.4 KHz, 3.9 KHz and 2.3 KHz VCO channels. The continuous analogue magnetic information is separately telemetered using the subcarrier at 960 Hz. The output of the individual VCO'S were fed to a mixer amplifier, the output of which modulated the 108 MHz transmitter. A quarter-wave antenna was used for transmitting the output of the transmitter to the ground.

3.15 Construction and Environmental Testing

The mechanical design of the payload as shown in figure 40, consisted of a circular platform, free to rotate about the centre, and was supported by cross bars with respect to a square shaped outer platform. The telescope assembly was enclosed in an aluminium box, with an open top and was mounted on the circular platform through an universal joint. The detector assembly was supported with the help of gimbals so as
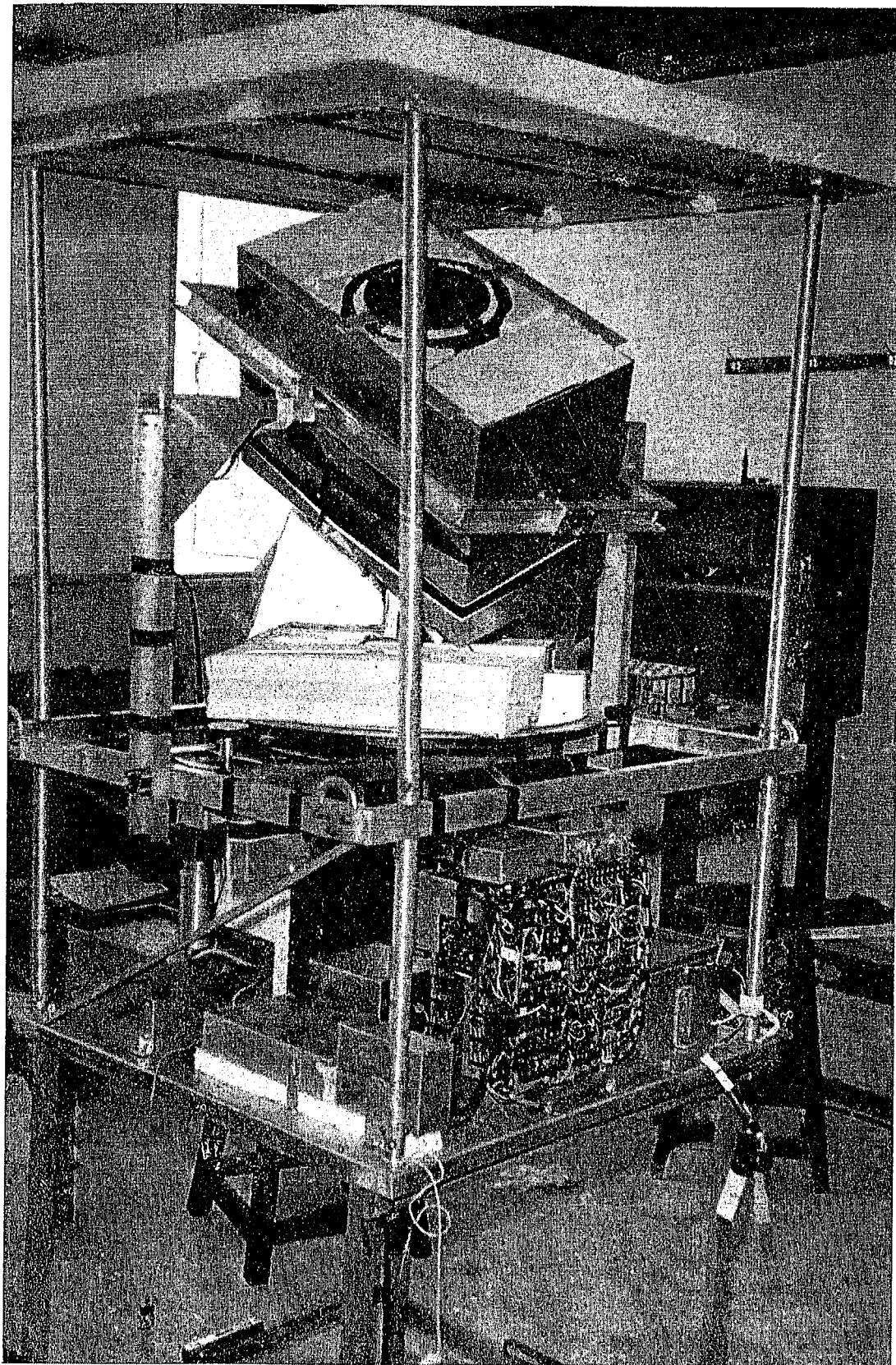
Figure 40 : Photograph of the Balloon borne X–ray payload flown on Nov. 15, 1971.

to enable the assembly to freely rotate about both azimuth and elevation. The magnetic sensor elements and the associated electronic packages were mounted on the circular platform. The sun sensor was placed inside the centre tube of the collimator system with its axis accurately aligned with the normal of the telescope.

The square shaped outer platform along with all the associated mechanical structures was tied to the balloon with strong tensile ropes. The electrical contacts between this outer platform containing battery packs, pulse height analyser system and telemetry packages and the inner platform was achieved through slip ring contacts. The antenna was mounted underneath this square platform at the centre. A wooden crash pad was provided for safe landing.

Extensive laboratory tests were performed on all the individual electronic units and detector system to test the ability of the detector system to withstand both low pressure and temperature environments. The photomultiplier base and high voltage units were potted with RTV60, silicone rubber compound, to prevent coronal effects. The individual modules were thermally insulated with 'Thermocole'. The entire payload was covered with 'Thermocole' sheets and was enclosed in a polythene bag to provide further thermal insulation. The performance of the detector shows that at no time the inside temperature went below $5^{o}C$ during the flight.
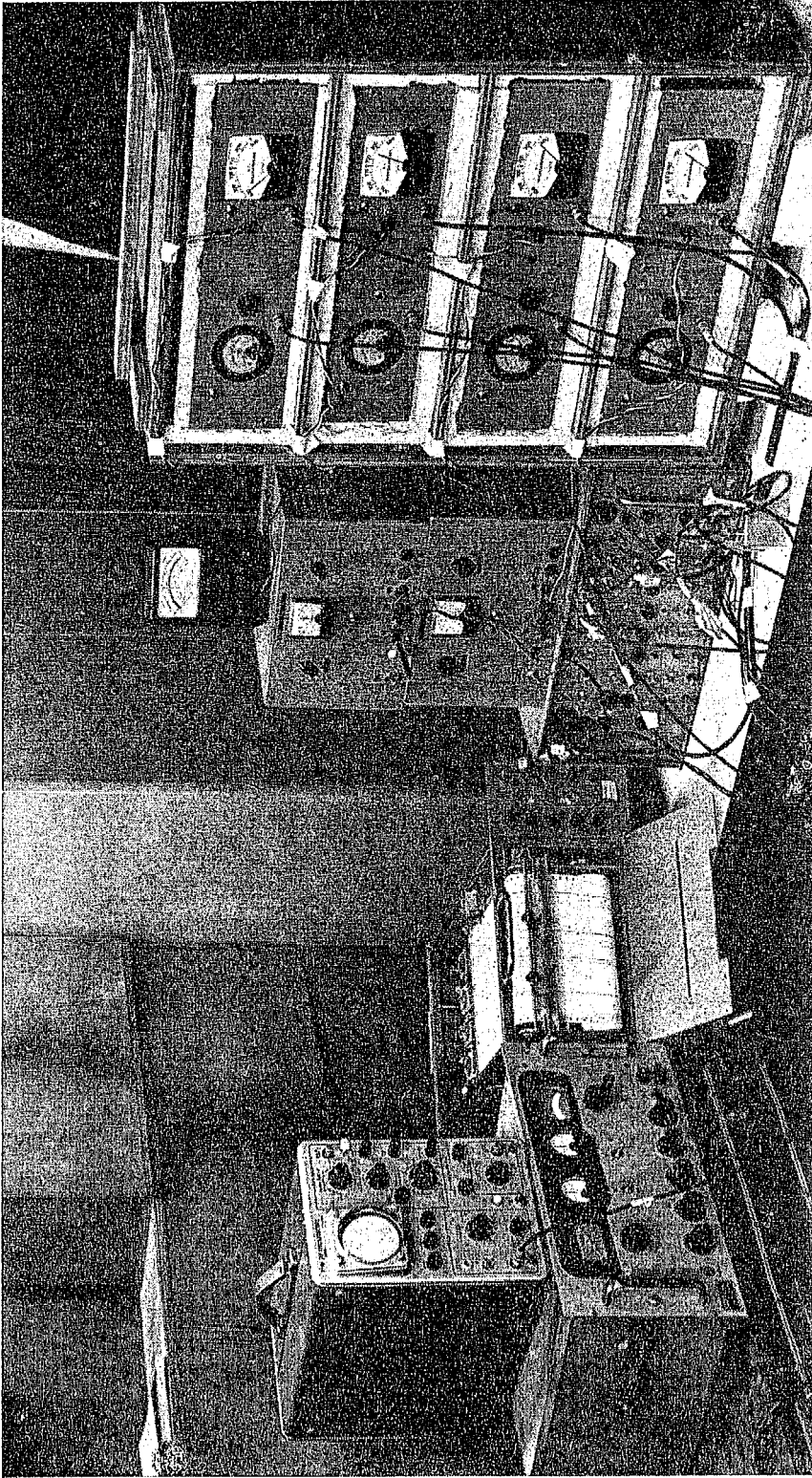
Figure 41 : Ground receiving system for Balloon experiments.

- 119 -
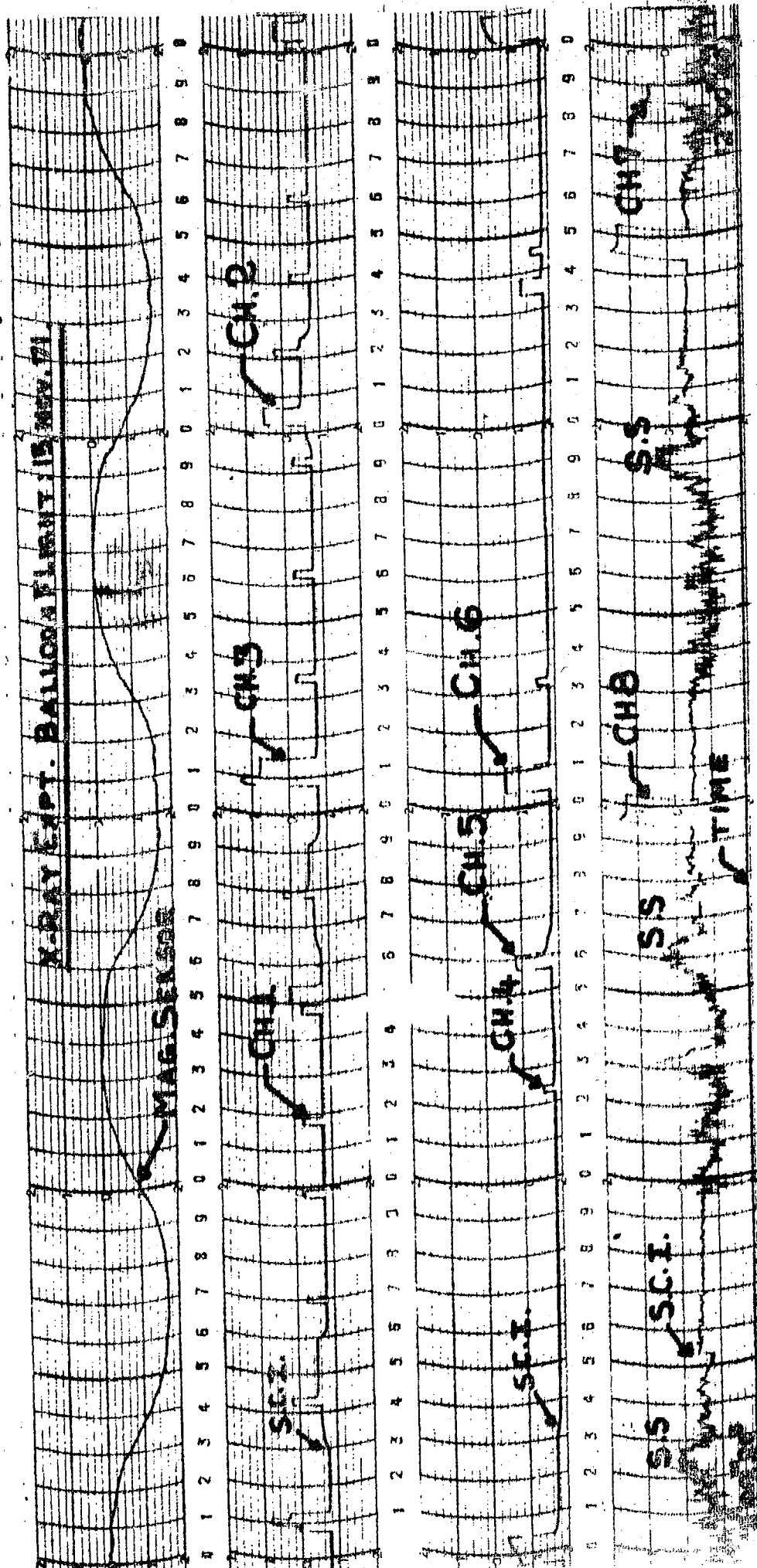
Fig. 42 - Sample chart record of Telemetry of the balloon flight. (CH. 1...8 - X-ray information, S.S - Sun Signal and S.C.I - Sector change information).

3.16 Launch and Recording

Sco XR-1 in its diurnal traversal, subtends a minimum zenith angle of 33° at Hyderabad. The detector elevation accordingly was adjusted prior to the flight and the magnetic sensors were properly aligned with respect to the earth's field. The launch was flawless and took place around 40 minutes after Sun rise in both the cases. The balloons remained over head till 1 p.m., after which they drifted east-wards to about 150 Km.

The ground receiving station for the experiments, consisted of an 8 element yagi antenna, FM receiver, compatible sub-carrier discriminators, D.C. amplifiers and a fast four channel recorder as shown in figure 41. Data was received continuously in real time, nearly till the touch down of the payloads. Figure 42 shows the sample record of the flight of November 17, 1971. The data also records 1 minute time marks, for easy identification of time.

3.2 Method of Analysis and Results

In this section we present the analysis and results of the flight conducted on November 15, 1971. The time-altitude curve, showing the performance of the 3 million cu.ft. stratospheric balloon with the 95.7 kg. X-ray payload launched at 0718 hrs. IST (0148 UT) is presented in figure 43, where the atmospheric depth in millibars and height in kilometers are plotted as a function of time. The balloon reached a float altitude of
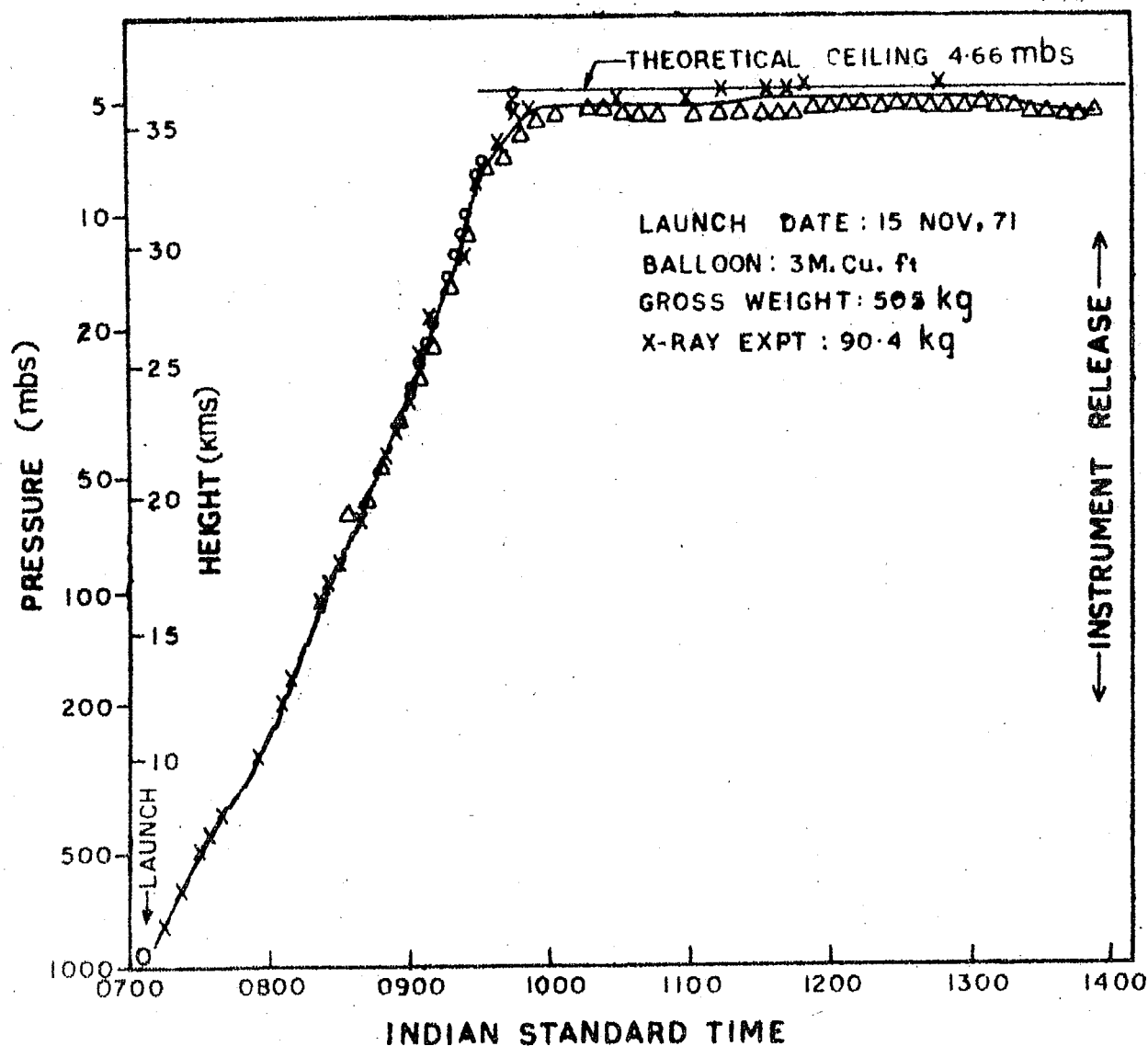
Fig. 43 - Time-altitude history of the balloon flight.
Radar data (O), W.T. data (△), Radio sonde
data (X).

35.6 Kms. at about 1000 hrs. IST and floated for about 4 hrs. at altitudes varying between 5.2 to 5.6 gms. cm^{-2}. The payload which functioned well throughout the flight was parachuted down to earth after cut off. Extensive calibrations were done after recovery to check the changes in the performance level of the detector in flight.

3.21 Data Processing

The X-ray data from the balloon as shown in figure 42, consisted of events for which the energy loss in the X-ray detector lies in the preset energy ranges. The X-ray detector was programmed to scan the sky at 33° zenith angle along the transit path of the Sco XR-1 source. The time profile of the data consisted of events recorded by the detector which was programmed to look in the direction due South for approximately 3.5 mts, and in the exactly opposite direction namely due North for 1.4 mts. The data recorded when the detector in motion changing from one direction to the other has been neglected for the analysis. The counting rates of the various energy channels in both directions are read and finally expressed as counts per minute as a function of time for the two modes of detector look directions separately.

The major contribution to the detector counting rate on the ground comes from the natural radio activity. As the detector ascends above the ground, the counting rate at first registers a sharp fall and then starts increasing due to the

increase in cosmic radiation intensity till it reaches a maximum at around a depth of about 150 gms. cm^{-2}, generally referred to as pfotzer maximum. Above the pfotzer maximum the detector counting rate starts dropping till it reaches a minimum at a depth of 10-15 gm. cm^{-2} of residual atmosphere and in fact should continue to further decrease, if there were no contribution from extra terrestrial sources. Inspite of the atmospheric absorption, the celestial X-rays can penetrate upto 10-15 gm. cm^{-2} depending on their energy, the degree of penetration being less at greater depths. Consequently from the upturn and the observed progressive increase in count rate at altitudes greater than 10 gm. cm^{-2}, the contribution due to the celestial X-rays can be evaluated.

Any X-ray telescope pointed in the direction of an X-ray source registers count rate due to two components. A small fraction of the total counting rate arises due to the X-ray emission from the source and the rest of it is contributed by the general diffuse X-ray background and secondary cosmic ray induced events. The balloon altitude data indicates an almost uniform depth of floating from 1115 to 1320 IST. In figure 44, the count rate obtained when the telescope looks due South, averaged over 10 mts interval for improved statistics, is plotted as a function of time in various energy channels. The average counting rate obtained during this time when the telescope looks due North and which registers only the background is also plotted for evaluating the source count rate.
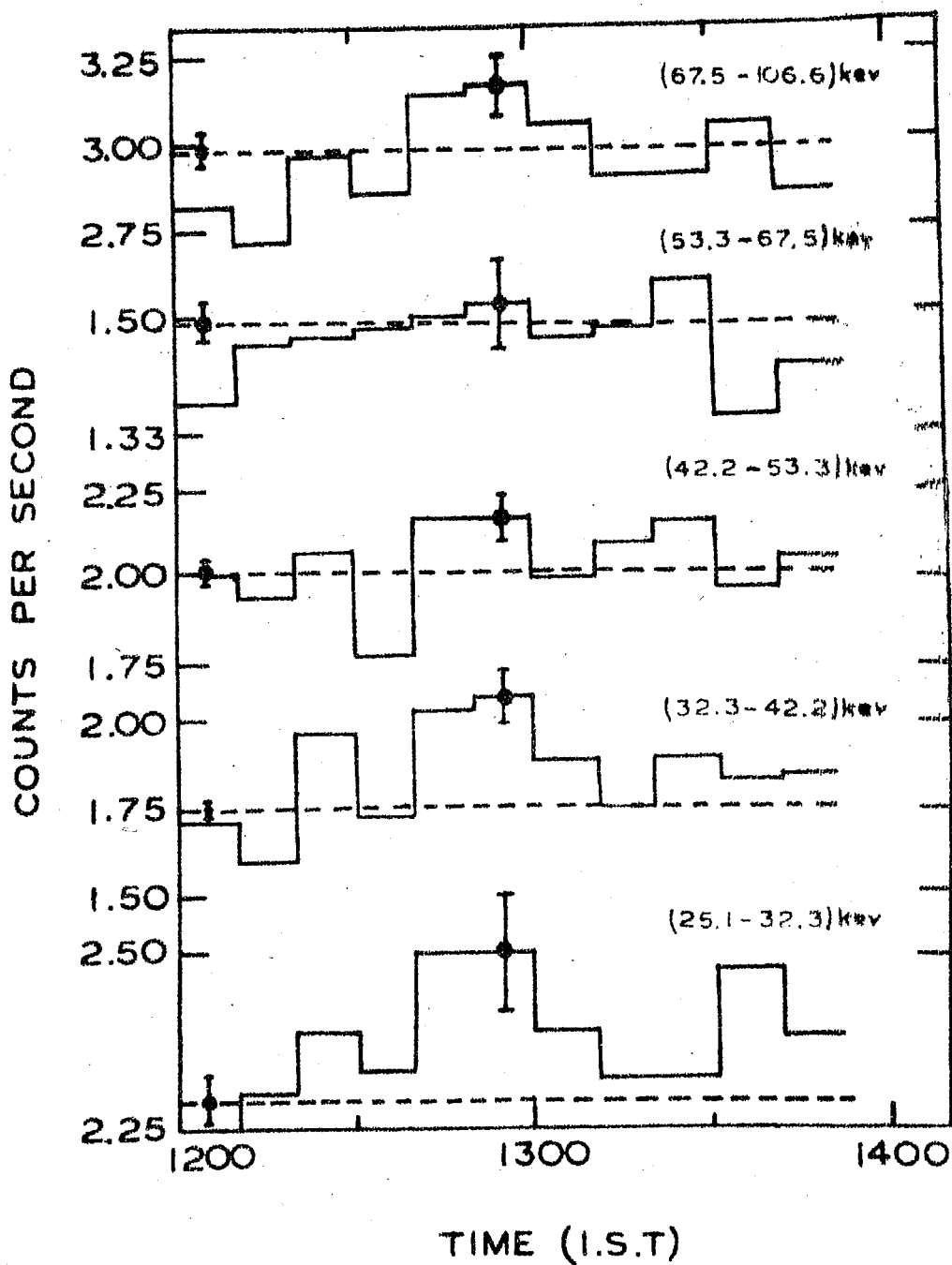
Fig. 44 — Counting rates of the telescope in the various energy channels due to Sco XR-1 (———) and general background is indicated by dashed line.

The back ground being omnidirectional, can be subtracted from the observed count rate to obtain counts due to the source.

3.22 Exposure Efficiency of the Detector

In order to evaluate the absolute flux from any point source it is necessary to compute the exposure efficiency of the detector as a function of time. The exposure efficiency of the detector depends on the collimation response of the telescope and the elevation of the telescope axis with respect to the source, which continuously changes as the source moves with respect to the stationary telescope axis.

A beam incident parallel to the detector axis, illuminates the full area of the detector. As the angle θ between the source beam and the detector increases, the illuminated area progressively decreases till it becomes zero at an angle θmax. The value of the limiting angle $\theta_{max.}$ is given by

$$\tan \theta_{max} = \frac{2r}{h} \qquad .. \ 3.2$$

where r and h are the radius and height of the collimator. The area exposed to the parallel beam at an angle θ is given by

$$A(\theta) = \frac{2}{\pi} A_o \cos\theta \left[\cos^{-1} (\cot \theta_{max.} \cdot \tan \theta) - \cot \theta_{max.} \cdot \tan\theta \sqrt{1 - (\cot \theta_{max.} \tan \theta)^2} \right] \qquad .. \ 3.3$$

where A_o is the area of the detector. Figure 45 represents the telescopic collimator response used in the flight. The full width at half maximum (FWHM) for the system is 11.6 degrees. For the 11.6° FWHM, the telescope traces two
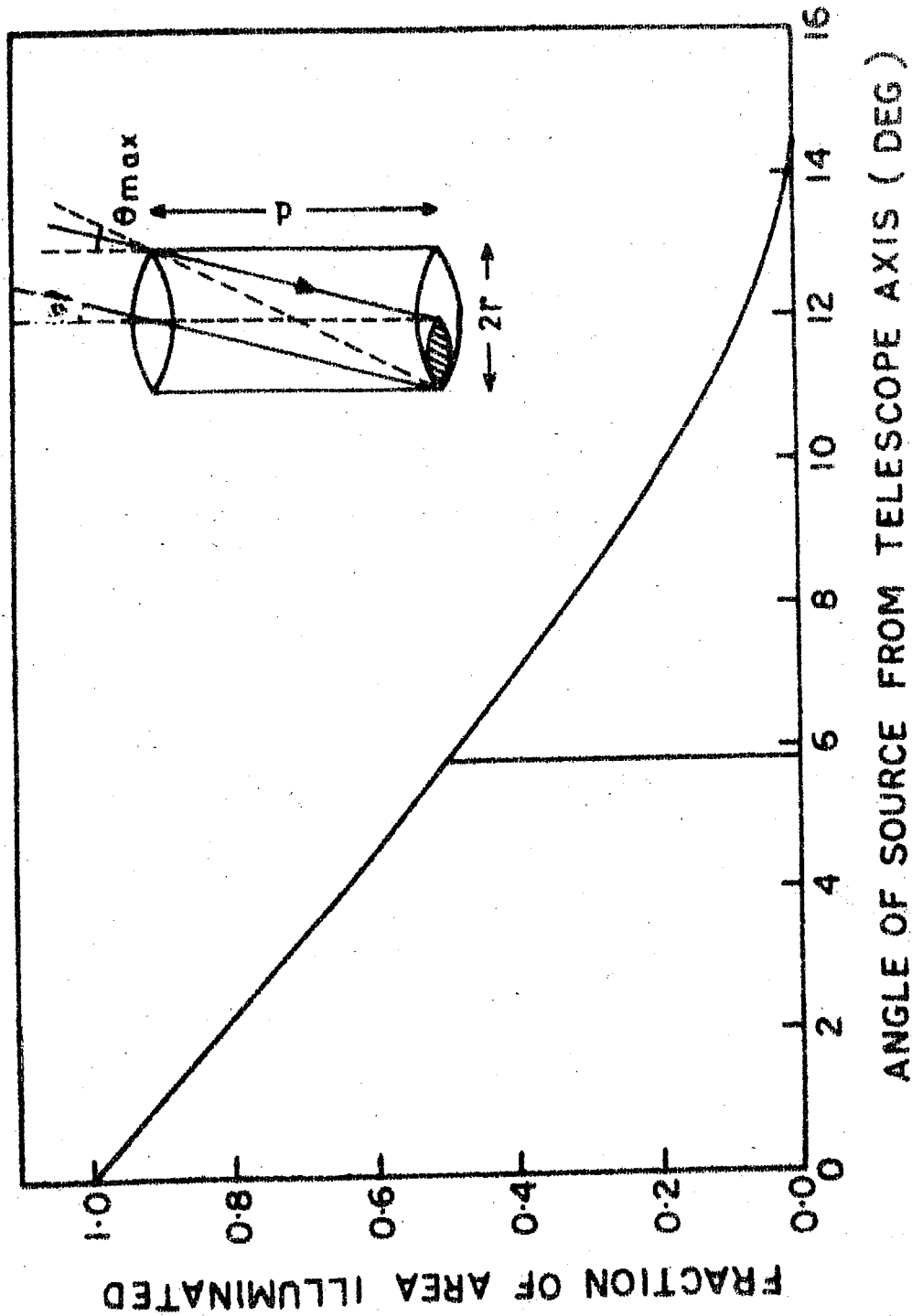
Fig. 45 – Angular response of the telescope as a function of the angle between the source and the telescope.

bands in the celestial sky in North and South directions with average declinations $+50.5^{\circ}$ and -15.5° respectively. In figure 46 we have plotted the trajectory of the various sources including Sco XR-1 on Nov.15, 1971, as they drift in time into the field of view of the telescope.

The angle θ between the source and telescope axis can be calculated from the relation

$$Cos\,\theta = Cos\,(A_T - A_S)\,Sin\,Z_T\,Sin\,Z_s + Cos\,Z_s\,Cos\,Z_T$$

.. 3.4

where A_S and Z_S refer to the Azimuth and Zenith angle of the source and A_T and Z_T are the respective angles defining the direction of the telescope axis. Combining equations 3.3 and 3.4, the exposure efficiency $\eta(t)$ of the telescope for any source at time 't' can be written as

$$\eta\,(t) = \frac{A\,(\theta)}{A_o}$$

.. 3.5

The total exposure ξ (cm^2-sec) for a source during its observation by the telescope can be computed, by integration over n equal intervals of time Δt, and is given by

$$\xi = A_o \sum_{i=1}^{n} \eta_i\,(t).\Delta t_i$$

.. 3.6

The total exposure time $T_o = \xi/A_o$ corresponds to time duration for normal incidence of X-rays from the source during the total observational period.
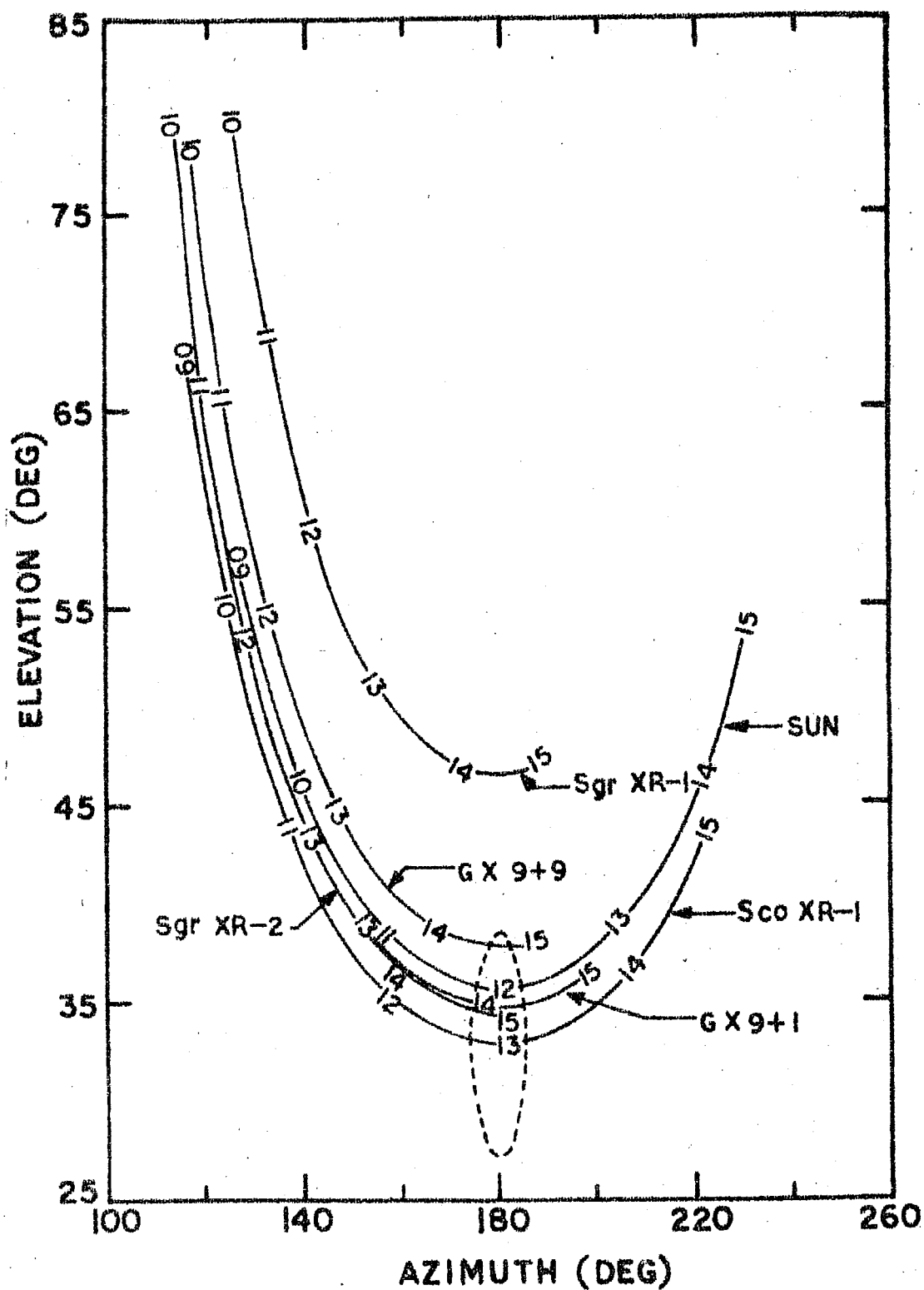
Fig.46 — Position of various X-ray sources in sky as a
function of IST over Hyderabad on 15th
November 1971. The dashed contour is the half
field of view of the telescope.

3.23 Evaluation of the Count Rate Flux of Sco XR-1 for Normal Incidence

Referring to the trajectory diagram it is observed that Sco XR-1 has a meridional transit at 1255 hours IST on Nov.15, 1971. The Sun was in the field of view of the detector till 1220 hours. The cluster of sources in the galactic centre region start drifting into view after 1315 hours. Consequently the count rate observed between 1220 to 1310 hours will have contribution only from Sco XR-1 source superimposed over the general background. The excess flux due to Sco XR-1 is evaluated, by subtracting the count rate recorded when the telescope looked 180° away in azimuth i.e. due North, from the count rate observed when Sco XR-1 is in the field of view. For the purposes of calculations the total excess counts in each channel during the period of time 1235-1310 IST, where the collimation admittance efficiency is greater than 60%, has been used. The differential count rate C_j due to the source at the depth of observation is

$$C_j \ (E_j) = \frac{S_j}{\xi \cdot \triangle E_j} \quad counts.cm^{-2}.sec^{-1}.KeV^{-1} \qquad .. \ 3.7$$

where Sj represents the total excess flux in the jth channel of average energy E_j and width $\triangle E_j$ for the duration of time ξ.

3.24 Absorption of X-Rays in the Atmosphere

A beam of X-rays passing through the atmosphere, undergoes attenuation by photoelectric and compton processes, the amount of attenuation varying with the energy of the incident X-rays.
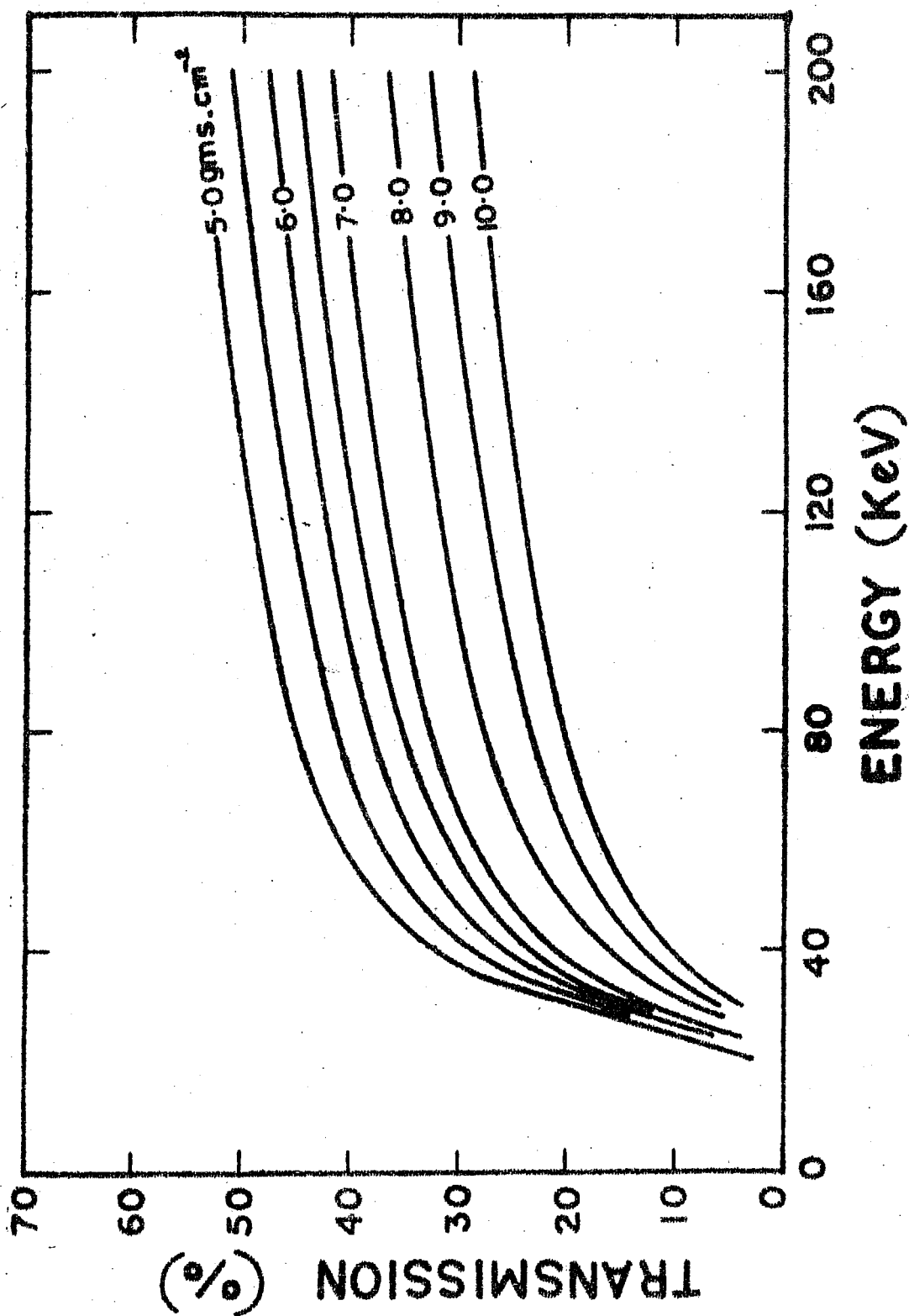
Fig. 47 - Transparency of X-rays of various energies in Atmosphere of different grammages.

At typical balloon altitudes of 5 gm.cm^{-2} of atmosphere, about 97% of 20 KeV X-rays and 85% of 30 KeV X-rays are absorbed. At higher energies the attenuation becomes less being 67% at 50 KeV and 53% at 100 KeV.

Considering the interaction of X-rays in the atmosphere, below 30 KeV, photoelectric process dominates while for X-rays above 40 KeV, the compton scattering becomes the important mode of interaction. In the calculation of diffuse background it has now been shown by Kasturirangan and Rao (1971) that consideration of multiple compton scattering is very important to arrive at the spectral shape and flux of X-rays. In the case of point sources the effect is relatively insignificant even though compton scattering of X-rays generally tend to slightly broaden the angular size of the source. The atmospheric attenuation factor for X-rays due to absorption can be written as

$$A(E) = e^{-\mu_a(E) X_a} \qquad\qquad .. 3.8$$

where $\mu_a(E)$ is the mass absorption coefficient for X-rays of energy E and X_a refers to the thickness of the atmosphere in gms.cm^{-2} along the line of sight. In figure 47 the transmission factor versus energy is plotted for various grammages of atmosphere traversed. As the zenith angle of the source practically remained constant during the period employed for our calculation of flux, the variation of attenuation factor with zenith angle, is negligible.

3.25 Spectral Analysis

Any form of incident spectra undergo distortions in propagation through the overlying atmosphere and in the detector. The flux $F^1(E^1)$ at energy E^1 for a spectral form $J(E)$ of the incident spectrum can be written as

$$F^1(E^1) = \int_0^\infty J(E) \, A(E) \, \in(E) \, R(E, E^1) \, dE \qquad .. \ 3.9$$

where $A(E)$ represents the absorption in the air and $\in(E)$ the efficiency of the detector system given by expressions 3.8 and 3.1 respectively. The resolution spread, $R(E, E^1)$ due to statistical process has the gaussian form

$$R(E, E^1) = \frac{1}{\sqrt{2\pi}\,\sigma} \exp\left[-\frac{(E - E^1)^2}{2\sigma^2}\right] \qquad .. \ 3.10$$

where $\sigma = \frac{FWHM}{2.355}$ E. The flux $F^1(E^1)$ is integrated between energy bands E_{1j} and E_{2j} of the jth channel to give the average count rate flux C_j^1 and is

$$C_j^1 = \frac{1}{\Delta E_j} \int_{E_{1j}}^{E_{2j}} F^1(E^1) \, dE^1 \quad counts.sec^{-1}.cm^{-2}.KeV^{-1}$$
$$.. \ 3.11$$

where ΔE_j is the channel width in KeV.

The functions representing absorption in the atmosphere and the efficiency of the detection system exhibit steep linear variations below 30 KeV, but are practically constant above this energy. The effect of limited resolution, which flattens the spectrum is small especially at higher energies. So to a first approximation, the incident spectrum can be directly inferred from the observed count rate C_j (expression 3.10) by

taking average values for $A(E)$ and $\in(E)$ and neglecting the effect of $R(E)$. Later this spectral form is substituted in the convolution integral 3.9 and by successive iterations the functional form for the incident spectrum can be obtained.

In our calculations we assumed two different spectral forms — a power law and an exponential form for the energy spectra. The photon power law spectrum representing the synchrotron emission mechanism

$$J(E) \; dE = K \; E^{-\lambda} \quad dE \quad photons.cm^{-2}.sec^{-1}.KeV^{-1} \qquad .. \; 3.12$$

and the thermal bremsstrahlung emission

$$J(E) \; dE = K \; E^{-1} \exp(-E/T_e) \; dE \quad photons.cm^{-2}.sec^{-1}.KeV^{-1}$$
$$.. \; 3.13$$

where λ and T_e represent the electron spectra responsible for the X-ray emission and K is the intensity constant, have been considered.

3.26 Sco XR-1 Spectrum

In figure 48, we have plotted the energy spectrum of Sco XR-1 on a log-linear scale. The count rate in the first two channels are significant at 3 σ level. Only upper limits could be provided for the 53-67 KeV channel as no positive flux is observed (figure 43). The other channels including the sum channel have ~2σ level significance. The figure 48 shows the energy spectrum above about 40-50 KeV becoming flat. The energy flux in the first three channels was fitted to an
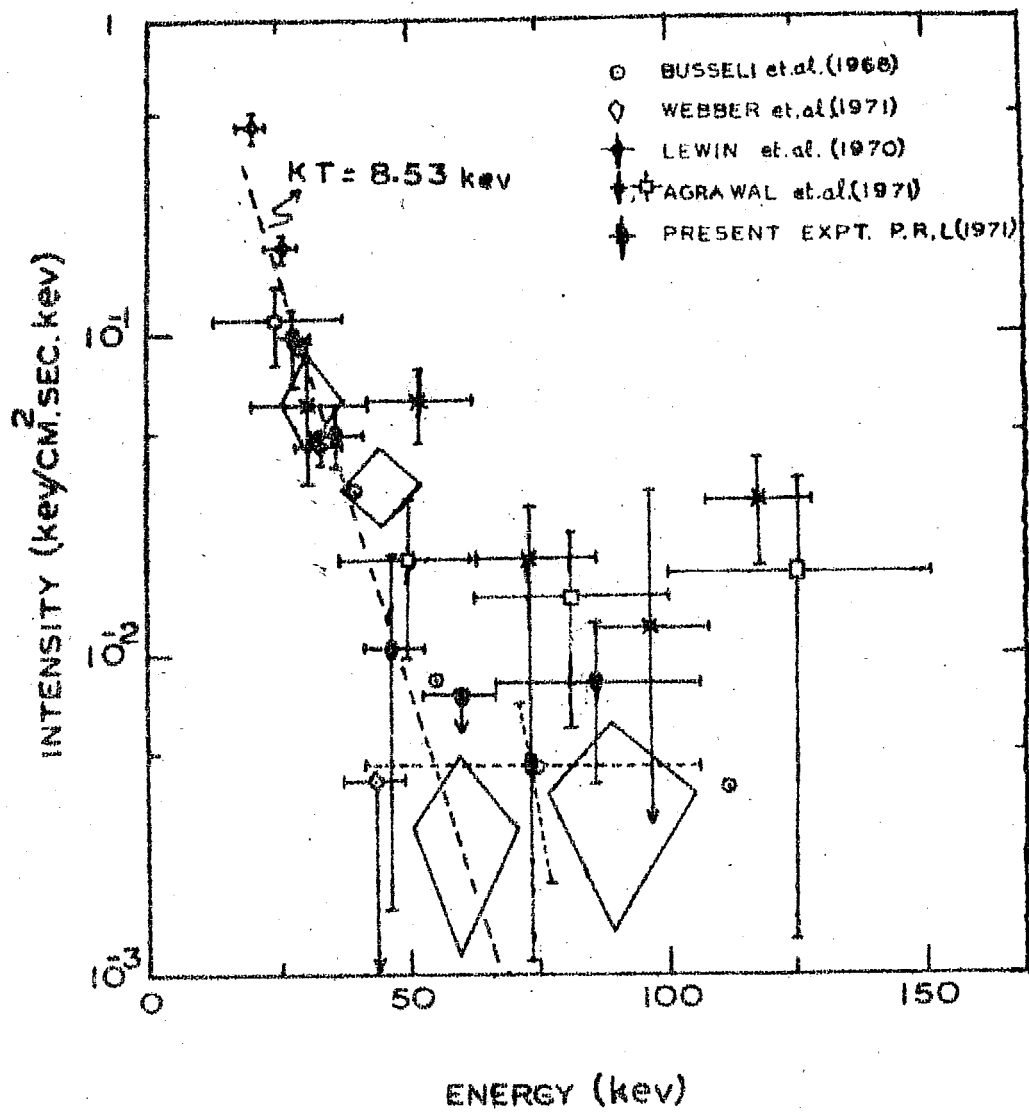
Fig. 48 - Observed energy spectrum of Sco XR-1.
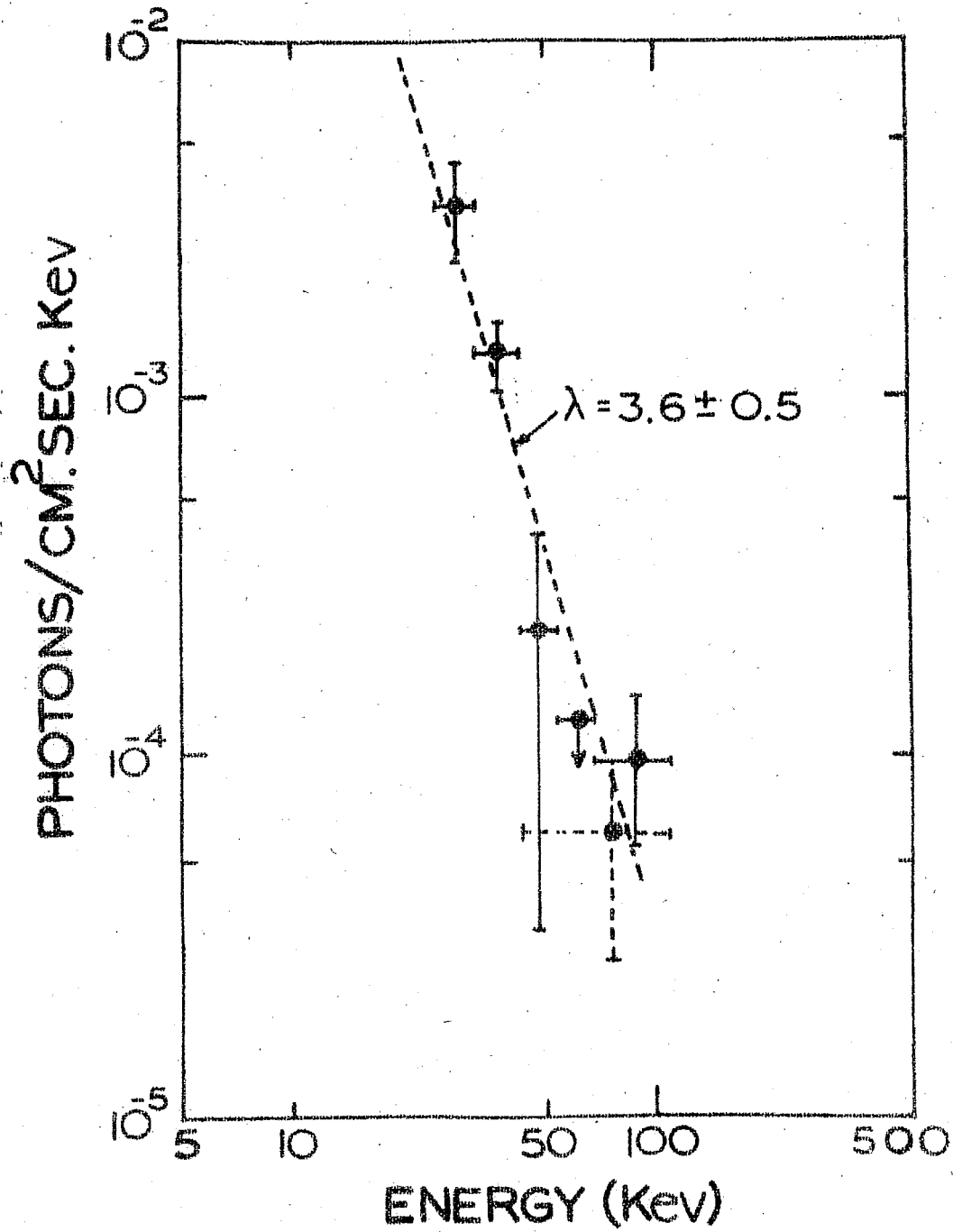
Fig.49 - Photon flux of Sco XR-1 versus X-ray energy.

exponential spectrum, as no single temperature can represent the entire spectrum upto 100 KeV. The characteristic temperature associated with bremsstrahlung emission from a hot thin plasma was found to be $\sim 9 \times 10^{7}$ ^{0}K, a value which agrees with the observations obtained at energies below 20 KeV. Along side are plotted the results of other experimenters and are in general agreement with the results obtained by us. The power law fit for all the channels show a good fit with a photon exponent of 3.6 ± 0.5. In figure 49 we have plotted the photon flux against energy with this power law spectral fit. The spectrum, if it represents a synchrotron emission mechanism, has a slope much steeper than Tau XR-1 or Cyg XR-1. The discussion of these results along with other similar observations are presented in the next chapter.

. . . . .

DISCUSSION ON SCO XR-1 RESULTS

In this chapter we discuss the results presented previously and determine the spectral characteristics as well as the physical parameters of the star Sco XR-1. We attempt to formulate a self consistent model from the observational features and discuss them in terms of the model proposed. In this process we examine not only X-ray observations but also the observations in the other regions of the source and their interrelations.

4.1 Low Energy X-Ray Observations

The differential X-ray flux measurements reported earlier have been fitted to a simple exponential spectrum

$$I(E) \, dE = A \, e^{-E/kT} \qquad \ldots 4.1$$

which represents the radiation emitted from a hot thin plasma, to a first degree approximation. In the above equation I(E) represents the differential energy spectrum and k is Boltzman's constant. In this expression the gaunt factor that occurs in the bremsstrahlung collision cross section is assumed to be constant, and its variation with electron energy (E_e) and photon energy (E) is neglected. For a more exact expression, we use the non-relativistic bremsstrahlung collision cross section without nuclear screening (Koch & Motz 1965) which can be expressed as

$$\frac{d\sigma}{dE} = \frac{16}{3}\alpha \quad \frac{Z^2 r_e^2}{\beta^2} \cdot \frac{1}{E} \cdot \left\{ \ln\left[\frac{\beta+\beta^1}{\beta-\beta^1} \right] \right\} \cdot$$

$$\frac{\beta}{\beta^1} \cdot \left[\frac{1 - \exp\left(\frac{-2\pi Z\alpha}{\beta}\right)}{1 - \exp\left(\frac{-2\pi Z\alpha}{\beta^1}\right)} \right] \right\} \qquad \ldots 4.2$$

where α is the fine structure constant, r_e is the classical electron radius, $\beta \left(=\sqrt{\frac{2E_e}{mc^2}}\right)$ and $\beta^1\left(=\sqrt{\frac{2(E_e - E)}{mc^2}}\right)$ are the velocities of the electron before and after collision. In this expression the term $\frac{\beta}{\beta^1}$ times the last term is the Elwert factor. At low frequencies ($E \ll kT$) the Elwert factor is unity. At high frequencies ($E \gg kT$) this factor departs from unity, however, for low Z materials this correction is not large. Setting this factor at unity, the intensity can be obtained by folding this bremsstrahlung crosssection with the maxwellian electron energy distribution and can be expressed for all photon energies as

$$I(E)\ dE = A_1\ e^{-E/kT} \left[e^{E/2kT} K_0\left(\frac{E}{2kT}\right) \right] dE \qquad \ldots 4.3$$

where $K_0(X)$ is a modified Bessel function of the second kind. The function $K_0(X)$ has the form for $E \ll kT$

$$K_0\left(\frac{E}{2kT}\right) = \ln\left(\frac{4kT}{E}\right) - 0.577$$

and for $E \gg kT$ $\qquad\qquad\qquad\qquad\qquad\qquad \ldots 4.4$

$$K_0\left(\frac{E}{2kT}\right) = \sqrt{\frac{\pi}{2}} \cdot e^{-E/2kT} \cdot (E/2kT)^{-\frac{1}{2}}$$

Thus the intensity spectrum $I(E)$, due to bremsstrahlung process will have a form which is not a simple exponential function but depends on the form as expressed by equations 4.3 and 4.4.

TABLE IV

Comparison of Intensity Functions Describing Bremsstrahlung

Photon Energy (KeV)	Modified Bessel Function (Equation 4.3)	Simple Exponential Function (Equation 4.1)
0.01	7.2	1.87
0.1	4.72	1.82
1.0	2.19	1.52
3.0	1.02	1.02
5.0	0.56	0.68
8.0	0.25	0.37
10.0	0.15	0.25
15.0	0.048	0.093
20.0	0.015	0.051
30.0	1.7×10^{-3}	4.5×10^{-3}
40.0	2.0×10^{-4}	6.2×10^{-4}
50.0	2.5×10^{-5}	8.4×10^{-5}
80.0	4.8×10^{-8}	2.1×10^{-7}
100.0	8.0×10^{-10}	3.8×10^{-9}

Table showing the intensities derived using simple exponential formulation and using gaunt factor variation expression. Both these intensities have been computed for $Z = 1$, $kT = 5$ KeV and normalised at photon energy = 3 KeV.

In Table IV we present a comparison between the results obtained using this modified Bessel formulation and the simple exponential which has been often used in X-ray astronomy literature. These expressions have been computed for $\bar{Z} = 1$ and kT = 5 KeV and have been normalised at the X-ray photon energy, E = 3 KeV. It is clear from the table that at very low photon energies ($\angle$ 2 KeV), the estimates from equation (4.3) are higher than the simple exponential function and vice versa - in the higher X-ray energy range(>15 KeV). In the X-ray region 2-15 KeV they are nearly equal.

Using this modified expression the spectrum of Sco XR-1 has been derived for each of the four rocket flights N.A.40.04, N.A.40.05, K-9M-27 and S-210, observations. Figure 50a shows the spectral fit for the energy flux in the case of experiments conducted on 26th and 28th April from TERLS and figure 50b for the two experiments performed on August 7th and 8th from KSC. The temperatures derived by including the gaunt factor calculations are shown in the respective figures. It is seen that the derived temperatures (7 KeV and 9 KeV) with the exact expressions for the N.A.40.04 and N.A.40.05 observations are significantly higher than the simple exponential fit values (5 KeV and 7 KeV).

In Table VI are listed the temperatures obtained for the epoch corresponding to each of the rocket flights conducted by us. An examination of table clearly indicates that the temperature of the source varies from epoch to epoch in a
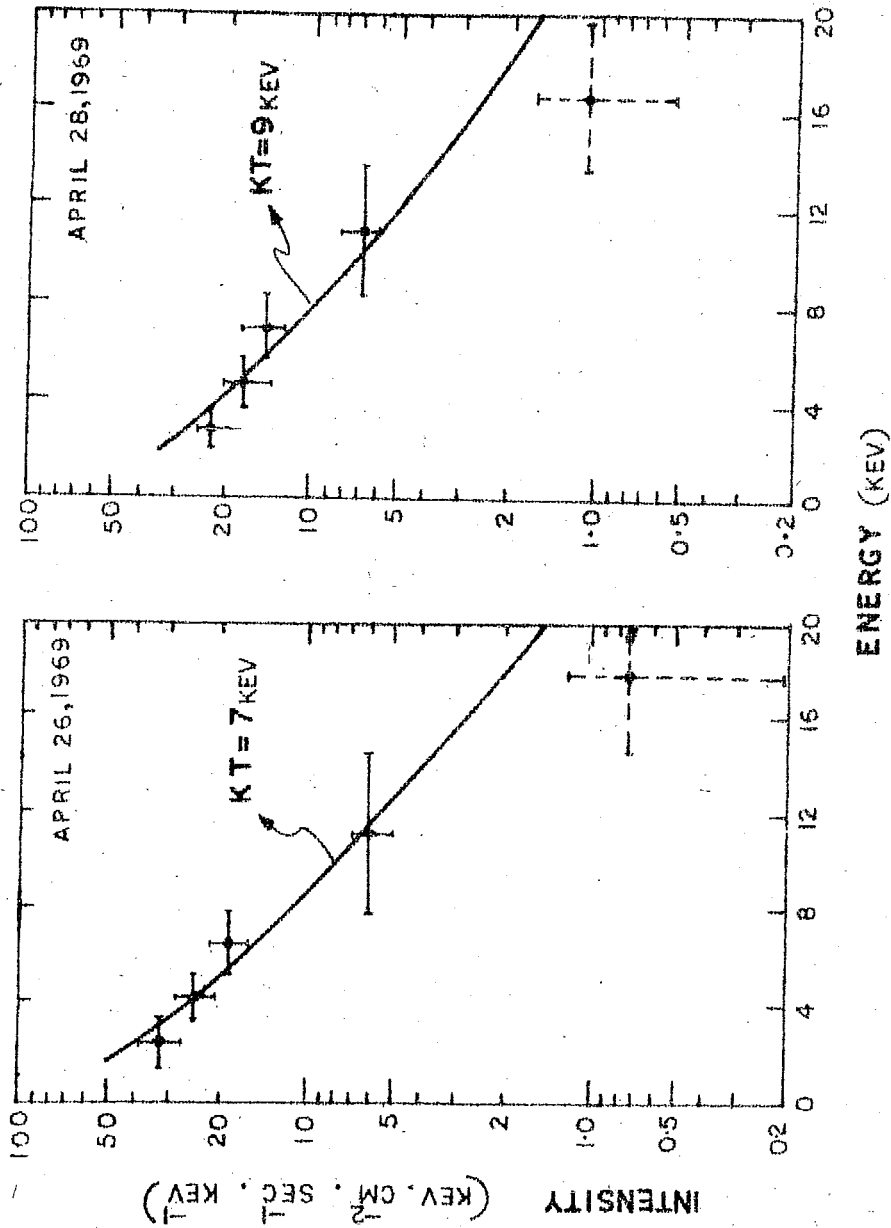
Fig. 50a — The energy spectra of X-rays from Sco XR–1 observed from TERLS.
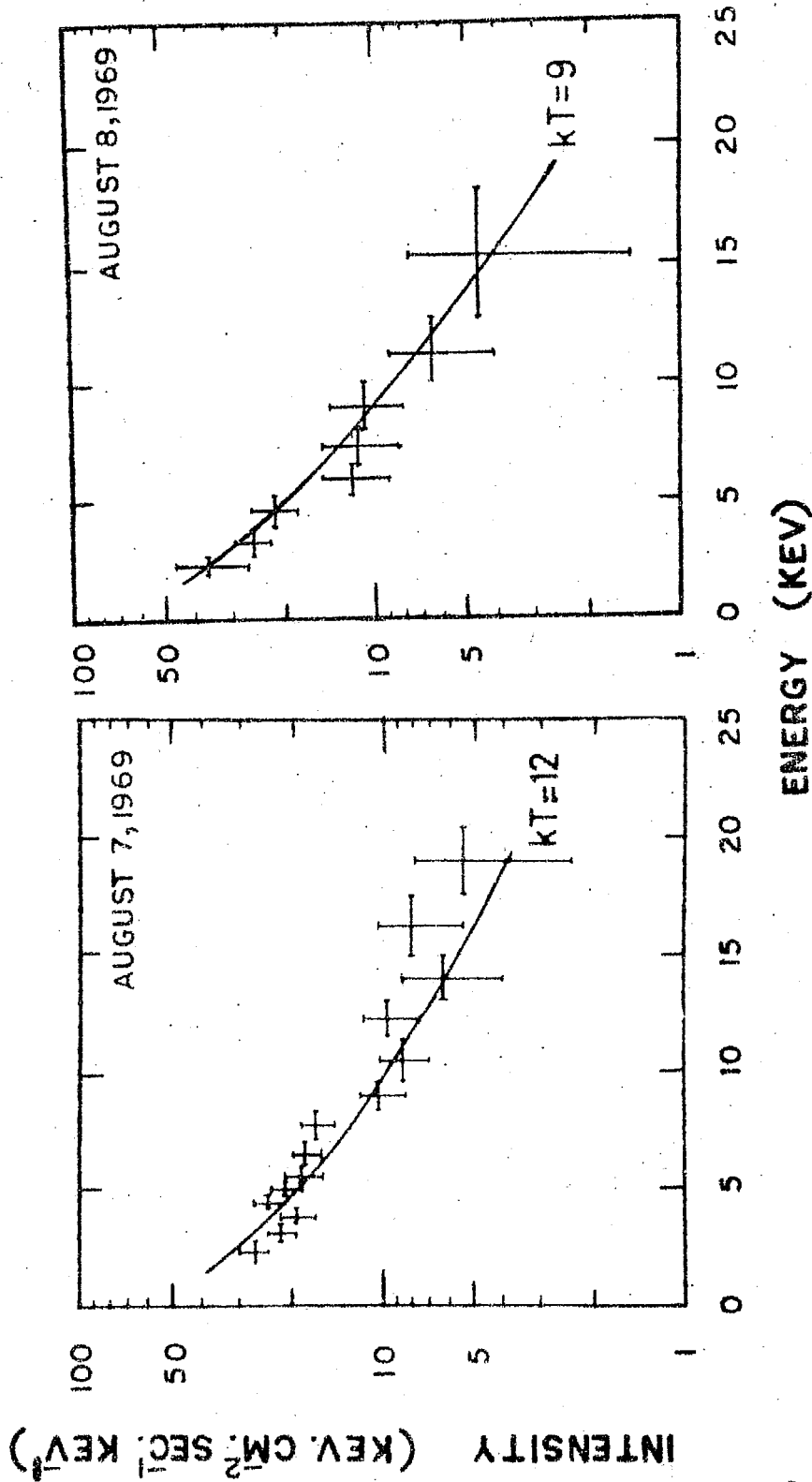
Fig.50b- The energy spectra of X-rays from Sco XR-1 observed from Kagoshima space centre.

significant manner. The existence of such variations in the
energy flux and spectrum has been observed by other workers as
the table indicates (Burginyon et al. 1970). Since it is now
recognised that the low energy X-ray flux from Sco XR-1 is
representative of thermal bremsstrahlung emission from hot thin
plasma, the observed variation in temperature of the plasma and
the flux of X-ray emission have been utilised to understand the
physical parameters of the source.

We assume a simple model for the source namely a spherical
cloud of hot plasma at a uniform temperature. Even though such
simple models are not completely realistic, nevertheless they
help us in gaining a quantitative insight into the physical
mechanism responsible for X-ray emission of the source. The
free-free emission flux at a distance d from a source consisting
of
of a spherical cloud/hot plasma of radius r at a uniform tempe-
rature T and having uniform particle density n, can be repre-
sented by

$$I_{ff}(E) = 3 \times 10^{-15} . \frac{n^2 r^3}{3d^2} . g . \exp\left(\frac{-E}{kT}\right).(kT)^{-\frac{1}{2}}$$

$$KeV.sec^{-1}.cm^{-2}.KeV^{-1} \qquad \ldots 4.5$$

where g is the gaunt factor, r and d are in cms, n is in cm^{-3}
and the photon energy E and kT are in KeV. If the cloud is
fully transparent to X-rays, the X-ray emission measure $n^2 r^3$
can be evaluated for the observed temperature T, assuming a
reasonable value for the distance d. The emission parameter
$\frac{n^2 r^3}{3d^2}$ of Sco XR-1 is evaluated for each observation, utilising
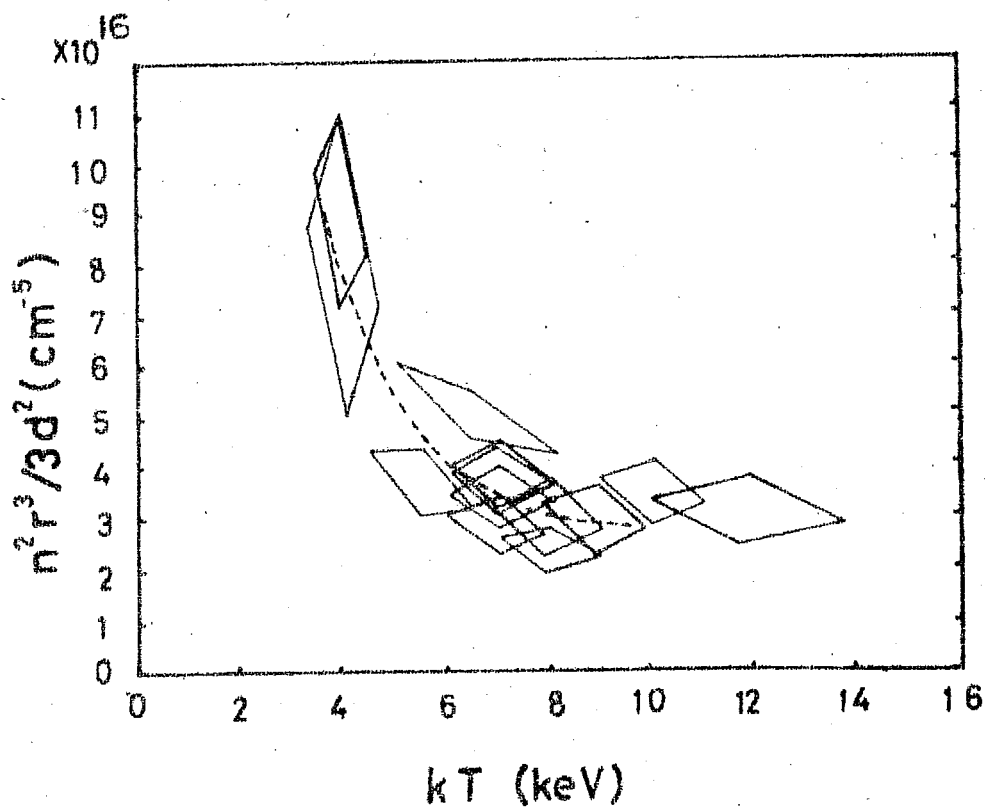
Fig. 51 - The relation between the temperature KT and the value of $\frac{n^2 r^3}{3d^2}$ of Sco XR-1 compiled from the results obtained by rocket observations.

the intensity observations at 6 KeV, where the efficiency for
the observation in general is maximum and is also tabulated in
table VI.

Figure 51, presents a plot of $\frac{n^2 r^3}{3d^2}$ versus temperature kT
for many observations both from our group and LRL group. The
plot indicates a definite unique relationship between $\frac{n^2 r^3}{3d^2}$ and
temperature as represented by the dashed line. The emission
measure is inversely proportional to kT. The relationships
between kT and individual parameters n and r cannot be obtained
from X-ray data alone and therefore we have used data from the
simultaneous optical observations for deducing the magnitudes
of individual physical parameters n and r and their interrelat-
ionship with kT.

4.2 High Energy X-Ray Region

Before proceeding with a discussion of the behaviour of
Sco XR-1, X-ray source at high energies, we will compare our
results obtained from balloon flight over Hyderabad with similar
results obtained by other workers. In figure 52 we have
plotted most of the available world data on the energy spectrum
of Sco XR-1 together with our observations. Above 20 KeV we
have shown practically all the available data points from
various balloon flight experiments. At low energies below
20 KeV we have included the results from our rocket flights and
these represent adequately the average flux generally observed.
In addition two rocket experiments of Grader et al. (1966) and
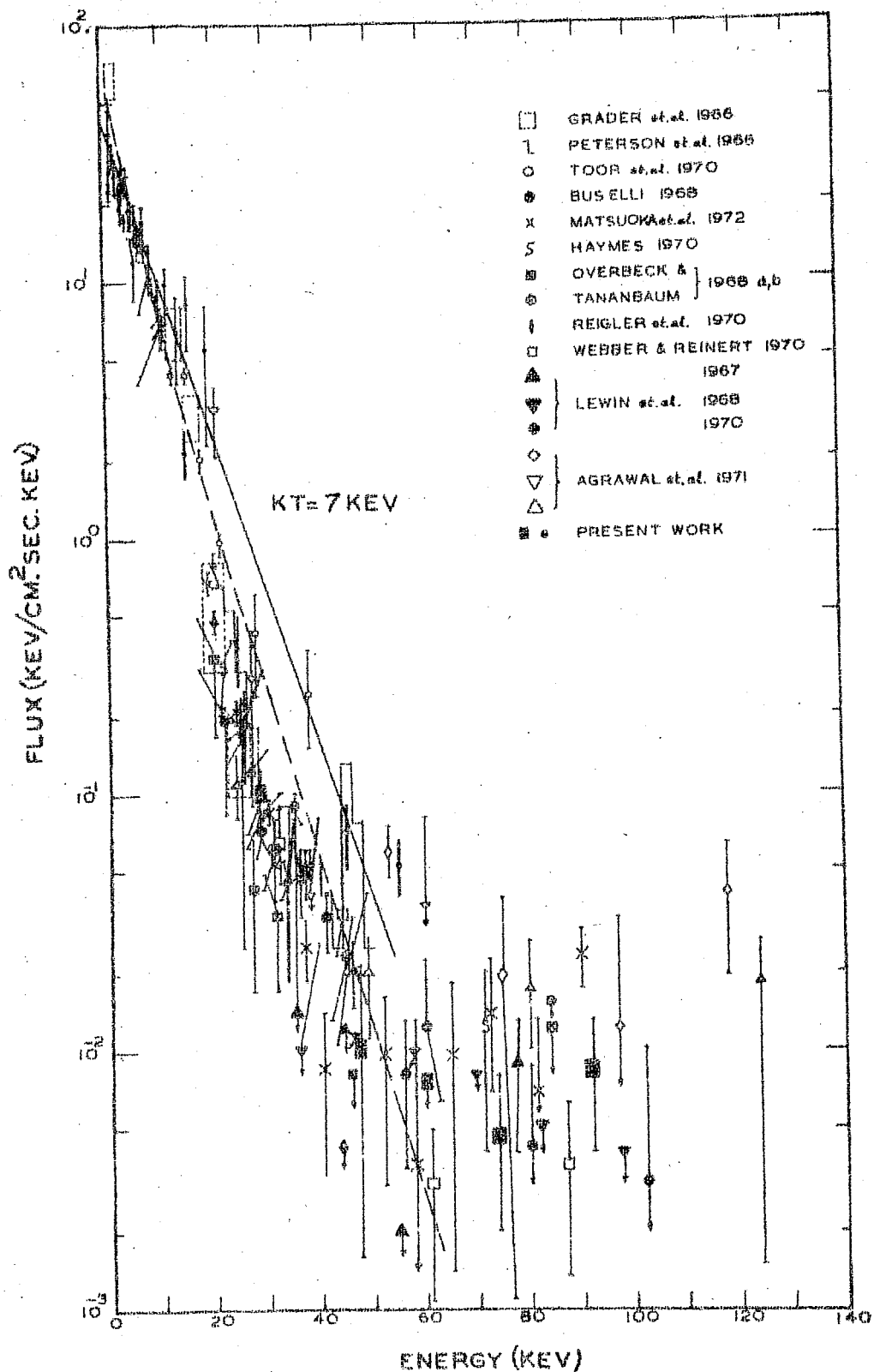
Fig. 52 - Energy spectrum of Sco XR-1 measured by various
investigators at different energies. Simple
exponential (straight line) and fit with gaunt
factor variation (dashed line) at temperature
kT = 7 KeV are shown.

line emission. A similar feature, though less significant, was observed by Reigler et al. in the 40-50 KeV band. However, since this feature is not confirmed by other workers we shall disregard this observation for the present.

Comparing the various observations above 50 KeV, it is apparent that even though most of the values reported are significant at only 1-2 σ level, and inspite of many disagreements between different observations, the observations clearly indicate the existence of positive high energy X-ray flux from the source. However, the large statistical errors associated with the observations preclude us from deriving definite conclusions regarding these flux variations. In spite of the large statistical errors, it is noticeable that there are definite instances, like that reported by Matsuoka et al. at 90 KeV and Agrawal et al. at 120 KeV where the observed fluxes have been significantly higher than most of the other observations which clearly indicate the existence of strong time variations, even at higher energies.

4.22 Spectrum

Even though a simple exponential fit can adequately represent the flux below 20 KeV, the situation becomes entirely different when rocket and balloon results are considered together. In figure 52, where both the observations at low and high energies are plotted, two theoretical fits one describing a simple exponential and another incorporating the gaunt factor

variation are considered. These fits are normalised at 5 KeV to adequately describe the low energy results. It is evident from the figure that the theoretical fit which employs a simple exponential fails to describe the high energy observations. Whereas the theoretical expression using the exact expression is better fit upto 40 KeV, it is still evident that the observation points in the 20-40 KeV fall below the theoretical curve. In other words the observed results in the limited range of 2-40 KeV are not consistent with a hot thin plasma at a single temperature.

As in the case of cosmic diffuse X-ray background, it can be suggested that the discrepancy or apparent break in the spectrum could be due to the difference in techniques viz. rockets and balloons. In the case of diffuse X-ray background, when multiple compton scattering of X-rays in residual atmosphere is taken into consideration, the discrepancy between rocket and balloon observations can be resolved satisfactorily. However, for a point source this correction is negligible and as such is not applicable. In order to avoid this ambiguity, we have closely examined the rocket observations of Grader et al. and Toor et al. which covers the entire 2-40 KeV energy range. Even though both these experimenters claim that their data can be fitted to a single exponential spectrum, a closer scrutiny of the observations between 15 to 40 KeV indicate a steeper slope than the 2-15 KeV range. Further, in view of the fact that the fluxes quoted by these authors are

TABLE V

Exponential and Power Law Fits for Intensity Observed by Various Experimenters

Experimenter	Flight Date	Exponent α	R_p	T_p	Temperature (KeV)	R_e	T_e
1. Peterson & Jacobson (1966)	5. 18.65	3.1 ± 0.5	0.84	5.6	11^{+3}_{-4}	0.79	4.8
2. Reigler & Ramatty (1970)	12.15.66	3.0 ± 0.8	0.89	3.9	12^{+7}_{-3}	0.80	2.7
3. Lewin et al. (1967)	2. 13.67	2.5 ± 1.3	0.76	2.0	22	0.65	1.5
4. Lewin et al. (1968)	10.15.67	2.2 ± 0.6	0.84	3.5	27^{+15}_{-8}	0.77	2.7
5. Lewin et al. (1970)	3. 20.69	3.2 ± 0.7	0.95	4.6	10^{+4}_{-2}	0.92	3.3
6. Overbeck & Tananbaum (1968)	5. 15.67	2.1 ± 0.9	0.82	2.5	25	0.69	1.6
7. "	6. 26.67	2.4 ± 0.7	0.90	3.5	22^{+16}_{-7}	0.81	2.4
8. Buselli et al. (1968)	2. 29.68	2.9 ± 0.3	0.97	9.7	19^{+4}_{-3}	0.94	5.4
9. "	"	3.8 ± 1.1	0.96	3.6	13^{+7}_{-3}	0.94	2.9
10. Agrawal et al. (1971)	4. 28.68	1.9 ± 0.9	0.73	2.1	36	0.55	1.42
11. "	4. 16.69	1.9 ± 1.0	0.74	1.9	40	0.54	1.1
12. "	5. 5. 70	0.8 ± 0.6	0.59	1.3	9	0.52	1.1
13. Webber & Reinert (1970)	5. 10.69	3.3 ± 1.0	0.92	3.3	17^{+10}_{-5}	0.88	2.7
14. Present Thesis	11.15.70	2.6 ± 0.6	0.91	4.5	22^{+9}_{-5}	0.85	3.2
15. Haymes et al. (1972)	11.25.70	2.7 ± 0.4	0.97	6.5	16^{+7}_{-4}	0.92	3.5
16. Matsuoka et al. (1972)	5. 1. 71	2.0 ± 0.8	0.72	2.4	30	0.60	1.7
17. "	"	3.2 ± 0.6	0.92	5.2	15^{+6}_{-4}	0.85	3.4

α and kT represent Intensity exponent and temperature for the power law and exponential fits for observations in X-ray range >20 KeV respectively. The corresponding regression and T test values R_p, T_p and R_e, T_e have been tabulated.

different we believe, it is not possible to reconcile with a
single spectral fit for the entire 2-40 KeV range.

At energies above 40 KeV (ref.fig.52) it is evident that
an exponential fit is completely inadequate. The observations
very clearly indicate a flattening of the energy spectrum. Many
attempts have been made to fit both exponential and power law
functions upto 100 KeV. Table V provides power law exponent
and temperature kT for each of the observations. In order to
verify the energy dependence of intensity we have performed T
test. $T > 2.5$ indicates that the intensity is a function of
energy. The observations,e.g.Agrawal et al., show that, at
higher energies, the intensity is practically independent of
energy indicating a flattening of the spectrum. In most of
other cases, the intensity shows a falling off with energy.
Assuming that the anomalous behaviour observed occasionally
is due to time variations, we have attempted to fit both power
law and exponential spectrum to the rest of the data. The
goodness fit of the observations in each case for both power
law and exponential fits is determined by the regression coeff-
icient between the relevant parameters. ~~The~~ Table V indicates
that the regression coefficient for flux above 20 KeV with the
power law fit is generally better than the regression coeffic-
ients obtained by using exponential fit even though the diffe-
rence is statistically not significant. In other words our
analysis show that the observations can be better fitted to a
power law spectrum with an index $\alpha \sim 3.0 \pm 0.5$. However, the

poor statistics of observations above 20 KeV makes it difficult
to conclusively prove this.

4.3 Simultaneous Optical and X-Ray Observations

Since the discovery of Sco XR-1 emission not only in X-ray
region but also in optical, radio and infrared regions all of
which seem to be time dependent, many attempts have been made
to measure and correlate simultaneous changes in X-ray, optical
and radio regions. During the period 1967-69, Lawrence Radiation
Laboratory group at Livermore have made nearly eight observations
with proportional counters and halide crystals. The X-ray
observations were conducted for a range of optical luminosity
varying between 12.4 to 13.2 magnitudes.

Under the collaborative programme between Prof. Oda's
group at the University of Tokyo and ours, we have attempted
to conduct simultaneous optical and X-ray observations. The
X-ray observations were carried out when the star was on the
Thumba Horizon. Since at this time the star had an elevation
$\sim 35^{\circ}$ to 40° as seen from Okayama Observatory (Tokyo), it was
only suitable to carry out/optical photographic observations from Okayama. Also
the moon set during this period occured nearly one hour after
the launchings from Thumba. Photographic observations at
Okayama were conducted with 20 cm refractor mounted on the
91 cm reflector. Extensive communication lines were set up to
successfully conduct the simultaneous X-ray and optical obser-
vations under clear sky conditions and to decide, in advance,
on the 15 mt window for both optical and X-ray observations.

For the rocket flights from Kagoshima, a temporary station at Taniyama, Kagoshima (Japan), was set up for observing Sco XR-1 during the launchings. A 10.4 cm camera (F/4.8) with a combination of blue sensitive plate and ultraviolet blocking filter was used. The error is estimated at ± 0.3 mag. In spite of all the extensive arrangements, due to bad weather patches and other mishaps it was possible to make simultaneous observations during only one flight. This occured when Sco XR-1 was in its darkest phase.

TABLE VI

Simultaneous X-Ray and Optical Observations

Date	Group	Temperature (kT in KeV)	$\dfrac{n^2 r^3}{3d^2} \times 10^{-15}$ (cm^{-5})	B (mag)
1967, May 18	LRL	7 ± 1	37 ± 6	12.8
1967, Sept. 29	"	4 ± 0.7	80 ± 29	12.5
1968, May 9	"	7 ± 1	28 ± 6	13.15
1968, May 19	"	5.5 ± 1	38 ± 6	13.2
1969, April 26	PRL-ISAS	6.8 ± 1	31 ± 6	–
1969, April 28	"	8.6 ± 1.2	25 ± 5	–
1969, Aug. 7	"	12 ± 2	30 ± 7	13.4
1969, Aug. 8	"	9 ± 1	28 ± 8	–
1969, May 17	LRL	8	23 ± 5	13.19
1969, May 24	"	6.5 ± 1.5	50 ± 5	12.56

Rocket observations of Sco XR-1. LRL : Observations by Lawrence Radiation Laboratory (Livermore). PRL – ISAS : Physical Research Laboratory (Ahmedabad) and Institute of Space & Aeronautical Science (Tokyo). Effective temperatures have been determined in the energy range 2-20 KeV taking the gaunt factor into account.
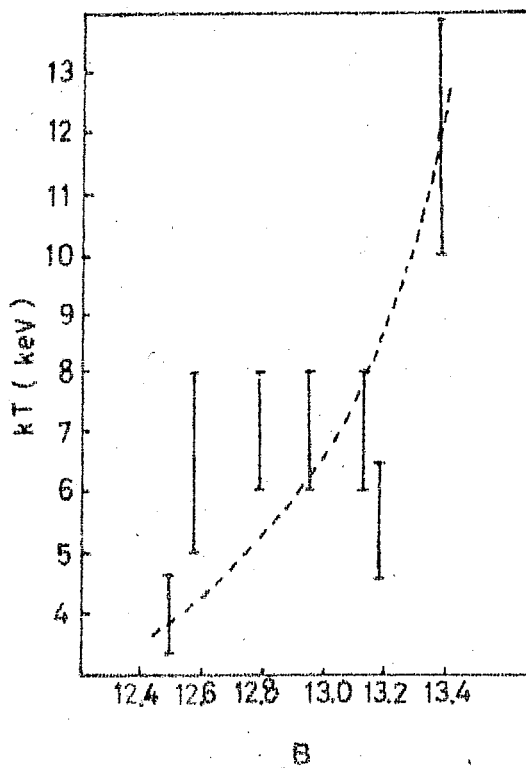
Fig. 53- The relation between optical blue magnitude
B and the temperature KT of Sco XR-1 compiled
from results obtained by rocket observations.

In Table VI we have presented the various X-ray and optical observations that have been conducted. The temperature obtained from X-ray data and the emission measure along with the optical luminosity in terms of blue magnitude are given in the table. In figure 53 the relationship between blue magnitude and temperature observed during the various flights are plotted. It is seen from the figure (excluding the result of May 15, 1968 which coincided with a flare observation) Sco XR-1 tends to be brightest when its temperature is lowest, inspite of large scatter. A best fit curve defining the relationship between B and kT is also shown in the figure. The relationships plotted in figures 51 and 53 indicate a definite relationship between X-ray and optical flux through kT. On the basis of the emperical relationships between B and kT and the volume emission measure $\frac{n^2 \, r^3}{3d^2}$ and kT, we have determined the emission measure and blue magnitude for a set of kT values and are tabulated in Table VII. This will be used for further analysis.

TABLE VII

Compilation of Physical Parameters of Sco XR-1

kT (KeV)	$\frac{n^2 \, r^3}{3d^2}$ (cm^{-3})	B (mag)
4	8×10^{16}	12.5
6	4×10^{16}	12.9
8	3×10^{16}	13.1
10	3×10^{16}	13.3
12	3×10^{16}	13.4

This compilation is based on the relationships shown in figures 51 and 53.

4.4 Hot Plasma Cloud Model for Sco XR-1

The inter-relationship between the optical brightness and temperature derived from X-ray data implies a common emission mechanism for X-ray and optical flux in the spherical cloud of hot plasma. On the basis of thermal bremsstrahlung emission from a hot thin plasma, the expected flux in the optical region is calculated for the parameters listed in Table VII using the energy dependent gaunt factor equation (4.3). As the optical observations of Sco XR-1 have shown the color excess to be essentially constant or B-V = 0.2 ± 0.05, we have obtained the corresponding V magnitude for each set. These apparent optical magnitudes were converted into energy flux values F(V) and F(B) using the table given by Mathews and Sandage (1965). The observed energy flux values at V (5500 $\overset{o}{A}$) wavelength are much below the extrapolated estimates $I_{ff}(V)$ as shown in Table VIII.

TABLE VIII

Optical Data of Sco XR-1

kT (KeV)	B (mag)	F(B)	F(V)	$I_{ff}(V)$
		(KeV/cm ^{2} sec. KeV)		
4	12.5	62.5	69.1	600
6	12.9	43.2	47.8	242
8	13.1	32.8	39.8	159
10	13.3	29.9	33.1	143
12	13.4	27.3	30.2	130

For the kT and B values of Table VII, the optical flux in Blue and Visual has been obtained using table provided by Mathews and Sandage (1963). The theoretical value in Visual $I_{ff}(V)$ has been obtained by extrapolating from X-ray data.

The attenuation factor necessary to explain the optical observations as an extension of thermal bremsstrahlung emission from thin plasma cannot be understood in terms of the interstellar absorption of optical photons. The interstellar absorption is stronger in Blue than in Visible region. From the strength of interstellar Ca II lines the extinction in V $\gtrsim$ 0.75 mag. observed in the case of near by stars (Wallerstein 1967), is believed to be a reasonable value for Sco XR-1 which, however, is less than what is needed to explain the optical continuum from X-ray data. Besides, the optical spectrum cannot be explained by interstellar reddening alone and needs less steeper extinction than observed in the near by stars. Thus the data requires an additional attenuation in the source material to explain the observed spectrum and intensity in the optical region. We have assumed free-free absorption in the source material which has more absorption in Visible than in Blue. Using the free-free absorption coupled with interstellar absorption, simultaneous observations can be used to determine the source parameters T, n and r and the relationships between them.

The energy spectrum of the free-free emission generated by a semi-opaque plasma can be expressed by the approximate relation

$$I(E) = \frac{1 - \exp(-\tau_{ff})}{\tau_{ff}} I_{ff}(E) \qquad \qquad \dots 4.6$$

where τ_{ff} is the optical depth for free-free absorption and is expressed as :

$$\tau_{ff} = 7.7 \times 10^{-4} \cdot g \, (kT)^{-3/2} \cdot E^{-2} \cdot n^2 \, r \qquad \ldots \, 4.7$$

The interstellar absorption A_V can be represented by an extinction curve with R = 3, where R is the total to selective absorption and is written as

$$R = \frac{A_V}{A_B - A_V} \qquad \ldots \, 4.8$$

Assuming different values for the extinction A_V and the optical depth τ_{ff}, we have corrected the observed optical data of Table VIII through equations 4.8 and 4.6. The best values of A_V and τ_{ff} for which the convergence of the optical data and the extrapolated values occurs is computed for the combinations of $n^2 \, r^3$, B and kT of Table VII. The optical depth so obtained, for any particular temperature allows evaluation of the parameter $n^2 \, r$ using the expression 4.7. From the parameters $n^2 \, r^3$ and $n^2 \, r$, it is possible to determine the density n and radius r of the plasma.

TABLE IX

Physical Parameters of Sco XR-1 on the Basis of Isothermal Hot Plasma Cloud.

kT (KeV)	A_V (mag)	r(cm)	n(cm^{-3})	τ_{es}
4	1.2	2.9×10^8	9.1×10^{16}	17.6
6	1.1	2.2×10^8	9.7×10^{16}	14.3
8	1.0	1.4×10^8	1.6×10^{17}	15.2
10	1.0	1.2×10^8	2.1×10^{17}	16.8
12	1.0	1.0×10^8	2.7×10^{17}	18.1

Distance 'd' is assumed to be 300 pc.

In Table IX we present the value of A_V /n and r for the cloud, for each set of observation of table VII for the assumed distance of 300 pc for Sco XR-1. These observations show that the size and density of the source are of the order of about $10^8 - 10^9$ cm and $10^{16} - 10^{17}$ atoms cm^{-3} respectively. These values are in essential agreement with the previous investigations of Chodil et al. (1968) and Nageaubauer et al. (1968). The resultant A_V values are some what larger than are expected for the assumed distance of 300 pc (Sandage et al. 1966). The difference may be due to the fact that the distance is little larger than is assumed or that part of the extinction is due to circumstellar dust cloud.

The attenuation depth for electron scattering may be expressed as :

$$\mathcal{T}_{es} = \sigma_T \cdot n.r \qquad \ldots 4.9$$

where σ_T is the Thomson scattering cross section (=6.65 x 10^{-25} cm^{-2}). In the earlier estimates photons are considered to exchange energy with the plasma by free-free absorption. However, the optical scattering depths $\mathcal{T}_{es}$ obtained, for the values of n and r obtained, are quite high as shown in Table IX. As such, the photons produced in the cloud are scattered many times before they come to surface which may result in distortion of the emergent photon spectrum. Chodil et al. (1968) used a conventional diffusion theory to take this into account. Loh and Garmire (1971) have considered the effects of electron scattering on the photon spectrum.

Loh and Garmire treated the problem by means of Monte-Carlo calculations to estimate the distortion of the spectrum from X-ray to infrared regions. The energy shifting mechanism indicates thermalisation of photons. The electron scattering therefore increases the X-ray emissivity for a given temperature. This makes the electron temperature of the source T_0, less by as much as a factor of two or three than the observed radiation temperature T, which increases with increasing optical depth for a given T_0. In addition the spectral shape at small optical depth although can be characterised by a single temperature, at larger optical depths, $\tau_{es} \geqslant 10$, the emitted spectrum show deviations, so that a single temperature is not valid over the entire spectrum and at higher optical depths the source behaves like a black body.

The results of Loh and Garmire (1971) obtained for a limited number of computations are simulated by the approximate formulae :

$$
\left.
\begin{aligned}
T &= T_0 \, (1 + 0.00475 \, \tau_{es}^{2.5}) \\
I &= \frac{1 - \exp(-\tau_a)}{\tau_a} \, I_{ff}(T) \quad \text{and} \\
\tau_a &= \left(3 \left[\tau_{ff}(T_0) \right]^3 \tau_{es} \right)^{\frac{1}{4}}
\end{aligned}
\right\} \qquad \ldots \; 4.10
$$

Assuming that these expressions are valid for wider ranges of T, n and r we have extrapolated Loh and Garmire calculations and produced modified model spectra for various combinations of the parameters. We have fitted the modified spectrum to the observed spectrum in the X-ray range and the optical range.

TABLE X

Physical Parameters of Sco XR-1 Calculated as
an Isothermal Hot Plasma Cloud
(Including Electron Scattering)

kT(KeV)	A_V(mag)	kT_0(KeV)	r (cm)	n(cm^{-3})	τ_{es}
4	1.1	1.5	9.3×10^8	1.6×10^{16}	9.9
6	0.9	2.7	5.6×10^8	2.4×10^{16}	9.1
8	0.9	3.7	4.3×10^8	3.1×10^{16}	8.9
10	0.9	4.4	3.8×10^8	3.7×10^{16}	9.4
12	1.0	4.8	3.5×10^8	4.3×10^{16}	9.9

Distance 'd' is assumed to be 300 pc.

The results from these modified calculations are tabulated in
Table X. We obtain lower temperatures compared to those obtain-
ed by neglecting electron scattering; kT_0 = 2 to 5 KeV while
kT = 4 to 12 KeV. The cloud will be little larger, by a
factor of about three to four and less dense approximately by
a factor of six than those of the previous estimates. Essen-
tially the free-free emission estimates are valid except for
small numerical factors and clearly any further calculations
require detailed understanding of the electron scattering
effects.

Examination of Tables IX and X, indicates that Sco XR-1
is a compact object with dimensions comparable to or lower
than a white dwarf. This suggests a possible generic relation-
ship between the X-ray source and a white dwarf or perhaps
even a neutron star. The size is consistent with the distance
at which a gas of this temperature is confined by a gravitat-
ional force of a central body of a solar mass as given by

$$r = \frac{\in G\, M_c\, m_p}{kT} \quad cm \qquad \qquad \dots 4.11$$

where G is the gravitational constant, m_p is proton mass and M_c
represents the mass of the central star and $\in$ is the efficiency
of conversion of gravitational energy into thermal energy. The
variation of the size of the cloud with temperature is consis-
tent with the gravitational confinement of plasma. In addition
the change in density is not proportional to r^{-3} thus indicating
accretion of matter in the bright phase. All these features
support the binary hypothesis for Sco XR-1 where in the gravita-
tional infall of material from an extended component on to a
compact central star supplies the energy for radiation.

In the above discussion we have considered the observat-
ions of the LRL group which are similar to our experiments.
Satellite measurements of the X-ray intensity of Sco XR-1 by
Vela 5 satellite have been reported for two periods of approxi-
mately 4 hours each (Evans et al. 1970). In one of the periods
simultaneous optical observations were made and an optical flare
was observed. The other period contained large and rapid
changes in the X-ray intensity. Assuming that the thin hot
cloud model is applicable in flare period, we estimated the
$\frac{n^2 r^3}{3d^2}$ and kT for the pre-optical flare period of August 2nd,
and for the period of sudden X-ray increases or X-ray flares
of October 17th, from the published data. We have plotted
the results on the diagrams $\frac{n^2 r^3}{3d^2}$ Vs. kT and B Vs. kT and are
shown in figures 54 and 55. For the X-ray flare period of
October 17, as optical data is lacking we assumed an optical
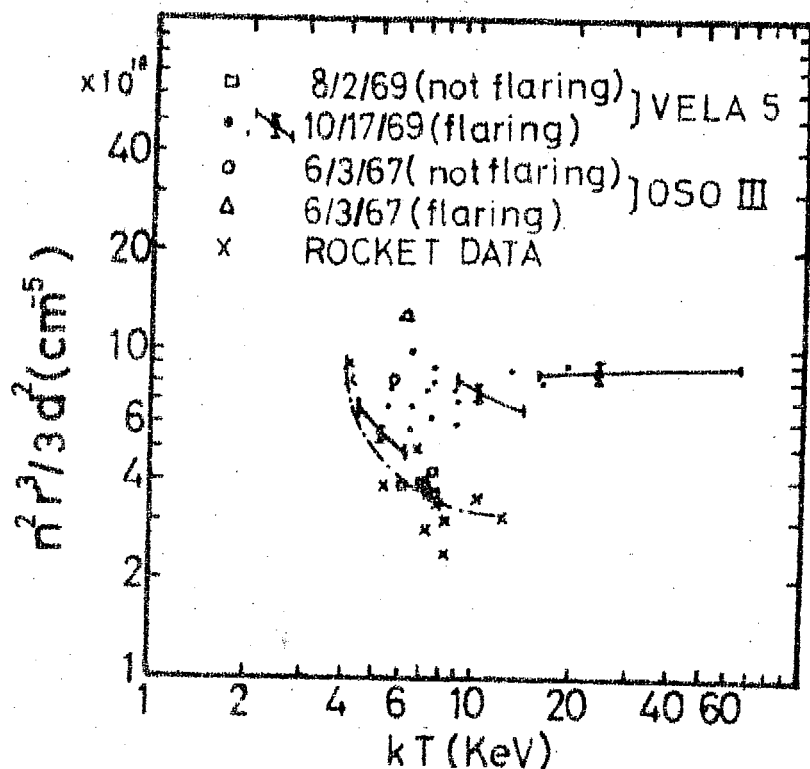
Fig. 54 - The relation between the temperature KT and values of $\frac{n^2 r^3}{3d^2}$ of Sco XR-1 compiled from Satellite data. For comparison, the data obtained by rockets are shown by X.
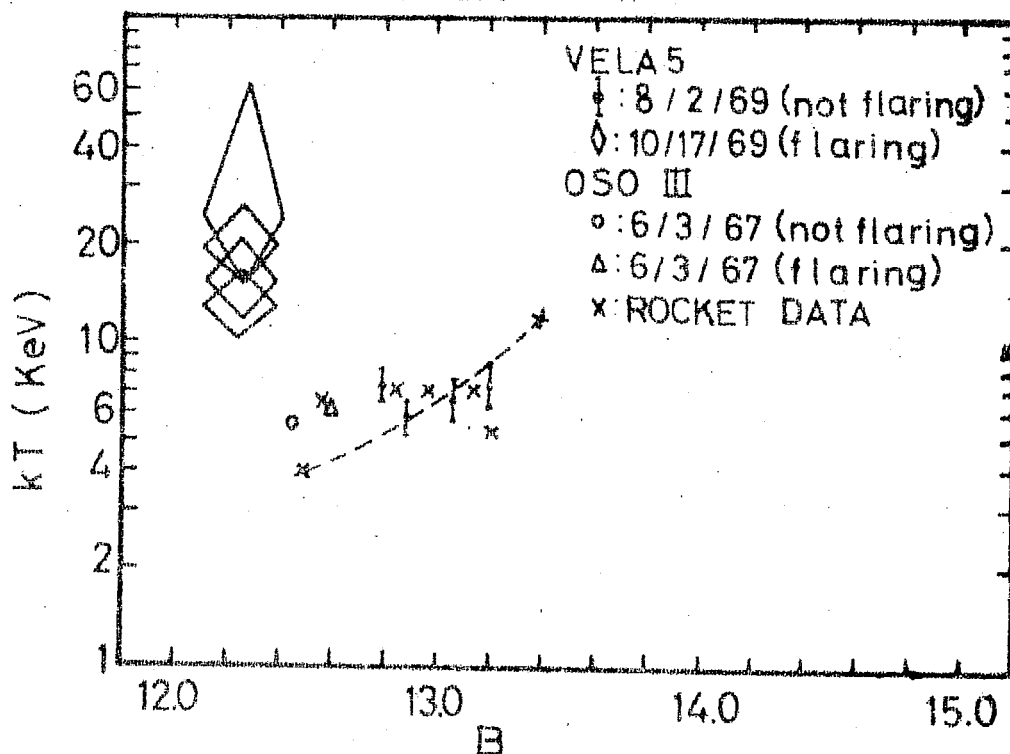
Fig. 55- The relation between the optical blue magnitude B and the temperature KT of Sco XR-1 compiled from the satellite data. For comparison the data

flare to coincide with the X-ray flare and as the optical flare in general appears when Sco XR-1 is in its brightest phase (B $\gtrsim$ 12.4), we obtain the square representing a flare on the B Vs. kT diagram. Similarly, the OSO III satellite observations of Hudson et al. (1970) during flare and quiet period are also plotted in the same figures.

The satellite OSO III observations show relatively high intensities compared to other observations. The two channel spectral informations from the Vela satellite are inadequate to determine the kT values to good degree of accuracy. From the figures it is clear that the observations related to flare conditions, fall in a separate category compared to all the quiet time variations. From the observations we have, we can only conclude that the flare type variations are completely different from the normal quiet type variations exhibited by the source and unlike the quiet time variations, the flare type variations cannot be understood in terms of the simple theoretical model presented above.

4.5   Theoretical Models for Sco XR-1

Before proceeding with the discussion of an appropriate theoretical model for explaining the observed X-ray emission, we first summarise the various observed features which have been discussed earlier.

1.   Assuming the star to be at a distance of 300 pc (Hiltner & Mook 1971), the observed intensity at earth

indicates that the total luminosity of the star is in excess of 5 x 10^{36} ergs/sec. The assumed distance of the object is in good agreement with other estimates such as by Wallerstein et al. (1967) from Ca II line absorptions (>270 pc), by Sofia et al. (1969) from proper motion data (⌄200 pc) and by Oda et al. (1971) using interstellar reddening (⌄300 pc).

2. The emission spectrum in the X-ray range (2-15 KeV) can be adequately described by an exponential with an 'e' folding energy of 4-10 KeV. The high energy flux >20 KeV can be considered as an extension of the low energy spectrum upto ⌄45 KeV. Alternatively, the flux in the range 20-100 KeV can be considered to follow a power law with an exponent α ⌄3.0 ± 0.5. The flux at all energies above 2 KeV show both irregular variation as well as flare like enhancements.

3. Below 1 KeV, different X-ray flux observations show mutually inconsistent results. The results of Fritz et al. (1968) and Rappaport et al.(1970) indicate that the observed flux at these energies is consistent with the extension of the exponential spectrum implying a neutral hydrogen density ⌄0.2 x 10^{21} cm^{-2}. This means that the value of N_H is much smaller than expected or alternately the source is an intense emitter in the soft X-ray region. On the other hand the flux values reported by Grader et al. (1971) are very much below compared to Fritz et al. and Rappaport et al. These values require an absorption due to matter greater than 10^{21} cm^{-2} atoms, if the low energy X-ray flux is assumed to be a

continuation of 2-10 KeV flux observations.

4.   The visible counter part is ~12.5 mag. blue star, whose
luminosity seems to vary from 12.2 to 13.4 mag. and exhibits
features similar to old novae. Below 12.4 mag. it exhibits
flare like enhancements.

5.   Emission lines in the visible portion of the spectrum
indicate electron temperatures $\leq 10^5$ $^{\circ}$K with volume emission
measure $\sim 10^{55}$ cm^{-3} for a distance ~ 300 pc (Johnson et al. 1969).
The emission lines apparently do not change in intensity and
it is the continuum that changes and hence they are decoupled
(Johnson and Golson 1968).

6.   A weak radio source has been identified with Sco XR-1 at
cm wavelengths with spectra characteristic of non-thermal
emission.

7.   There is no evidence of polarisation in X-ray and optical
bands. No positive evidence for the existence of X-ray line
emission has yet been discovered.

    The flux density from Sco XR-1 as a function of frequency
in various bands of observations is shown in the figure 10. The
dashed line represents the thermal bremsstrahlung emission
from an optically thin plasma at temperature kT = 5 KeV. As
already mentioned the observed flux values in the optical,
infrared and radio regions are clearly below that derived from
the extrapolation of the thin plasma approximation valid at

X-ray energies. On the basis of the earlier mentioned hot thin plasma model we try to explain the observed features in all the various wavelength regions.

The hot plasma cloud model for the Sco XR-1 source assumes a spherical volume $\sim 10^{25} - 10^{28}$ cm^3 for containing the plasma at a uniform density (n $\sim 10^{16} - 10^{17}$ cm^{-3}) and a uniform temperature (varying between 4-10 KeV). Even if the 20-40 KeV X-ray flux is considered as an extension of the low energy (2-20 KeV) flux and to have a common origin from this source, the higher energy flux above 40 KeV needs the presence of electrons with high energy tail. On the other hand if the whole 20-100 KeV region is assumed to follow a power law fit, typical of synchrotron mechanism, it needs the presence of high energy electrons with power law distribution in the presence of magnetic field, the intensity of field dependent on the electron energy. On the other hand one can explain this power law as due to bremsstrahlung if there are temperature gradients inside the source. Clearly the origin of high energy X-ray flux $>$ 20 KeV cannot be the same as that of low energy X-rays and will require either the presence of higher energy electrons or of thermal gradients. On the other hand it is difficult to reconcile the observed flux features in the soft X-ray region ($<$ 1 KeV) in terms of this model basically because of the inconsistency in the flux values reported.

The large optical depths present in the hot plasma cloud model will broaden the emission lines and detection may be

difficult. The upper limit obtained for X-ray polarisation is within the estimates expected because of the electron scattering.

The semi-opaque hot plasma model based on the simultaneous optical and X-ray flux changes, cannot explain the optical emission lines and consequently have a different origin. In view of the observation that the optical emission intensity is constant relative to the continuum and it is the continuum that varies, this is justified. Besides, the emission lines require temperatures $\lesssim 10^5$ °K compared to the X-ray emission which is much greater ($\gtrsim 10^7$ °K) and have a volume emission measure of 10^{55} cm^{-3} which is low compared to X-ray region estimates.

The semi opaque plasma model which explains the observed optical flux, by self absorption and interstellar reddening predicts a decrease of intensity as wavelength increases into the infrared. The infrared observations of Naugebauer et al. 1969 indeed show that at longer wavelengths the plasma is optically thick and radiates like a blackbody.

The radio emission of nonthermal character cannot have origin in this plasma of $\sim 10^{16}$ atoms cm^{-3} because of the plasma effects and synchrotron reabsorption and as such the emission would decrease sharply below 10^{14} and cannot have a common origin with the X-ray emission. As proposed by Reigler and Ramatty (1969) the radio emission may arise due to gyrosynchrotron of electrons enveloping the dense plasma. Taking a power

law energy distribution for electrons and assuming 5×10^9 Hz as the peak frequency of self synchrotron source, they computed the various radiation parameters for Sco XR-1 for a range of source radii. From the stability considerations a value of $\sim 10^{12}$ cm is obtained for the radius which corresponds to a plasma density of 10^9 cm^{-3} and a magnetic field of 5 gauss. A similar value for $R(\sim 10^{13}$ cm) was deduced by Hjellming and Wade (1970) from radio flare data.

Thus the radio flux may have origin from a circumstellar plasma of dimension $R \leq 10^{13}$ cm. However, the life time associated with synchrotron losses is $10^5 \sim 10^6$ secs, because the electrons of energy ~ 15 MeV loose quickly their energy in the presence of magnetic fields of ~ 5 gauss. The suggestion that these same electrons responsible for radio radiation may be responsible for hard X-ray emission is not valid. First the spectral indices in both the cases differ being 1.5 and 3.0 respectively. Secondly the volume emission measure 3×10^{55} cm^{-3} in the radio region is approximately two to three orders of magnitudes lower than that required for X-rays, and as such significant X-ray flux cannot be produced.

Thus no single mechanism can account for all the observed flux and spectral features as well as the time variations in the different wavelength bands. The hot semi-opaque plasma cloud model with peripheral electrons can account for the observed X-ray, optical, infrared and radio features.

The above discussed hot plasma configuration for Sco XR-1 has a thermal content comparable to the energy emission ($\sim 10^{36}$ ergs/sec.). This means the source needs continuous heating of the plasma. Among the various models suggested for Sco XR-1 for this energy supply are the conversion of gravitational energy in binary systems and conversion of rotational energy in neutron stars. From the variation of the source parameters our model study favours accretion mechanism. Further, the optical data of Sco XR-1 suggests an association of old nova with the star and it is generally known that old novae are close binaries. Our study favours a hot plasma cloud for Sco XR-1 coupled with a binary system in which accretion of matter of about 2×10^{-6} solar mass per year occurs. The binary system may have a central star of a solar mass with dimensions of a white dwarf with the circumstellar plasma surrounding it. In the next section we briefly discuss various binary and neutron star models suggested for Sco XR-1.

4.51 Binary Models for Sco XR-1

Based on the apparent binary nature of Sco XR-1 Prendergast and Burbidge (1968) and Shklovsky (1967) have proposed models for Sco XR-1. The two models differ in details of the compact star in binary being either a neutron star or a white dwarf and the manner of accretion. We describe below these models briefly.

(a) Model by Prendergast and Burbidge

The accretion of matter as gas streams from a secondary on to a primary in the binary system may produce X-rays, with the corresponding temperature T, approximately given by

$$T = 10^7 \left(\frac{M}{M_\odot}\right)\left(\frac{R_\odot}{R}\right) \text{ K} \qquad \ldots 4.12$$

where M and R/the mass and radius of the primary. Thus if
             are
$T = 10^7$ to 10^8K, M/R in solar units must be 1 to 10, provided that the bulk of gravitational energy released can be converted into photons which are emitted in an optically thin region.

The matter from the secondary cannot, however, fall directly on to the primary because of the large angular momentum typical of the binary orbit. This difficulty is overcome in the model by assuming that the incoming gas streams go into orbital motion about the X-ray source. This leads to the formation of a gaseous disk surrounding the primary. Because of viscosity, the matter losses its centrifugal support and gradually falls on to the primary. A crude estimate indicates that roughly half the mass leaving the secondary terminates at the primary. A number of detailed models of the gaseous disk have been constructed for efficient transformation of the gravitational energy into KeV X-rays.

The geometrical configuration in which the flow near the primary is axisymmetric is considered, so as to avoid complications because of the presence of the secondary. A steady state is assumed wherein the disk is supported by its rotation

against the gravitational field by the primary, and that radial and tangential velocities are independent of the distance from the central plane with negligible longitudinal velocities. Under these conditions the hydrodynamic and radiative transfer equations are set up and solved, for the assumed initial parameters like temperature, density and tangential velocity along with the flux of mass. The authors considered a white dwarf of $R = 0.2 R_{\odot}$, $M = 0.5 M_{\odot}$ and flux of mass $\sim 2 \times 10^{19}$ gms/sec. With initial temperatures $\sim 3 \times 10^{4}$K, associated with spectrotopic binaries, they have examined the dependence of the physical parameters of the disk on the distance from the centre of star.

The study showed a temperature of about $1-2 \times 10^{6}$ K near the surface of the primary with total flux of 4×10^{36} ergs/sec. This temperature is too low compared to the observed temperatures. If the friction between the orbiting disk and the stellar surface is taken into account it is probably possible to achieve higher kinetic temperatures. The decrease in the radius of the central star can also increase the gravitational release per unit mass of accretion.

In this model the optical lines will be emitted from the outer part of the disk where there is a large amount of gas outflow at temperatures of $10^{4} - 10^{5}$ K while X-rays will be produced from the inner part near the hot stellar surface. Variability of the optical and X-ray flux can be understood as due to variations in accretion rate. The presence of cool matter near the source requires the thin disk approximation

to have no absorption in the direction of the observer.

(b) Shklovsky Model

From the analysis of the observational data a three layer
model for Sco XR-1 was proposed with accretion of matter on to
a neutron star.   The model associates soft X-ray flux ($\leqslant 1$ KeV)
and optical radiation with the outer most layer and two concen-
tric plasma regions for X-rays > 1 KeV.

The dimension R_1 of the outer most region, with temperat-
ure

$$2 \times 10^5 \leqslant T_1 < 2 \times 10^6 \quad K \qquad \ldots 4.13$$

has an upper limit to explain the occurence of soft X-ray flux
and optical flux from this region and a lower limit set to
explain the transparency of this region to X-rays > 1 KeV from
the inner layers, and is given by

$$3 \times 10^8 \left(\frac{r}{200}\right) < R_1 < 10^9 \left(\frac{r}{200}\right) \text{ cms} \qquad \ldots 4.14$$

where r is the distance of the source in parsecs.   For r = 200 pc
the dimension of the soft X-ray emitting source is $\sim 5 \times 10^8$ cm
and with a mean density, $\sim 2 \times 10^{17}/cm^3$, will have a total mass
for the plasma $\sim 3 \times 10^{20}$ gms.

The lower X-ray energy region with temperature of $\sim 5 \times 10^7$ K
derived from X-ray data in a similar fashion has limits for R_2

$$2 \times 10^6 < R_2 < 1.5 \times 10^8 \left(\frac{r}{200}\right) \text{ cms} \qquad \ldots 4.15$$

Assuming the region with $T \sim 5 \times 10^7$ K has a dimension $R_2 \sim 10^7$ cm, we obtain $N_e \sim 10^{19}/cm^3$ and a total mass $\sim 10^{17}$ gms. X-rays with energies > 35 KeV can come from the inner most region ($R_3 \sim 10^6$ cms). The binary system with the components separated by $10^{10} \sim 10^{11}$ cms supposes the optical emission lines to occur from gas streams. From the observed intensities of the emission lines, the volume emission measure of the comparatively cold plasma in the stream $\sim 10^{55}$ cm^{-3}, we estimate the electron concentration to be about 10^{13} cm^{-3}. The emission in H lines originate in the remotest part of the stream from the neutron star where $T \sim 10^4$ K, the C III - N III lines in the part of the stream nearer to the neutron star and the He lines from regions still nearer. From the density of the stream ($\sim 2 \times 10^{-11}$ gm/cm^2) and for an assumed velocity of $\sim 10^8$ cm/sec, the mass flow is $10^{16} - 10^{17}$ gm/sec. As the energy release in the gravitational system of the neutron star is $\sim 10^{20}$ ergs/gm the radiated power for the X-ray source is $\sim 10^{36}$ ergs/sec in agreement with the observed energy emission.

In the above binary model the details of accretion mechanism are not discussed. Prendergast and Burbidge have shown that the calculation of the efficiency of transformation of gravitational energy into radiation is very complicated. In addition Sofia (1968) has also cast doubt on the survival of a secondary in a binary system composed of a neutron star as the explosion of a supernova is likely to completely disrupt it. The lack of definite identification of Sco XR-1 with a binary to date

makes these binary models less plausible.

4.52 Pulsar Models for Sco XR-1

Pulsars in which the signature of pulsations is possibly destroyed by absorption in the thick gaseous cloud surrounding the plasma, may account for sources like Sco XR-1. Hjelliming and Wade (1970) point out that the time scales of irregular variations in radio flux from Sco XR-1 are similar to those observed by them in pulsar PSR 0329 + 54 when the data is averaged over times much greater than the pulsar period. Therefore it may be a rotating neutron star or a white dwarf whose rotational kinetic energy is converted into a source of radiation. Cocppn pulsar models on these lines have been proposed by Davidson et al. (1971) Coppi and Treves (1970), Apparao (1971), etc.

In their model Davidson et al. assume a rapidly rotating neutron star surrounded by a dense shell of gas as the X-ray source. They assume that this gas is somehow supported at a radial distance 10^9 cms, which is larger than the speed of light circle. The gaseous envelope is assumed to be thick as required by the observed optical and infrared data.

The rotational energy of the pulsar, through a modified form of magnetic dipole radiation (Pacini 1968), is assumed to accelerate particles. These semi-relativistic protons of several hundred MeV move inside the cloud and heat up the thick envelope. They consider a small amount of gas near the

equitorial plane at a distance $r > R_c$ from the pulsar, where $R_c = C/\Omega$, is the radius of the speed of light circle, and Ω is the angular rotation frequency. The gas cloud absorbs a part ΔL of the pulsar energy loss rate and in turn transfers a torque $\Delta L/\Omega$ to the gas. This torque induces the gas cloud to revolve around the axis of rotation of the pulsar. The observed energy is then thermally radiated isotropically in the rest frame of the gas and thus preferentially in the forward direction seen from the revolving frame. They find that the gaseous shell moving in the gravitational field of the star has a stable orbit at a distance $r = R_o$ where $R_o = \xi R_c$, and ξ is a dimensionless parameter which is always $\gg 1$ for any pulsar, and is given by

$$\xi = R_c / R_G \qquad \ldots 4.16$$

where $R_G = \dfrac{GM}{C^2}$, being the Schwarzschild radius, equal to 1.5×10^5 cms for $M = M_\odot$. In the potential of the system, the hydrostatic equilibrium of the gas with typical sound velocity W , has scale heights $\mathcal{A} = \dfrac{R}{R_o} = \dfrac{W}{C} \xi$ $\qquad \ldots 4.17$

or in terms of temperature attained

$$T = 10^8 \left(165 \frac{\mathcal{A}}{\xi} \right)^2 \; {}^\circ K \qquad \ldots 4.18$$

It is supposed that there is a sufficient turbulent motion in the gas to stabilise the rotating toroidal configuration. In that case there will be an equipartition between thermal and kinetic energies. If the total energy output in the form of semirelativistic particles is L and if σ is the cross-section for absorption in the gas with electron density n, the total

energy providing heat in a column length Δr is given by L.σ.n.Δr. The cooling due to X-ray emission for conventional abundances is estimated as $C.n^2.W.4\pi R_o^2.\Delta r$, where $C = 1.6 \times 10^{-31}$ ergs-cm^2 (Cox and Tucker, 1969). The equation for thermal balance is

$$\frac{L}{4\pi R_o^2} \sigma \cdot n = C n^2 W \qquad \ldots 4.19$$

Under these conditions of stability the gas fills the potential well and $\Delta R/R_o \simeq 1$. For the observed temperatures $T \leq 10^8$ K the value of $\xi \gtrsim 100$.

Now R_o ($= R_G \xi^2$) is $\sim 10^9$ cm and from the X-ray data $n = 10^{16}$ cm^{-3}. The energy loss by protons is $\gtrsim 10^{-25}$ cm^{2} (Ginzburg 1967) and hence $L \simeq 4 \times 10^{37}$ ergs/sec which is few times L_X, the observed X-ray luminosity. The value of $\xi = 100$ corresponds to angular rotation frequency $\Omega = 2000$/sec or a pulsar period of 3 m. sec (t_p). Using the values of Ω and L, the surface magnetic field B of the pulsar is estimated to be $\sim 5 \times 10^9$ gauss which is much smaller than that expected for the pulsar and therefore the pulsar can rotate at this high frequency for several million years. The period of rotation of the gas is $\xi^2 t_p \sim 30$ sec and the cooling time $t_{cool} \sim 0.3$ sec. Since $t_{cool} \gg t_p$ the thermally radiated photons will not show periodic pulsation. The time scale for dynamic equilibrium is $t = \xi^2 t_{cool} \sim 50$ mts. In order that the mass loss from the gaseous shell be small, the life time of ions against escape should be $\gtrsim t$. This life time requires accretion of gas from interstellar matter at a rate of $\sim 10^{-9}$ $M_\odot$/Yr.

The Cocoon pulsar model described above is consistent with physical characteristics of Sco XR-1. However, the short time variationst $\leqslant$ 1 hour are difficult to explain. In addition the formation of the gas cloud around the pulsar and its equilibrium stability will be difficult as the radiation pressure of the pulsar will tend to disperse the gaseous envelope. The proton energies needed to heat the plasma are difficult to achieve and besides the presence of these are doubted as γ-rays which arise out of π^0 decay are not observed from Sco XR-1.

The model of Apparao considers a white dwarf for the X-ray source. The oblique rotating white dwarf with a period of 10 sec., magnetic field of $\sim 10^8$ gauss, radius of $\sim 10^9$ cm, and mass about one half solar mass was considered for Sco XR-1. The low frequency electromagnetic radiation corresponding to the rotation period of the dwarf was considered to heat the plasma situated at distance beyond the velocity of light circle, $\sim 5 \times 10^{10}$ cm. It is estimated that the energy is radiated at a rate of 10^{38} ergs/sec. If the input energy due to the low frequency radiation is shared by the electrons with densities $\sim 3 \times 10^{13}/cm^3$, then the energy of each electron is $\sim 4 \times 10^{-9}$ ergs and corresponds to an electron kinetic temperature of $\sim 3 \times 10^7$ K, which is close to the observed temperature of the plasma. No periodicity will be observed as the cooling time of the plasma is longer than the rotation period.

This model also has similar difficulties as in the model of Davidson et al. (1971) like the origin of the plasma, the short period flaring, etc. The density assumed in this model is rather low compared to the hot plasma X-ray estimates and the temperature will become smaller if higher densities are assumed. Both the models do not explain the radio and high energy X-ray emission.

From the discussion of the various models, outlined above, we can conclude that at present there is no single model which can satisfactorily explain all the observed features of Sco XR-1. The binary models however look promising as there are some X-ray sources like Cyg X-1, Cen XR-3 where binary nature is identified.

. . . . .

REFERENCES

1. Ables, J.G., Astrophys.J.Lett., <u>155</u>, L27, 1969.

2. Acton, L.W., Cutura, R.C., Culhane, J.L. and Fisher, P.C., Astrophys.J.Lett., <u>161</u>, L175, 1970.

3. Adams, D.J., Cooke, B.A., Evans, K. and Pounds, K.A., Nature, <u>222</u>, 757, 1969.

4. Agrawal, P.C., Biswas, S., Ghokale, G.S., Iyengar, V.S., Kunte, P.K., Manchanda, R.K. and Sreekantan, B.V., Nature, <u>224</u>, 31, 1969.

5. Agrawal, P.C., Biswas, S., Gokhale, G.S., Iyengar, V.S., Kunte, P.K., Manchanda, R.K. and Sreekantan, B.V., Intl.Conf.Cosmic Rays <u>1</u>, 20, Hobart, 1972.

6. Agrawal, P.C., Ph.D. Thesis, University of Bombay, 1972.

7. Ananthkrishnan, S. and Ramanathan, K.R., Nature, <u>223</u>, 488, 1969.

8. Andrew, B.H. and Purton, C.R., Nature, <u>218</u>, 855, 1968.

9. Angel, J.R.P., Novick, R., Vandenbout, P., Weisskoff, H. and Wolff, R.S., Astrophys.J.Lett., <u>140</u>, L309, 1969.

10. Angel, J.R.P., Kestenbaum, H. and Novick, R., Astrophys. J., <u>169</u>, L57, 1971.

11. Apparao, M.V.K., Nature, <u>229</u>, 114, 1971.

12. Apparao, M.V.K., Nature <u>232</u>, 153, 1971.

13. Barkas, W.H. and Berger, M.J., "Tables of Energy Losses and Ranges of Heavy Charged Particles", NASA SP-3013, 1964.

14. Bergamini, R., Londrillo, P. and Setti, G., Nuovo Cimento, <u>52</u> B, 495, 1967.

15. Bertotti, B., Cavaliere, A. and Pacini, F., Nature, <u>221</u>, 624, 1969.

16. Biermann, L., Proc.Roy.Soc.Lond., <u>A 313</u>, 357, 1969.

17. Bleeker, J.A.M. and Deerenberg, A.J.M., Astrophys.J., <u>159</u>, 215, 1970.

18. Bless, R.C., Fishel, D. and Stecher, T.D., Astrophys.J., <u>151</u>, L 117, 1968.

19. Boldt, E.A., Desai, U.D., Holt, S.S.& Serlimitsos, P., Nature, 224, 677, 1969.

20. Brecher, K. and Morrison, P., Astrophys.J., 150, L61, 1967.

21. Brecher, K. and Morrison, P., Phys.Rev.Lett., 23, 802, 1969.

22. Brecher, K. and Burbidge, G.R., Nature, 230,440, 1972.

23. Breitenberger, E., Prog.Nucl.Phys., P.55., Ed.by Fisher, R. Pergamon Press, New York, 1955.

24. Brini, D., Fuligini, F. and Hortsman - Morretti, E., Preprint, Univ.of Bologna, 1971.

25. Bunner, A.N., Coleman, P.C., Kraushar, W.L., McCammon, D., Palmieri, T.M., Shilepsky, A. and Ulmer, M., Nature, 223, 1222, 1969.

26. Burginyon, G.A., Grader, R.J., Hill, R.W., Hiltner, W.A., Mannery, E.J., Price, R.E., Rodrigues, R., Seward, F.D. and Swift, C.D., Astrophys.J., 161, 987, 1970.

27. Buselli, G., Clancy, M.C., Davison, P.J.N., Edwards, P.J., McCracken, K.G. and Thomas, R.M., Nature, 219, 1124, 1968.

28. Byram, E.T., Chubb, T.A. and Friedman, H., Science, 152, 66, 1966.

29. Cameron, A.G.W. and Mock, M., Nature, 215, 464, 1967.

30. Charles, M.W. and Cooke, B.A., Nucl.Insts. and Methods, 61, 31, 1968.

31. Chiu, H.Y. and Salpeter, E.E., Phys.Rev.Lett., 12, 413, 1964.

32. Chodil, G., Mark, H., Rodrigues, R., Seward, F., Swift, C.D., Hiltner, W.A., Wallerstein, G. and Mannery, E.J., Phys.Rev.Lett., 19, 681, 1968a.

33. Chodil, G., Mark, H., Rodrigues, R., Seward, F.D., Swift, C.D., Turiel, I., Hiltner, W.A. and Mannery, E.J., Astrophys.J., 154, 645, 1968b.

34. Clark, G.W., Garmire, G.P. and Kraushar, W.L., Proc.XII Int.Conf.Cosmic Rays, Hobart, Tasmania, OG-29, 1971.

35. Coppi, B. and Ferrari, Astrophys., J.Lett., 161, L65, 1970.

36. Coppi, B. and Treves, A., Astrophys.J., 167, L9, 1971.

37. Cox, D.P. and Tucker, W.H., Astrophys.J., 157, 1157, 1969.

38. Curran, S.C. and Wilson, H.W., "Alpha, beta and gamma ray spectroscopy", North-Holland Pub.Co., Amsterdam, 1965.

39. Damle, S.V., Daniel, R.R., Joseph, G. and Lavakare, P.J., Preprint, TIFR CR-NE-71-8, 1971.

40. Davidsen, A., Shulman, S., Fritz, G., Meekins, J.F., Henry, R. and Friedman, H., Submitted to Astrophys.J., 1972.

41. Davidson, K., Pacini, F. and Salpeter, E.E., Astrophys.J., 168, 45, 1971.

42. de Loore, C. and de Jager, "Non Solar X and Gamma Rays Astronomy", 37, I.A.U. Symp., 238, 1969.

43. Dyer, C.S. and Morfil, G.E., Preprint, Imp.College of Sci. and Tech. London, 1971.

44. Edwards, P.J., Burt, G.J. and Knox, F., Nature, 222, 1052, 1969.

45. Evans, W.D., Belian, R.D., Conner, Strong, I.B., Hiltner, W.A. and Kunkel, W.E., Astrophys.J.Lett., 162, L115, 1970.

46. Feldman, P.A., Gribbin, J.R. and Plagemann, S.H., Nature, 226, 432, 1970.

47. Felton, J.E. and Morrison, P., Astrophys.J., 146, 686, 1966.

48. Felton, J.E. and Rees, M.J., Astron. and Astrophys., 1971.

49. Finzi, A. and Wolf, R.A., Astrophys.J., 155, L107, 1969.

50. Friedman, H., Byram, E.T. and Chubb, T.A., Science, 153, 1527, 1966.

51. Friedman, H., Ann.Rev.Nucl.Sci., 17, 317, 1967.

52. Friedman, H., Proc.Roy.Soc.London, A 313, 301, 1969.

53. Fritz, G., Meekins, J.F., Henry, R.C., Byram, E.T. and Friedman, H., Astrophys.J.Lett., 153, L199, 1968.

54. Fritz, G., Meekins, J.F., Henry, R.C. and Friedman, H., Astrophys.J., 155, 1, 1969.

55. Fritz, G., Davidsen, A., Meekins, J.F. and Friedman, H.,
     Astrophys.J., <u>164</u>, L81, 1971.

56. Garmire, G.P., Moore, W. and Stevens, J.C., Proc.Int.Conf.
     Cosmic Rays (Hobart), <u>1</u>, 7, 1971.

57. Giacconi, R., Gursky, H., Waters, J.R., Rossi, B., Clark,G.,
     Oda, M. and Wada, M.,'Proc.Intl.School of Physics',
     Enrico Fermi Course XXXV, P.73, Ed.Gratton, L. Academic
     Press, New York, 1966.

58. Ginzburg, V.L. and Syrovatsky,S., Ann.Rev.of Astr. and
     Astrophys., <u>3</u>, 297, 1965.

59. Ginzburg, V.L. and Syrovatskii, S.,   "The Origin of
     Cosmic Rays", Pergamon Press, London, 1966.

60. Ginzburg, V.L., Zhelezniakov, V.V. and Zaitsev, V.V.,
     Astrophys.Space.Sci, <u>4</u>, 464, 1969.

61. Gold, T., Nature, <u>218</u>, 731, 1968.

62. Gold, T., Nature, <u>221</u>, 25, 1969.

63. Goldreich, P. and Julian, W.H., Astrophys.J., <u>157</u>, 869,
     1969.

64. Goldstein, H., 'Classical Mechanics', Addison-Wesley Publ.
     Co., Mass., 1951.

65. Gorenstein, P., Gursky, H. and Garmire, G., Astrophys.J.,
     <u>153</u>, 885, 1968.

66. Gorenstein, P., Kellog, E.M. and Gursky, H., Astrophys.J.,
     <u>156</u>, 315, 1969.

67. Gorenstein, P., Kellog, E.M. and Gursky, H., Astrophys.J.,
     <u>160</u>, 199, 1970.

68. Gorenstein, P., Harris, B., Gursky, H., Giacconi, R.,
     Novick, R. and Vandenbout, P., Science, <u>172</u>, 369,
     1971.

69. Gould, R.J., Am.J.Phys., <u>35</u>, 376, 1967.

70. Grader,R.J.,Hill, R.W., Seward, F.D. and Toor, A., Science,
     <u>152</u>, 1499, 1966.

71. Grader, R.J., Hill, R.W., Seward, F.D. and Hiltner, W.A.,
     Astrophys.J., <u>159</u>, 201, 1970.

72. Gunn, J.F. and Ostriker, J.P., Nature, <u>221</u>, 454, 1969a.

73. Gunn, J.F. and Ostriker, J.P., Phys.Rev.Lett., 22, 728, 1969b.

74. Gursky, H., Giacconi, R., Gorenstein,P., Waters, J.R., Oda, M., Bradt, H., Garmire, G. and Sreekantan, B.V., Astrophys.J., 146, 310, 1966.

75. Gursky, H., Gorenstein, P. and Giacconi,R., Astrophys.J., 150, L75, 1967.

76. Gursky, H., Kellog, E.M., Leong, C., Tananbaum, H. and Giacconi, R., Astrophys.J., 165, L43, 1971.

77. Harris, J.R., Ph.D. Thesis, University of Adelaide, 1968.

78. Hayakawa, S. and Matsuoka, M., Prog.Theor.Phys.Kyoto, Supp., 30, 204, 1964.

79. Hayakawa, S., Matsuoka, M. and Sugimoto, D., Space Sci. Rev., 5, 109, 1966.

80. Hayakawa, S., Kato, T., Makino, F., Ogawa, H., Tanaka, Y., Yamashita, K., Matsuoka, M., Miyamato, S., Oda, M. and Ogawara, Y., Astrophys. & Spa.Sci., 12, 104, 1971.

81. Hill, R.W., Grader, R.J. and Seward, F.W., Astrophys.J., 154, 655, 1968.

82. Hiltner, W.A., Mook, D.E. and Graham, D., Astrophys.J., 148, L47, 1967.

83. Hiltner, W.A. and Mook, D.E., Astrophys.J., 150, L23, 1967a.

84. Hiltner, W.A. and Mook, D.E., Astrophys.J., 150, 851, 1967b.

85. Hiltner, W.A. and Mook, D.E., Ann.Rev.Astro.& Astrophys, 3, 1970.

86. Hjellming, R.M. and Wade, C.M., Astrophys.J,Lett., 161, L1, 1971.

87. Holt, S.S., Boldt., E.A. and Serlemitsos, P,J., 'Non Solar X and Gamma Ray Astronomy', 138, Ed,L.Gratton, Reidel Publishing Comp., Holland, 1970.

88. Holt, S.S., Boldt, E.A., Shwartz, D.A., Serlemitsos, P.J. and Bleach, R.D., Astrophys.J., 166, L65, 1971.

89. Hudson, H.S., Peterson, L.E. and Schwartz, D.A., Astrophys. J., 159, L51, 1970.

90. Ichumura, K., Ishada, G., Jugaku, J., Oda, M., Osawa, K. and Shimizu, M., Tokyo Astron.Obs.Reprint 301, 1966.

91. Jackson, J.D., 'Classical Electrodynamics', John Wiley and Sons, New York, 1962.

92. Jain, A.K., Jayanthi, U.B., Kasturirangan, K. and Rao, U.R., Astrophys. & Spa.Sci.,(In Press), 1973.

93. Johnson, H.M. and Stephenson, C.B., Astrophys.J., 146, 602, 1966.

94. Johnson, H.M. and Golson, J.C., Astrophys.J., 153, 307, 1968.

95. Jordan, C., Mon.Not. Roy.Astro.Soc., 142, 501, 1969.

96. Kasturirangan, K., Ph.D. Thesis, Gujarat University, 1971.

97. Kasturirangan, K. and Rao, U.R., Astrophys.Space Sci., 15, 161, 1972.

98. Kellog, E., Gursky, H., Murray, S., Tananbaum, H. and Giacconi, R., Astrophys.J., 169, L99, 1971.

99. Kestenbaum, H., Angel, J.R.P. and Novick, R., Astrophys. J.Lett., 164, L87, 1971.

100. Kestenbaum, H., Angel, J.R.P., Novick, R. and Cocke, U.J., Astrophys.J., 169, L49, 1971.

101. Kitamura, T., Matsuoka, M., Miyamato, S., Nakagawa, M., Oda, M., Ogawara, Y., Takagishi, K., Rao, U.R., Chitnis, E.V., Jayanthi, U.B., Prakasarao, A.S. and Bhandari, S.M., Astrophys.Spa.Sci., 12, 378, 1971.

102. Lampton, M., Bower, S., Welch, J. and Grasdalen, G., Astrophys.J., 164, L61, 1971.

103. Lewin, W.H.G., Clark, G.W. and Smith, W.B., Astrophys.J., 150, L153, 1967.

104. Lewin, W.H.G., Clark, G.W. and Smith, W.B., Astrophys.J. Lett., 152, L55, 1968.

105. Lewin, W.H.G., McClintock, J.E., Ryckman, S.G., Glass, I.S. and Smith, W.B., Astrophys.J.Lett., 162, L109, 1970.

106. Loh, E.D. and Garmire, G.P., Astrophys.J., 166, 301, 1971.

107. Manchanda, R.K., Ph.D. Thesis, Bombay University, 1971.

108. Manchanda, R.K., Iyengar, V.S., Agrawal, P.C., Gokhale, G.S., Kunte, P.K. and Sreekantan, B.V., Nature, 232, 190, 1971.

109. Manchanda, R.K., Biswas, S., Agrawal, P.C., Ghokale, G.S., Iyengar, V.S., Kunte, P.K. and Sreekantan, B.V., Astrophys.& Spa.Sci., 15, 272, 1972.

110. Manley, O.P., Astrophys.J., 144, 1253, 1966.

111. Manley, O.P. and Olbert, S., Astrophys.J., 157, 223, 1969.

112. Morgan, B., Bowyer, S., Lampton, M. and Cruddance, R., Astrophys.J., 169, L45, 1971.

113. Mark, H., Price, R., Rodrigues, R., Seward, F.D., Swift, C.D. and Hiltner, W.A., Astrophys.J.Lett., 156, L67, 1969.

114. Mathews, T.A. and Sandage, A.R., Astrophys.J., 138, 30, 1963.

115. Matsuoka, M., Oda, M., Ogawara, Y., Hayakawa, S. and Kato, T., Can.J.Phys., 46, S466, 1968.

116. Matsuoka, M., Fujii, M., Miyamato, S., Nishumura, J., Oda, M., Ogawara, Y., Ohta, S., Hayakawa, S., Kasahar, I., Makino, F., Tanaka, Y., Agrawal, P.C., Sreekantan, B.V., Hatanaka, Y. and Sreedhararao, S., Nature Phys. Sci., 236, 53, 1972.

117. Metzger, A.E., Anderson, E.C., Van Dilla, M.A. and Arnold, Jr. J.R., Nature, 204, 766, 1964.

118. Michel, F.C. and Tucker, W.H., Nature, 223, 277, 1969.

119. Mook, D.E., Astrophys.J., 150, L25, 1967.

120. Neugebauer, G., Oke, J.B., Beeklin, E. and Garmire, G., Astrophys.J., 155, 1, 1969.

121. Novick, R., Weisskopf, M.C., Berthelsdorf, R., Linke, R. and Wolff, R.S., Columbia Astrophys.Lab.Reprint, 56, 1972.

122. Oda, M., Intl.Conf.Cosmic Rays, London, 1, 68, 1965.

123. Oda, M., Space Sci.Rev., 8, 507, 1968.

124. Oda, M., Gorenstein, P., Gursky, H., Kellog, E., Schreier, E., Tananbaum, H. and Giacconi, R., Astrophys. J.Lett., 166, L1, 1971.

125. Overbeck, J.W. and Tananbaum, H.D., Astrophys.J., 153, 899, 1968.

126. Pacini, F., Nature, 216, 567, 1967.

127. Pacini, F., Nature, 219, 145, 1968.

128. Palmieri, T.M., Burginyon, G.A., Hill, R.W., Seward, F.D. and Stoering, J.P., Astrophys.J., 169, 33, 1971.

129. Pelling, R.M., Matteson, J.L., Peterson, L.E. and Johnson, H.M., Bull.Am.Astr.Soc., 1, 256, 1969.

130. Peterson, L.E. and Jacobson, A.S., Astrophys.J., 145, 62, 1966.

131. Peterson, L.E., 'Non Solar X and Gamma Ray Astronomy', P.65, Ed.Gratton, L., Reidel Publishing Co., Holland, 1970.

132. Prakasarao, A.S., Sharma, D.P., Jayanthi, U.B. and Rao, U.R., Astrophys.Space Sci., 10, 150, 1971.

133. Prendergast, K.H. and Burbridge, G.R., Astrophys.J., 151, L83, 1968.

134. Reigler, G.R., Boldt, E. and Serlemitsos, P., Astrophys.J. 153, L95, 1968.

135. Reigler, G.R. and Ramatty, R., Astrophys.J., 4, 27, 1969.

136. Reigler, G.R., Nature, 226, 104, 1970.

137. Rao, U.R., Prakasarao, A.S. and Jayanthi, U.B., Nature, 222, 864, 1969.

138. Rao, U.R., Chitnis, E.V., Prakasarao, A.S. and Jayanthi, U.B., Astrophys.J., 157, L127, 1969.

139. Rao, U.R., Jayanthi, U.B. and Prakasarao, A.S., Astrophys. J.Lett., 157, L133, 1969.

140. Rao, V.R., Kulkarni, P.V. and Ramanathan, K.R., Pure and Appl.Geophys.(In Press), 1973.

141. Rappaport, S., Bradt, H.V., Naranan, S. and Spada, G., Nature, 221, 428, 1969.

142. Rees, M.J. and Setti, G., Nature, 219, 127, 1968.

143. Rossi, B.B. and Staub, H.H., 'Ionisation Chambers and Counters', McGrahill Co., New York, 1950.

144. Sandage, A., Osmer, P., Giacconi, R., Gorenstein, P., Gursky, H., Waters, J., Bradt, H., Garmire, G., Sreekantan, B.V., Oda, M., Osawa, K. and Juguku, J., Astrophys.J., 146, 316, 1966.

145. Sartori, L. and Morrison, P., Astrophys.J., 150, 385, 1967.

146. Schwartz, D.A., Boldt, E.A., Holt, S.S., Serlemitsos, P.J. and Bleach, R.D., Nature, Phys.Sc., 233, 110, 1971.

147. Sciama, D.W., Proc.Roy. Soc.London, A313, 349, 1969.

148. Schmidt, M., Astrophys.J., 151, 393, 1968.

149. Setti, G. and Rees, M.J., 'Non-Solar X- and Gamma Ray Astronomy', No.37, I.A.U. Symposium, 352, 1970.

150. Seward, F., Chodil, G., Mark, H., Swift, C. and Toor, A., Astrophys.J., 150, 845, 1967.

151. Sharma, D.P., Jain, A.K., Chakravarty, S.C., Kasturirangan, K., Ramanathan, K.R. and Rao, U.R., Astrophys.Spac.Sci., 17, 409, 1972.

152. Sheshadri, K.S.V., Prakasarao, A.S. and Rao, U.R., J.Inst. Telecom.Engrs., 16, 434, 1970.

153. Shklovsky, I.S., Astrophys.J.Lett., 148, L1, 1967.

159. Shukla, P.G. & Wilson, B.G., Astrophys.J., 164, 265, 1971.

160. Silk, J., Astrophys.J., 151, L19, 1968.

161. Silk, J., Nature, 221, 347, 1969.

162. Silk, J. and McCray, R., Astrophys.Lett., 3, 33, 1969.

163. Sofia, S., Astrophys.J., 149, L59, 1967.

164. Sofia, S., Eichhorn, H. and Gatewood, G., Astron.J., 74, 20, 1969.

165. Stepein, K., Astrophys.J.Lett., 151, L15, 1968.

166. Tananbaum, H., Kellog, E., Gursky, H., Murray, S., Schreier, E. and Giacconi, R., Astrophys.J., 165, L37, 1971.

167. Toor, A., Seward, F.D., Cathey, L.R. and Kunkel, W.E., Astrophys.J., 160, 209, 1970.

168. Tucker, W.H. and Gould, R., Astrophys.J., 144, 244, 1966.

169. Tucker, W.H., Astrophys.J., 148, 745, 1967.

170. Tucker, W.H., 'Non-Solar X- & Gamma ray Astronomy', Ed. Gratton, L., P.221, D.Reidel Pub.Co., Holland, 1970.

APPENDIX

Reprints of the following papers:

1. Energy Spectrum and the Absolute
    Flux of Various Celestial X-Ray
    Sources

2. Diffuse X-Ray Background Measure-
    ments in the Energy Range
    2-18 KeV.

3. X-Ray Observations from Cen XR-4
    and Nor XR-2.

. . . . .

ENERGY SPECTRUM AND THE ABSOLUTE FLUX OF VARIOUS CELESTIAL X-RAY SOURCES

By

U. R. RAO, E. V. CHITNIS, A. S. PRAKASA RAO AND U. B. JAYANTHI

ENERGY SPECTRUM AND THE ABSOLUTE FLUX OF VARIOUS CELESTIAL X-RAY SOURCES

By U. R. RAO, F.A.Sc., E. V. CHITNIS, A. S. PRAKASA RAO

AND

U. B. JAYANTHI

(*Physical Research Laboratory, Ahmedabad, India*)

ABSTRACT

The results on the flux of low energy X-rays in the range 2–18 Kev from Sco-X1, Tau-X1 and Cen-X2 celestial sources observed during two rocket flights, flown from the Thumba Equatorial Rocket Launching Station (TERLS), Trivandrum, India, are presented. The absolute flux and the energy spectrum obtained for these sources are compared with other similar observations. The results indicate a long-term exponential decrease in the energy flux of X-rays from Sco-X1 over the period 1965–1968. The X-ray source Cen-X2, which showed a remarkable outburst of X-rays in April 1967, had ceased to be active after May 1967. We present here the first evidence of the rediscovery of the low energy, X-ray flux from Cen-X2 since May 1967. These short-lived X-ray outbursts may be attributed to a shock wave from the nova outburst expanding into the circumstellar medium.

INTRODUCTION

SINCE the discovery of stellar X-ray source Sco-X1 by Giacconi et al.[1] in 1962, a number of experiments have been performed by different groups for determining the absolute flux and the energy spectrum of various galactic as well as extra-galactic X-ray sources. After the optical identification of Sco-X1 by Sandage et al.,[2] a large number of photometric observations have been conducted by Hiltner and Mook[3] and others. Such studies have clearly revealed that the optical intensity of Sco-X1 undergoes very rapid variations between 12·2 and 13·2 magnitudes, large flare type enhancements occurring during nearly 50% of the time when Sco-X1 is brighter than 12·6 magnitude. A search by Rao et al.[4] for hidden periodicities has shown that, besides rapid fluctuations, Sco-X1 optical intensity varies by about a factor of two with a periodicity of about 3 hours. Recent radio observa-

257

tions by Andrew and Purton[5] and Ables[6] have also shown the existence of similar variations in the radio emission from Sco-X1. The possibility of finding correlated changes in X-ray, optical and radio emissions from the same object is truly exciting and will reveal a common origin for the widely different radiations. The observation of X-ray flare from Sco-X1 at balloon altitudes by Lewin *et al.*[7] and the discovery of the highly variable source Cen-X2 by Harries *et al.*[8] have focussed a great attention on the systematic measurements of the absolute flux and the time variation of X-ray lumi-nosity from different celestial sources.

In this paper, we describe the results of the two rocket flights carried out from the Thumba Equatorial Rocket Launching Station (TERLS), Trivandrum (Geogr. Latitude 8° 32′ N; Geogr. Longitude 76° 51′ E), India. Two identical X-ray payloads were launched, one on a Centaure rocket at 0319 UT on November 3, 1968 and the second on a Nike-Alpache rocket at 0305 UT on November 7, 1968 almost vertically (85° elevation) such that the X-ray detector mounted with its axis perpendicular to the spin axis of the rocket scanned the rocket horizon. The launch time was chosen when the Sco-X1, Cen-X2 and Tau-X1 were all in the rocket horizon. The present experiments were conducted with the following objectives:

(a) To measure the absolute flux and the energy spectrum of Sco-X1, Tau-X1 and Cen-X2 in the energy range 2–20 Kev.

(b) To measure the time variability of the X-ray flux from these sources in the above energy range.

(c) To conduct a survey of the southern sky with a view to detect hitherto undiscovered X-ray sources.

INSTRUMENTATION

The X-ray detector consisted of a proportional counter filled with Xenon (90%) and Methane (10%) at one atmospheric pressure and having a 2 mil. thick Berylium entrance window. The counter had an effective path length of 2 inches. The counter resolutions were typically 15% full width half-maximum at 6·0 Kev (Fe[55]) and 22% full width half maximum at 22 Kev (Cd[109]). A slat type collimator mounted in front of the proportional counter dafined a 8·7° × 17·2° full width half-maximum field of view, with the long axis parallel to the spin axis of the rocket. The effective area of the counter, after taking into account the collimator occultation, was 60·8 cm.[2]. Figure 1 shows the detector. In Fig. 2 is shown the calculated efficiency of the

counter as a function of X-ray quantum energy. The efficiency of the counter $\mathscr{E}(\lambda)$ is calculated using the well-known equation

$$\mathscr{E}(\lambda) = e^{-\mu_\omega \chi^\omega}\left(1 - e^{-\mu_g \chi^g}\right)$$

where μ_ω and μ_g are the absorption coefficients of the window and the gas and χ_w and χ_g are the respective path lengths.
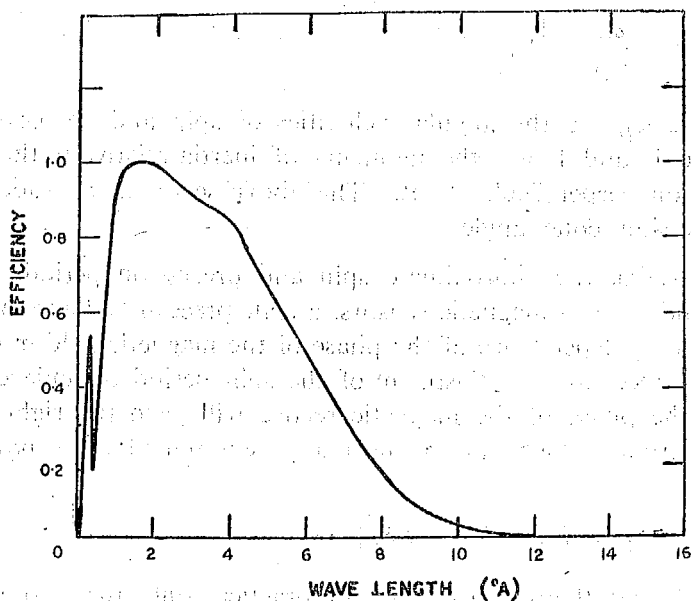

FIG. 2. Efficiency of the proportional counter filled with Xenon (90%) and Methane (10%) at 1 atmospheric pressure and having a 2 mil. thick Berylium window.

The pulses from the proportional counter were amplified, shaped and pulse height analysed in the energy range 2–18 Kev into four consecutive energy windows. A redundant analogue signal giving the actual pulse height of each pulse was also telemetered separately. The entire information was telemetered by FM/FM telemetry system. Monitoring of the 6·0 Kev line from the Fe[55] radioactive source mounted on the split nose-cone provided the inflight calibration upto 70 Km., at which altitude, the source and the nosecone were explosively ejected.

The attitude of the rocket was determined by two suitably mounted geomagnetic aspect sensors, one along the spin axis and another perpendicular to it. The alignment of the detector and the geomagnetic aspect sensors were made to an angular accuracy better than 0·1°. Both the Centaure and Nike-Apache rockets reached an apogee of about 160 Km. Out of

the total flight time of about 420 seconds, useful X-ray data above 90 Km. altitude were obtained for about 200 seconds.

ASPECT ANALYSIS

Assuming the rocket to behave like a rigid body, one can estimate the half apex-angle of the precession cone α, using the well-known formula

$$\cos \alpha = \frac{\omega_s}{\omega_p} \frac{I_1}{I_2 - I_1}$$

where ω_s and ω_p are the angular velocities of spin and precession respectively and I_1 and I_2 are the moments of inertia relative to the spin axis and a direction perpendicular to it. The above serves as a crude estimate of the precession cone angle.

After deriving the approximate spin and precession periods from the horizontal and vertical magnetic sensors, a spin precession diagram is drawn showing the time dependence of the phase of the magnetic field in each spin during each precession. Adjustment of the spin period to achieve synchronization of the phase of the magnetic record will yield the right spin and precession periods which can be normally represented as a power series in time t as

$$\omega_s + \omega_p = W_0 + At + Bt^2 + \cdots$$

where W_0, A and B are constants. In practice, only the first two terms are of importance.

The peak-to-peak amplitude of the horizontal magnetic sensor (2M) is equal to $2M_{max.} \sin \theta$ where θ is the angle between the spin axis and the magnetic vector. The equation $\sin^{-1} \theta = 2M/2M_{max.}$ is used to determine θ at each maximum of the magnetometer, taking into account the variation of $M_{max.}$ with altitude using the Finch and Leaton expansion of the geomagnetic field. Knowing θ for each spin, one can construct the precession circle which is correct to probably within a few degrees. It must be noted that θ will vary between the two limits of $\alpha + \delta$ and $\alpha - \delta$ where α is the half-cone precession angle and δ is the inclination of the precession axis to the vertical. The celestial co-ordinates calculated using the well-known formulas of spherical astronomy at the time of two launches are given in Table I.

A further refinement of the attitude was accomplished by using the successive Sco-X1 sighting. From the spin phase diagram for the passage

of X-ray source Sco-X1, the average spin phase difference between Sco-X1 and the magnetic direction which was about 118° and the variation of X-ray intensity in each precession cycle has been employed to refine the precession axis of the rocket to better than 1° using the method described by Wada et al.[9]

TABLE I

Celestial Co-ordinates at the Time of Launching

		Flight I		Flight II	
		R.A.	Declination	R.A.	Declination
Sun	..	$14^h 33'$	$-15°\ 1'$	$14^h 49'$	$-16° 14'$
Zenith	..	$11^h 18'$	$8° 33'$	$11^h 16'$	$8° 33'$
Magnetic field	..	$0^h 42'$	$81° 54'$	$0^h 40'$	$81° 54'$

The spin stabilized Centaure rocket flown on November 3, 1968, with a spin rate of about 8 RPS, had its axis centered at $10^h 18'$ Right Ascension and 15·0° N. declination on the celestial sphere. Consequently, the X-ray detector was able to look at Sco-X1 and Cen-X2 sources during the entire duration of the flight (about 200 seconds from 90 Km. altitude to the time of entry into the atmosphere). The Nike-Apache rocket launched on November 7, 1968, however, got into precession after the ejection of the nosecone at 70 Km. and its spin rate which was initially about 9 RPS, changed to about 2·8 RPS. after the nosecone ejection. The precession axis of the rocket, as derived from the attitude sensor analysis described above and Sco-X1 sighting, is $10^h 8'$ R.A. and 36° N. declination with the half-cone precession angle being 54°. In the 7 precessions containing 93 spins each, Sco-X1, Tau-X1 and Cen-X2 sources were all scanned for about 8–9 consecutive spins. Figure 3 shows the relevant trajectories of the detector axis in the celestial sphere for both the flights.

The data from all the spins from the Centaure rocket launched on November 3, 1968 have been summed up. Figure 4 shows the observed X-ray counting rates in the energy range 2–6 Kev, as a function of the rocket azimuth. For the flight of November 7, 1968 (Nike-Apache), the data for all consecutive scans during which each source could be observed are summed up and presented in Fig. 5. The relevant scan numbers are also indicated in the figure. In both the figures, the position of Sco-X1, Tau-X1 and

Cen-X 2 sources are marked. The observed data in each scan (spin) was fitted to a theoretical response function of the type A.g. $(t - t_0)$ where A is the absolute strength of the source, t_0 is time of maximum response and $g(0) = 1$. The response is obviously a triangular one with a base equal to $17/360 \times \tau_s$ where τ_s is the spin period. A and t_0 are chosen for least square fitting, i.e., when

$$E = \sum_i [X(t_i) - A.g. (t_i - t_0)]^2$$

is a minimum. Having obtained the source strength as observed in each scan, the least square method is applied again for consecutive scans, in an identical manner as explained above to obtain the absolute flux of the source.
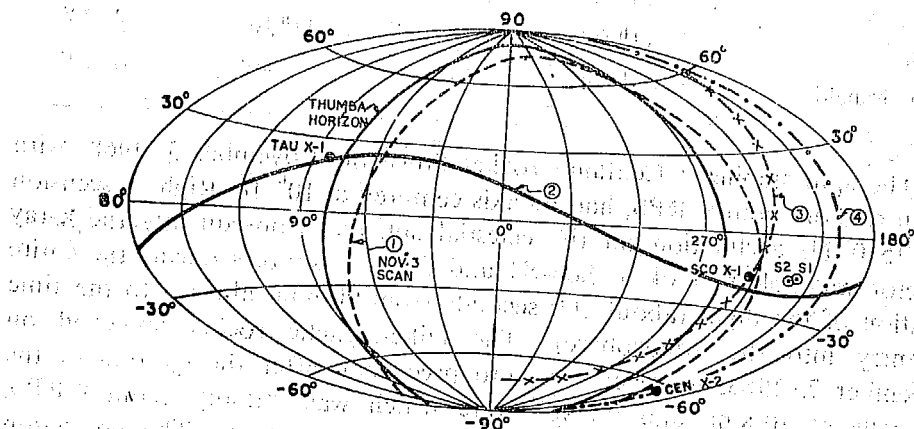

FIG. 3. Trajectories of sky scans for the two flights of November 3, 1968 (Number 1) and November 7, 1968 (Numbers 2, 3 and 4). The Thumba horizon at the time of launching is also indicated. S1, S2 indicate positions of sun on November 3 and November 7 respectively.

ABSOLUTE FLUX OF TAU-X1 SOURCE

Figure 6 shows the energy spectrum of Tau-X1 in the range 2–18 Kev. The observations by Chodil et al.[10] and Boldt et al.[11] are also plotted in the same figure. Our results show an excellent agreement with the observations made by other workers and are consistent with a power law energy spectrum of the type

$$f(E) = 8 \cdot 0 \, E^{-0.9 \pm 0.2} \, dE$$

The flux in the energy range 2–5 Kev is found to be $(1 \cdot 6 \pm 0 \cdot 3) \times 10^{-8}$ ergs/cm.² sec.

The recent discovery of an X-ray pulsa by Fritz *et al.*[12] in the general direction of the crab nebula and its tentative identification with the optical
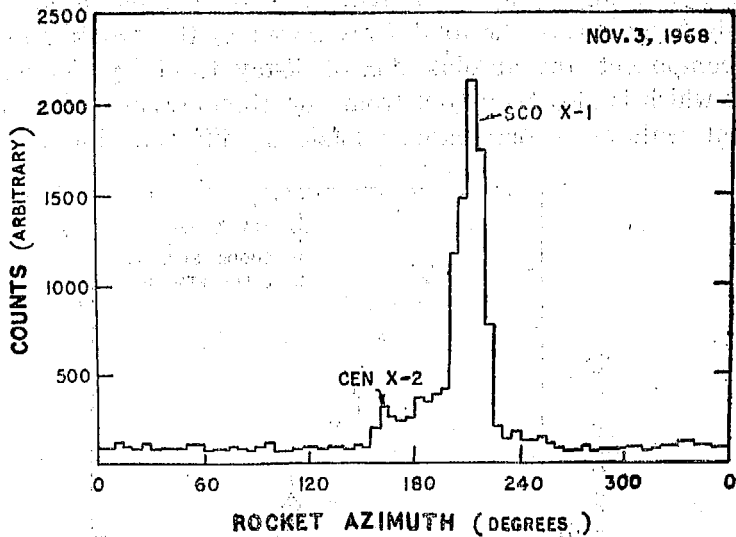

FIG. 4. Observed X-ray counting rates in the energy range 2-6 Kev as a function of rocket azimuth for the flight of November 3, 1968.
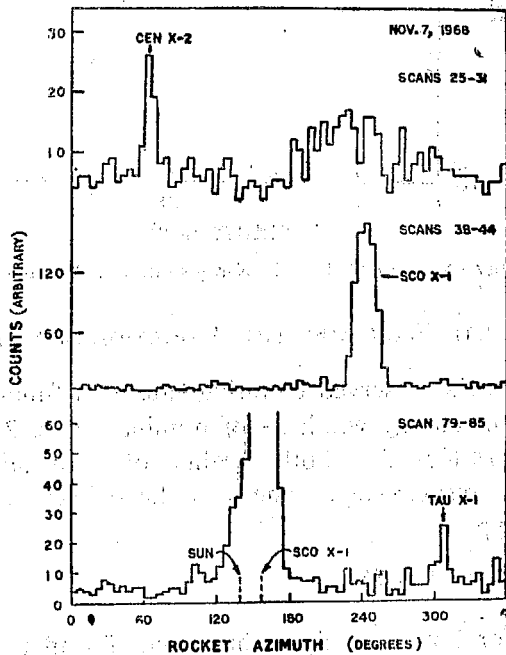

FIG. 5. Observed X-ray counting rates in the energy range 2-6 Kev as a function of rocket azimuth for the flight of November 7, 1968.

pulsar NP 0532 has increased the importance of the study of this X-ray source. The frequency of the X-ray pulsations in the crab nebula is in close agreement with the frequency of radio and optical pulsations. However, since only 5 per cent of the total X-ray power of the nebula appears in the pulsed component, the absolute flux of X-ray from Tau-X1 is practically constant which is also borne out from our observations which are in close agreement with other observations made at different times.
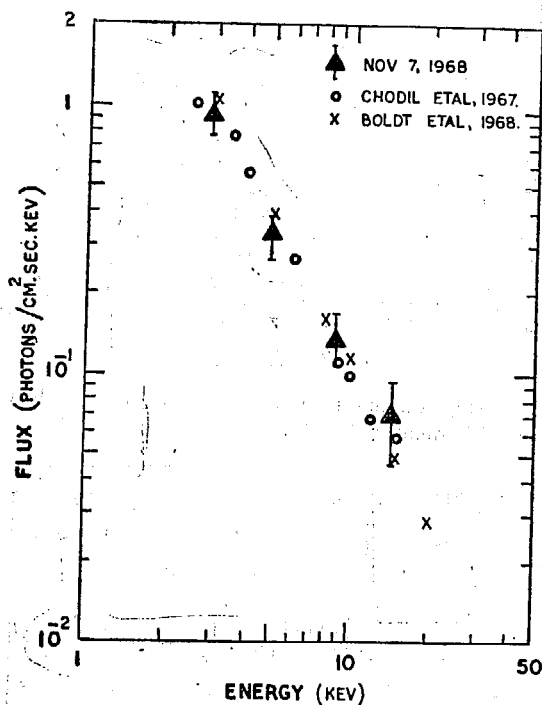

FIG. 6. Energy spectrum of Tau-X1 X-ray source in the range 2-18 Kev.

ABSOLUTE FLUX AND TIME VARIATION OF SCO-X1

Figure 7 shows the observed counting rate as a function of the rocket azimuth for different energy windows of nominal value 2–4 Kev; 4–6 Kev; 6–12 Kev and 12–18 Kev for both flights of November 3, 1968 and November 7, 1968 respectively. The data have been fitted to an energy spectrum of the type

$$f(E) = K \exp^{-E/E_0} dE$$

The value of E_0 for both the flights has been found to be $4 \cdot 4 \pm 0 \cdot 2$ Kev corresponding to a temperature of a hot thin plasma of $5 \cdot 1 \times 10^7$ °K. The

energy spectrum beyond 12 Kev, however, is consistent with only $E_0 \approx 18$ Kev in agreement with the observations of Busseli *et al.*[13] The flattening of the spectrum at higher energies has been explained in terms of the multi-layer complex model for Sco-X1 proposed by Shklovsky,[14] the higher energies being emitted from the higher temperature plasma in the core of the object.
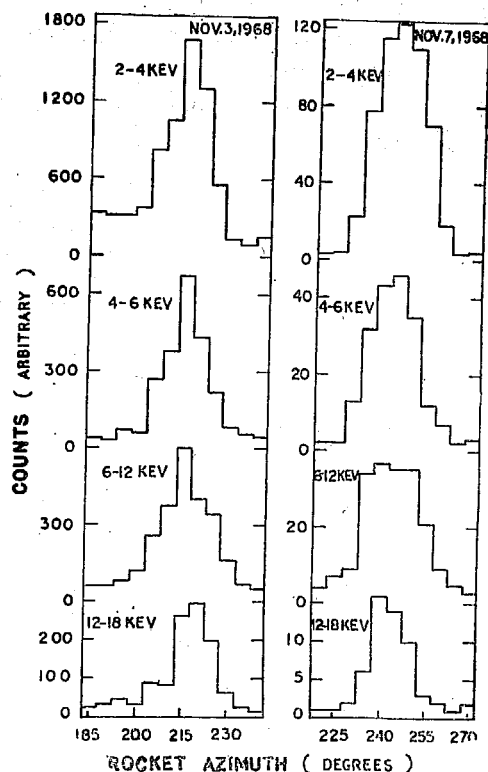

Fig. 7. X-ray count rate of Sco-X1 source for different differential energy windows.

In Fig. 8 are plotted the observational data on the intensity of low energy X-ray flux in different windows observed during the two flights. The observations of Chodil *et al.*,[15] Hill *et al.*[16] and Overbeck *et al.*[17] are also plotted in the same figure. Our observations are in quite a good agreement with the observations by other workers.

Investigation of the time variation of the absolute flux of Sco-X1 is of great importance in understanding the nature of the source. The large number of observations in the visible, in the near ultraviolet by Hiltner and Mook and by Stepien,[18] in the near infrared by Neugebauer *et al.*[19] and in

the radio region by Andrew and Purton have all pointed out to the large
variability of Sco-X1. Simultaneous optical and X-ray measurements by
Chodil et al.[15] has shown that the brighter optical intensity is accompanied
by a lower temperature and a bluer emission spectrum. The measurements
seem to be consistent with the model of both the X-ray and optical conti-
nuum being produced by thermal bremsstrahlung from the same hot thin
plasma. Observations of X-ray flares from Sco-X1 at balloon altitudes by
Lewin et al. and Agarwal et al.[20] seem to add strength to the above hypo-
thesis, even though a large number of simultaneous optical and X-ray
observations of Sco-X1 are needed to make any positive conclusion regard-
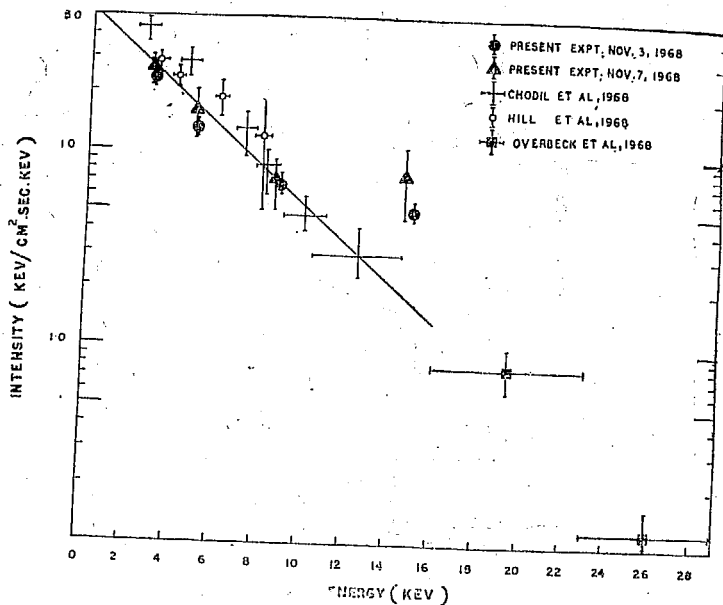ing the nature of the source.

FIG. 8. Energy spectrum of Sco-X1 X-ray source in the energy window 2–18 Kev.

Taking reasonable numbers for the distance of Sco-X1 and the total
energy flux as 1000 light-years and 6×10^{36} ergs/sec. respectively, the radius
of Sco-X1 has been estimated to be between 3×10^{10} and 10^{13} cm. In
order to keep the X-ray source going, the cooling time of the cloud, which is
variously estimated between 10 and 10^5 seconds, should be of the same order
as the heating time. This would indicate the possible existence of time varia-
tions in the X-ray flux from Sco-X1, having a time scale of 10 to 10^5 seconds.
We do not observe any statistically significant variation between the abso-
lute flux of Sco-X1 measured on November 3, 1968 and November 7, 1968.
Addition over shorter periods of time have also been intercompared to make

sure that statistically significant variations of Sco-X1 flux over periods of about 4 minutes do not exist. We may, however, point out that Overbeck *et al.* have reported significant time variations over time scales of about a month for X-rays in the energy range 16–30 Kev at balloon altitudes. Even though such large variations in the high energy flux can result from very small changes in temperature, nevertheless, the evidence together with the flare-like increases of X-ray flux strongly indicate the time variability of Sco-X1 X-ray source.

In Fig. 9 is shown the measurements of absolute flux of X-rays from Sco-X1 since 1965. Since many of the observations in the past did not have their sensor and attitude well calibrated, only those measurements from which reasonably accurate measurements can be derived are plotted in the figure. Table II gives the flux at 4·0 Kev, 6·0 Kev and the energy in the range 2–5 Kev as well as the temperature. It is evident from the figure as well as the table that the absolute flux of Sco-X1 has undergone significant time variations. The most conspicuous result from Fig. 9 is that the flux and the energy of Sco-X1 has steadily decreased over the period 1965–1968. Sporadic short time variations are superimposed upon
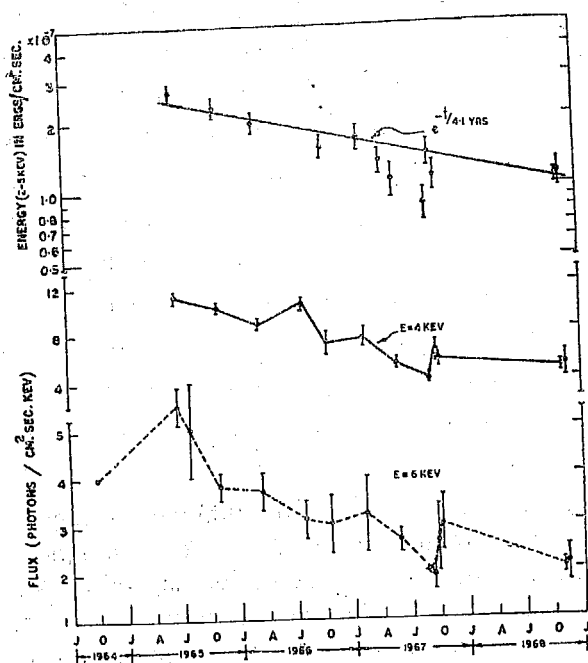

FIG. 9. Time variation of the flux and energy spectrum of Sco-X1 X-ray source during 1964–1968.

this general decrease in flux. The observations indicate that the general pattern of the time variation of Sco-X1 is consistent with an exponential decay of X-ray luminosity with a time constant of about 4·1 years which would mean that the flux of Sco-X1 would decrease by two orders of magnitude in a period of about 20 years.

TABLE II

Time variation of Sco-X1

Experimenter	Flight date	Flux of 4 Kev photons/cm.^{2} sec. Kev	Flux of 6 Kev photons/cm.^{2} sec. Kev	Energy (2-5 Kev range) $\times 10^{-7}$ ergs/ cm.^{2} sec.	Temperature $\times 10^7$ °K
Fisher et al.[21]	1 October 1964	··	4·0	··	··
Chodil et al.[22]	12 June 1965	11·25±0·6	5·5±0·4	2·65±0·23	1·6
Hayakawa et al.[23]	26 July 1965	··	5·0±1·0	··	4·8
Grader et al.[24]	28 October 1965	10·3 ±0·4	3·8±0·3	2·28±0·22	3·8
Gursky et al.[25]	8 March 1966	8·8 ±0·5	3·7±0·4	1·93±0·21	4·6
Chodil et al.[26]	28 July 1966	10·5 ±0·5	3·1±0·4	··	5·0
Gursky et al.[27]	11 October 1966	7·1 ±0·9	3·0±0·6	1·49±0·17	5·8
Matsuoka et al.[28]	6 February 1967	7·6 ±0·8	3·2±0·8	1·64±0·20	4·8
Cooke et al.[29]	10 April 1967	··	··	1·30±0·15	5·0
Chodil et al.[15]	18 May 1967	5·2 ±0·4	2·6±0·2	1·08±0·18	··
Fritz et al.[30]	8 September 1967	4·0 ±0·4	1·3±0·3	0·85±0·11	8·1
Chodil et al.[15]	29 September 1967	6·3 ±0·8	2·6±0·6	1·41±0·17	10·4
Hill et al.[16]	2 October 1967	5·4 ±0·6	2·9±0·6	1·12±0·16	4·6
Rao et al. (present experiment)	3 November 1968	4·9 ±0·3	2·1±0·2	1·07±0·15	10·4
„	7 November 1968	5·2 ±0·7	2·2±0·3	1·12±0·16	5·1
					5·1

Different theoretical models give different estimates ranging from 10–50 years for the lifetime of Sco-X1. For example, if we consider Manley's[31] model of a protostar shedding its magnetic field, where the high energy electrons are produced through the utilisation of magnetic energy, which upon interaction with the same field, can produce X-rays an estimated lifetime of about 30 years is obtained for an extar like Sco-X1. Such an estimate is obtained from considerations of energy for the magnetic field

required to supply energy to electrons. The experimental observation of about 20 years for the lifetime of Sco-X1 obtained from the long-term variation of the absolute X-ray flux of Sco-X1 is consistent with the theoretical models.

ABSOLUTE FLUX AND TIME VARIATION OF CEN-X2

The rediscovery of low energy X-ray flux in the range 2–18 Kev from Cen-X2 source is the most important result of these flights. The presence of low energy flux from Cen-X2 is unambiguously proved in both the flights as may be seen from Figs. 4 and 5. The level of detection of Cen-X2 on November 3, 1968 flight is more than 10 standard deviation level and on November 7, 1968 flight at about 6 standard deviation level. The best estimate of the position of Cen-X2 as determined from our experiment is $201 \pm 2°$ R.A. and $-62 \cdot 5 \pm 2°$ declination, which is consistent with the position of Cen-X2 observed by Harries *et al.* and Chodil *et al.*

In Fig. 10 is plotted the energy spectrum of the X-ray intensity from Cen-X2 observed during both the flights. Even though the data from both the flights can be adequately represented by an exponential spectrum with a characteristic temperature of about $5 \cdot 4$ Kev ($T = 6 \cdot 3 \times 10^{7°}$ K), a power law spectrum fits the data better. The X-ray flux on November 3, 1968 can be represented by the spectrum

$$f(E) = 5 \cdot 8 \; E^{-1 \cdot 2 \pm 0 \cdot 2} \; dE$$

and that on November 7, 1968 by the spectrum

$$f(E) = 5 \cdot 1 \; E^{-0 \cdot 9 \pm 0 \cdot 2} \; dE.$$

We conclude that the energy spectrum of the X-ray flux measured on November 3, 1968 and November 7, 1968 are same within the statistical error. In the same figure, the observations of high energy flux observed at balloon altitudes by Lewin *et al.*[32] on October 15, 1967 are also plotted. The low and high energy observations taken one year apart seem to fit a single power law spectrum with an exponent of $1 \cdot 2$.

Figure 11 summarizes the remarkable time variation of the X-ray flux from Cen-X2, the numerical data being given in Table III. It was not detected in October 1965, was observed as a time-varying object in April–May 1967 and again could not be detected in September 1967. The decreases in the X-ray flux during the period April–May 1967 was found

to be exponential, with a time constant of 23·4 days. This decrease was also accompanied by a softening of the spectrum. Even though Cen-X2 was again sighted in the high energy range in October 1967, no low energy flux from the same source was detected in June 1968, by Pounds *et al.* They provide an upper limit of 0·15 photons/cm.^{2} sec. for the flux in the energy range 2–5 Kev, which is more than an order of magnitude below the low energy flux that has been detected in our experiments in November 1968. Our observations are the first evidence for the existence of the low energy X-ray flux from Cen-X2 in the range 2–20 Kev since May 1967.
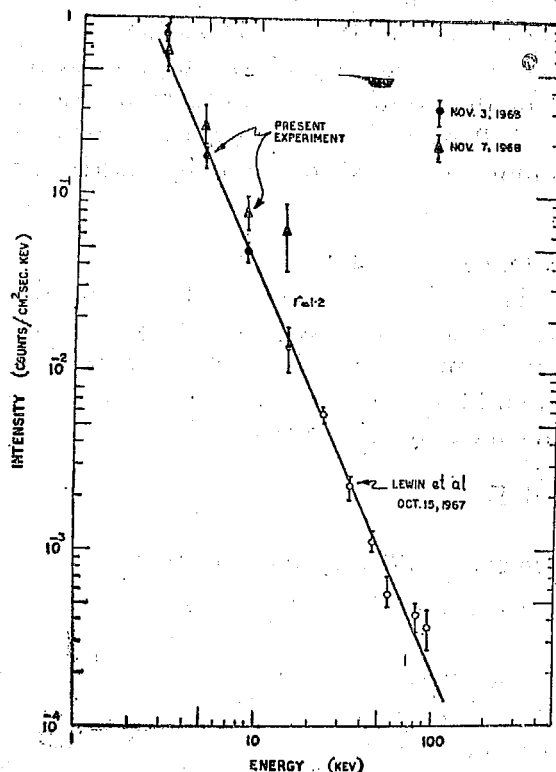

FIG. 10. Energy spectrum of Cen-X2 X-ray source in the range 2–18 Kev.

The remarkable time variability of Cen-X2 makes this extar a unique object of interest. The spectacular outburst in April–May 1967 was followed by the outbursts in October 1967 as observed by Lewin *et al.*, and in November 1968 as observed in the two rocket flights conducted by us from India. The totality of observations made so far clearly indicate that Cen-X2 is a nova-like source giving rise to recurring X-ray outbursts, each

TABLE III

Time variation of X-ray Intensity from Cen-X2

Experimenter	Flight date	Energy flux in 2–5 Kev range 10^{-8} ergs/cm.^{2} sec.
Grader et al.[24]	28 October 1965	< 0·25
Harries et al.[8]	4 April 1967	11·0 ±1·0
Cooke et al.[29]	10 April 1967	16·0 ±1·0
Francey et al.[33]	20 April 1967	7·5 ±1·0
Chodil et al.[34]	18 May 1967	2·6 ±0·4
Chodil et al.[15]	28 September 1967	< 0·3
Lewin et al.[32]	15 October 1967	0·62 (extrapolated)
Pounds et al.[35]	12 June 1968	< 0·1
Rao et al. (present experiment)	3 November 1968	0·68±0·08
,,	7 November 1968	0·83±0·14

outburst lasting probably a short period of time. In order to explain this behaviour, Manley proposed an expanding constant mass plasma model for the source, according to which a dense plasma cloud of radius ~ 10^{14} cm. was heated at constant volume to nearly 2×10^7 °K which then proceeded to expand isothermally and cool off. The recurring short-lived outbursts like the one observed by Lewin *et al.* and more recently our low energy observations can be attributed to a shock wave from the nova
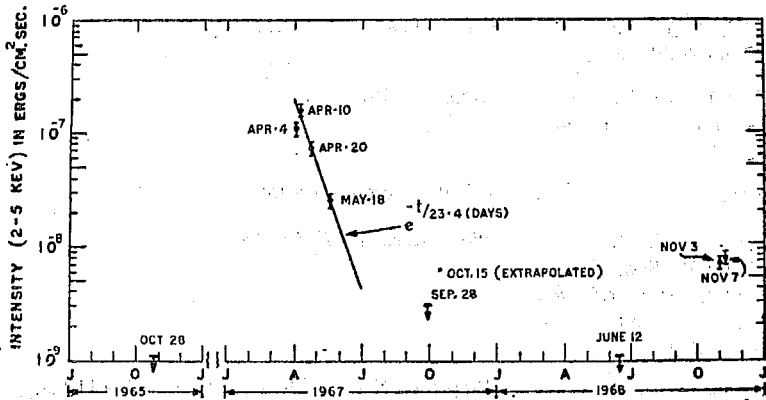

FIG. 11. Time variation of the X-ray flux from Cen-X2 source.

outburst expanding into the circumstellar medium. Such a shock could accelerate and heat the gas to a high temperature as it propagates into a medium of decreasing density.

REFERENCES

1. Giacconi, R., Gursky, H., Paolini, F. R. and Rossi, B.   *Phys. Rev.*, 1962, **9**, 439.

2. Sandage, A., Osmer, P., Giacconi, R., Gorenstein, P., Gursky, H., Waters, J., Bradt, H., Garmire, G., Sreekantan, B. V., Oda, M., Osawa, K. and Jugaku, J.   *Ap. J.*, 1966, **146**, 316.

3. Hiltner, W. A. and Mook, D. E.   *Ibid.*, 1967, **150**, 851.

4. Rao, U. R., Prakasarao, A. S. and Jayanthi, U. B.   *Nature*, 1969, **222**, 864.

5. Andrew, B. H. and Purton, C. R.   *Ibid.*, 1968, **218**, 855.

6. Ables, J. G.   ..   *Ap. J. (Letters)*, 1969, **155**, L 27.

7. Lewin, W. H. G., Clark, G. W. and Smith, W. B.   *Ibid.*, 1968, **152**, L 55.

8. Harries, J. R., McCracken, K. G., Francey, R. J. and Fenton, A. J.   *Nature*, 1967, **215**, 38.

9. Wada, M.   ..   Private Communication.

10. Chodil, G., Mark, H., Rodrigues, R., Seward, F., Swift, C. D., Hiltner, W. A., Wallerstein, G. and Mannery, E. J.   *Phys. Rev.*, 1967, **19**, 681.

11. Boldt, E. A., Desai, U. D. and Holt, S. S.   Preprint—NASA Document No. X-611-68-353

12. Fritz, G., Henry, R. C.,   *Science,* 1969, **155**, 709.
    Meekins, J. F., Chubb,
    T. A. and Friedman, H,

13. Busseli, G., Clancey, M. C.,   *Nature,* 1968, **219**, 1124.
    Davison, P. J. N., Edwards,
    P. J., McCracken, K. G.
    and Thomas, R. M.

14. Shklovsky, I. S.   .. *Ap. J.* (Letters), 1967, **148**, L1.

15. Chodil, G., Mark, H.,   *Ap. J.,* 1968, **154**, 645.
    Rodrigues, R., Seward,
    F. D., Swift, C. D.,
    Turiel, I., Hiltner, W. A.,
    Wallerstein, G. and
    Mannery, E. J.

16. Hill, R. W., Grader, R. J.   *Ibid.,* 1968, **154**, 655.
    and Seward, F. D.

17. Overbeck, J. W. and   *Ibid.,* 1968, **153**, 899.
    Tananbaum, H. D.

18. Stepien, K.   .. *Ap. J. (Letters),* 1968, **151**, L 15.

19. Neugebauer, G., Oke, J. B., *Ap. J.,* 1969, **155**, 1.
    Becklin, E. and Garmire, G.

20. Agarwal, P. C., Biswas, S., Presented at Symposium No. 37 of the I.A.U. on Non-
    Gokhale, G. S., Iyengar,   Solar Gamma and X-ray Astronomy at Rome, 1969.
    V. S., Kunte, P. K.,
    Manchanda, R. K. and
    Sreekantan, B. V.

21. Fisher, P. C., Johnson,   *Ap. J.,* 1966, **143**, 203.
    H. M., Jordan, W. C.,
    Meyerott, A. J. and
    Acton, L. W.

22. Chodil, G., Jopson, R. C., *Phys. Rev.,* 1965, **15**, 605.
    Mark, H., Seward, F. D.
    and Swift, C. D.

23. Hayakawa, S., Matsuoka, *Report of Ionosphere and Space Research in Japan.*
    M. and Yamashita, K.

24. Grader, R. J., Hill, R. W., *Science,* 1966, **152**, 1499.
    Seward, F. D. and Toor, A.

25. Gursky, H., Gorenstein, P. *Ap. J. (Letters),* 1967, **150**, L 50.
    and Giacconi, R.

26. Chodil, G., Mark, H.,   *Ap. J.,* 1967, **150**, 57.
    Rodrigues, R., Seward,
    F. D. and Swift, C. D.

27. Gursky, H., Gorenstein, P.   *Ap. J.* (*Letters*), **150**, L 85.
     and Giacconi, R.

28. Matsuoka, M., Oda, M.,   *Can. J. Phys.*, 1966, p. 8466.
     Ogawara, Y., Hayakawa,
     S. and Kato, T.

29. Cooke, B. A., Pounds,   *Ap. J.* (*Letters*), 1967, **150**, L 18?.
     K. A., Stewardson, E. A.
     and Adams, D. J.

30. Fritz, G., Meekin, J. F.,   *Ibid.*, 1968, **153**, L 199.
     Harry, R. C., Byram, E. T.
     and Friedman, H.

31. Manley, O. P.   *Ap. J.*, 1966, **144**, 1253.

32. Lewin, W. H. G., Clark,   *Ap. J.* (*Letters*), 1968, **152**, L 49.
     G. W. and Smith, W. B.

33. Francey, R. J., Fenton,   *Nature*, 1967, **216**.
     A. G., Harries, J. R. and
     McCracken, K. G.

34. Chodil, G., Mark, H.,   *Ap. J.* (*Letters*), 1968, **152**, L 45.
     Rodrigues, R. and
     Swift, C. D.

35. Pounds, K. A.   Presented at Symposium No. 37 of the I.A.U. on Non-
                                        Solar Gamma and X-ray Astronomy at Rome, 1969.
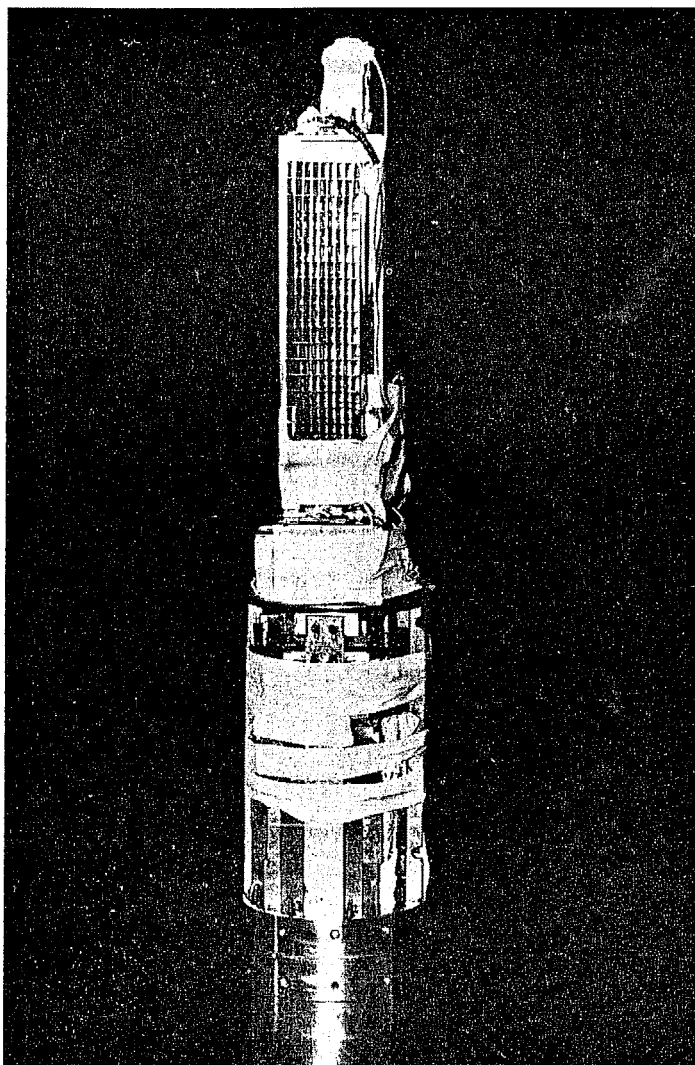
FIG. 1. Rocket-borne X-ray payload to measure extra-terrestrial X-rays.

DIFFUSE X-RAY BACKGROUND MEASUREMENTS
IN THE ENERGY RANGE 2–18 keV

A. S. PRAKASARAO, D. P. SHARMA, U. B. JAYANTHI, and U. R. RAO

Physical Research Laboratory, Navrangpura, Ahmedabad, India

Abstract. Rocket measurements, of the diffuse X-ray background in the energy range 2–18 keV, conducted from Thumba Equatorial Rocket Launching Station (TERLS), India, are presented. The estimates of the cosmic background are derived by the method which employs the Earth and its atmosphere as a shutter to intercept the celestial X-rays. The results are shown to be consistent with a power law photon spectrum.

$13.6\,^{+4.3}_{-3.3}\,E^{-1.73}\,\pm 0.15$ photons/cm²-sec-keV-ster the spectrum being much flatter than that observed at higher energies.

1. Introduction

Precise estimation of the energy spectrum and the anisotropy of the celestial diffuse X-ray background over a large energy range is of vital importance in the understanding of its production mechanism, and its cosmological implications (Setti and Rees, 1969). In this paper, we report the results obtained from the analysis of data over the energy range 2–18 keV from two spin stabilised, Centaure rocket flights, conducted on November 3, 1968 (35.01) and December 7, 1969 (45.03), from the Thumba Equatorial Rocket Launching Station (TERLS), Trivandrum, India. Reliable estimation of cosmic background is rendered difficult due to contamination of secondary X-rays of terrestrial origin. Therefore experiments done at equator have a great special value since the contribution from the secondary X-rays at these latitudes is least due to the high geomagnetic cut-off rigidity. Besides, to derive the cosmic background, we have employed a new powerful method of analysis which uses the Earth and its atmosphere as an effective shutter.

2. Experimental Details

The detector systems used in both the rocket experiments, consisted of proportional counters filled with xenon and methane and having thin beryllium entrance windows. The physical details of the counters are described elsewhere (Rao *et al.*, 1969; Rao *et al.*, 1970). The counters having an effective area of about 60 cm², had an energy resolution of about 15% FWHM for 6 keV X-rays from Fe⁵⁵ radioactive source. The detectors, mounted perpendicular to the spin axis of the rocket, scanned in the direction of the rocket horizon during each spin. Slat type collimators with full width half maximum transmission angles of 8.7° × 17.2° and 7° × 15°, defined the geometrical apertures of the detectors in the two flights. The X-ray data were analysed into four contiguous discrete energy channels 2–4, 4–6, 6–12, 12–18 keV in the flight 35.01 and into eight equal energy windows over 2–10 keV in the flight 45.03. The

calibration of the detectors and the associated electronics were checked during a part
of the flight, by using an Fe^{55} radioactive source mounted on the nose cone in front
of the counter, the nose cone portion being explosively ejected at about 60 km
altitude. The attitudes of the rockets were derived from suitably located Sun sensor
and crossed magnetic sensors, using standard techniques, details of which are
published elsewhere (Rao et al., 1969; Rao et al., 1970). The regions of celestial sky
scanned by the detector in each of these two flights are shown in Figure 1.

3. Method of Analysis

A number of methods have been used in the past for estimating the cosmic X-ray
flux, which are summarised by Matsuoka et al. (1969). One of these is to use the Earth
and its atmosphere as a shutter to intercept the celestial X-rays, when the counter
views the Earth during some parts of the spin of the rocket. The detector registers
both the secondary background and the diffuse cosmic X-rays, when it views the
celestial sky. When the detector faces the Earth completely, the counts it registers are
only due to the secondary charged particle background. The difference in count
rate, when the counter field of view is intercepted by the Earth and other periods can
provide a reliable estimate of the diffuse X-ray background.

The above simple situation exists only for low rocket elevations and small opening
angles of the telescope. In practice, when the elevation of the rocket is not very far
from 90° and the detectors have a fairly large opening angle, intermediate situations
exist, and even in the best case a small portion of the solid angle of the detector will be
looking at the celestial sky. The elevation of the two rockets in the present experiment

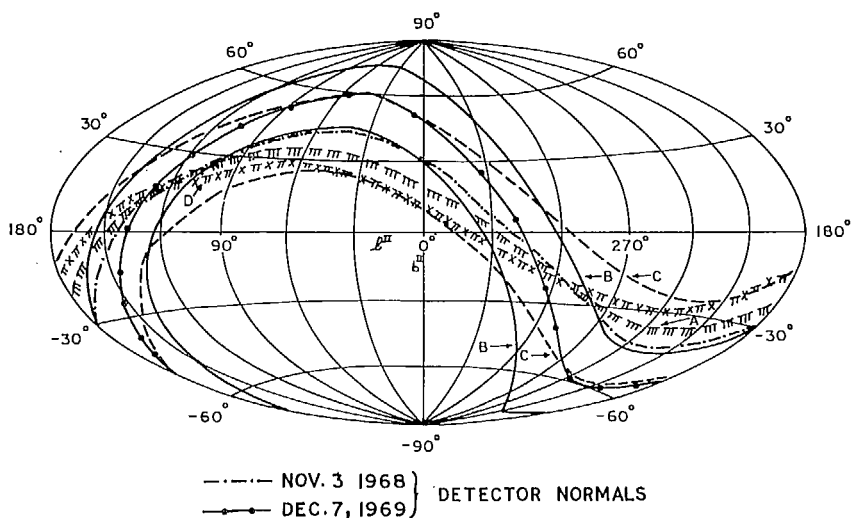—·—·— NOV. 3 1968 ⎫ DETECTOR NORMALS
—•—•— DEC. 7, 1969 ⎭

Fig. 1.   Regions of celestial sky scanned by the detector during the two rocket flights. A and D are
local horizons, CC and BB are belts scanned during November 1968 and
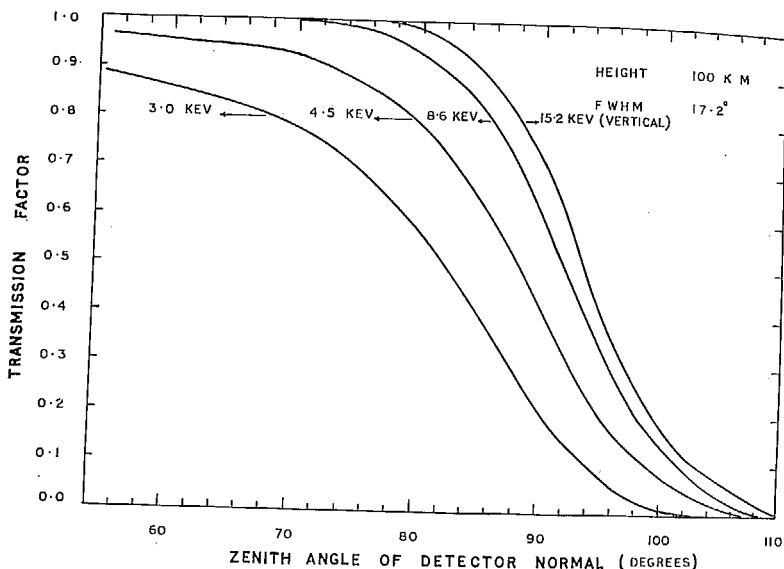December 1969 flights respectively.

Fig. 2. Effective transmission factor of the detector with a field of view with FWHM of 15° along the spin axis, at four specific energies, for an altitude of 100 km.

being 73° and 64° respectively, effective solid angles have to be evaluated for different portions of the spin azimuths to estimate the background flux.

The geometrical sensitivity (as a fraction of total geometrical aperture) of an element of the detector, between zenith angle θ and $\theta + d\theta$ is given by

$$G(\theta) = \left(1 - \frac{\tan(|Z - \theta|)}{\tan F}\right) \frac{d\theta}{F},$$

where Z is the zenith angle of the detector normal and F is the half angle of opening of the collimator along the spin axis of the rocket. The effective transmission factor of the detector at a zenith Z is given by

$$TR(Z, E) = \int_{Z-F}^{Z+F} G(\theta) \exp(-\mu(E) m(\theta)) \, d\theta,$$

where $\mu(E)$ is the mass absorption coefficient of air for X-rays of energy E, and $m(\theta)$ is the mass of air in the line of sight along the zenith angle Z. These factors, for four different energies for the detector at 100 km altitude have been calculated and are shown in Figure 2. Weighted means of these transmission factors for different energies have been computed for each flight, taking into account the time spent by the detector at different altitudes.

Figure 3 shows the plot of count rate in the energy range 2–10 keV as a function of spin azimuth for the rocket experiment 45.03. The absolute photon flux in each differential energy channel was derived by deconvoluting the count rate data with the
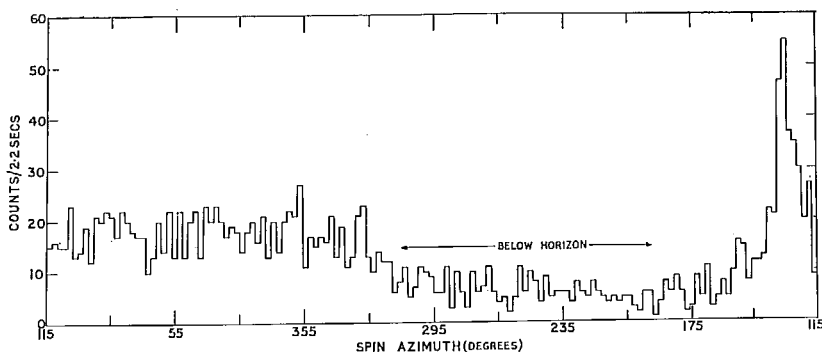
Fig. 3.   The count rate in the energy range 2–10 keV, plotted versus spin azimuth of rocket, for
the flight 45.03.

detector efficiency $\varepsilon(E)$, and the computed transmission factors $TR(E)$, using the
expression

$$C(E_1, E_2) = TBG + \int_{E_1}^{E_2} P(E)\,\varepsilon(E)\,TR(E)\,dE,$$

where $C(E_1, E_2)$ are the observed counts in an energy interval E_1 to E_2 keV, TBG is
the contribution from terrestrial background and $P(E)$ is the true photon flux at
energy E.

4. Results

The results of the diffuse X-ray background from the two rocket flights are shown in
Figure 4, along with the spectral fits given by Gorenstein et al. (1969) and Baxter et al.
(1969). Since the results obtained in the two rocket flights agree within the experimental
errors, data from both the flights have been combined to obtain the best fit power law
spectrum given by

$$13.6^{+4.3}_{-3.3}\, E^{-1.73\pm0.15}\ \text{photons/cm}^2\text{-sec-keV-ster}.$$

The spectral behaviour of the cosmic X-ray flux obtained in our experiment is
consistent, with the results obtained by other workers (Gorenstein et al., 1969;
Baxter et al., 1969) for the low energy cosmic X-ray flux but much flatter than the
spectral exponent of 2.45 reported by Bleeker and Deerenberg (1970) for energies
greater than 20 keV.

5. Discussion

The results, besides establishing the effectiveness of the method which uses the Earth
as a shutter, clearly confirm that the spectrum of diffuse X-ray background in the
energy range 2–18 keV is flatter than at higher energies (Rao et al., 1967 and Bleeker
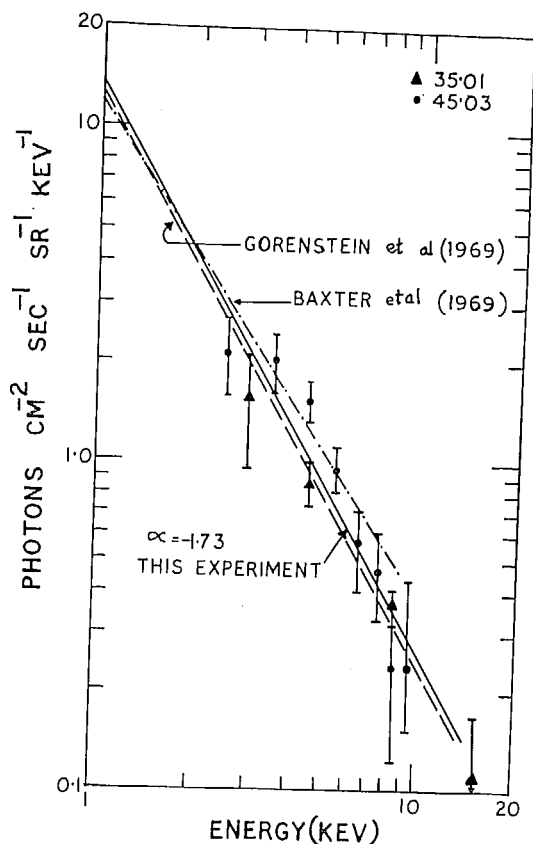and Deerenberg, 1970). The existence of such a break in the spectrum at about

Fig. 4.   Energy spectrum of diffuse X-ray background in the energy range 2–18 keV.

20–40 keV has also been reported by other workers and consequently any theoretical model proposed must be able to explain this feature of the spectrum. The models proposed till now can generally be classed under two categories (a) those which interpret X-ray background as the effect of superposition of discrete sources and (b) those which invoke emission mechanisms that operate over extended diffuse regions, possibly throughout the intergalactic space. Both these categories of models fail from the intensity considerations when the cosmological evolutionary effects are not considered. The discrete source model (Silk, 1969) which takes into account cosmological effects, though capable of explaining the observed magnitude of the flux by appropriate choice of evolutionary parameters, fail to satisfactorily explain the change of spectral exponent, as the contribution from the distant galaxies would be integrated even if objects having power law spectra with different exponents are assumed. The model based on inverse Compton scattering of blackbody photons by relativistic electrons from radio sources at large red shifts (Setti and Rees, 1969) seems to give the most satisfactory explanation of the diffuse background. Change in this spectral exponent can be explained (Rees and Setti, 1968) by invoking additional adiabatic energy

losses, such that the Compton life time for the relevant electrons is equal to the time required for the radio source to expand to twice its radius. However, for this process to be effective one needs to assume that the X-ray emission is mainly from a region of small window of redshift, so that the break is not smeared out.

Acknowledgements

References

Baxter, A. J., Wilson, B. G., and Green, D. W.: 1969, *Can. J. Phys.* **47**, 2651.
Bleeker, J. A. M. and Deerenberg, A. J. M.: 1970, *Astrophys. J.* **159**, 215.
Gorenstein, P., Kellogg, E. M., and Gursky, H.: 1969, *Astrophys. J.* **156**, 315.
Matsuoka, M., Oda, M., Ogawara, Y., Hayakawa, S., and Kato, T.: 1969, *Astrophys. Space Sci.* **4**, 44.
Rao, U. R., Chitnis, E. V., and Prakasarao, A. S.: 1967, *Proc. Ind. Acad. Sci.* **66A**, 353.
Rao, U. R., Chitnis, E. V., Prakasarao, A. S., and Jayanthi, U. B.: 1969, *Proc. Ind. Acad. Sci.* **70A**, 257.
Rao, U. R., Chitnis, E. V., Sharma, D. P., Prakasarao, A. S., and Jayanthi, U. B.: 1970, communicated for publication.
Setti, G. and Rees, M. J.: 1969, in L. Gratton (ed.), 'Non-Solar X- and Gamma-Ray Astronomy', *IAU Symp.* **37**, 352, D. Reidel, Dordrecht.
Silk, J.: 1969, *Nature* **221**, 347.

X-ray Observation of Cen XR-4 and Nor XR-2

WE wish to present the results of an X-ray astronomy experiment conducted from a Centaure rocket launched from Thumba Equatorial Rocket Launching Station (TERLS), India, at 0035 UT on December 7, 1969. The detector consisted of a xenon–methane proportional counter of useful area of 55 cm² with a 18 mg cm⁻² thick beryllium window and a slat collimator with a field of view of 7°×15°. It had a resolution of 20% for 6 keV X-rays from a ^{55}Fe radioactive source. The rocket aspect[1] determined from onboard magnetic and Sun sensors showed that it had a spin rate of 5.5 r.p.s. and a precession with a half cone angle of about 3° around an axis centred at R.A. 8 h 56 m ±4 m and declination 3°±1°. The X-ray data were pulse height analysed into three contiguous energy channels in the energy range 2–18 keV.

Fig. 1 shows the plot of count rate in the 2–9 keV range as a function of spin azimuth. Various sources within the scan region of the detector are marked in the figure, the source positions having been obtained from earlier observations[2-4]. As the figure shows, the fluxes from Cen XR-1, Cen XR-2 and Cen XR-4 are much below the limit of detectability and hence only upper limits of flux for these sources are derived (Table 1).

All available observations of Cen XR-4 at different epochs[3,5,6] are plotted in Fig. 2. Data from Vela satellites used in this diagram have been corrected for transmission efficiency of the

Table 1 Upper Limits for the X-ray Flux from Cen XR-1, Cen XR-2 and Cen XR-4 in the Energy Range 2–18 keV (2 σ level)

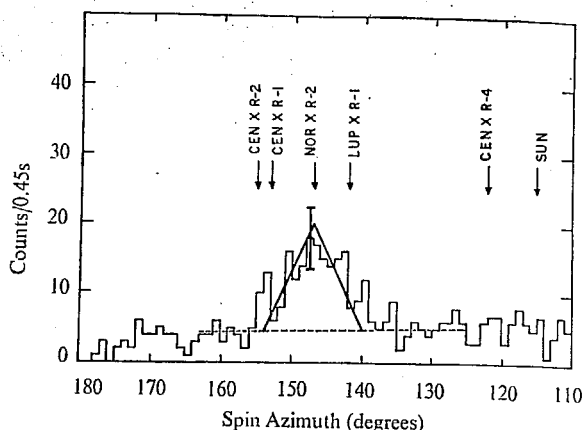| Energy range (keV)	Flux in photons cm⁻² s⁻¹ keV⁻¹		
	Cen XR-1	Cen XR-2	Cen XR-4
2–5	1.4×10^{-2}	3.6×10^{-2}	1.5×10^{-2}
5–9	0.95×10^{-2}	2.4×10^{-2}	1.0×10^{-2}
9–18	0.52×10^{-2}	1.3×10^{-2}	0.55×10^{-2}

Fig. 1 Total counts in 2–9 keV range for 0.45 s plotted as a function of spin azimuth.

detector window. Cen XR-4, which erupted suddenly as an X-ray star in July 1969, decayed to less than 0.5% of its peak intensity by September 24, 1969 (ref. 6). Our observation on December 7, 1969, yields an upper limit of 0.13 photons cm^{-2} s^{-1} for the flux from this source in the energy range 2–18 keV.

The similarity between the concentration of X-ray sources and that of novae along the galactic plane has already been pointed out by L. Gratton (at the IAU symposium on non-solar γ and X-ray astronomy in Rome in 1969). The spectacular time variation, shown by X-ray sources like Cen XR-2 and Cen XR-4[6], is very much like the optical luminosity variation of novae. Arp[7] has established a definitive relationship between the maximum magnitude attained by novae and their total duration, the lesser magnitude novae corresponding to lesser duration. Novae with a duration similar to Cen XR-4 will have a typical apparent magnitude of about 17. Since the novae in the galaxy M31 have the same characteristics as our galactic novae, we have plotted in Fig. 2 the light curves for No. 13 nova in M31 which has an apparent magnitude of about 17. The similarity between the light intensity of a typical fast nova and the X-ray flux of Cen XR-4 is very striking, indicating that Cen XR-4 is a nova-like object.

Considering the triangular response of the collimator, the main peak in the count rate (Fig. 1) can be attributed entirely to Nor XR-2 at R.A. 234° 30′ ± 2° and declination −56°

2

Photons/cm²/s

50

10

5

1

0.05
.5

0.01
.1

50

10

5

1

0.5

0.1

17

18

19

20

21

Photographic magnitude (mpg)

1   5   10   50   100   500 1,000
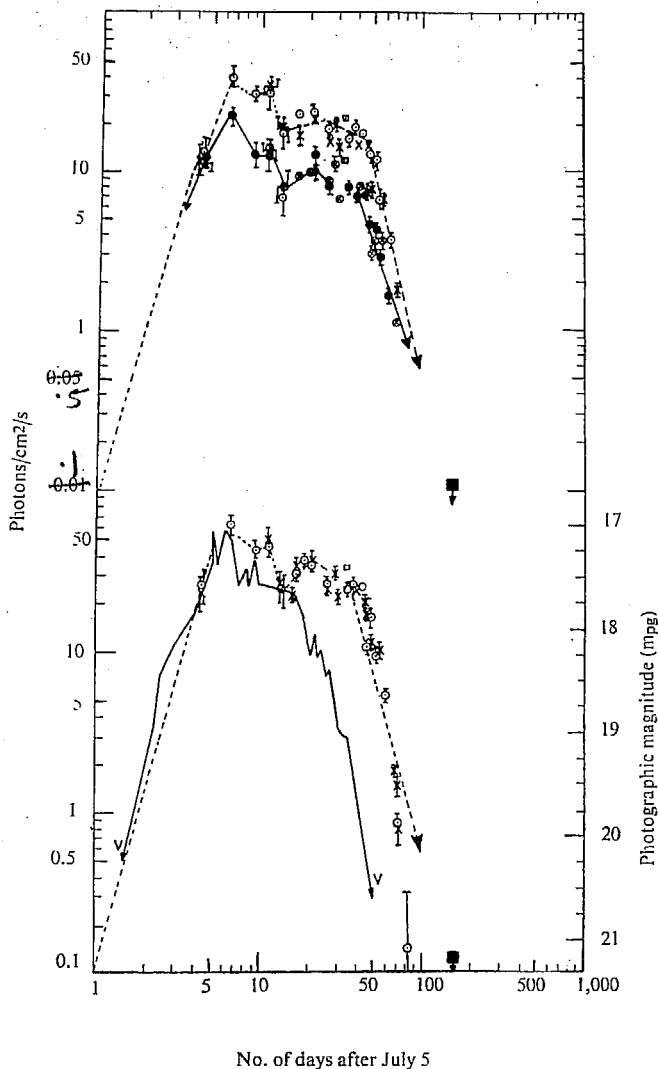
No. of days after July 5

Fig. 2 X-ray flux from Cen XR-4 as a function of time after July 5. The lower curves show the light curve of nova No. 13 in Andromeda nebula (———) and the X-ray flux in the energy range 3–12 keV (- - -). The upper curves show X-ray flux from the same source in two energy bands 3–6 (- - - -) and 6–12 (———) keV. ⊗, ●, ⊙, ×, Vela (Evans *et al.*)[6]; ▫, Kitamura *et al.*[5]; ▪, present experiment.

3

$22' \pm 2°$ consistent with the position coordinates given by Friedman *et al.*[2].

Even though Chodil *et al.* observed a flux of ~ 1.6 photons cm^{-2} s^{-1} (2–10 keV) for Lup XR-1 in 1967, subsequent low energy observations by Peterson (reported in Rome) and MacGregor *et al.*[8] have failed to confirm this. Further, the high energy balloon observation of Lewin *et al.*[9] has indicated the absence of this source. In spite of the reported location of Lup XR-1 only 3° away from collimator normal as compared with 8° for Nor XR-2, we do not observe a significant flux (at 2σ level) from the direction of Lup XR-1, which taken with Chodil *et al.*'s[4] observation indicates that Lup XR-1 is also a time varying X-ray source.

The counts in different energy channels 2–5, 5–9, 9–18 keV for Nor XR-2 source were obtained by subtracting the background, which was derived from the mean counts on both sides of the source position. The absolute flux $N_p(E)$ was derived from the count rates by folding the efficiency $\varepsilon(E)$ of
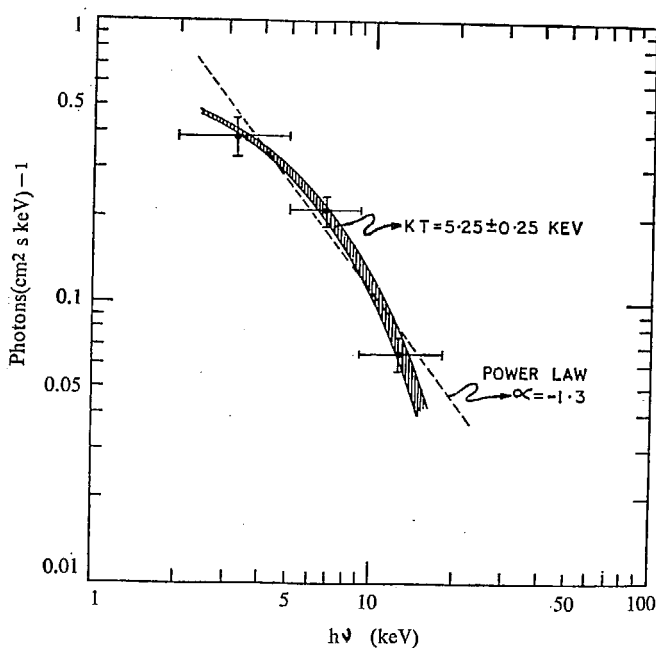

Fig. 3   The differential photon spectrum of the Nor XR-2 source.

4

the detector and the atmospheric transmission along the line of sight $Tr(E)$ as

$$N(E_1, E_2) = \int_{E_1}^{E_2} N_p(E)\, Tr(E)\, \varepsilon(E)\, dE$$

and considering the geometrical response of the detector system. In the energy range 2–10 keV, we observe a flux of 2.0 ± 0.3 photons cm^{-2} s^{-1} for the Nor XR-2 source, which can be compared with the value of ~ 2.6 photons cm^{-2} s^{-1} obtained by MacGregor *et al.*

Fig. 3 shows the plot of the differential photon flux for Nor XR-2 which can be fitted to either an exponential spectrum $N_p(E) = 0.75\, e^{-E/5.25 \pm 0.25}$ photons cm^{-2} s^{-1} keV^{-1} corresponding to a hot thin plasma at 6×10^7 K or to a power law spectrum $N_p(E) = 2.1\, E^{-1.3 \pm 0.2}$ photons cm^{-2} s^{-1} keV^{-1}.

Even though a power law spectrum is generally considered as indicative of the synchrotron mechanism for X-ray production, Manley[10] has shown that consideration of a sharp high energy cut off in the relativistic electron spectrum can modify the power law spectrum for X-rays into an exponential one. It is extremely interesting to note that a supernova remnant[11] P 1548–55 at R.A. 237° 15′ and decln −55° 59′ and a pulsar[12] MP 1530–53 at R.A. 232° 35′ 45″ ±30″ and decln −53° ±1° are located within the uncertainty circle of Nor XR-2 coordinates. Since Poveda and Woltjer[11] first suggested the possibility that all supernova remnants were X-ray emitters, only two X-ray sources have been definitely identified with supernova remnants. The likelihood of Nor XR-2 being also associated with a supernova remnant, coupled with the possibility of its X-ray spectrum favouring a synchrotron emission, makes this a source of great astrophysical interest.

U. R. Rao
E. V. Chitnis
D. P. Sharma
A. S. Prakasarao
U. B. Jayanthi

Physical Research Laboratory,
Ahmedabad-9.

[1] Rao, U. R., Chitnis, E. V., Prakasarao, A. S., and Jayanthi, U. B., *Proc. Ind. Acad. Sci.,* **70***A*, 257 (1969).
[2] Friedman, H., Byram, E. T., and Chubb, T. A., *Science,* **156**, 374 (1967).

3 Conner, J. P., Evans, W. D., and Belian, R. D., *Astrophys. J. Lett.*, **157**, L157 (1969).

4 Chodil, G., Mark, H., Rodrigues, R., Seward, F., Swift, C. D., Hiltner, W. A., Wallerstein, G., and Mannery, E. D., *Phys. Rev. Lett.*, **19**, 681 (1968).

5 Kitamura, T., Matsuoka, M., Miyamoto, S., Nakagawa, M., Oda, M., Ogawara, Y., and Takagishi, K., *Nature*, **224**, 784 (1969).

6 Evans, W. D., Belian, R. D., and Conner, J. P., *Astrophys. J. Lett.*, **159**, L57 (1970).

7 Arp, H. C., *Astron. J.*, **61**, 15 (1956).

8 MacGregor, A., Seward, F., and Turiel, I., *Astrophys. J. Lett.*, **161**, 979 (1970).

9 Lewin, W. H. G., Clark, G. W., and Smith, W. B., *Astrophys. J. Lett.*, **152**, L49 (1968).

10 Manley, O. P., *Astrophys. J.*, **144**, 1253 (1966).

11 Poveda, A., and Woltjer, L., *Astron. J.*, **73**, 65 (1968).

12 Taylor, R., *Astrophys. Lett.*, **3**, 205 (1969).